

DISSERTATION

DAMAGE ANALYSIS AND MITIGATION FOR WOOD-FRAME STRUCTURES
SUBJECTED TO TORNADO LOADING

Submitted by

Christine Diane Standohar-Alfano

Department of Civil and Environmental Engineering

In partial fulfillment of the requirements

For the Degree of Doctor of Philosophy

Colorado State University

Fort Collins, Colorado

Spring 2016

Doctoral Committee:

Advisor: John W. van de Lindt

Bruce R. Ellingwood

Paul R. Heyliger

Russ S. Schumacher

Copyright by Christine D. Standohar-Alfano 2016

All Rights Reserved

ABSTRACT

DAMAGE ANALYSIS AND MITIGATION FOR WOOD-FRAME STRUCTURES SUBJECTED TO TORNADO LOADING

Tornadoes are one of the most devastating natural hazards that occur in the United States. While there is an average of approximately 1200 tornadoes per year across the country, the annual likelihood of experiencing a tornado at a particular location is quite small due to their relatively small size. However, the high consequence of a tornado strike necessitates the determination of geographic tornado hazard. A methodology to estimate the annualized probabilistic tornado hazard over the contiguous U.S. was developed and used the most recent 38 years of climatological tornado data. Furthermore, with the use of detailed damage surveys after the April 3-4, 1974 and April-May, 2011 tornado outbreaks, an empirical method was developed and applied to account for the gradient of wind speed along a tornado's path length and path width. From this, a probabilistic tornado hazard index was developed across the United States which quantified the annual probability of experiencing a tornado of any strength on the Enhanced Fujita scale.

Tornado hazard curves were developed from the tornado hazard analysis at six illustrative locations which varied as a function of location-specific occurrence rates. Five different residential wood-frame building archetypes were designed at each of the locations based on current residential building code and/or practice. Fragilities for the roof sheathing, truss to wall top-plate, and wall-to-foundation connections were developed for each archetype. At each of the six locations, the fragility curves for the locally adopted residential building code were

convolved with the tornado hazard curve at that specific location in order to compute annual failure probabilities for select components along the vertical load path. This was one of the first times unconditional risk of component failure due to tornadoes has been computed since the tornado hazard curve was convolved with the fragility curves. These probabilities quantify failure probabilities of residential wood-frame construction components to tornado winds. In addition, the more wind-resistant Florida residential building code is applied to other locations in the U.S., fragilities are developed and convolved, and failure probabilities for these modified buildings are computed. This resulted in a quantitative measure of risk reduction from tornadoes by using strengthened construction at various locations across the country. The convolved failure probabilities were first developed for individual components. The system level behavior of the entire structure was also assessed and included the correlated dependencies between individual components. Results indicate that stricter building codes may be beneficial in areas with a high annual tornado risk, such as Tornado Alley.

The final portion of this work used a simplified property loss model applied to the April 25-28, 2011 tornado outbreak. This was one of the largest tornado outbreaks in U.S. history and resulted in over \$5B in property loss. In order to determine property loss over a broad area, census data regarding household income and home market value was utilized. The performance of manufactured homes had to be considered in conjunction with wood-frame residential construction since the tornado outbreak impacted the southern U.S. which has a high number of manufactured homes. Using the system level fragility analysis, property loss was estimated based on both locally adopted residential codes and the stricter guidelines described in the Florida Residential Building Code. Results indicate that using strengthened construction methodologies would reduce property loss up to 40% as compared to current design guidelines.

ACKNOWLEDGEMENTS

First I would like to express my deepest gratitude to my advisor, Dr. John van de Lindt for seeing the potential of multidisciplinary work. His patience and understanding throughout my time as his student are greatly appreciated. He provided substantial guidance and motivation that pushed me outside my comfort zone so that I could successfully transition into the field of structural engineering. I would also like to thank and recognize my committee members Dr. Bruce Ellingwood, Dr. Paul Heyliger, and Dr. Russ Schumacher for providing me with additional support, ideas, and valuable critique. Additionally, I'd like to thank the Civil Engineering faculty members at Colorado State University and the University of Alabama.

I would also like to thank the University of Alabama Graduate Council Fellowship Office and acknowledge the financial support of Colorado State University and the George T. Abell Professorship funds.

Finally, I'd like to thank the many people who supported me during my graduate care. I am especially grateful to my colleagues Omar Amini, Eric Holt, Hassan Masoomi, Elaina Sutley, Negar Nazari, and countless others for their invaluable assistance and patience. In addition, I'd like to thank my dad and siblings for providing the encouragement necessary for completing my graduate career. Lastly, I'd like to thank my husband Joel for his patience and support.

TABLE OF CONTENTS

ABSTRACT	ii
ACKNOWLEDGEMENTS	iv
LIST OF TABLES	viii
LIST OF FIGURES	xi
INTRODUCTION AND MOTIVATION	1
1.1 Statement of Problem.....	1
1.2 Impact of Tornadoes on Woodframe Residential Structures	3
1.3 Framework of the Solution	9
1.4 Limitations of the Study	11
TORNADO HAZARD ESTIMATION	16
2.1 Historical Evaluations of Tornado Risk.....	16
2.2 Description of Data	17
2.3 Methodology.....	23
2.3.1 Obtaining Tornado Area	23
2.3.2 Obtaining Wind Speed Probabilities from a Weibull Distribution.....	24
2.3.3 The Gradient Technique for Reduced Area	27
2.4 Annual Tornado Probability Estimation	35
2.5 Determining the Annual Tornado Hazard at a Location.....	40
2.6 Results of Probabilistic Tornado Hazard Analysis	43
2.7 Development of Tornado Hazard Curves	48
2.8 Uncertainty in the Tornado Hazard Analysis	49
FRAGILITY ANALYSIS	58
3.1 Introduction to Fragility Analysis.....	58
3.2 Sample Locations.....	65
3.3 Uncertainty in Tornado Wind Loads	67
3.4 Wind Load Statistics.....	70
3.5 Dead Load and Resistance Statistics	77
3.5.1 Roof Sheathing Connection	77
3.5.2 Roof-to-Wall Connection.....	80

3.5.3 Wall-to-Foundation Connection	82
3.6 Results of the Fragility Analysis.....	93
3.6.1 Roof Sheathing Results.....	94
3.6.2 Roof-to-Wall Connection Results.....	101
3.6.3 Wall-to-Foundation Connection Results.....	108
3.7 System Level Analysis.....	115
3.7.1 Introduction to Positive Quadrant Dependence	116
3.7.2 Fragility Curves	122
3.8 Summary	128
CONVOLUTION OF FRAGILITY AND TORNADO HAZARD CURVES.....	130
4.1 Introduction to Convolution Analysis.....	130
4.2 Roof Sheathing	132
4.3 Roof-to-Wall Connection	141
4.4 Wall-to-Foundation.....	144
4.5 System Level Analysis.....	147
4.6 Summary	152
PROPERTY LOSS ESTIMATION FOR THE APRIL 25-28, 2011 TORNADO OUTBREAK.....	155
5.1 Summary of the April 25-28, 2011 Tornado Outbreak	155
5.1.1 Subset used for Analysis	160
5.2 Loss Estimation.....	162
5.2.1 Building Code Assignment	162
5.2.2 Manufactured Homes.....	164
5.2.3 Number of Homes Impacted.....	168
5.2.4 Archetype Assignment.....	171
5.2.5 Determining Real Market Value of Impacted Homes	172
5.2.6 Determining Failure Probability	172
5.2.7 Property Loss Estimation	181
5.3 Comparison of Standard versus Strengthened Construction	183
5.4 Conclusions.....	186
ANTICIPATED CONTRIBUTIONS TO THE PROFESSION.....	188
6.1 Tornado Hazard Curves	188
6.2 Unconditional Failure Methodology for Tornadoes	188

6.3 Positive Quadrant Dependence for Wood-frame Residential Structures.....	189
6.4 Property Loss Estimation.....	189
MITIGATION STRATEGY AND CONCLUSIONS.....	191
7.1 Mitigation Strategy	191
7.1.1 Historical Approach to Residential Design against Tornadoes	191
7.1.2 Distribution of Tornado Winds.....	192
7.1.3 Adoption and Enforcement of Residential Building Codes.....	193
7.1.4 Routine Maintenance	195
7.1.5 Improved Connections	195
7.1.6 Additional Measures	198
7.1.7 Adoption of High Wind Provisions in Tornado Alley.....	199
7.2 Summary.....	200
7.3 Conclusions.....	204
7.4 Recommendations for Future Work	206
REFERENCES.....	208
GC_p VALUES FOR EACH STRUCTURAL ARCHETYPE.....	221
LOGARITHMIC PARAMETERS FOR THE ROOF SHEATHING FRAGILITY CURVES	228
LOGARITHMIC PARAMETERS FOR THE ROOF-TO-WALL FRAGILITY CURVES	231
LOGARITHMIC PARAMETERS FOR THE WALL-TO-FOUNDATION FRAGILITY CURVES	234
LOGARITHMIC PARAMETERS FOR THE SYSTEM LEVEL (VERTICAL LOAD PATH) FRAGILITY CURVES.....	237
SYSTEM LEVEL FRAGILITY CURVES FOR AN EAST-WEST ORIENTED WIND. 240	
PROPERTY LOSS ESTIMATES FOR INDIVIDUAL TORNADOES	246
LIST OF ABBREVIATIONS AND SYMBOLS	248

LIST OF TABLES

Table 2.1: Comparison of the Fujita scale versus the Enhanced Fujita scale (modified from Wind Science and Engineering Research Center 2006)	20
Table 2.2: Damage indicators utilized in the Enhanced Fujita scale (modified from Wind Science and Engineering Research Center 2006)	21
Table 2.3: Degree of Damage for One- or Two-Family Residences	22
Table 2.4: Summary of the variation of intensity along the length of tornadoes from five surveyed tornado outbreak cases (modified from Schaefer <i>et al.</i> 1986).....	29
Table 2.5: Variation of intensity of the damage area for EF1-EF5 tornadoes presented as percentages of the total path length, width, and area (e.g. 4.1 represents that 4.1% of the tornado area is rated as EF5). The variation of width was obtained from the Tuscaloosa and Joplin tornadoes of 2011 and the variation of length was obtained from Schaefer <i>et al.</i> (1986).....	33
Table 2.6: Number of tornadoes per decade investigated	50
Table 3.1: Summary of the 6 select locations and the adopted building code	67
Table 3.2: Values for select wind load parameters	72
Table 3.3: Summary of K_z statistics for differing structure types.....	76
Table 3.4: Summary of GC_p Values for Uplift and Wall Racking.....	77
Table 3.5: Roof sheathing statistics for panel uplift resistance based on local residential building code	78
Table 3.6: Roof sheathing statistics for panel dead load based on local residential building code	79
Table 3.7: Roof-to-wall uplift resistance statistics based on local residential building code	80
Table 3.8: Summary of Wall Types and Loading Protocol.....	87
Table 3.9: Resistance Statistics for the Wall-to-Foundation Connection	92
Table 3.10: Summary of Dead Load Statistics for the Wall-to-Foundation Connection Analysis.....	93
Table 3.11: Event Tree Component Details	118
Table 4.1: Upper Bound Roof Sheathing System 50 year failure probabilities for Tornado Alley.....	134
Table 4.2: Lower Bound Roof Sheathing System 50 year failure probabilities for Tornado Alley.....	135
Table 4.3: Upper Bound Roof Sheathing System 50 year failure probabilities for Dixie Alley.....	136

Table 4.4: Lower Bound Roof Sheathing System 50 year failure probabilities for Dixie Alley.....	136
Table 4.5: Upper Bound Roof Sheathing System 50 year failure probabilities for the Midwest.....	137
Table 4.6: Lower Bound Roof Sheathing System 50 year failure probabilities for the Midwest.....	138
Table 4.7: Upper Bound Roof Sheathing System 50 year failure probabilities for the High Plains.....	139
Table 4.8: Lower Bound Roof Sheathing System 50 year failure probabilities for the High Plains.....	139
Table 4.9: Upper Bound Roof Sheathing System 50 year failure probabilities for the Northwest.....	139
Table 4.10: Lower Bound Roof Sheathing System 50 year failure probabilities for the Northwest.....	140
Table 4.11: Upper Bound Roof Sheathing System 50 year failure probabilities for the Florida Peninsula.....	140
Table 4.12: Lower Bound Roof Sheathing System 50 year failure probabilities for the Florida Peninsula.....	141
Table 4.13: Upper Bound Roof-to-wall connection 50 year failure probabilities for the six sample locations.....	142
Table 4.14: Lower Bound Roof-to-wall connection 50 year failure probabilities for the six sample locations.....	143
Table 4.15: Wall-to-foundation 50 year failure probabilities for Tornado Alley	145
Table 4.16: Wall-to-foundation 50 year failure probabilities for Dixie Alley	145
Table 4.17: Wall-to-foundation 50 year failure probabilities for the Midwest.....	146
Table 4.18: Wall-to-foundation 50 year failure probabilities for the High Plains	146
Table 4.19: Wall-to-foundation 50 year failure probabilities for the Northwest	146
Table 4.20: Wall-to-foundation 50 year failure probabilities for the Florida Peninsula.....	147
Table 4.21: System Level 50-year Failure Probabilities for Tornado Alley.....	148
Table 4.22: System Level 50-year Failure Probabilities for Dixie Alley.....	148
Table 4.23: System Level 50-year Failure Probabilities for the Midwest	149
Table 4.24: System Level 50-year Failure Probabilities for the High Plains.....	149
Table 4.25: System Level 50-year Failure Probabilities for the Northwest.....	150
Table 4.26: System Level 50-year Failure Probabilities for the Florida Peninsula	150
Table 5.1: Number of Tornadoes Reported per State.....	157
Table 5.2: Number of Tornadoes for each EF Intensity.....	157

Figure 5.3: Number of Tornadoes with over \$1M in Property Loss per State	162
Figure 5.4: Locally Adopted Building Code and Assigned Fragility	163
Figure 5.5: Income and Archetype Assignment.....	171
Figure 5.6: Sample Housing Matrix.....	173
Figure 5.7: Logarithmic Parameters for Hurricane Fragility Curves.....	176
Figure 5.8: Logarithmic Parameters for Tornado Fragility Curves	179
Figure 5.9: Sample Estimate of Property Loss from Tornadoes.....	183
Figure 5.10: Loss Estimation for the April 25-28, 2011 Tornado Outbreak	184

LIST OF FIGURES

Figure 1.1: All reported tornado paths from 1973-2011	2
Figure 1.2: Failure of roof sheathing during the May 20, 2013 Moore, OK tornado. The remainder of the home performed well.....	4
Figure 1.3: Toe-nail connection at the roof-to-wall interface.....	5
Figure 1.4: Failure of the roof-to-wall connection at a home during the May 20, 2013 Moore, OK tornado.....	6
Figure 1.5: Two homes moved off their foundation due to inadequate wall-to-foundation connections during the April 28, 2014 Flintville, TN tornado	7
Figure 1.6: Overturning failure of a residential structure during the April 27, 2011 tornado in Tuscaloosa, AL	8
Figure 1.7: Failure of the wall-to-foundation connection due to wall stud pull out. Note the bottom plate is still attached to the foundation and the nails to the wall studs remain in place	8
Figure 1.8: Effect of increasing swirl ratio, S , on tornadic vortex flows. (a) Very weak swirl flow in boundary layer results in no tornado formation; (b) Low S is a smooth-flowing one-cell weak tornado; (c) Moderate S results in a tornado with vortex break down and a two-cell vortex aloft; (d) Slightly higher S results in a vortex break down stagnation point near the ground surface; (e) Turbulent two-cell tornado with the central downdraft impinging on the surface; (f) Large S and the tornado ‘splits’ into multiple vortices.....	12
Figure 2.1: Locations of the 6 test regions. These locations were chosen based on the varying degrees of tornado activity that each represent.....	25
Figure 2.2: Simulated wind speeds and fitted Weibull distribution with $1^\circ \times 1^\circ$ resolution for the test regions of (a.) Tornado Alley, (b.) Dixie Alley, (c.) the Midwest, (d.) the High Plains, (e.) the extreme Northwest U.S., and (f.) the Florida Peninsula. Simulated wind speeds are based on tornado reports at each location over the 38 year period. Dashed lines indicate the boundary between EF categories	26
Figure 2.3: Sample transect measurements for the Tuscaloosa tornado (Graettinger <i>et al.</i> 2012).....	31
Figure 2.4: Illustration of the variation of tornado intensity along its path used in this study (See Table 2.4 for numerical values.....	34
Figure 2.5: Flow chart visualizing the process to determine the annual tornado hazard at a location.....	37
Figure 2.6: Probabilistic tornado hazard index for (a.) EF0- (f.) EF5. The hazard is labeled as the power of ten per year	42
Figure 2.7: Reported tornado paths plotted for (a.) EF0-(f.) EF5 based on tornado reports from 1973-2011	44

Figure 2.8: Hazard curves for each of the 6 locations investigated. Values below 10^{-10} are not shown	49
Figure 2.9: Tornado hazard curve and 95% confidence intervals for Tornado Alley. The hazard curve is generated from the probabilistic tornado hazard maps while the upper and lower confidence intervals were obtained from bootstrap resampling	51
Figure 2.10: Tornado hazard curve and 95% confidence intervals for Dixie Alley. The hazard curve is generated from the probabilistic tornado hazard maps while the upper and lower confidence intervals were obtained from bootstrap resampling	52
Figure 2.11: Tornado hazard curve and 95% confidence intervals for the Midwest. The hazard curve is generated from the probabilistic tornado hazard maps while the upper and lower confidence intervals were obtained from bootstrap resampling	53
Figure 2.12: Tornado hazard curve and 95% confidence intervals for the High Plains. The hazard curve is generated from the probabilistic tornado hazard maps while the upper and lower confidence intervals were obtained from bootstrap resampling	54
Figure 2.13: Tornado hazard curve and 95% confidence intervals for the Florida Peninsula. The hazard curve is generated from the probabilistic tornado hazard maps while the upper and lower confidence intervals were obtained from bootstrap resampling	55
Figure 2.14: Tornado hazard curve and 95% confidence intervals for the Northwest. The hazard curve is generated from the probabilistic tornado hazard maps while the upper and lower confidence intervals were obtained from bootstrap resampling	56
Figure 3.1: Structure Type 1 taken from Amini and van de Lindt (2014). Dimensions are shown in meters	59
Figure 3.2: Structure Type 2 taken from Amini and van de Lindt (2014). Dimensions are shown in meters	60
Figure 3.3: Structure Type 3 taken from Amini and van de Lindt (2014). Dimensions are shown in meters	61
Figure 3.4: Structure Type 4 taken from Amini and van de Lindt (2014). Dimensions are shown in meters	62
Figure 3.5: Structure Type 5 taken from Amini and van de Lindt (2014). Dimensions are shown in meters	63
Figure 3.6: Cities and regions investigated in this research (Standohar-Alfano and van de Lindt 2015)	66
Figure 3.7: Location of roof wind zones for a.) ASCE 7-10 and b.) ASCE 7-16. The left hand side is for gable roofs while the right hand side shows hip roofs (ASCE 2010, Vickery 2015) ...	74
Figure 3.8: Simpson Strong-Tie H2.5 reinforcing clip connecting the roof rafter to a double top plate (Simpson Strong-Tie 2015).....	81
Figure 3.9: Design of the wood shear walls used in this study (wall sheathing not shown)	85
Figure 3.10: Simpson Strong-Tie RSP4 stud plate tie used as reinforcement for Wall Types C and D (Simpson Strong-Tie 2014).....	86

Figure 3.11: Experimental set-up for the combined shear and uplift test	88
Figure 3.12: Commonly observed failure with Wall Types A and B due to nail withdrawal	90
Figure 3.13: Commonly observed failure with Wall Types C and D due to the wood splitting around the anchor bolt	90
Figure 3.14: Interaction curves for Wall Types A-D. The top figure is in klf and the bottom figure is in kN/m	91
Figure 3.15: Roof system fragility curves for Structure Type 1 where a.) is the upper bound performance estimated using ASCE 7-10 and K_c and b.) is the lower bound performance found using ASCE 7-16 wind provisions without any tornado amplification. The improved performance of the Florida Residential Building Code is evident by the rightward shift of the curves	96
Figure 3.16: Roof system fragility curves for Structure Type 2 where a.) is the upper bound performance estimated using ASCE 7-10 and K_c and b.) is the lower bound performance found using ASCE 7-16 wind provisions without any tornado amplification. The improved performance of the Florida Residential Building Code is evident by the rightward shift of the curves	97
Figure 3.17: Roof system fragility curves for Structure Type 3 where a.) is the upper bound performance estimated using ASCE 7-10 and K_c and b.) is the lower bound performance found using ASCE 7-16 wind provisions without any tornado amplification. The improved performance of the Florida Residential Building Code is evident by the rightward shift of the curves	98
Figure 3.18: Roof system fragility curves for Structure Type 4 where a.) is the upper bound performance estimated using ASCE 7-10 and K_c and b.) is the lower bound performance found using ASCE 7-16 wind provisions without any tornado amplification. The improved performance of the Florida Residential Building Code is evident by the rightward shift of the curves	99
Figure 3.19: Roof system fragility curves for Structure Type 5 where a.) is the upper bound performance estimated using ASCE 7-10 and K_c and b.) is the lower bound performance found using ASCE 7-16 wind provisions without any tornado amplification. The improved performance of the Florida Residential Building Code is evident by the rightward shift of the curves	100
Figure 3.20: Fragility curves for Structure Type 1 for individual roof-to-wall connections prescribed by local residential building codes where a.) is the upper bound performance estimated using ASCE 7-10 and K_c and b.) is the lower bound performance found using ASCE 7-16 wind provisions without any tornado amplification	103
Figure 3.21: Fragility curves for Structure Type 2 for individual roof-to-wall connections prescribed by local residential building codes where a.) is the upper bound performance estimated using ASCE 7-10 and K_c and b.) is the lower bound performance found using ASCE 7-16 wind provisions without any tornado amplification	104
Figure 3.22: Fragility curves for Structure Type 3 for individual roof-to-wall connections prescribed by local residential building codes where a.) is the upper bound performance	

estimated using ASCE 7-10 and K_c and b.) is the lower bound performance found using ASCE 7-16 wind provisions without any tornado amplification105

Figure 3.23: Fragility curves for Structure Type 4 for individual roof-to-wall connections prescribed by local residential building codes where a.) is the upper bound performance estimated using ASCE 7-10 and K_c and b.) is the lower bound performance found using ASCE 7-16 wind provisions without any tornado amplification106

Figure 3.24: Fragility curves for Structure Type 5 for individual roof-to-wall connections prescribed by local residential building codes where a.) is the upper bound performance estimated using ASCE 7-10 and K_c and b.) is the lower bound performance found using ASCE 7-16 wind provisions without any tornado amplification107

Figure 3.25: Fragility curves for Structure Type 1 for the wall-to-foundation where a.) is the upper bound performance estimated using ASCE 7-10 and K_c and b.) is the lower bound performance found using ASCE 7-16 wind provisions without any tornado amplification. It is evident that the inclusion of reinforcing ties did not drastically improve wall performance by comparing the curves for A and C for each wind direction110

Figure 3.26: Fragility curves for Structure Type 2 for the wall-to-foundation where a.) is the upper bound performance estimated using ASCE 7-10 and K_c and b.) is the lower bound performance found using ASCE 7-16 wind provisions without any tornado amplification. It is evident that the inclusion of reinforcing ties did not drastically improve wall performance by comparing the curves for A and C for each wind direction111

Figure 3.27: Fragility curves for Structure Type 3 for the wall-to-foundation where a.) is the upper bound performance estimated using ASCE 7-10 and K_c and b.) is the lower bound performance found using ASCE 7-16 wind provisions without any tornado amplification. It is evident that the inclusion of reinforcing ties did not drastically improve wall performance by comparing the curves for A and C for each wind direction112

Figure 3.28: Fragility curves for Structure Type 4 for the wall-to-foundation where a.) is the upper bound performance estimated using ASCE 7-10 and K_c and b.) is the lower bound performance found using ASCE 7-16 wind provisions without any tornado amplification. It is evident that the inclusion of reinforcing ties did not drastically improve wall performance by comparing the curves for A and C for each wind direction113

Figure 3.29: Fragility curves for Structure Type 5 for the wall-to-foundation where a.) is the upper bound performance estimated using ASCE 7-10 and K_c and b.) is the lower bound performance found using ASCE 7-16 wind provisions without any tornado amplification. It is evident that the inclusion of reinforcing ties did not drastically improve wall performance by comparing the curves for A and C for each wind direction114

Figure 3.30: Event tree utilized for the system level performance117

Figure 3.31: System level fragility curves for Structure Type 1 a.) is the upper bound performance estimated using ASCE 7-10 and K_c and b.) is the lower bound performance found using ASCE 7-16 wind provisions without any tornado amplification123

Figure 3.32: System level fragility curves for Structure Type 2 a.) is the upper bound performance estimated using ASCE 7-10 and K_c and b.) is the lower bound performance found using ASCE 7-16 wind provisions without any tornado amplification124

Figure 3.33: System level fragility curves for Structure Type 3 a.) is the upper bound performance estimated using ASCE 7-10 and K_c and b.) is the lower bound performance found using ASCE 7-16 wind provisions without any tornado amplification125

Figure 3.34: System level fragility curves for Structure Type 4 a.) is the upper bound performance estimated using ASCE 7-10 and K_c and b.) is the lower bound performance found using ASCE 7-16 wind provisions without any tornado amplification126

Figure 3.35: System level fragility curves for Structure Type 5 a.) is the upper bound performance estimated using ASCE 7-10 and K_c and b.) is the lower bound performance found using ASCE 7-16 wind provisions without any tornado amplification127

Figure 5.1: Map of all the reported tornadoes from the April 25-28, 2011 outbreak156

Figure 5.2: Image of ground (top) and road (bottom) scouring from the Philadelphia-Kemper, MS EF5 tornado. Image courtesy of the Jackson, MS NWS Office (NWS JAN 2011).....159

Figure 5.3: Map of all the reported tornadoes from the April 25-28, 2011 outbreak which caused over \$1M in property damage.....161

Figure 5.4: Basic wind zone map for manufactured homes. Image courtesy of the Manufactured Housing Institute (MHI 2016)165

Figure 5.5: Catastrophic damage to a manufactured home from an EF2 tornado in Perry County, Alabama. Tie-downs are indicated in the black circles167

Figure 5.6: Fragility curves for manufactured homes where a.) is the upper bound performance estimated using ASCE 7-10 and K_c and b.) is the lower bound performance found using ASCE 7-16 wind provisions without any tornado amplification180

CHAPTER 1

INTRODUCTION AND MOTIVATION

1.1 Statement of Problem

Tornadoes are one of the most damaging natural disasters in the United States on a local scale. They are relatively rare, localized events, but can have a high impact on communities that receive a direct hit. While tornadoes are, in theory, a worldwide occurrence, the overwhelming majority occur in the United States (Goliger and Milford 1998), specifically the region contained between the Rocky and Appalachian Mountains, especially in the areas defined as Tornado Alley and Dixie Alley. According to the American Meteorological Society, Tornado Alley is the region of the central U.S. with a north-south orientation containing Texas, Oklahoma, Kansas, and Nebraska, where tornadoes are most frequent. Similarly, Alabama, Mississippi, Tennessee, and Arkansas are commonly referred to as “Dixie Alley” due to frequent tornado occurrence (Dixon *et al.* 2011). According to the Storm Prediction Center (SPC), approximately 800-1,400 tornadoes strike the United States annually (Ashley 2007). Figure 1.1 illustrates all reported tornado paths in the U.S. from 1973 to 2011. This clearly shows the high density of tornadoes that impact the central and southeastern portions of the U.S., although as one can see from Figure 1.1, tornadoes have been reported in all 48 contiguous states since systematic tornado reporting began.

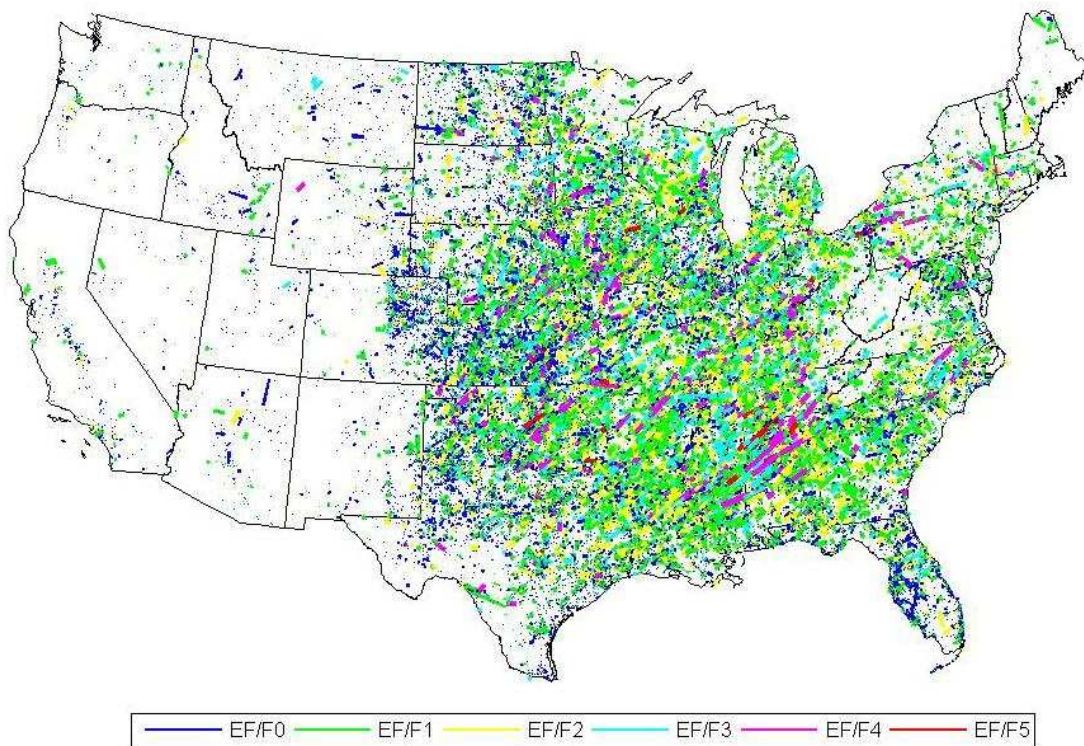


Figure 1.1: All reported tornado paths from 1973-2011.

While there is a broad area of tornado occurrence across the United States, the probability of a tornado hitting one particular city or structure in any given year is quite low. This is due to the fact that while tornadoes occur frequently across the central U.S., an individual tornado itself is typically rather short lived, spanning only a few kilometers in length and is often less than 100 meters (328 feet) wide. The majority of tornadoes have a very short lifetime, and only a small percentage actually cause serious structural damage, injuries, or even death. That being said, it is still critical to understand the climatology of severe weather at a particular location, especially tornadoes, since they have a high potential to be life threatening when they do correspond to populous locations. From 1973-2011, there have been almost 4,000 deaths and 68,000 injuries reported from tornadoes. While improvements in technology have drastically reduced the

number of injuries and fatalities due to increased warning time, the extreme 2011 season serves as a reminder of the destructive and deadly potential of tornadoes.

1.2 Impact of Tornadoes on Woodframe Residential Structures

When strong tornadoes impact densely populated locations, as recently observed in Tuscaloosa, AL, Joplin, MO, and Moore, OK, catastrophic damage can occur, especially to wood-frame structures (Minor *et al.* 1977, Marshall 2002, Prevatt *et al.* 2011a, 2011b, 2012b). Wood-frame construction has been observed to perform poorly under tornado wind loads, even in weak to moderate tornadoes (Jordan 2007). There are several failure modes commonly observed in tornadoes. These include translation, overturning, racking, and/or material or component failure (Jordan 2007). Material/component failure is the most common failure mode seen in the aftermath of a tornado and includes failure of the roof sheathing, roof-to-wall, and/or wall-to-foundation connections.

Often portions of a roof or the complete roof will fail first (Mehta *et al.* 1976, Conner *et al.* 1987, Pan *et al.* 2002, Jordan 2007, Chowdhury *et al.* 2012). In some cases, the structure may lose its entire roof while the remaining portion of the home performs relatively well. This is due to the significant uplift forces imparted on the structure as strong winds from the tornado move over the roof (Mehta *et al.* 1976). High winds from a tornado induce uplift in two ways. These include the aerodynamic lift from wind passage over a sloped roof, similar to an airplane wing, and the strong uplift from the tornado suction itself. Commonly observed roof damage is the result of failure of either the roof sheathing and/or roof-to-wall connection. Figure 1.2 illustrates a home that lost a portion of the roof sheathing in the Moore, OK tornado on May 20, 2013. As is evident in the figure, the home lost a significant portion of the roof sheathing while the remainder of the house performed relatively well. Property loss due to rain water intrusion is

a large source of insured losses from tornadoes and could be prevented if the roof sheathing had performed better (Lee and Rosowsky 2005, Dao and van de Lindt 2012, van de Lindt and Dao 2012).



Figure 1.2: Failure of roof sheathing during the May 20, 2013 Moore, OK tornado. The remainder of the home performed well.

Another common material/component failure observed after tornadoes is the failure of the roof-to-wall connection. This is the connection at the intersection of the roof joists and wall top plate. The roof is commonly attached to the wall with a toe-nail connection which involves 2-3 nails driven at an angle as shown in Figure 1.3. While this connection performs well with gravity loads, it does not provide significant resistance to uplift forces.

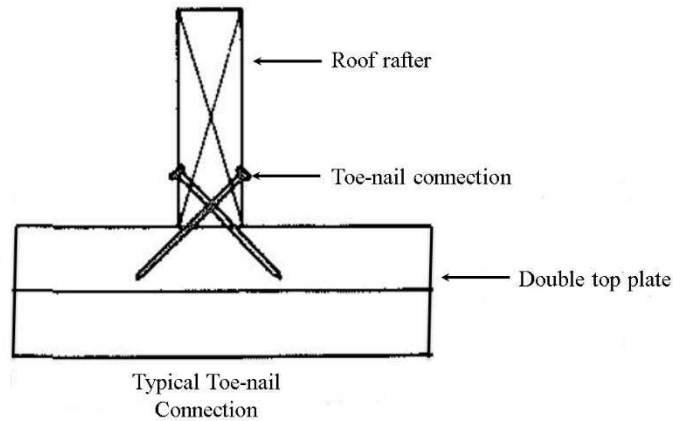


Figure 1.3: Toe-nail connection at the roof-to-wall interface.

Due to the common practice of using a toe-nail connection, failure of the roof-to-wall connection is often observed in the aftermath of tornadoes as shown in Figure 1.4. This particular structure was investigated after the May 20, 2013 tornado that struck Moore, OK. The majority of the house performed well. The door and windows remained intact and were not broken. In addition, hanging plants remained in place after the tornado. However, the house experienced complete removal of the roof system and as a result was uninhabitable and required major rehabilitation or demolition.



Figure 1.4: Failure of the roof-to-wall connection at a home during the May 20, 2013 Moore, OK tornado.

In addition to failure of either the roof sheathing or roof-to-wall connections, inadequate wall-to-foundation connections can result in translation or overturning of a residential structure as shown in Figures 1.5 and 1.6. The wall-to-foundation connection typically utilizes anchor bolts that connect the bottom plate of the wall to the concrete slab or masonry foundation. Improper construction is often attributed to wall-to-foundation failures in that anchor bolts are missing, improperly spaced, or are missing the nut or washer. In some cases, nails are used instead of anchor bolts. In addition, pull out of the wall studs from the bottom plate is commonly observed in the aftermath of tornadoes even when the anchor bolts perform adequately. Failure of the wall-to-foundation connection can occur in moderate wind speeds, and in some cases the majority of the home will perform relatively well as observed in Figure 1.5. The two homes were swept off their foundations but retained structural integrity with some roof sheathing failures. Unfortunately, due to inadequate wall-to-foundation anchorage, the occupants will need

to completely rebuild. In addition, Figure 1.7 illustrates failure of the wall-to-foundation connection due to wall stud pull out from the bottom plate. This represents a weak point along the vertical load path since the wind load was unable to be successfully transferred to the foundation.



Figure 1.5: Two homes translated off their foundation due to inadequate wall-to-foundation connections during the April 28, 2014 Flintville, TN tornado (courtesy of SellersPhoto 2014).



Figure 1.6: Overturning failure of a residential structure during the April 27, 2011 tornado in Tuscaloosa, AL.



Figure 1.7: Failure of the wall-to-foundation connection due to wall stud pull-out. Note the bottom plate is still attached to the foundation and the nails to the wall studs remain in place.

The structural failures described above can be prevented in low to moderate tornado winds by improving the components along the vertical load path (Mehta *et al.* 1976). While the number of injuries and fatalities from tornadoes has dropped in the past decades, the cost of

damage has continued to rise (Prevatt *et al.* 2011b, Amini and van de Lindt 2014). According to Changnon (2009), the annual average loss due to tornadoes is \$982 million dollars. Due to the low probability of occurrence, modern engineering design codes have not included tornado design provisions, yet light frame wood construction is some of the most vulnerable structures from high wind events. This type of construction comprises about 90% of the housing in the United States and is the single largest asset for most individuals (Ellingwood *et al.* 2004).

Due to the large societal and economic disruptions from recent tornado events, there is increased interest in understanding the performance of wood frame construction subjected to tornado wind loads. Current pressure coefficients are insufficient to account for the strong uplift loads experienced by a roof during a tornado. The lack of tornado design provisions in residential construction is due in part to the low probability of occurrence of tornadoes (Twisdale and Dunn 1983, van de Lindt *et al.* 2013). More specifically, it is highly improbable for a given community or individual home to be struck by a tornado in a year as discussed in more detail below. However, due to the high impact of violent tornadoes in urban settings, there is an increased push to understand the improvement in structural performance of residential structures subjected to tornado wind loads (Prevatt *et al.* 2011a, 2011b, 2012b). Thus the work presented in this dissertation details a methodology to quantify the impact of tornado provisions in the residential design code across the United States in order to assess the feasibility of implementing stricter building codes in high risk areas.

1.3 Framework of the Solution

When trying to determine the practicality of a tornado design provision, the tornado occurrence rate had to first be quantified. In order to estimate an annual probabilistic tornado hazard for the contiguous United States, the climatology of reported tornadoes from 1973-2011

was used. This dataset included the tornado intensity, location, path length, path width, and property loss. In order to quantify the hazard, the methodology proposed by Schaefer *et al.* (1986) was used but modified to account for the variation of intensity along the tornado path length and width. Maps of the estimated tornado hazard were created for tornado wind speeds of each tornado intensity on the Enhanced Fujita scale. With the maps, a tornado hazard curve at any location could be developed. A detailed summary of the calculation of the tornado hazard is described in Chapter 2.

Once hazard curves were generated, fragility analysis was used to determine structural performance. This was done for the three major components along the vertical load path: the roof sheathing, roof-to-wall, and wall-to-foundation connections. Five structural archetypes were selected to represent commonly observed residential construction. These archetypes were applied to six different geographic locations across the country with varying tornado activity and fragility analysis was performed. At each respective location, the five structural archetypes were designed based on the residential building codes current at the time of this work. In addition, each structural archetype was designed with the Florida state residential building code to represent strengthened construction. This is discussed in more detail in Chapter 3.

The fragility analysis briefly discussed above presents a conditional failure probability. Thus, this represents the probability of failure assuming the structure is subjected to tornado winds. In order to understand the unconditional failure probabilities for each connection, the fragility curves and tornado hazard curves had to be convolved. The unconditional failure probabilities obtained from convolution were calculated over a 50 year period consistent with the service life used in ASCE 7-10 wind provisions. More information on the convolution analysis can be found in Chapter 4. Structural performance using strengthened construction was

investigated for the historic April 2011 tornado outbreak. This is described in Chapter 5. Remaining chapters include anticipated contributions to the profession, a mitigation strategy, and conclusion.

1.4 Limitations of the Study

While the work described in this dissertation details a methodology to assess tornado failure probabilities, there are some issues which must be considered when interpreting results. The first limitation involves the nature of the tornado rating. Currently, tornado intensity is based on damage and not on wind speed. It is difficult to obtain in situ tornado wind speeds since that would require meteorological instruments to be placed directly in the tornado damage path. Developments in Doppler radar have allowed for remotely sensed wind speed measurements, but these have occurred at heights ranging from 30 – 1000 m (100 – 3280 ft) above the surface (Wurman *et al.* 2013). This presents two issues when trying to determine wind speeds at the surface. The first is that the vertical wind profile within a tornado is not known and varies based on the individual tornado swirl ratio, defined as the ratio of the vortex circulation to the rate of inflow. As the swirl ratio varies, the vortex structure changes (Davies-Jones *et al.* 2001) as illustrated in Figure 1.8 which indicates the varying vertical wind profiles for different swirl ratios. With each varying wind profile, the surface ground motion is different and thus it is difficult to ascertain ground wind speeds from measurements made at any height above ground level. This is an area of continued research in the meteorological community.

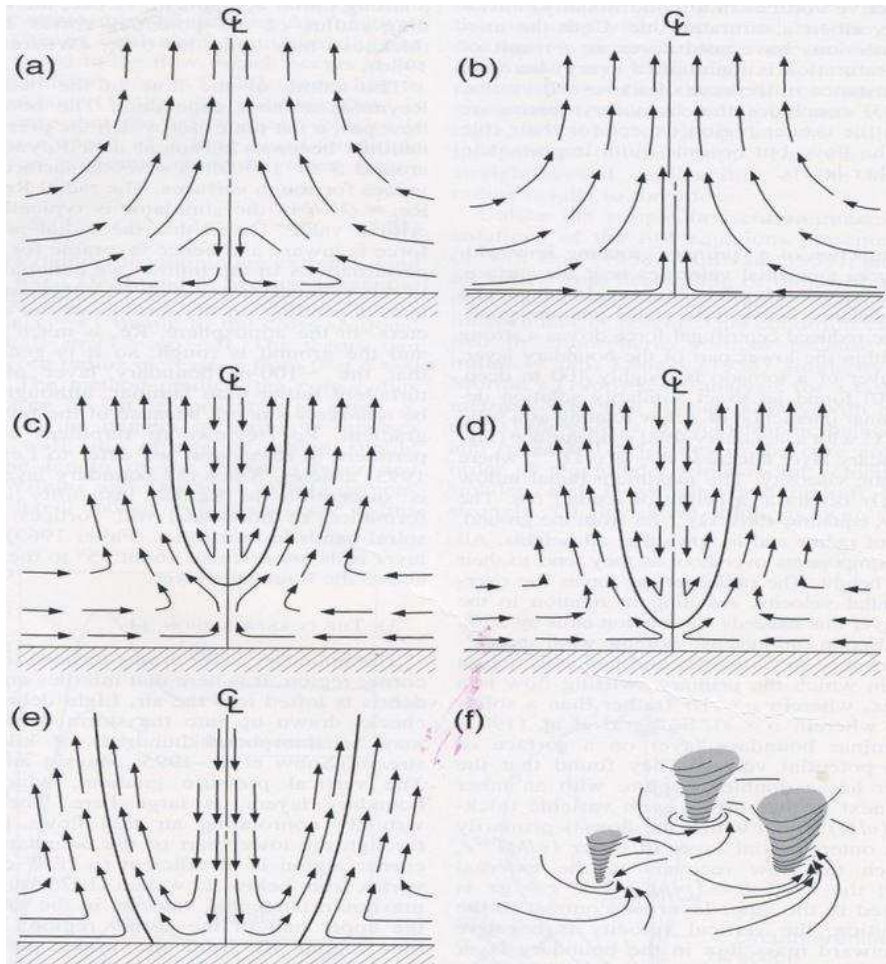


Figure 1.8: Effect of increasing swirl ratio, S , on tornadic vortex flows. (a) Very weak swirl flow in boundary layer results in no tornado formation; (b) Low S is a smooth-flowing one-cell weak tornado; (c) Moderate S results in a tornado with vortex break down and a two-cell vortex aloft; (d) Slightly higher S results in a vortex break down stagnation point near the ground surface; (e) Turbulent two-cell tornado with the central downdraft impinging on the surface; (f) Large S and the tornado ‘splits’ into multiple vortices (Davies-Jones *et al.* 2001).

In addition, in order to properly verify Doppler radar measurements, in situ wind speed measurements are necessary. Overall, since obtaining direct tornado wind speeds is problematic, the current scale used for rating tornado intensity is based on tornado damage and not wind speed and is referred to as the Enhanced Fujita (EF) scale.

The EF scale was created after collaboration with various engineering and meteorological entities (Wind Science and Engineering Research Center 2006). It was developed to try to standardize tornado rating within the multiple National Weather Service offices across the country. This was done by including several damage indicators. These are described as man-made or natural bodies that can be damaged from a tornado. Each damage indicator has several degrees of damage which qualitatively assesses the degree of damage observed and provides an associated wind speed. The included wind speed is based on damaged states observed and the quality of construction. While it was an improvement on the previous Fujita scale, there are some concerns about the subjective nature of the current tornado rating methodology. However, since a standardized method for obtaining direct tornado wind speed has not been implemented, the EF scale is currently the best method for rating tornado intensity and will be used in this work.

For determination of the empirically-based probabilistic tornado hazard maps, a record of all reported tornadoes from 1973-2011 was used. Tornado reports prior to 1973 were not used due to issues with inconsistent tornado reporting prior to the implementation of the Fujita scale. The tornado data set prior to 1973 is plagued with issues of under reporting due to lack of population in rural areas of the U.S. (Anderson *et al.* 2007). Improvements in technology (such as Doppler radar), the popularity of storm chasing, and the increase in population (Brooks *et al.* 2003) have reduced the likelihood of missing tornadoes since 1973 (Reinhold and Ellingwood 1982). However, while there may not be a reported tornado in some locations, that does not guarantee that no tornado has touched down in a particular location. In addition, while all reported tornadoes were included in the data set, some individual tornado reports are lacking

information on intensity, length, width, etc. These tornadoes could not be used in the tornado hazard estimation.

The tornado dataset utilized in this work included information pertaining to path length and width but was limited in the amount of detail each report included, specifically, information about the variation of intensity along the tornado path length and width is typically not obtained in post-tornado investigations. However, it has long been observed that tornado strength is commonly highest at its center and reduces along its width transversely away from the center of the path (see e.g. Reinhold and Ellingwood 1982). Similarly, maximum damage commonly occurs at the center of tornado path length and is weakest at touch down and lift up. In order to account for this variability in intensity, damage analyses from Tuscaloosa, AL and Joplin, MO 2011 tornadoes were used. These datasets included a high degree of detail along the tornado path width. Historical data from the 1974 Super Outbreak was used for variation of intensity along the tornado path length. Using statistics from these tornado outbreaks allowed for an estimation of the typical gradient of intensity along both the tornado path length and width. Thus, the gradients used in this work were based on a limited sample of reported tornadoes. Ideally, the gradation of intensity along the path length and width would be obtained for every tornado. This would provide a better understanding of the variation of tornado intensity for each EF intensity. However, since this was not feasible with the given data, the intensity variation used in this work was based on information from the 1974 and 2011 tornado outbreaks.

Finally, wind loading from straight line winds has been extensively studied and is currently used in design across the country (ASCE 2010). However, the impact of tornado wind loads has received less attention. For the fragility analysis discussed later, a tornado amplification factor was utilized as described by Haan *et al.* (2010). There has been some

discussion about the applicability of the Haan *et al.* (2010) work since the amplification factor would imply failure of structural components at wind speeds lower than expected from straight line winds. However, due to limited direct observations of tornado wind loads on low-rise structures, the work presented in this dissertation was bounded by two methodologies to estimate tornado wind loads. The first was defined as the upper bound and used the experimental results from Haan *et al.* (2010) in order to calculate tornado wind loads with an amplification due to the tornado vortex. The second method did not have any amplification of the wind load, essentially treating tornado wind loads as straight line winds. This was defined as the lower bound. It is hypothesized that wood-frame construction performance in tornadoes will be bounded by these two methodologies.

CHAPTER 2

TORNADO HAZARD ESTIMATION

2.1 Historical Evaluations of Tornado Risk

Significant work has been done on evaluating tornado risk (Reinhold and Ellingwood 1982, Schaefer *et al.* 1986, Hossain *et al.* 1999, Brooks *et al.* 2003, Ramsdell *et al.* 2005). The estimation of tornado hazard utilized in this dissertation is a combination of two earlier studies by Reinhold and Ellingwood (1982) and Schaefer *et al.* (1986). Reinhold and Ellingwood (1982) evaluated several models current at the time of their study for predicting tornadic wind speeds in order to develop a comprehensive model that combined tornado occurrence probabilities with tornado damage potential. Their work was motivated by the design of nuclear structures and evaluation of tornado risk across broad regions of the country. Ultimately, their goal was to create a unified model and determine an annual tornado probability. Their work considered the variation of intensity along a tornado path length and path width, as well as classification and random errors resulting from misclassification of a tornado's intensity.

Reinhold and Ellingwood (1982) estimated the risk over a broad geographic region in which they utilized several regionalization schemes that divided the country into areas based upon regional dewpoints, temperatures, and wind speed contours. Each of these schemes had 3 to 4 regions that encompassed differing portions of the country and the risk for each region was estimated based on tornado occurrence rates, variation of intensity along the path width and length, and the correction factors that accounted for misclassification of tornado intensity. Their results indicated that the area east of the Rocky Mountains had the highest geographic

probability with F0 tornado probability having a magnitude of 10^{-4} consistent with Schaefer *et al.* (1986) and the results of the work presented in this dissertation.

Similar to Reinhold and Ellingwood (1982), additional work was done to develop a tornado hazard across the entire contiguous U.S. Schaefer *et al.* (1986) aimed to determine the probability of a tornado of specified intensity at any point in the country rather than based on geographic regions. Their approach is discussed later in more detail, however, the results differed from earlier studies in that contours of risk were created for each F-scale intensity. For their hazard assessment, variation of intensity along the tornado path length and path width was not considered, resulting in an overestimation of the tornado hazard for the strongest F-scale intensities. Thus, for the work presented in this study, a combination of Reinhold and Ellingwood (1982) and Schaefer *et al.* (1986) is utilized in order to create contours of tornado hazard at any point in the continental U.S. while also considering the variation of intensity along tornado path length and width.

2.2 Description of Data

Data on tornadoes has been systematically collected from 1950 to present and is available from the Storm Prediction Center (SPC) website for download. For this work, only data from 1973 to 2011 was included. Earlier years of the data set were excluded because the Fujita scale was first developed and implemented in 1973. In addition, due to improvement in reporting and technological advances, essentially all tornadoes since 1973 have been reported (Reinhold and Ellingwood 1982). The Fujita scale is a method to measure the intensity of a tornado based on the degree of damage observed following the event. Values range from F0, which is the weakest tornado and is associated with little structural damage, to F5, which is complete destruction of a structure, often with the slab swept clean of any debris. The implementation of the Fujita scale

offered better consistency with reporting methodology among National Weather Service (NWS) offices, and drastically reduced the information that was lacking from tornado reporting. Finally, the Fujita scale introduced a method of standardization of several tornado characteristics such as length and width. Thus, only tornado reports after the implementation of the Fujita scale are utilized in this work.

The data obtained in the tornado reports includes the date and time of the tornado touchdown, injuries, and deaths (if any were a direct result of the tornado). The path length is also recorded in miles and is defined as the distance from the touchdown and lift up points, assuming a straight line (Twisdale and Dunn 1983). In addition, the width of the tornado (in yards) is also included in the data. It is measured at the widest point along a tornado path and is assumed constant along the entire path. Tornado start and end coordinates are included; however, end coordinates are commonly not reported in the earlier years of the data set. Finally, the intensity of the tornado is also included. There have been no in-situ wind speed measurements at the surface from inside the tornado core, thus information on the magnitude of the actual wind speed is lacking. Since tornado intensity is based on damage, the wind speed is a 'best guess' of the magnitude of wind that would cause the degree of structural damage observed.

There were a total of 43,048 tornadoes included in the dataset for this study spanning over 38 years. There were some issues with missing data, however, since tornadoes prior to 1973 were not included, this reduced the likelihood of tornado characteristics being left out. A common source of missing data prevalent in the early part of the dataset was the exclusion of end coordinates within the tornado report. Likewise, in a small number of cases, start coordinates, intensity, path length, or path width were not reported and these tornadoes were not included in

the analysis. The tornadoes missing intensity, path length, path width, or start coordinates reduced the total count by 2.65% resulting in a sample of 41,906 tornadoes that contained start coordinates, path length and width information, and intensity.

One caveat to this dataset is that it includes intensity reported with both the Fujita scale (F scale) and the Enhanced Fujita scale. The Enhanced Fujita scale was implemented in 2007 after significant collaboration between meteorologists and structural engineers (Wind Science and Engineering Research Center 2006). After multiple field studies and damage investigations, the original Fujita scale was found to have wind speeds that were too strong based on observations from Doppler radar and damage to structures. A side by side comparison of the two scales is shown in Table 2.1. The Enhanced Fujita scale contains 28 damage indicators (DI) such as buildings, structures, and trees (Wind Science and Engineering Research Center 2006) shown in Table 2.2. For each DI, there are several degrees of damage (DOD) identified. Based on the DOD, a range of wind speed can be determined with an expected, upper, and lower bound estimate based on the quality of construction. An example of the DOD for one- or two-family residences is included in Table 2.3. The Enhanced Fujita scale has provided a better standard for determining the strength (and wind speed) of a tornado among the geographically distributed NWS offices.

Since the data employed in this research includes intensity ratings from both scales, the intensity ratings were not separated (e.g. F0 was in the same category as EF0). This was due to the fact that direct wind measurements during tornadoes are almost never available so that it is not possible to reclassify the tornado intensity. Overall, since the scale is based on damage and not wind speeds, the EF scale can be thought of as a modification to the Fujita scale. The EF scale will be used in the remainder of this work. It should also be noted that the tornado dataset

suffers from issues including the subjective nature of rating tornado damage and determining wind speed from observed damage patterns. This was not considered in the current work. To date, there has not been any measured wind speed inside a strong tornado. Doppler radar has been useful but lacks any in situ measurement as a check for Doppler indicated wind speeds.

Table 2.1: Comparison of the Fujita scale versus the Enhanced Fujita scale (modified from Wind Science and Engineering Research Center 2006).

Fujita Scale			Operational EF Scale		
F Number	3 Second Gust (kph)	3 Second Gust (mph)	EF Number	3 Second Gust (kph)	3 Second Gust (mph)
0	72-126	45-78	0	105-137	65-85
1	127-188	79-117	1	138-177	86-110
2	189-259	118-161	2	178-217	111-135
3	260-336	162-209	3	218-266	136-165
4	337-420	210-261	4	267-322	166-200
5	421-510	262-317	5	Over 322	Over 200

Table 2.2: Damage indicators utilized in the Enhanced Fujita scale (modified from Wind Science and Engineering Research Center 2006).

DI No.	Damage Indicator (DI)
1	Small Barns or Farm Outbuildings (SBO)
2	One- or Two- Family Residences (FR12)
3	Manufactured Home – Single Wide (MHSW)
4	Manufactured Home – Double Wide (MHDW)
5	Apartments, Condos, Townhouses [3 stories or less] (ACT)
6	Motel (M)
7	Masonry Apartment or Motel Building (MAM)
8	Small Retail Building [Fast Food Restaurants] (SRB)
9	Small Professional Building [Doctor’s Office, Branch Banks] (SPB)
10	Strip Mall (SM)
11	Large Shopping Mall (LSM)
12	Large, Isolated Retail Building [K-Mart, Wal-Mart] (LIRB)
13	Automobile Showroom (ASR)
14	Automobile Service Building (ASB)
15	Elementary School [Single Story; Interior or Exterior Hallways] (ES)
16	Junior or Senior High School (JHSH)
17	Low-Rise Building [1-4 Stories] (LRB)
18	Mid-Rise Building [5-20 Stories] (MRB)
19	High-Rise Building [More than 20 Stories] (HRB)
20	Institutional Building [Hospital, Government or University Building] (IB)
21	Metal Building System (MBS)
22	Service Station Canopy (SSC)
23	Warehouse Building [Tilt-up Walls or Heavy-Timber Construction] (WHB)
24	Electrical Transmission Lines (ETL)
25	Free-Standing Towers (FST)
26	Free-Standing Light Poles, Luminary Poles, Flag Poles (FSP)
27	Trees: Hardwood (TH)
28	Trees: Softwood (TS)

Table 2.3: Degree of Damage for One- or Two-Family Residences

DOD	Damage Description	Lower Bound	Expected	Upper Bound
1	Threshold of visible damage	53	65	80
2	Loss of roof covering material (<20%), gutters, and/or awning; loss of vinyl or metal siding	63	79	97
3	Broken glass in doors and windows	79	96	114
4	Uplift of roof deck and loss of significant roof covering material (>20%); collapse of chimney; garage doors collapse inward; failure of porch or carport	81	97	116
5	Entire house shifts off foundation	103	121	141
6	Large sections of roof structure removed; most walls remain standing	104	122	142
7	Exterior walls collapsed	113	132	153
8	Most walls collapsed, except for small interior rooms	127	152	178
9	All walls	142	170	198
10	Destruction of engineered and/or well constructed residence; slab swept clean	165	200	220

In this dissertation, a method that estimates the probability of being struck by a particular wind speed from a tornado is developed. However, rather than simply disaggregating geographically and applying historical data, an empirical approach to divide each tornado into its gradient is used. Reinhold and Ellingwood (1982) used the same motivation to do this theoretically with a Rankine vortex model. Since that time, a significant amount of tornado-specific data has become available making an empirical approach possible.

2.3 Methodology

The development of a quantitative estimate of the annual tornado hazard was based on the minimum assumption method proposed by Schaefer *et al.* (1986) in which the probability of tornado occurrence is determined by the ratio of total tornado area to the total area of interest. The total tornado area was the sum of all tornado areas (length multiplied by width) that had start coordinates contained in the area of interest *A*, as was the approach utilized by Schaefer *et al.* (1986). This method assumes that the damage area from tornadoes that form outside of *A* and move into *A* is equal to the damage area from tornadoes that form within *A* and move outside the bounds of *A*. The area of interest is defined by the user and can be set as a city, county or state. For the purposes of this work, a U.S. map highlighting geographic hazard was the final product desired. To obtain a regional hazard index, the United States was broken up into grid boxes. Several different grid sizes were sampled and they include $2^{\circ} \times 2^{\circ}$, $1^{\circ} \times 1^{\circ}$, and $0.5^{\circ} \times 0.5^{\circ}$. For the $1^{\circ} \times 1^{\circ}$ grid size, a hazard index was estimated at every 0.5° so that at any particular point, the area of interest was a grid box that extended 0.5° in the north, south, east, and west directions ultimately resulting in a $1^{\circ} \times 1^{\circ}$ box. For continuity, the resolution was set at every 0.5° which resulted in grid boxes that were nested across the United States. The same approach was used for the $2^{\circ} \times 2^{\circ}$ and $0.5^{\circ} \times 0.5^{\circ}$ grid boxes with a resolution of 1° and 0.25° respectively, however, since the $1^{\circ} \times 1^{\circ}$ box provided the best resolution, the results for the $1^{\circ} \times 1^{\circ}$ grid box will be used in the remainder of the work. This corresponds to a square grid box with dimensions of approximately 111.2 km (69 miles).

2.3.1 Obtaining Tornado Area

An iterative loop was performed which isolated a single grid box of interest. To obtain the hazard at that point, the total tornado area had to be estimated from all tornado paths that

started within that particular grid box. For the 38 years of tornado information, the path length, path width and ultimately, a total tornado area were found. The tornado area was calculated by multiplying the path length and width since aerial damage survey documentation supports the use of a rectangular path model (Twisdale and Dunn 1983). Once the tornado area was estimated for every tornado in the grid box, it was summed to obtain the total tornado area. The total grid box area was also calculated accounting for the curvature of the earth.

2.3.2 Obtaining Wind Speed Probabilities from a Weibull Distribution

To obtain a breakdown of the probability of occurrence of each EF scale rating in the event of tornado occurrence, simulated wind speeds based on tornado occurrence in a given grid box were fit to a Weibull distribution. Since a range of wind speeds for each EF intensity is known (shown in Table 2.1), wind speeds were simulated using a uniform distribution based on the number of tornadoes reported for each intensity and multiplied by 100 to get enough data points for low activity regions (i.e. there were 2000 values of wind speed generated between 105-137 kph (65-85 mph) for 20 reported EF0 tornadoes). It should be kept in mind that these are conditional Weibull distributions (conditional on the occurrence of a tornado) so generating more points only provides better precision for the fit. This simulated wind speeds were summed in 8 kph (5mph) increments between 105 and 402 kph (65 and 250 mph). A histogram was generated based on this data set and a Weibull distribution was fit appropriately.

The Weibull distribution was determined to be a suitable statistical fit after several sensitivity tests were performed based on visual inspection. It was found the Weibull distribution performed better than a Gumbel or lognormal distribution across the U.S. by highlighting the six specific geographic regions shown in Figure 2.1. These regions included two fairly active areas found in the center of Tornado Alley and the southeast area commonly

referred to as Dixie Alley. In addition, there were three regions of moderate activity investigated. These include the Florida Peninsula, which sees a high occurrence of weaker tornadoes due to the effects of sea breeze interaction and land falling hurricanes, the High Plains, and the Midwest. The final location was in the extreme northwest U.S. Areas west of the Rocky Mountains typically experience a lower occurrence of tornadoes. While there is a low probability of tornado occurrence, the probability is, of course, never zero.

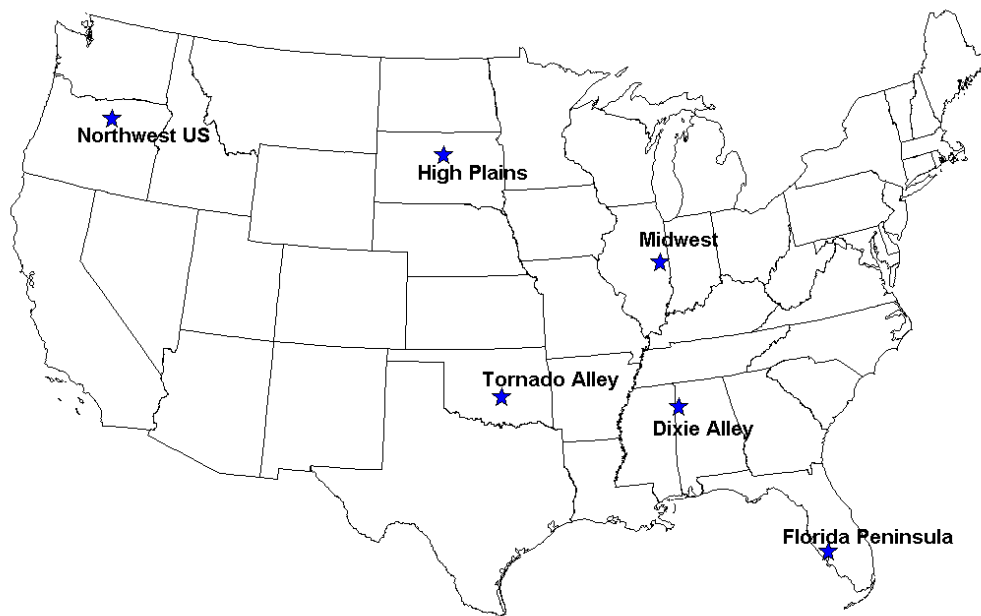


Figure 2.1: Locations of the 6 test regions. These locations were chosen based on the varying degrees of tornado activity that each represent.

The Weibull probability density functions (PDF) and simulated wind speeds for each of the six geographic regions are shown in Figure 2.2. The Weibull distribution performed better in low/moderate tornado occurrence regions (NW U.S., Florida, and the High Plains) and it was observed that the Gumbel and lognormal distributions did not handle these regions adequately, even though they were appropriate in the high activity regions. In addition, the Weibull

distribution is commonly used to model wind speed distributions (Brooks 2004). Due to the adequate performance of the Weibull distribution across the entire U.S., it was selected for use in this study and was fit to the histograms of simulated wind speeds.

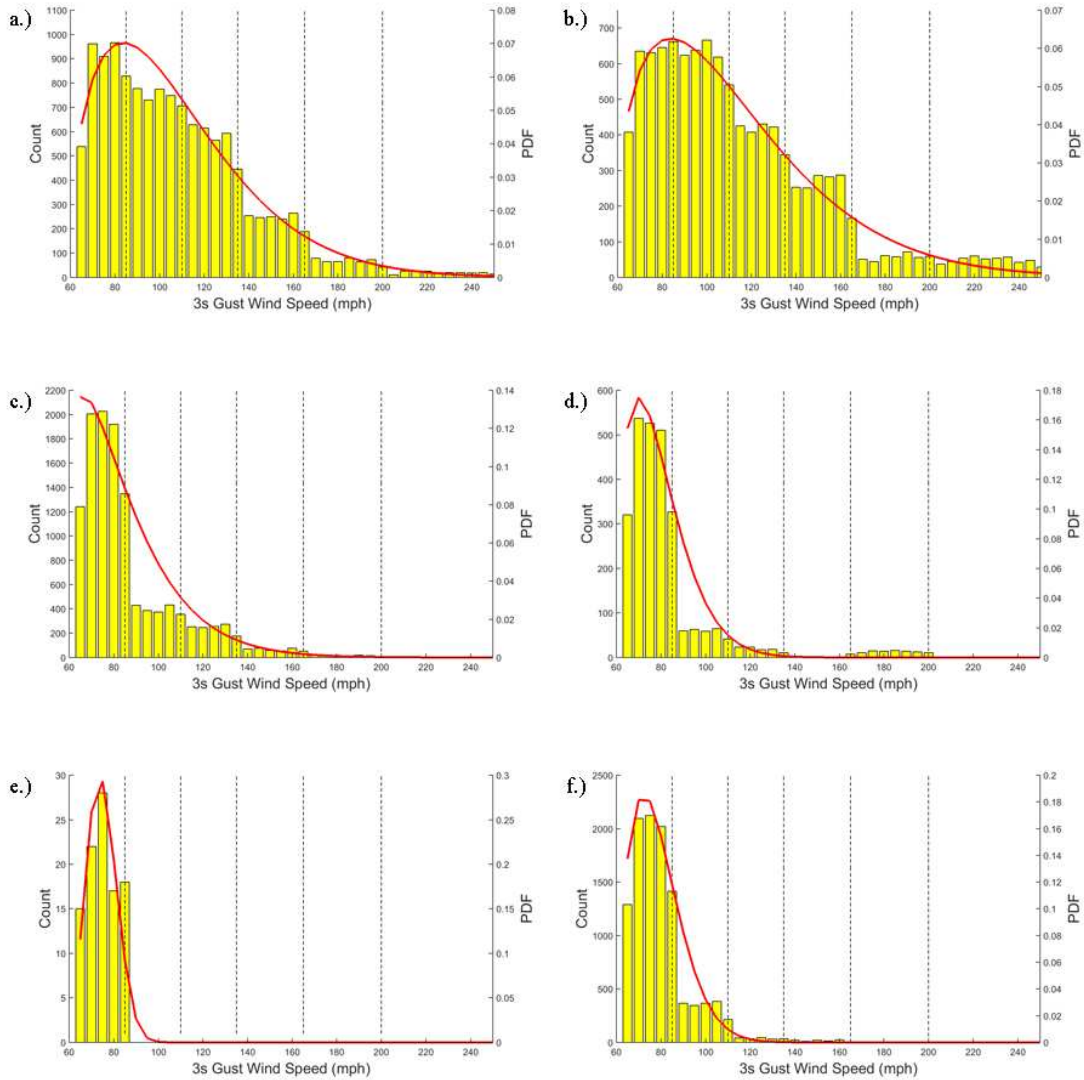


Figure 2.2: Simulated wind speeds and fitted Weibull distribution with $1^\circ \times 1^\circ$ resolution for the test regions of (a.) Tornado Alley, (b.) Dixie Alley, (c.) the Midwest, (d.) the High Plains, (e.) the extreme Northwest U.S., and (f.) the Florida Peninsula. Simulated wind speeds are based on tornado reports at each location over the 38 year period. Dashed lines indicate the boundary between EF categories.

The purpose of fitting a Weibull distribution (or any parametric distribution) to the simulated wind speeds was that it allowed for the estimation of the probability that in the event of a tornado, it would have a specific intensity rating. This value was estimated as p_0 - p_5 for EF0-EF5 tornadoes respectively. This probability was found by taking the area under the Weibull PDF curve for each wind speed range. Since an EF0 ranges between 105-137 kph (65-85 mph), the area under the curve between 105 kph and 137 kph (65 mph and 85 mph) was calculated and resulted in the probability of a wind speed categorized as an EF0. This was performed for each EF intensity to obtain the values of p_0 - p_5 . The probability is needed to estimate the tornado hazard at a location as described in more detail below.

2.3.3 The Gradient Technique for Reduced Area

Tornado intensity is reported solely by the local NWS office or offices near where a tornado strikes. The goal of the NWS assessment is to determine the maximum strength, the path length, maximum path width, touch down point, and lift up point. Their surveys do not typically include information that details the variation of intensity along the path width and length. However, it has long been observed that tornado strength is commonly highest at its center and reduces along its width transversely away from the center of the path (see e.g. Reinhold and Ellingwood 1982). This is consistent with a Rankine vortex and is also consistent with the tornado damage contours found in Tuscaloosa, AL and Joplin, MO. Although the damage paths in strong tornadoes may be cycloidal, the highest level of damage is typically found at the core. This is because the tornado's center moved directly over the area resulting in a longer duration in the tornado vortex. In addition, wind speeds are higher at the core and are reduced as one moves away from the vortex, thus structures on the outer fringes experience lower wind speeds. Furthermore, at the center, the wind changes direction before the core, at the

core, and behind the core due to the circular shape of the wind field. This fact likely causes more damage. Finally, at the core, the updraft is commonly strongest, resulting in higher tornado uplift force. Overall, the simplification of tornado intensity along the path is made to provide an estimate of the area of damage associated with each EF wind speed range for a given tornado. While the distribution of wind speeds will vary for each individual tornado, the method described below details a generic wind distribution for use in the tornado hazard estimation. This implies that while a tornado may be rated high, e.g. EF4, there are variations of this intensity along both the path width and length. Unfortunately, the NWS does not have the resources necessary to conduct in-depth damage surveys that would have the resolution to provide information on variations of intensity along the path width and length for every tornado. However, after major tornadoes, detailed damage surveys are often conducted that investigate damage along the path at many of the homes or structures impacted. This information is often available to the public in the form of internet websites, event reports, or scholarly publications which will be discussed later.

To better understand the variation of intensity along the tornado path, information was obtained from both the devastating 1974 and 2011 tornado outbreaks. Reinhold and Ellingwood (1982) and Schaefer *et al.* (1986) both included information related to the break down of intensity along tornado path lengths. After the April 3-4, 1974 Super Outbreak and other significant outbreaks of the time, detailed surveys were performed documenting segments of tornado paths and their intensity. A summary of this table is presented in Table 2.4. The sum of the six individual F5 tornado paths was 486 km (302 miles), yet only 72.4 km (45 miles) were actually rated as F5 damage based on inspection. Thus, along the tornado path length, only 15%

was actually determined to be rated F5, even though the tornadoes were all rated as F5. Similar results were found for tornadoes rated F1-F4.

Table 2.4: Summary of the variation of intensity along the length of tornadoes from five surveyed tornado outbreak cases (modified from Schaefer *et al.* 1986).

F-Scale	# of Tor.	Segment Path Length												Total Path Lengths	
		F0		F1		F2		F3		F4		F5			
		km	mi	km	mi	km	mi	km	Mi	km	mi	km	mi	km	mi
1	34	292.3	181.6	217.0	134.8									509.3	316.5
2	40	235.2	146.1	295.1	183.4	308.1	191.4							838.4	521.0
3	41	149.8	93.1	313.4	194.7	408.2	253.6	411.3	255.6					1282.7	797.0
4	29	223.2	138.7	247.3	153.7	436.2	271.0	329.9	205.0	333.7	207.4			1570.4	975.7
5	6	64.4	40.0	49.9	31.0	91.7	57.0	117.5	73.0	90.1	56.0	72.4	45.0	486.0	302.0
Total	150	964.9	599.6	1122.7	697.6	1244.2	773.1	858.7	533.6	423.8	263.3	72.4	45.0	4686.8	2912.2

Table 2.4 illustrates the variation of intensity along path length, but does not include information on the variation along the width. In order to estimate the damage area for each intensity rating along a tornado path, information was needed along the width of the tornado path. To obtain this information, damage surveys after the April 27, 2011 Tuscaloosa, AL, tornado and the May 22, 2011 Joplin, MO, tornado were used. Detailed damage surveys were performed after each of these devastating tornadoes (Prevatt *et al.* 2012a; 2012b) and the results were made available to the public and are available online (Rapid Deployment Damage Assessment Team 2011a and 2011b). For each tornado, transverse cuts perpendicular to the tornado path were made across the damage path and were termed transects. Due to the limited path lengths of the damage surveys, the transects were made on altering sides of the center of the path and staggered to obtain a better variation of intensity along the path as shown in Figure 2.3. Results from transects across the entire path length are similar to the values of the transects over half the damage path. These transects spanned from EF4 damage to EF0 and to the point at which there was no damage. This allowed for the estimation of the breakdown of tornado

intensity along the EF4 portions of the damage path. This approach was used for the EF3, EF2, and EF1 portions of the path as well. Once the gradient along the width was found for each of the two tornadoes, the percentage of the path width rated as each EF scale intensity was estimated. This was found by averaging the transects of each tornado. Note that the intensity variation along the tornado path width is taken from a very limited sample. Ideally detailed maps of tornado damage would be generated for numerous other tornadoes so that a better understanding of intensity variations along the tornado path length and width could be developed. This would lead to a better understanding of the intensity distribution and continual improvement of tornado hazard assessment.

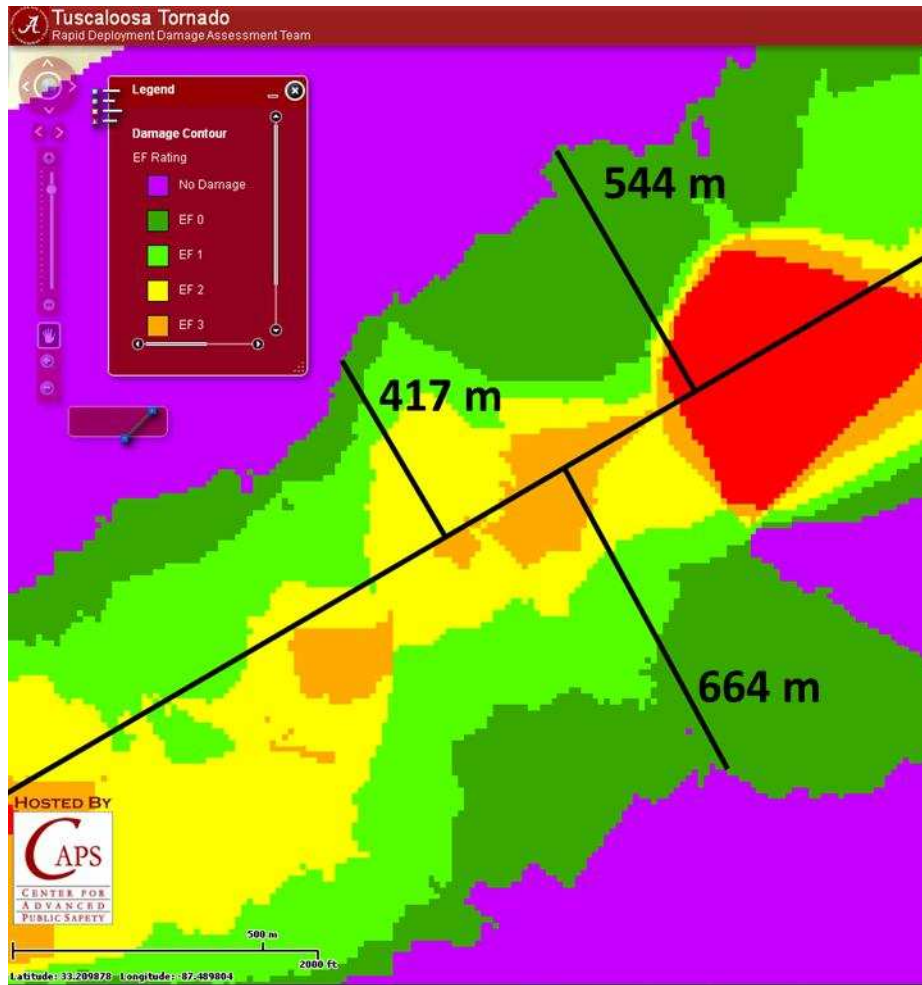


Figure 2.3: Sample transect measurements for the Tuscaloosa tornado (Graettinger *et al.* 2012).

Once the average breakdowns of intensity along the path width were estimated, the percentage of damage area associated with each EF category was estimated and is shown in Table 2.5. In the event that stronger tornado damage area was contained in a weaker EF strength area, the stronger tornado area was subtracted. For instance, when estimating the percentage of area rated EF4 associated with an EF5 tornado, the EF5 tornado area was subtracted. It is interesting to note that while a tornado may be rated an EF5, the area associated with that level of damage is estimated to be only 4% of the total tornado damage area. Illustrations of the reduced area gradient technique approach are shown in Figure 2.4 which illustrates the generic

intensity variations for EF1-EF5 tornadoes used from climatological averages of path length and path width and employs the empirical width approach in this paper for each category. These results will be used in the final tornado hazard estimation. The values for variation of intensity along the tornado path were defined deterministically using data from the 1974 and 2011 tornado season. In addition, the relationship between variations of intensity and path width and length, are assumed to occur in all tornadoes, that is, all tornadoes are assumed to exhibit common intensity distributions (Schaefer *et al.* 1986). Again, the variation of intensity shown in Figure 2.4 is based on a limited data set and would ideally be updated as more detailed damage surveys are performed and incorporated in the analysis. However, for this work, the generic intensity variations shown in Figure 2.4 will be used for the tornado hazard estimate.

Table 2.5: Variation of intensity of the damage area for EF1-EF5 tornadoes presented as percentages of the total path length, width, and area (e.g. 4.1 represents that 4.1% of the tornado area is rated as EF5). The variation of width was obtained from the Tuscaloosa and Joplin tornadoes of 2011 and the variation of length was obtained from Schaefer *et al.* (1986).

EF Category	Percent Width	Percent Length	Percent Area
<u>Adjusted EF5 Path</u>			
EF5	27.3	14.9	4.1
EF4	19.9	18.5	11.7
EF3	13.6	24.2	19.3
EF2	13.8	18.9	22.0
EF1	12.7	10.3	18.7
EF0	12.7	13.2	24.2
Total	100	100	100
<u>Adjusted EF4 Path</u>			
EF4	27.3	21.2	5.8
EF3	18.7	21.0	13.6
EF2	19	27.8	26.1
EF1	17.5	15.8	25.3
EF0	17.5	14.2	29.2
Total	100	100	100
<u>Adjusted EF3 Path</u>			
EF3	33.8	32.1	10.8
EF2	20.2	31.8	23.7
EF1	26.2	24.4	36.3
EF0	19.8	11.7	29.2
Total	100	100	100
<u>Adjusted EF2 Path</u>			
EF2	47.5	36.7	17.4
EF1	31.4	35.2	39.3
EF0	21.1	28.1	43.3
Total	100	100	100
<u>Adjusted EF1 Path</u>			
EF1	62.5	42.6	26.6
EF0	37.5	57.4	73.4
Total	100	100	100

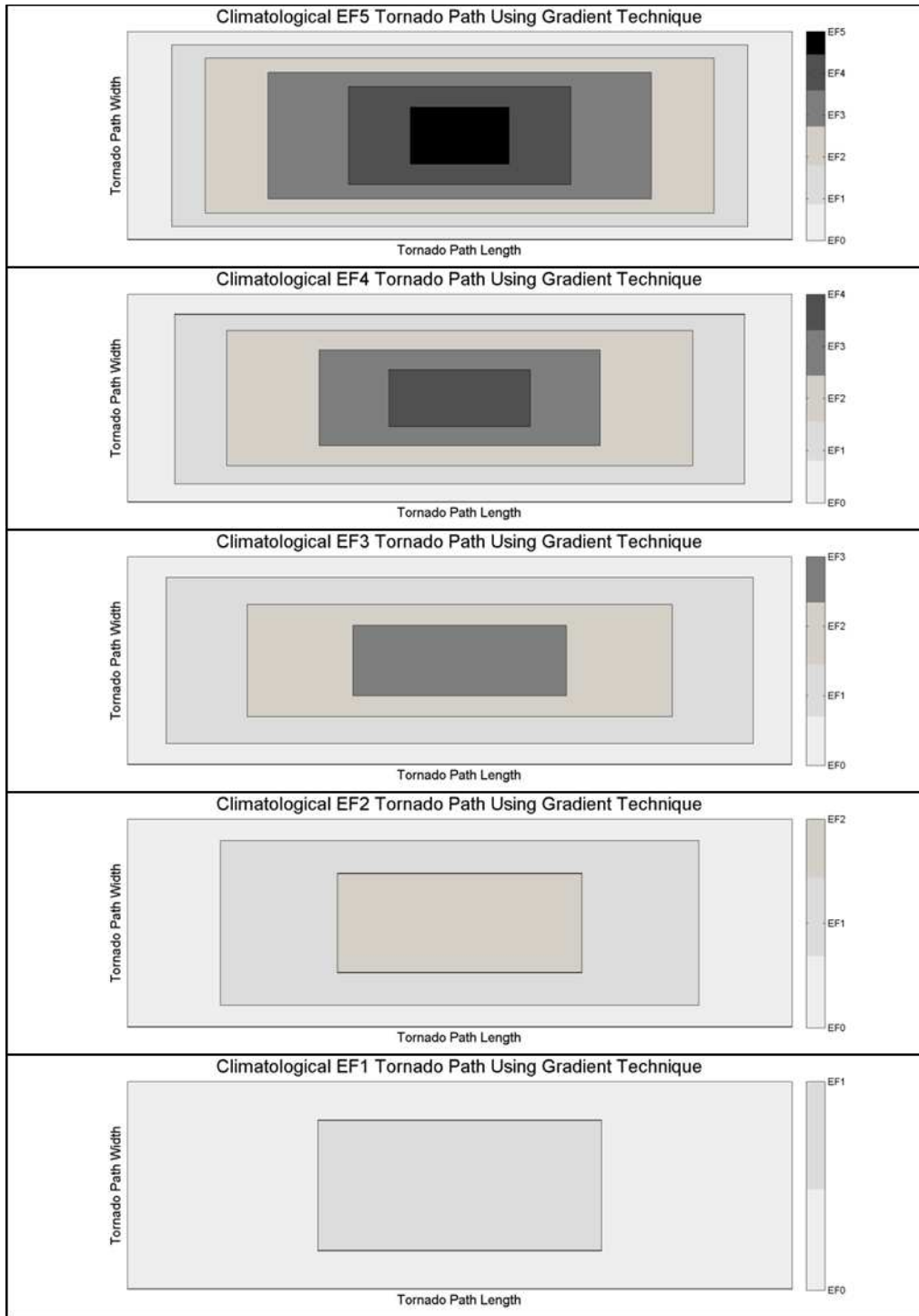


Figure 2.4: Illustration of the variation of tornado intensity along its path used in this study (See Table 2.5 for numerical values).

2.4 Annual Tornado Probability Estimation

Schaefer *et al.* (1986) proposed a minimum assumption model to estimate the annual tornado probability at a location. Their methodology logically summed all the tornado path areas in a grid box and divided that by the product of the grid box area and number of years in the data set. This allowed for a quantitative estimate of the annual probability of a tornado, P , described as

$$P = \frac{\sum_{i=1}^n l_i w_i}{AY} \quad (2.1)$$

where A is the regional area described earlier as a $1^\circ \times 1^\circ$ box, Y is the number of years in the data set, l_i is the length of tornado “ i ”, w_i is its width, and n is the number of tornadoes in area A . This model is particularly useful for analysis over a large area, such as the continental U.S.

While the minimum assumption model proposed by Schaefer *et al.* (1986) is useful in estimating an annual tornado probability, there are some issues to consider when interpreting the results. The first is that this methodology is based solely on climatology. In the event that a tornado did not occur over a region in the time frame of the data set, the value of P is set to zero. However, while there may not have been a tornado reported at a location in the data set, the probability of a tornado may be quite small, but is never zero. Similarly, the tornado data has issues with under reporting, especially in the earlier part of the time frame due to lack of population in certain areas of the U.S. Improvements in technology (such as Doppler radar), the popularity of storm chasing, and the increase in population have reduced the likelihood of missing tornadoes since 1973 (Reinhold and Ellingwood 1982). However, while there may not be a reported tornado, that fact does not imply that no tornado has touched down in the grid box.

In addition to the issue of missed storms, the annual probability may actually be overestimated in some locations, particularly when estimating the likelihood of strong or violent tornadoes. As shown with the method introduced by Schaefer *et al.* (1986), the entire tornado path of an EF5 tornado is used to estimate the EF5 tornado hazard. While a tornado may be rated as EF5, in actuality, the area that is EF5 rated damage is quite small compared to the total damage path as indicated in Figure 2.4. In the estimation of P in Equation (2.1), calculating the annual probability of an EF5 tornado sums the *total* tornado area of EF5 tornadoes in area grid box without accounting for the variation of intensity along a tornado's path length and width. This results in an overestimation of the probability of experiencing EF5 scale winds from a wind speed/damage perspective. Therefore, an enhanced estimation of P_{EFj} is proposed which employs the results from the gradient technique to account for the variation of intensity along a tornado path combined with the Weibull distribution for occurrence to populate locations with sporadic tornado reports. A summary of the procedure is shown in Figure 2.5.

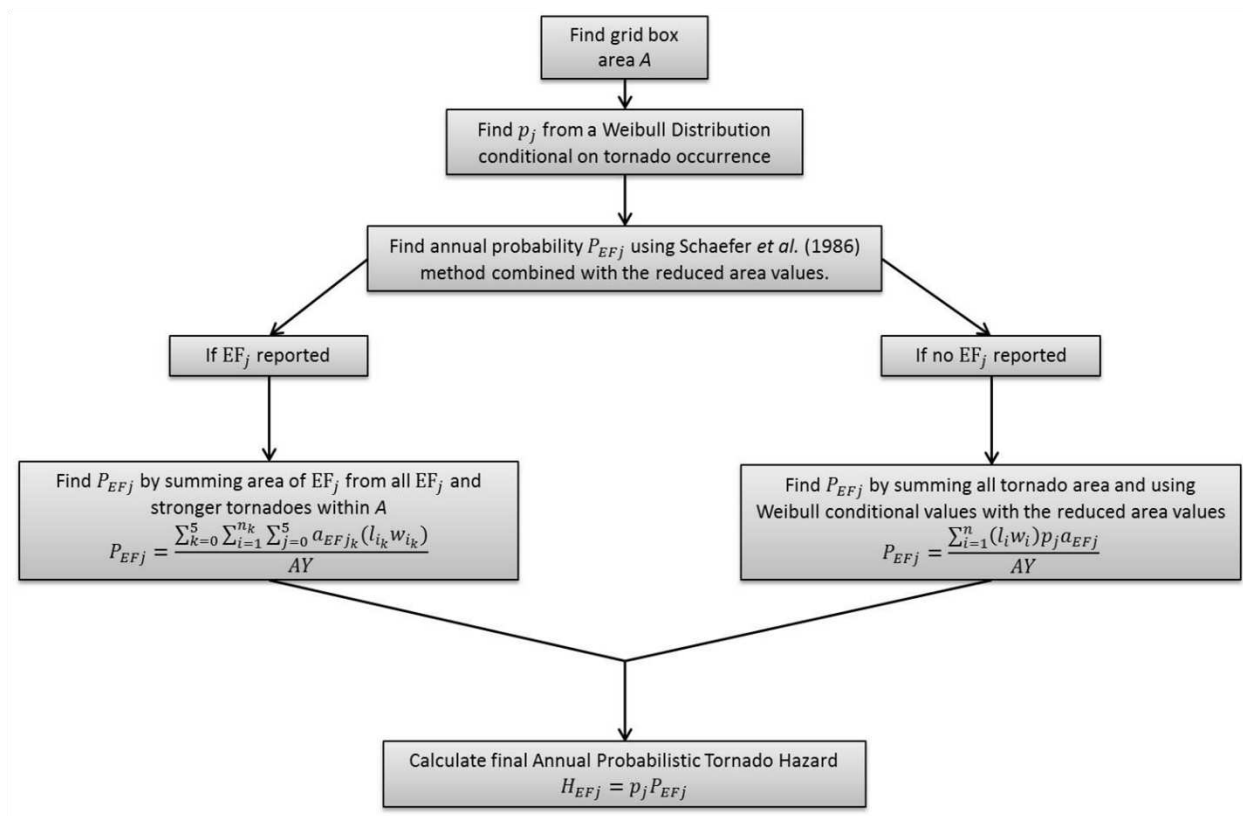


Figure 2.5: Flow chart visualizing the process to determine the annual tornado hazard at a location.

The reduced area approach previously described better illustrates the climatological probability of experiencing an EF scale tornado since it accounts for variations of intensity along a tornado path. This was a proposed modification to the minimum assumption approach described by Schaefer *et al.* (1986). However as briefly described before, this methodology has issues in locations where a low number of tornadoes are recorded. For instance, if no EF5 tornado was reported over the recorded timeframe, the annual probability is set to zero with the minimum assumption approach (Schaefer *et al.* 1986). However, the lack of EF scale tornadoes reported does not mean that the probability is zero. To account for this issue, a Weibull distribution is used within each bin to ensure the probability is never zero. The process of estimating the Weibull probability was described earlier. Thus, this new approach is helpful in

estimating probabilities of tornadoes in regions where a low number of tornadoes have been reported. However, in the event that a single tornado had never been reported over the grid box of interest, the default annual tornado hazard was set to zero due to lack of information, i.e. no way to fit parameters (and most likely lack of favorable atmospheric conditions). Ultimately this work will be applied to even smaller areas (i.e. city blocks), thus the hazard was set to zero rather than trying to smooth the data.

In the event that a low number of tornadoes were reported, a methodology to estimate the annual probability of any EF scale rating needed to be used. In these cases, the minimum assumption model of Schaefer *et al.* (1986) was still used, but modified. In the event a location had tornado activity but did not have a specific EF_j tornado reported, there is no way to estimate the tornado hazard at that location since there is no length, width, or area information provided using the Schaefer *et al.* (1986) method. By using Equation 2.2, however, the annual probability, P_{EF_j} can be estimated using the Weibull values described above. The method is shown:

$$P_{EF_j} = \frac{\sum_{i=1}^n (l_i w_i) p_j a_{EF_j}}{AY} \quad (2.2)$$

where j is an index ranging from 0-5 according to EF intensity, p_j is the probability that in the event of a tornado, it would be intensity j , n is the total number of tornadoes, Y is the number of years in the dataset, and a_{EF_j} is the area of the tornado path rated j (shown in Table 2.5). The value p_j comes from the Weibull fit of tornado reports over the area A and is very small when no EF_j tornadoes have been reported. Using a_{EF_j} accounts for the fact that only a portion of an EF_j tornado is actually rated as j . Employing this approach can result in a near zero annual

probability but indicates that there is still a chance of EF_j occurrence at any point. This methodology was employed for determining any intensity rating on the EF scale in the event that a tornado of specified intensity was not recorded over the timeframe.

In the event that tornadoes rated EF0-EF5 were reported in a grid box, a different approach was utilized. This calculation was straightforward for the strongest tornadoes, EF5, but became more complicated with weaker tornadoes. Estimating the annual probability of an EF4-EF0 strength wind was a bit more challenging due to the fact that the area of stronger tornadoes includes a large portion that is rated weaker as mentioned earlier and shown in Figure 2.4. Therefore, when estimating EF4 strength wind, one must account for the area of EF4 damage from both EF5 and EF4 tornadoes that have occurred in that grid during the time period of interest. An estimate of the annual probability can be expressed as:

$$P_{EF_j} = \frac{\sum_{i=1}^n a_{EFjk} (l_{ik} w_{ik})}{AY} \quad (2.3)$$

where j is the EF intensity of interest, k is a summing index between 0-5, and n is the total number of tornadoes in the grid box. Furthermore, l_{ik} and w_{ik} are the length and width of any tornado rated k , and a_{EFjk} is the area of the damage rated j in a tornado of k strength. If no tornado of intensity k is reported, a_{EFjk} is set to zero. A is the total grid box area, and Y is the total number of years in the dataset. This methodology allows for a more realistic estimation of the probability of a location experiencing a certain EF strength tornado since it accounts for variation of intensity along a tornado's damage path.

2.5 Determining the Annual Tornado Hazard at a Location

The Weibull method described earlier was used to estimate the probability of an EF strength wind speed in the event there was a lack of climatological tornado reports in area A. This value was estimated for EF0-EF5 wind speed ranges and was defined as $p0-p5$. In addition, the annual probability of an EF scale tornado was estimated using a minimum assumption model described earlier and was defined as P_{EFj} . The objective of the project was to calculate the annual probabilistic tornado hazard at any location in the U.S. To calculate this value, a combination of climatology and the Weibull procedure was utilized.

The multiplication rule of basic probability theory was utilized for the tornado hazard estimation. If A and B are two events, the probability of both A and B are not equal to zero, and the intersection of the two events is desired (e.g. both A and B occur), then

$$P(A \cap B) = P(A)P(B|A) \quad (2.4)$$

where $P(A \cap B)$ is the probability that both A and B occur, $P(A)$ is the probability of A, and $P(B|A)$ is the probability that B occurs given A. In the case of the tornado hazard, the probability of A, $P(A)$, is defined as the probability of a tornado at a location defined as $P_{EF0-P_{EF5}}$. $P(B|A)$ is the probability of an EF scale tornado in the event of tornado occurrence estimated using a Weibull distribution and calculated as $p0-p5$.

Finally, $P(A \cap B)$ is the probability of a location experiencing a certain EF scale wind speed. To find this for each EF scale rating, the multiplication rule was used. Thus, the probabilistic tornado hazard index was found by multiplying the annual tornado probability and the statistical probability estimated from the Weibull distribution and is shown below:

$$H_{EFj} = p_j P_{EFj} \quad (2.5)$$

where H_{EFj} is the probabilistic tornado hazard index, P_{EFj} is the annual probability of tornado occurrence, and p_j is the probability that if a tornado occurs, it will be a specific intensity. The variable j represents the EF scale ranging from $j=0-5$. The process to estimate H_{EFj} is summarized in Figure 2.5.

The probabilistic tornado hazard was estimated at every grid point in the U.S. for EF0-EF5 wind speeds using the methodology outlined in this paper and is shown in Figure 2.6. In Figure 2.6, the resolution was set to 0.5° . This resulted in overlapping grid boxes that were $1^\circ \times 1^\circ$ in size. In addition, the tornado hazard is presented, not as the calculated value, but rather is shown as the power of ten which is consistent with Schaefer *et al.* (1986) Thus if the contour is plotted as a -4, this indicates a probabilistic tornado hazard with a magnitude of 10^{-4} .

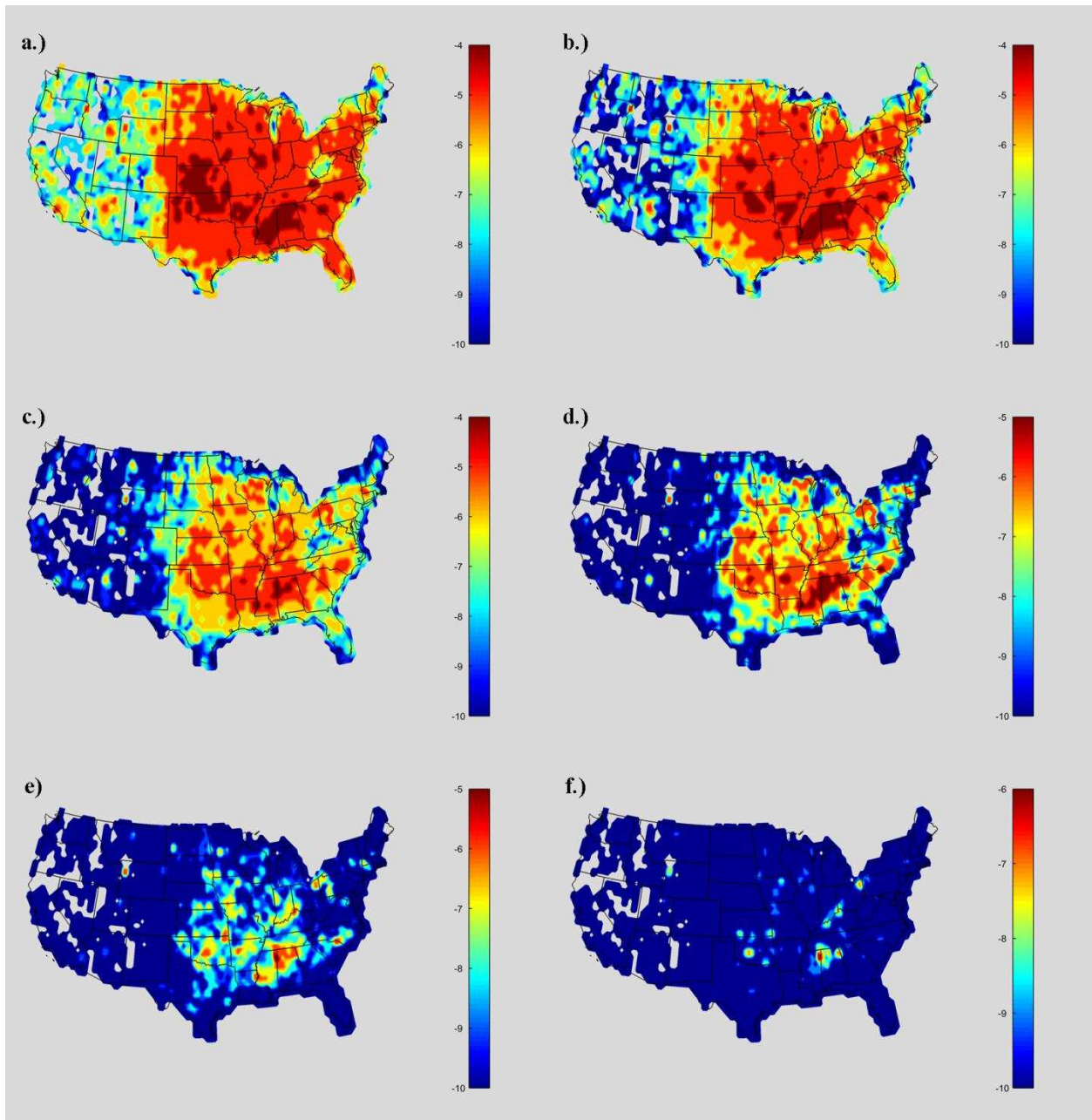


Figure 2.6: Probabilistic tornado hazard index for (a.) EF0- (f.) EF5. The hazard is labeled as the power of ten per year.

2.6 Results of Probabilistic Tornado Hazard Analysis

Contours of the probabilistic tornado hazard index were created to illustrate high probability zones across the U.S. as shown in Figure 2.6. The plots indicate the annual probability of experiencing an EF0-EF5 wind speed at any point in the continental U.S. Figure 2.6a illustrates the results for the annual probability of experiencing EF0 scale wind speed, which falls in the range between 105 and 137 kph (65-85 mph). The EF0 wind hazard covers a large area of high probability centered in the midsection of the U.S., incorporating most of Tornado Alley and portions of the Midwest. In addition, parts of the southeast including Alabama and Mississippi, commonly referred to as Dixie Alley, are also highlighted. Areas of very low probability (10^{-9}) in the EF0 hazard include most of the area west of the Rocky Mountains, the extreme Northeast, and West Virginia. However, compared to the remaining EF hazards, most of the continental U.S. has a relatively high probability (10^{-5}) in that the magnitude of the hazard is higher for EF0 than any other intensity, even in the low probability regions. This is likely due to the fact that EF0 tornadoes have occurred in all 48 states and these tornadoes account for a high percentage of tornado reports (approximately 50%).

The EF1 hazard is shown in Figure 2.6b and indicates the annual probability of experiencing wind speeds of 138-177 kph (86-110 mph). The spatial coverage of the EF1 hazard is nearly identical to the EF0 hazard with the highest hazard regions remain centered on the Mississippi River basin with a magnitude of 10^{-4} . However, one noticeable difference is that the areas of very low probability have increased drastically. This correlates well with the reported tornadoes in these areas as one might expect. There is a noticeable decrease in spatial coverage of tornado reports when EF0 tornadoes are not considered as can be seen by comparing Figures 2.7a and 2.7b. Thus, while there were not many EF1 or stronger tornadoes reported in these

areas, the EF1 wind speed hazard remains quite small as indicated by the blue contouring (10^{-8} to 10^{-10}) and was estimated using the Weibull procedure described earlier.

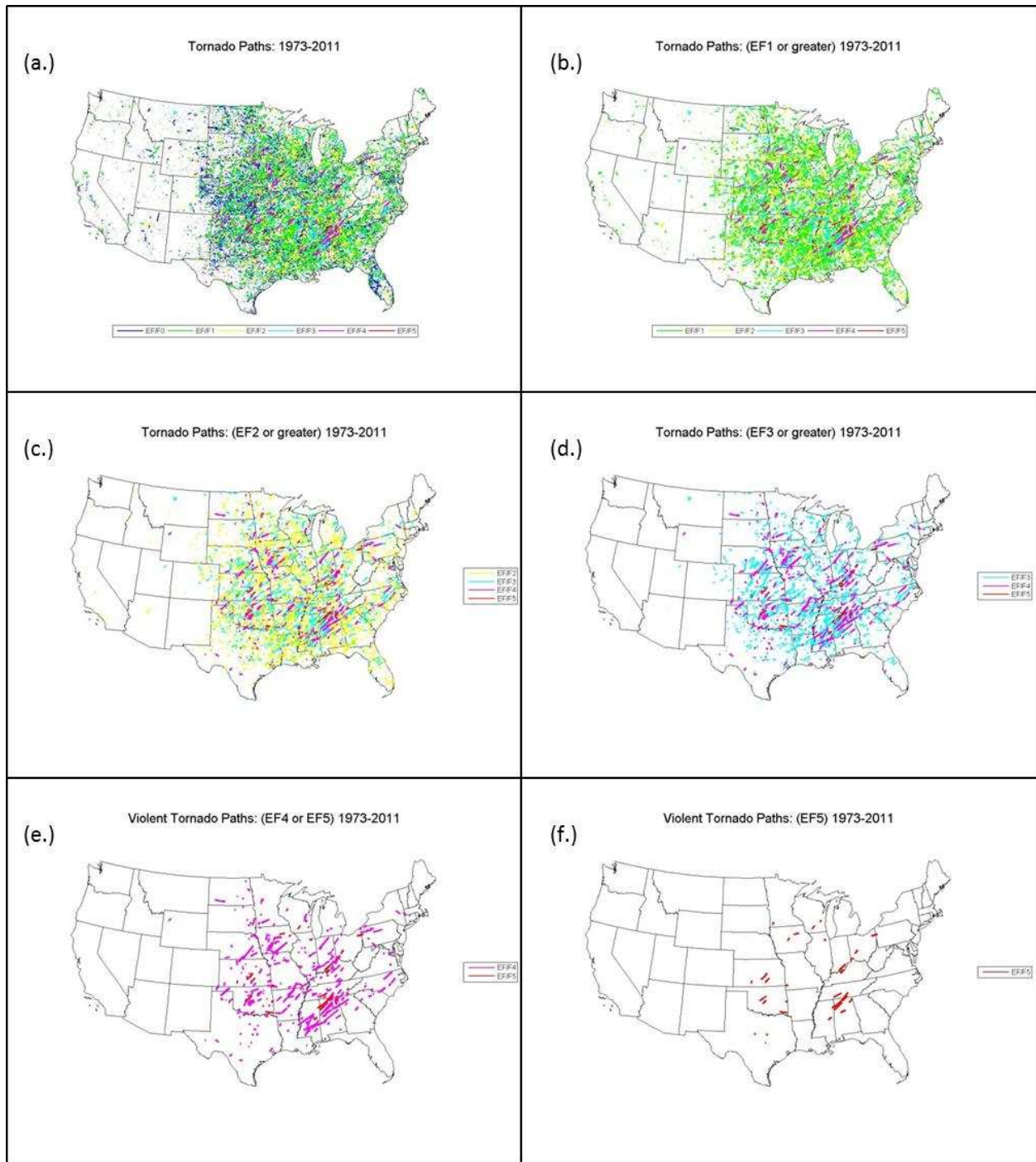


Figure 2.7: Reported tornado paths plotted for (a.) EF0-(f.) EF5 based on tornado reports from 1973-2011.

The EF2 wind speed hazard showed that the region of highest hazard was drastically reduced as shown in Figure 2.6c. Instead of a large region of relatively high hazard across the center of the country, there are areas of higher probability (10^{-5}) surrounded by a larger region of slightly lower probability (10^{-7}). The highest hazard regions (10^{-4}) included parts of Alabama, Mississippi, Louisiana, and Arkansas. However, a 10^{-5} region is still located in Tornado Alley, Dixie Alley, and the Midwest. This indicates that the probability of experiencing a wind speed between 178-217 kph (111-135 mph) is slightly smaller across the U.S., which is expected due to the fact that as tornado strength increases, the rate of occurrence decreases.

The EF3 tornado hazard denotes the annual probability of experiencing a tornado wind speed in the range of 218-266 kph (136-165 mph). The region between the Rocky and Appalachian Mountains is still the highest hazard area which correlates well with the tornado reports in this portion of the country seen in Figure 2.7d. The region between central Louisiana extending northeast to north Alabama has the highest hazard with a magnitude of 10^{-5} shown in Figure 2.6d. Relative minima are indicated in the Appalachian Mountain regions of Kentucky, West Virginia, and Virginia. Likewise, the occurrence probability in the Northeast and along the western U.S. is also very low.

The annual probability of experiencing a wind speed in the EF4 range of 267-322 kph (166-200 mph) is shown in Figure 2.6e. This figure illustrates that the highest occurrence probability remains in Tornado Alley and Dixie Alley with a hazard value with a magnitude of 10^{-5} that correlates well with reported EF4 and EF5 tornadoes as seen in Figure 2.7e. Observed minimums are seen in central Missouri associated with the Ozarks, the Florida peninsula, the Northeast and regions west of the Rockies. It is interesting to note the relative maximums in Wyoming, eastern Ohio and western Pennsylvania. While these regions are typically considered

outside the highest hazard zones, there were reported EF4 and EF5 tornadoes in these regions that resulted in significantly increased hazard at these locations compared to closely neighboring grid boxes. In addition, the locations of the highest hazard agree spatially with the results of Schaefer *et al.* (1986), however, the magnitude of the risk is reduced from 10^{-4} to 10^{-5} as would be expected since the analysis in this work considered variation of intensity along a tornado path length and width.

The strongest tornadoes, EF5, are very rare with only 44 reported tornadoes in the 38 year time frame investigated in this study as seen in Figure 2.7f. These tornadoes are associated with wind speeds over 322 kph (200 mph) and catastrophic damage. The majority of the continental U.S. has a very low probability of experiencing such strong tornadoes with the hazard well below 10^{-10} . However, regions in Tornado Alley, Dixie Alley, and the Midwest show a higher hazard as seen in Figure 2.6f. These include central Oklahoma and Kansas, northern Alabama and Mississippi, southern Indiana as well as parts of Iowa, Wisconsin, and Ohio. It should be noted that while there was higher annual hazard at these locations, it is quite small with a magnitude of approximately 10^{-6} to 10^{-9} . As with the EF4 tornadoes, the geographic location of the highest probability of EF5 correlates well with Schaefer *et al.* (1986), but the magnitude of the hazard is lower (i.e. 10^{-4} in earlier works to 10^{-6} with results presented in this dissertation). This is expected since the results presented in this paper considered only the small percentage of EF5 tornado area that is actually rated EF5.

It is important to note the limitations of the probabilistic tornado hazard maps since they were created using the tornado climatology from a rather short time set. This is especially evident in the maps for the violent EF4 and EF5 tornadoes. Areas of highest risk coincide with locations with reported EF4 and EF5 tornadoes as a result of the methodology to assess the

tornado risk across the country. As the tornado climatology continues to grow, the tornado hazard maps should be updated to obtain a better understanding of tornado risk. Additional limitations to the tornado hazard maps are discussed in Section 2.8.

Tornadoes can be extremely powerful and destructive and often their impacts can cripple a community in the immediate aftermath. While the annual probability of a tornado hitting a particular location is quite small (10^{-4} to 10^{-6}), there is an increasing interest in quantifying the relative hazard in a region. The high hazard areas shown in Figure 2.6 have a substantially higher probability of tornado occurrence (three orders of magnitude) as compared to the majority of the United States. It may be beneficial to consider regional modifications to construction procedures in these areas based on this quantified discrepancy in hazard, similar to enhanced building practices seen in Florida after Hurricane Andrew in 1992.

The tornado hazard maps indicated that high hazard areas were often found centered between the Rocky and Appalachian Mountains. This included the well documented region referred to as Tornado Alley which includes Texas, Oklahoma, Kansas, and Nebraska. Likewise, Dixie Alley was also highlighted as a high hazard area including the states of Alabama, Mississippi, and eastern Arkansas. The Midwest also saw a relatively high annual tornado hazard with maxima found in Indiana, Wisconsin, Iowa, Ohio, and Illinois. The probability in these areas was substantially higher (three orders of magnitude) than the rest of the United States. In fact, portions of Appalachia and regions west of the Rockies had an extremely small probability of tornadoes greater than EF0 as is well known. While it may not be economical to include a tornado provision in building codes at these locations, the high hazard areas mentioned above may benefit by considering implementation of fortified codes. This will be discussed in more detail in later chapters.

2.7 Development of Tornado Hazard Curves

Tornado hazard curves were developed for select locations across the United States shown in Figure 2.1. The choice of the locations is summarized in Section 3.2. To create the tornado hazard curves, the value of the tornado hazard for each EF category was found using the maps created by Standohar-Alfano and van de Lindt (2014). Interpolation between values for each EF intensity was performed to obtain a complete tornado hazard curve at those locations and the resulting curves are shown in Figure 2.8. As is evident from the curves, the Tornado Alley and Dixie Alley locations have the highest tornado hazard. Annual tornado probabilities below 10^{-10} are not shown even though the curves for the low-moderate activity regions do continue past this point.

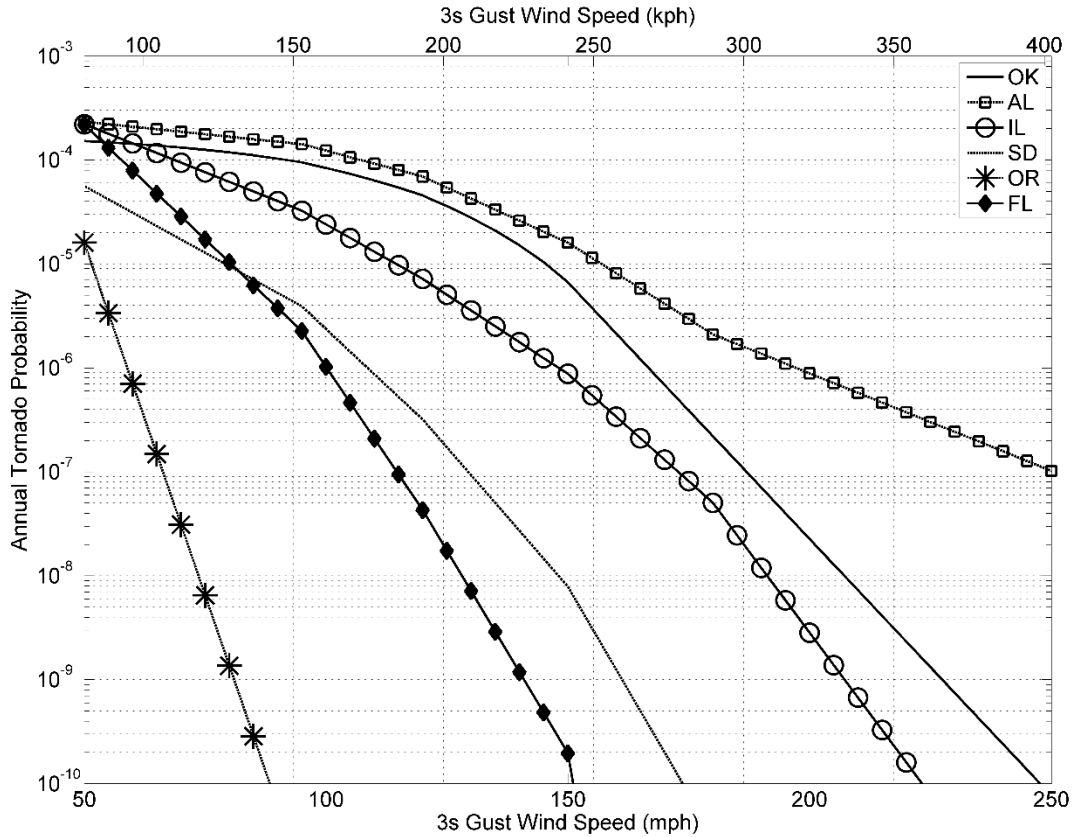


Figure 2.8: Hazard curves for each of the 6 locations investigated. Values below 10^{-10} are not shown.

2.8 Uncertainty in the Tornado Hazard Analysis

The probabilistic tornado hazard presented above and shown in Figure 2.6 was performed based on 38 years of tornado climatology. Thus, the results of the work are highly dependent on the location of reported tornadoes. For instance, neighboring locations could have values of tornado hazard that vary by a few orders of magnitude due to differences in the number of tornadoes reported in each grid box. To assess the variability of the tornado hazard, a bootstrap analysis was performed by estimating the probabilistic tornado hazard across the country for

several different decades, consistent with the work of Dixon *et al.* (2011). Table 2.6 includes information on the total number of tornadoes reported during each decade analyzed.

Table 2.6: Number of tornadoes per decade investigated

Decade	Number of Tornadoes
1973-1979	6389
1975-1984	8892
1980-1989	8313
1985-1994	9608
1990-1999	12277
1995-2004	12915
2000-2009	12974
2005-2011	9543
2010-2011	3094

To determine the uncertainty in the maps shown in Figure 2.6, the probabilistic tornado hazard was computed for each decade and a bootstrap resampling of the decadal hazard was utilized. Bootstrapping is a statistical method that relies on random sampling of a dataset with replacement in order to assess the accuracy of the sample estimates (Efron and Tibshirani 1994). In this work, accuracy was defined in terms of the 95% confidence intervals. For this analysis, 10,000 bootstrap replicates were generated at each point to reduce the Monte Carlo sampling error (Dixon *et al.* 2011). Figures 2.9-14 illustrate the actual tornado hazard curve shown in Figure 2.8, as well as the upper and lower confidence intervals (CI) for the six locations mentioned in Section 2.3.2.

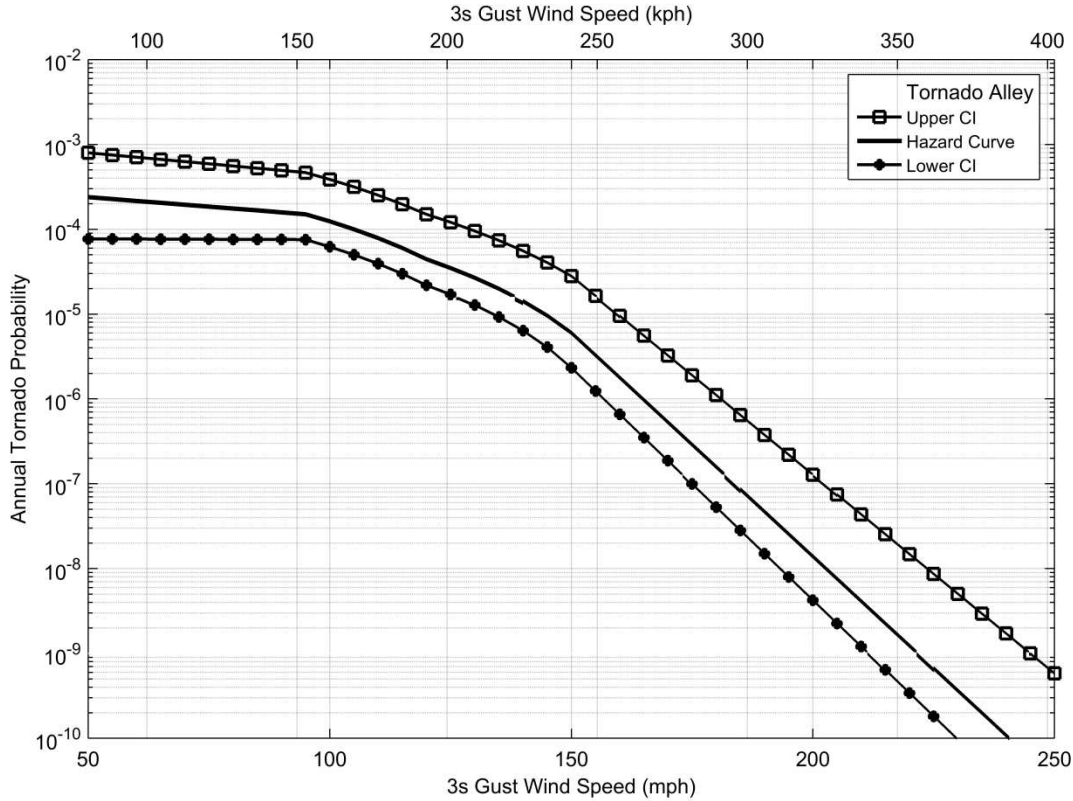


Figure 2.9: Tornado hazard curve and 95% confidence intervals for Tornado Alley. The hazard curve is generated from the probabilistic tornado hazard maps while the upper and lower confidence intervals were obtained from bootstrap resampling.

Figure 2.9 illustrates the tornado hazard curve and 95% confidence intervals for the Tornado Alley location. At this location, the upper and lower confidence intervals are very similar in shape to the actual tornado hazard curve. This was true for even the higher wind speeds and provides confidence in the tornado hazard curve for Tornado Alley. This behavior was not observed for the remaining locations as discussed below. It is hypothesized that the reason for this is due to the tornado climatology in Tornado Alley. While many locations across the country experience year-to-year and seasonal variability in tornado occurrence, Tornado Alley has long been known for its distinct tornado seasonality (Dixon *et al.* 2011). While there

is some year-to-year variability in the number of reported tornadoes, locations in Tornado Alley experience a well-observed tornado season between April and June.

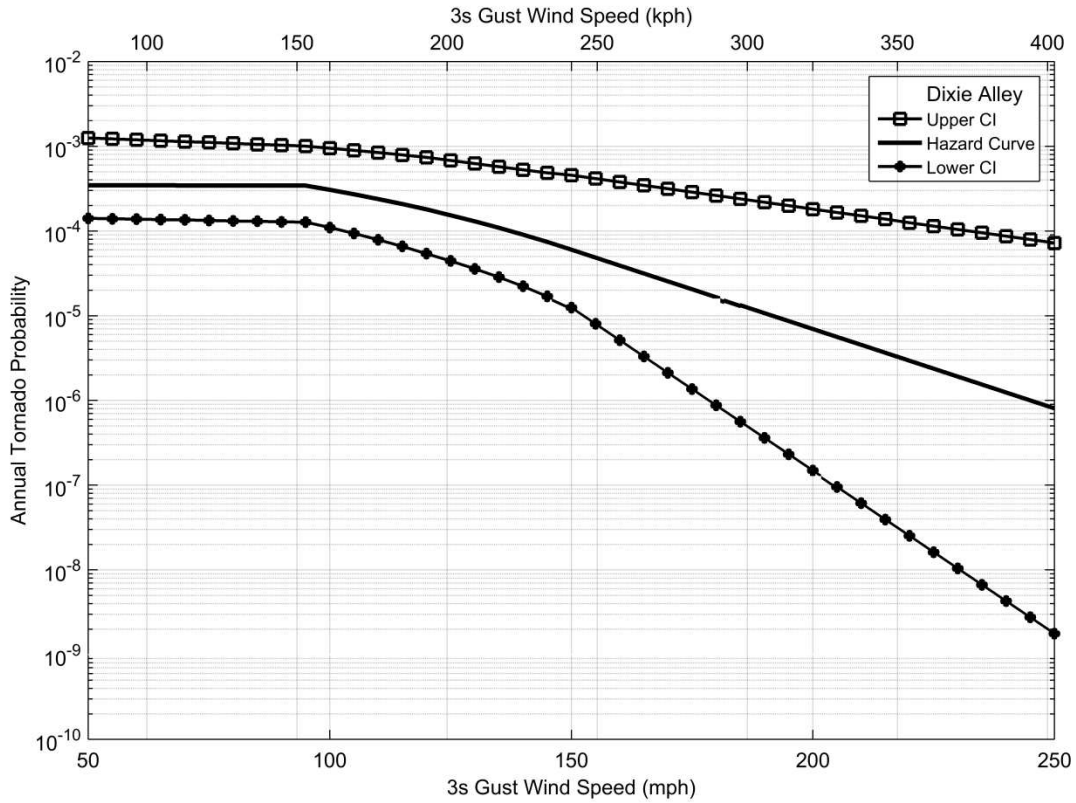


Figure 2.10: Tornado hazard curve and 95% confidence intervals for Dixie Alley. The hazard curve is generated from the probabilistic tornado hazard maps while the upper and lower confidence intervals were obtained from bootstrap resampling.

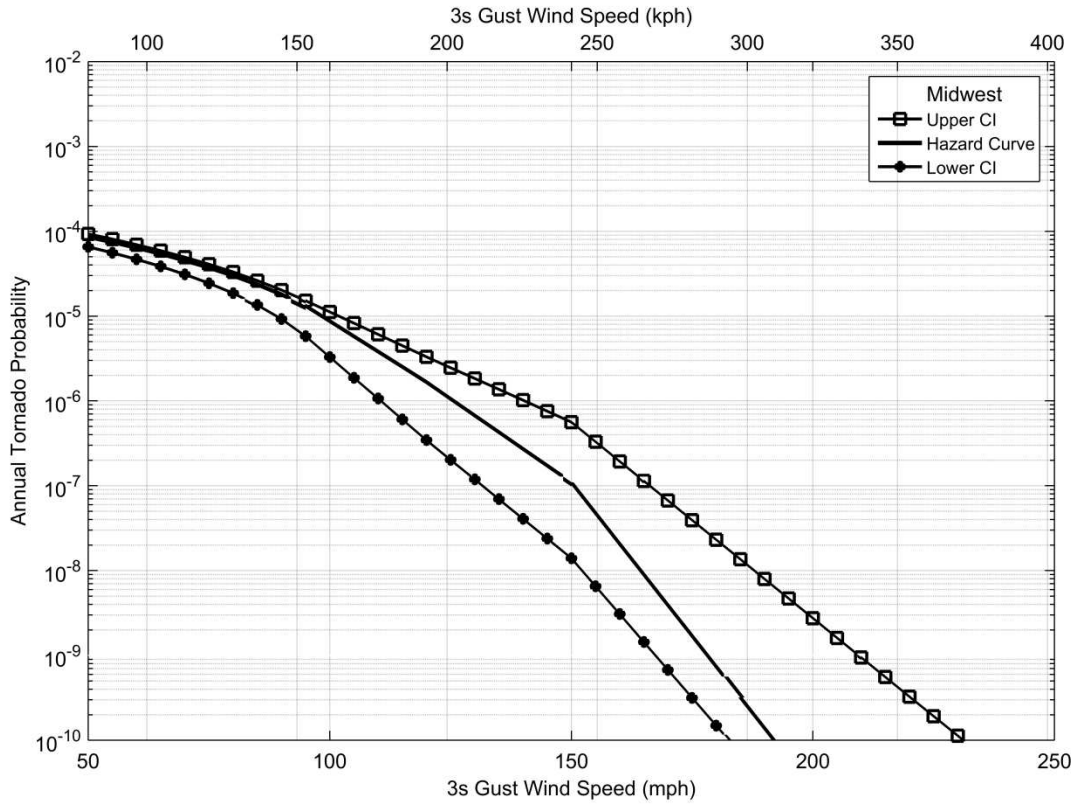


Figure 2.11: Tornado hazard curve and 95% confidence intervals for the Midwest. The hazard curve is generated from the probabilistic tornado hazard maps while the upper and lower confidence intervals were obtained from bootstrap resampling.

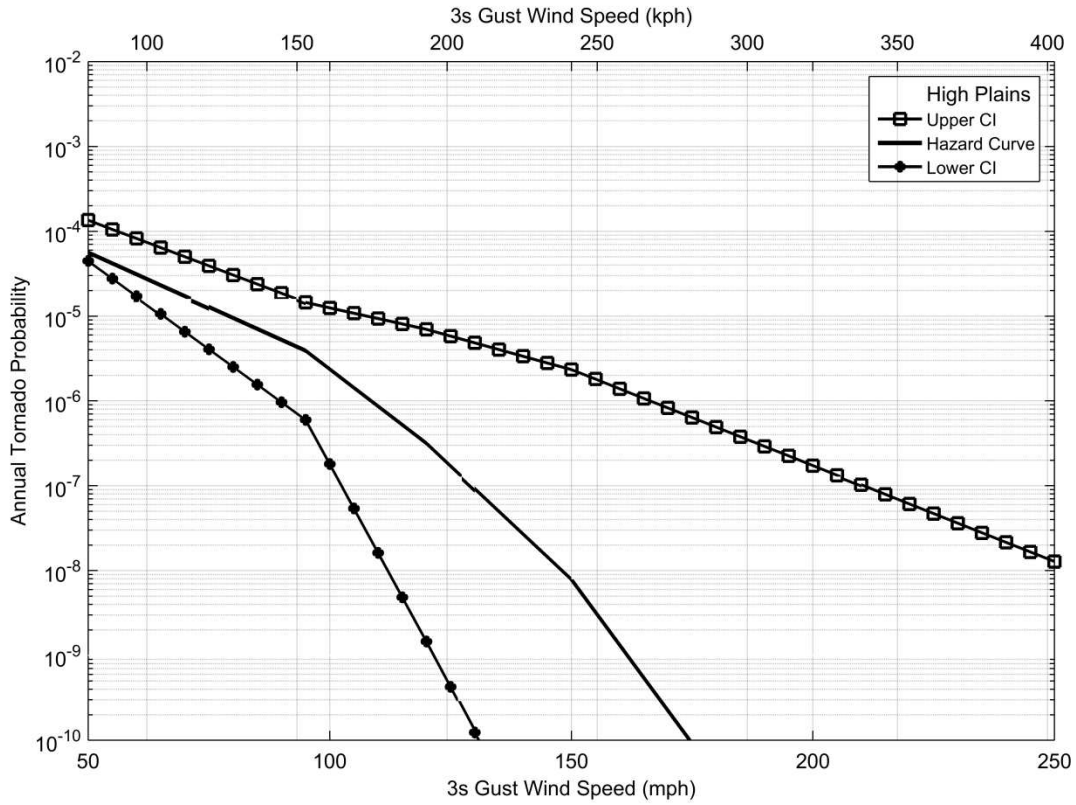


Figure 2.12: Tornado hazard curve and 95% confidence intervals for the High Plains. The hazard curve is generated from the probabilistic tornado hazard maps while the upper and lower confidence intervals were obtained from bootstrap resampling.

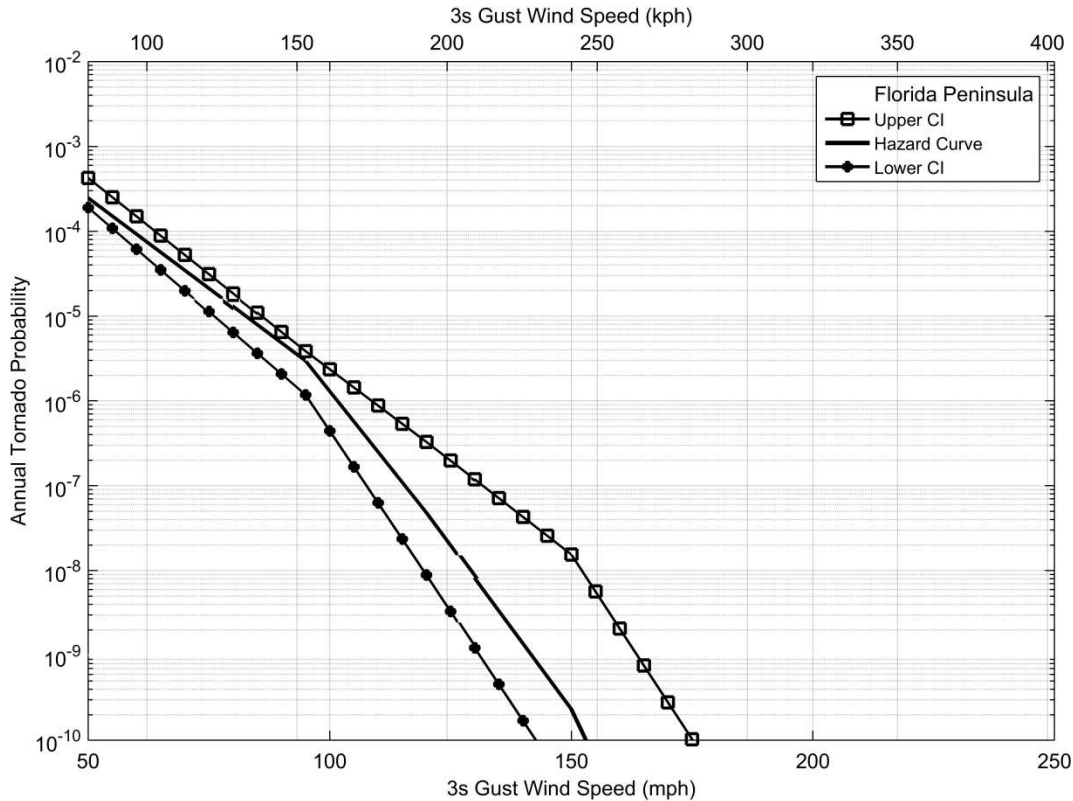


Figure 2.13: Tornado hazard curve and 95% confidence intervals for the Florida Peninsula. The hazard curve is generated from the probabilistic tornado hazard maps while the upper and lower confidence intervals were obtained from bootstrap resampling.

Figures 2.10-13 are the hazard curves and 95% confidence intervals for Dixie Alley, the Midwest, the High Plains, and the Florida Peninsula. These figures do not show a wide spread between the upper and lower confidence intervals until after 161 kph (100 mph) (EF1 tornado). However, as wind speed increases, the lower and upper confidence intervals begin to diverge implying there is limited confidence in the tornado hazard curve for tornado wind speeds rated EF2 or higher. These regions experience moderate to high tornado activity, but there is significant decadal variability with reported tornadoes rated EF3 or higher. For instance, Dixie Alley has a high rate of tornado occurrence especially tornadoes rated EF4 or EF5. However, these violent tornadoes are often associated with large outbreaks, such as the 1974 Super

Outbreak and the historic 2011 season. Unlike Tornado Alley, none of these regions experience a well-defined, yearly tornado season. The difference in tornado climatology in each of these 4 regions is likely the cause of the drastic divergence in tornado risk after 161 kph (100 mph).

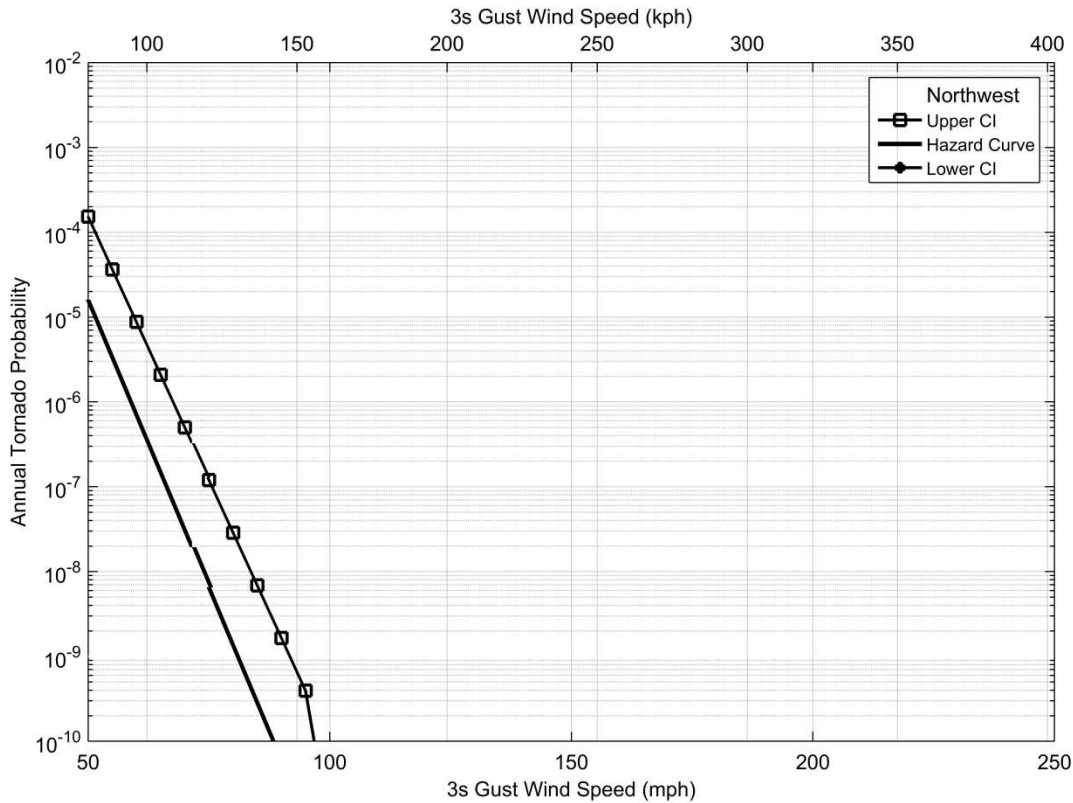


Figure 2.14: Tornado hazard curve and 95% confidence intervals for the Northwest. The hazard curve is generated from the probabilistic tornado hazard maps while the upper and lower confidence intervals were obtained from bootstrap resampling.

Figure 2.14 is the hazard and confidence interval curves for the location in the Northwest. Regions west of the Rocky Mountains do not experience a large number of tornadoes, as evident by the tornado hazard curve in Figure 2.8 and the tornado hazard maps illustrated in Figure 2.6. When developing the confidence intervals via bootstrap resampling, there was no value for the lower confidence interval. This is due to the method employed to create the bootstrap samples in

which the sample was created using replacement. The tornado hazard for the Northwest was calculated for each of the time periods shown in Table 2.5. Due to the limited number of tornadoes in that region of the country, many of the decadal values for the tornado hazard were set to zero since there were no reported tornadoes at that grid point during that time period. The mean tornado hazard at the grid point using bootstrap resampling was determined and was often zero due to the limited tornado reports. Thus, when determining the lower confidence interval, it was zero. As stated before, even though there were only a small number of tornadoes reported at the Northwest location, this does not imply that the tornado hazard itself is zero, but rather it is quite small.

The bootstrap analysis of the tornado hazard curves illustrates that uncertainty associated with the tornado hazard maps. The maps were generated using 38 years of climatological tornado information. Improvements in the tornado database will develop with time, allowing for a clearer understanding of the tornado hazard across the United States. Overall, the assessment described in Chapter 2 has allowed for an understanding of the geographic variability in tornado activity and has highlighted areas of enhanced risk. These regions may benefit from stricter residential design codes as described in more detail in the remaining chapters.

CHAPTER 3

FRAGILITY ANALYSIS

3.1 Introduction to Fragility Analysis

Chapter 2 summarized the development of the tornado hazard maps and curves. This was the initial step necessary to perform an analysis of unconditional failure probabilities described in Chapter 4. In this chapter the fragility analysis of common connections along the vertical load path is presented. These include the roof sheathing, roof-to-wall, and wall-to-foundation connections. In addition, fragility analysis was performed for the vertical load path as a system as discussed in more detail below.

For this work, five structures were selected to represent typical U.S. residential construction and are termed archetypes. These structures were originally developed by Amini and van de Lindt (2014) and the same floor plans and roof pitches were used for consistency in the current analysis. The use of several different residential structures was employed to capture some degree of building-to-building variability. Images of the archetypes are shown in Figures 3.1-3.5.

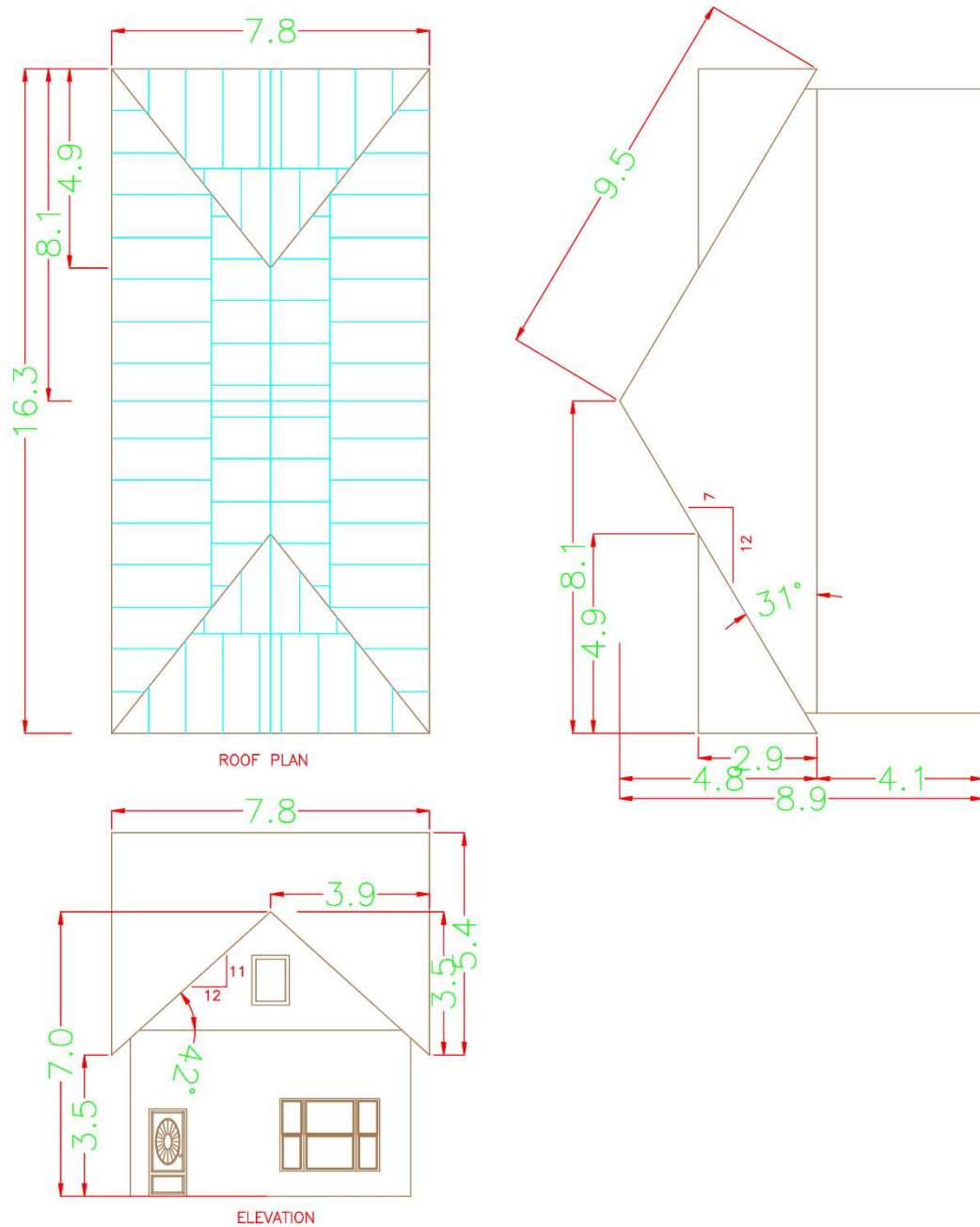


Figure 3.1: Structure Type 1 taken from Amini and van de Lindt (2014). Dimensions are shown in meters.

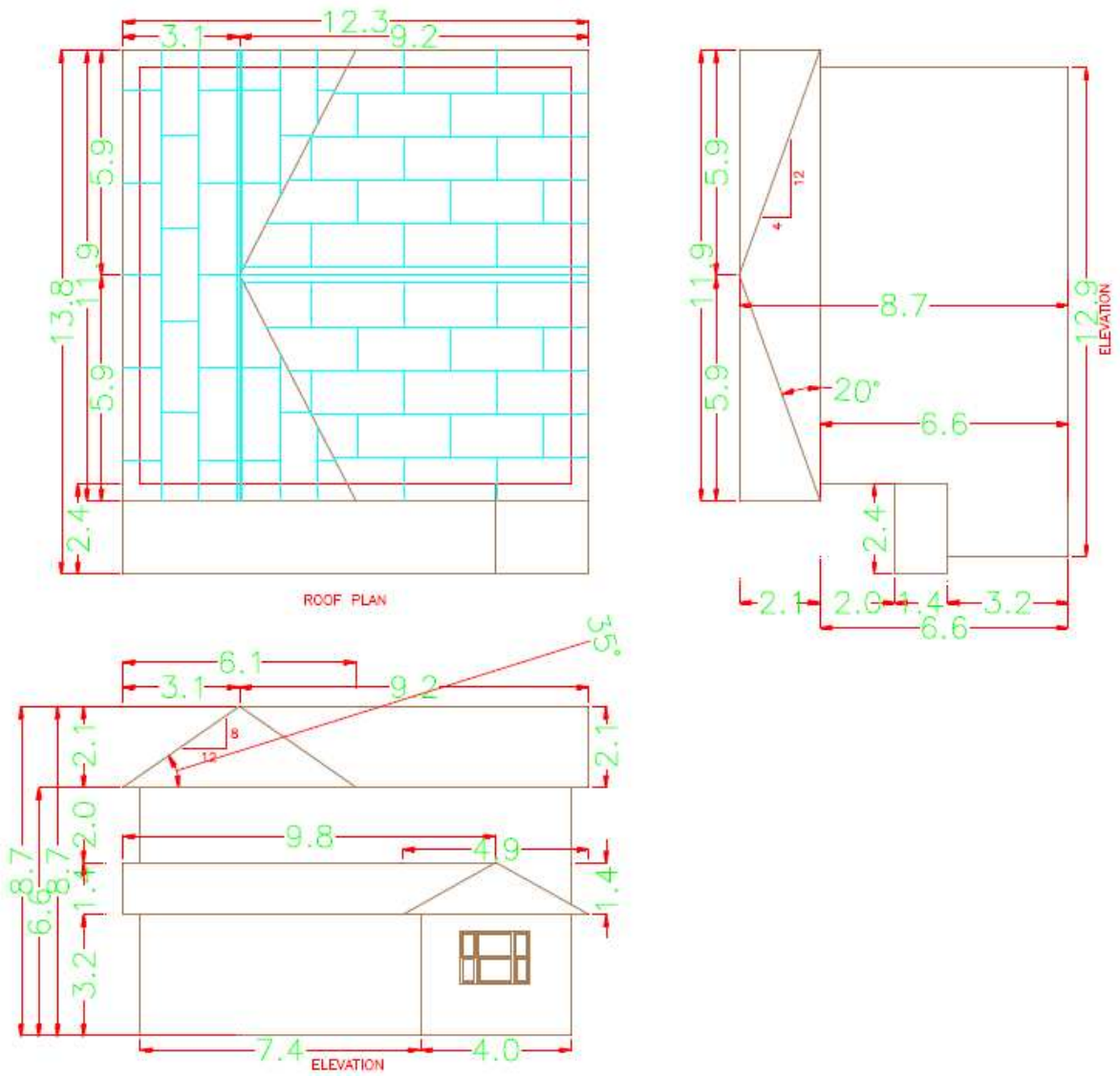


Figure 3.2: Structure Type 2 taken from Amini and van de Lindt (2014). Dimensions are shown in meters.

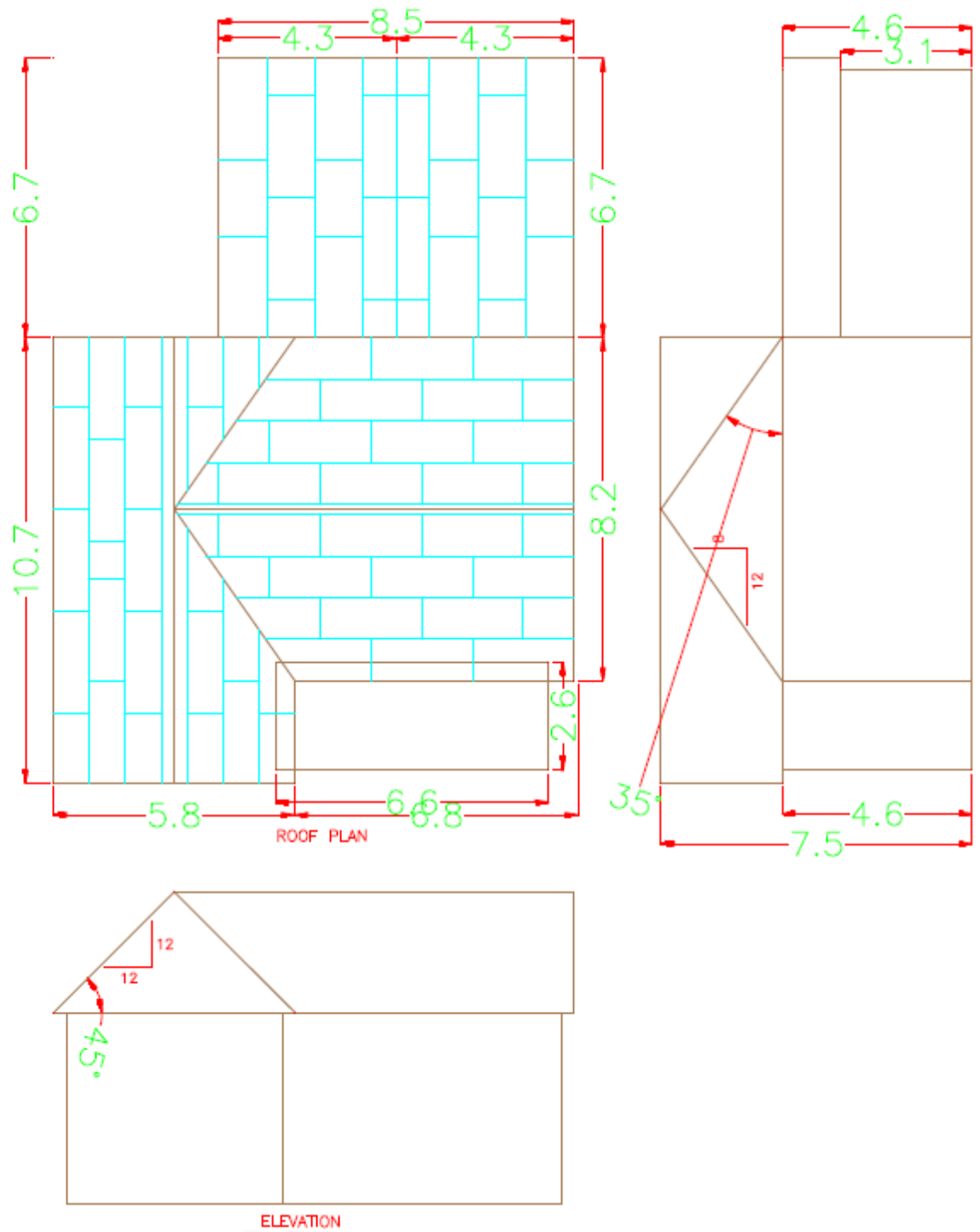


Figure 3.3: Structure Type 3 taken from Amini and van de Lindt (2014). Dimensions are shown in meters.

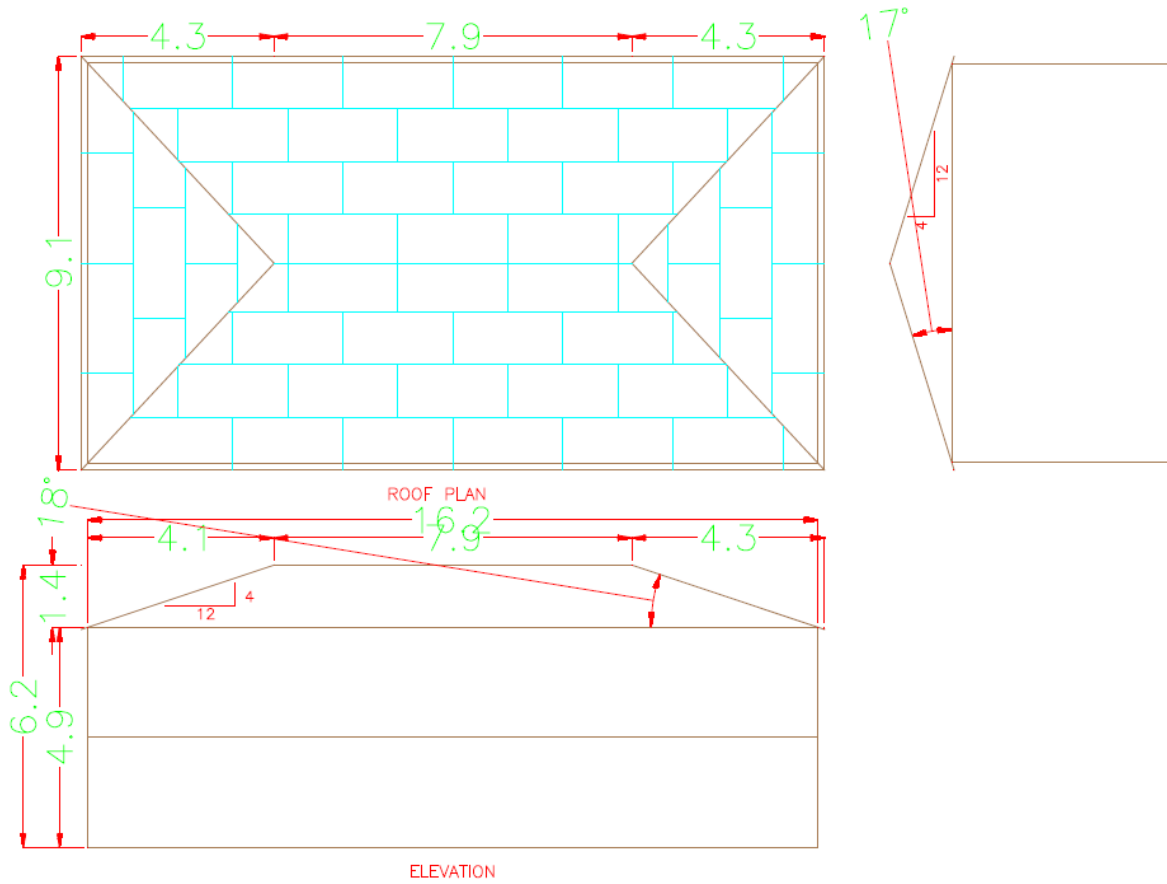


Figure 3.4: Structure Type 4 taken from Amini and van de Lindt (2014). Dimensions are shown in meters.

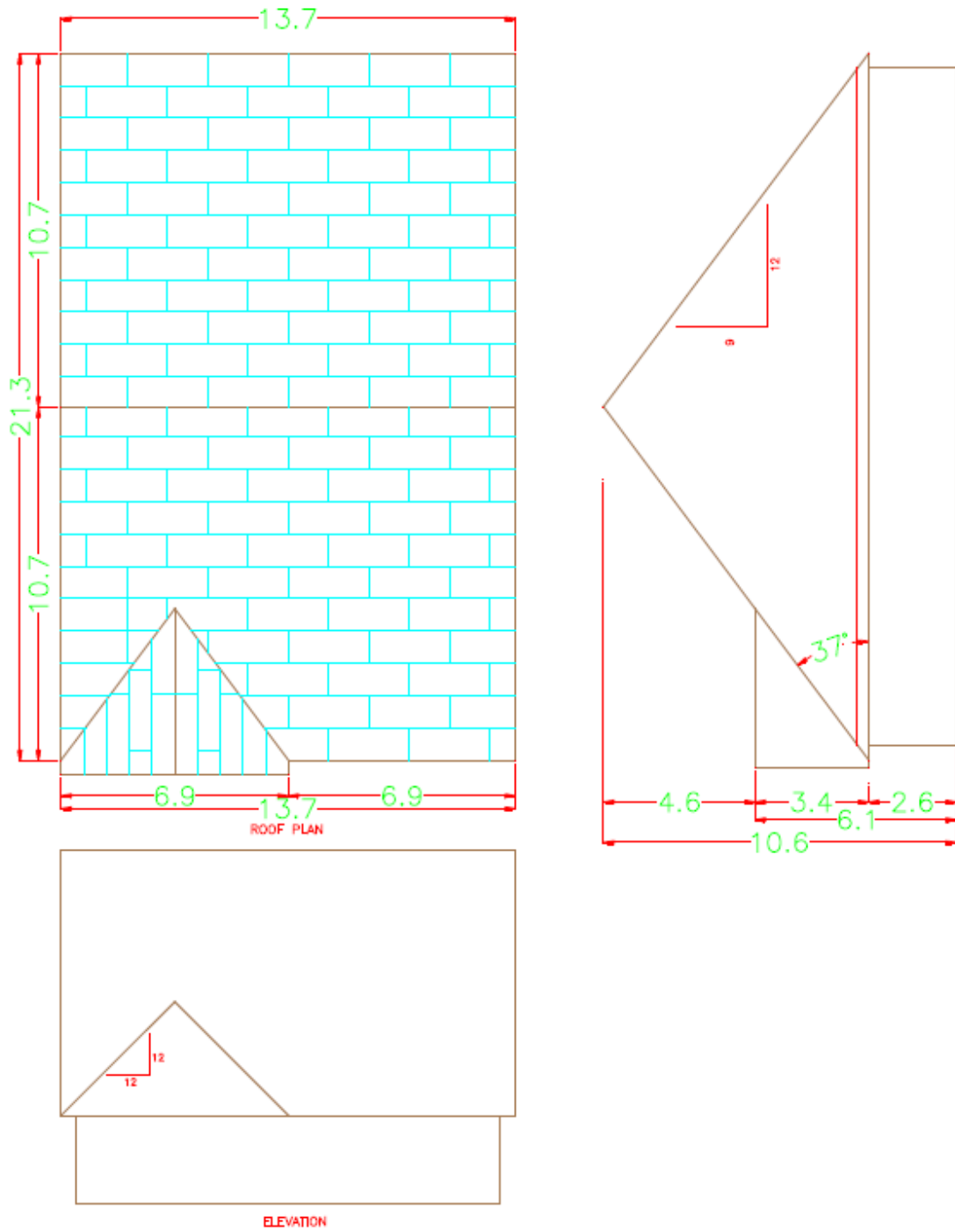


Figure 3.5: Structure Type 5 taken from Amini and van de Lindt (2014). Dimensions are shown in meters.

The fragility of a structure can be modeled using a lognormal distribution (Ellingwood *et al.* 2004, Lee and Rosowsky 2005) given as

$$F(x) = \Phi \left[\frac{\ln(x) - \lambda_R}{\xi_R} \right] \quad (3.1)$$

where $\Phi[\dots]$ is the standard normal cumulative distribution function, R is the capacity, λ_R is the logarithmic median of R , and ξ_R is the logarithmic standard deviation of R . For the purpose of this work, fragility analysis was performed for 3s gust wind speeds. Wind induced loading on a roof can result in failure of several components including the roof sheathing connections, roof-to-wall connections, and/or wall-to-foundation connections. In order to determine the structural performance, a limit state is therefore defined as

$$g(x) = R - (W - D) \quad (3.2)$$

where R is the uplift resistance capacity of the structural component, W is the uplift force due to wind induced loads acting on the structural component, and D is the dead load. When $g(x)$ becomes negative, failure occurs since the demand on the system exceeds the resistance of the connection. The structural components in this dissertation include the roof sheathing connection, roof-to-wall connection, and wall-to-foundation. As indicated in Eqn. 3.2, the dead load acts in a direction opposite of the wind uplift force and is thus beneficial to structural performance under wind loads.

In this dissertation, a probabilistic analysis for component performance was performed using Monte Carlo simulation in order to develop fragility curves. This methodology generates random demand and capacity variables from specified distributions or from statistical parameters of each component, thus allowing for an evaluation of structural performance under wind-induced loading. For this work, wind speeds between 80-402 kph (50-250 mph) were utilized

and component performance was assessed in this range at 8 kph (5 mph) increments. For the roof sheathing, roof-to-wall, and wall-to-foundation connections, the probability of failure at each wind speed was determined using 50,000 Monte Carlo simulations.

3.2 Sample Locations

Six locations were randomly selected across the United States based on their tornado risk. The cities closest to the selected points were used in this work since information on building codes was readily available. The first two cities were selected in regions of high tornado activity, namely Oklahoma City, OK and Winfield, AL in Tornado Alley and Dixie Alley, respectively. Two additional locations were selected in areas with moderate tornado activity including Champaign, IL in the Midwest and Sioux Falls, SD in the High Plains. Punta Gorda, FL was chosen as the location in the Florida Peninsula. Florida experiences a high number of weak tornadoes due to land falling hurricanes, sea breeze interaction, and water spouts moving from the water to land but strong tornadoes are rarer than in Tornado Alley and Dixie Alley. The final location was Fossil, OR in the Northwest U.S. representative of a location with a minimal tornado hazard. Regions west of the Rocky Mountains experience a very low number of tornadoes, however, while there is a low probability of tornado occurrence, the probability is never zero. Thus, a location with minimal tornado activity was selected for completeness. A map with the cities and the region they represent is shown in Figure 3.6.

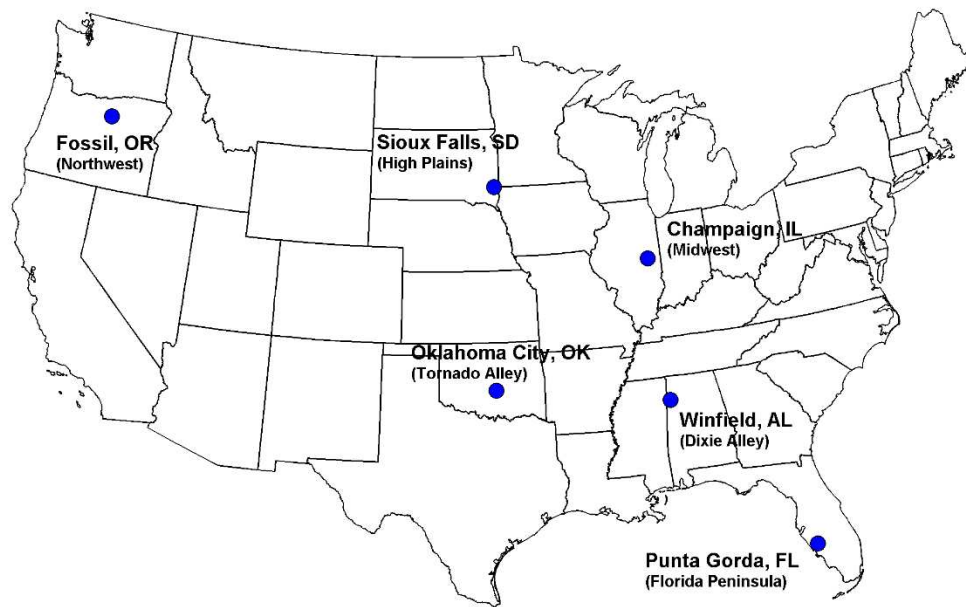


Figure 3.6: Cities and regions investigated in this research (Standohar-Alfano and van de Lindt 2015).

In order to perform fragility analysis, statistics on the resistance, dead load, and wind loads had to be established. Since fragility analysis was being performed at six different locations across the U.S., the current residential building codes at each site had to be considered in order to design the connections and determine the resistance. Table 3.1 summarizes the six locations and the adopted residential building code (if any) at the time of this work. The building codes in Table 3.1 will be referred to as IRC for the International Residential Code, ORC for the Oregon Residential Specialty Code, and FRC for the Florida Residential Building Code proceeded by the code year throughout the rest of this dissertation (i.e. IRC 2009).

Table 3.1: Summary of the 6 select locations and the adopted building code

Region	City	State	Building Code
Tornado Alley	Oklahoma City	Oklahoma	International Residential Code 2009
Dixie Alley	Winfield	Alabama	N/A
Midwest	Champaign	Illinois	International Residential Code 2009
High Plains	Sioux Falls	South Dakota	International Residential Code 2012
Northwest	Fossil	Oregon	Oregon Residential Specialty Code 2011
Florida Peninsula	Punta Gorda	Florida	Florida Residential Building Code 2010

3.3 Uncertainty in Tornado Wind Loads

Wind loading was determined using ASCE wind provisions. However, while loading from straight line and hurricane winds has been extensively documented, there is limited information on tornado wind loads. This is likely due to the difficulties in obtaining direct wind measurements within the tornado vortex itself. There has been significant research done on tornado wind loading in a laboratory setting, yet scientific consensus has not been reached on the best way to interpret and apply experiment results due to the lack of in-situ measurements regarding the magnitude and duration of tornado winds. Some studies have shown that tornadoes result in greater pressure on buildings than straight line winds (e.g. Haan *et al.* 2010). The pressure coefficients in ASCE 7-10 have been developed for straight-line winds. However, with tornadoes, there is a vertical component of the wind vector which is not present in straight line winds. Thus, the results of Haan *et al.* (2010) were used as a method to amplify the wind load from tornadoes by taking into account the vertical velocities of the tornado vortex. Unfortunately, there is no consensus on the actual intensity of the tornado wind loads. Due to this uncertainty, the work presented in this dissertation utilized two methods to estimate the

tornado wind loads as discussed in detail below. The goal of using two different methods was to attempt to bound failure probabilities by incorporating results from wind tunnel data and laboratory simulations of tornadoes.

The first method to determine structural behavior under tornado wind loads utilized ASCE 7-10 wind provisions in conjunction with laboratory simulations of tornadoes (e.g. Haan *et al.* 2010). Using a tornado simulator, Haan *et al.* (2010) were able to calculate the uplift forces imparted on a scale model one story, gable roof, and found that the uplift forces were higher than those calculated from ASCE 7-05 wind provisions for the same reference velocity. For the main wind force resisting system (MWFRS), the uplift coefficients were 1.8-3.2 times larger than those for straight line winds. Likewise, for components and cladding (C&C), the uplift coefficients exceeded estimates from the ASCE wind provisions by a factor of 1.4-2.4. Thus, when calculating wind loads on the structural archetypes used in this method, a tornado amplification factor, K_c , was used to account for the increased uplift consistent with the results of the tornado simulator. This method represents the upper bound on tornado wind loading and would result in higher failure probabilities for a given wind speed due to the inclusion of the tornado amplification factor.

There has been some discussion on appropriateness of the tornado amplification factors to study tornado wind loads (Kopp and Morrison 2011). Unfortunately, however, there is a fundamental gap in knowledge of the near surface tornado wind field which has presented a significant challenge in tornado research. One of the main arguments against the use of the tornado amplification factor is that comparable wind damage would occur at lower wind speeds in tornadoes as compared to straight-line winds. For example, failure of the roof sheathing connection would occur at a lower wind speed in a tornado than in a hurricane or severe

thunderstorm. However, the disparity in damage level and wind speed can likely be attributed to the large uplift forces associated with the tornado vortex itself. A structure subjected to any type of wind experiences uplift as wind moves over a sloped surface, in this case, the roof. In a tornado, the uplift forces associated with the tornado vortex itself can also be substantial and increase the net uplift that a structure experiences with tornado passage. Some analyses have suggested upward vertical velocities as high as 90-215 kph (55-135 mph) at heights ranging from 25-60 m (82-197 ft) above ground level (Davies-Jones *et al.* 2001). Likewise, recent observations with mobile mesonets and tornado probes have recorded atmospheric pressure with tornado passage directly over the instrumentation. Pressure deficits of 5-100 hPa (10-210 psf) were observed over the width of the tornado vortex (Karstens *et al.* 2010). Convergent uplift associated with these pressure drops can result in significant vertical velocities. Likewise, such a drastic change in ambient pressure over such a short distance can result in pressurization of an enclosed structure. Ultimately, without direct, near-surface wind speeds within a tornado, there is no way to validate if tornadoes cause the same damage as straight line winds at a lower velocity. Overall, due to experience in post-disaster investigations including tornadoes and hurricanes and the results of recent laboratory simulations (Mishra *et al.* 2008, Sengupta *et al.* 2008, Haan *et al.* 2010), the tornado amplification factor is utilized in the present study as an upper bound of structural performance subjected to tornado wind loads.

In order to estimate the lower bound fragilities, wind loading was also estimated using ASCE 7-16¹ pressure coefficients. In this case K_c is set to 1 so that no amplification of the wind load is occurring due to the tornado. The ASCE 7-16 provisions represent the best knowledge in pressure coefficients currently available for straight-line winds. These coefficients are notably

¹ It should be noted that at the time of this work ASCE 7-16 was not published. The ASCE 7-16 coefficients used in this dissertation were based on the public review version available at the time.

larger for roof pressures as compared to ASCE 7-10 due to recent wind tunnel test results (Kopp and Morrison 2014). The main difference between ASCE 7-10 and 7-16 is the product of the gust factor, G , and the external pressure coefficient, C_p , for C&C. There is no change in these values for the MWFRS in ASCE 7-16 provisions. Since the tornado wind load was estimated with two different methods, fragility curves for each component will be shown for both the upper and lower bound.

3.4 Wind Load Statistics

The results from Haan *et al.* (2010) and the wind provisions in ASCE 7-10 and 7-16 were used in this dissertation to assess wind loads from tornadoes and associated structural performance. To estimate the wind loads, the structures were classified as Risk Category II and all structures were assumed to be located in Exposure C (open terrain) since tornado winds are not believed to be dependent on the ground surface roughness or fetch length. The wind loading was calculated as

$$W = q_h [GC_p - GC_{pi}] \quad (3.3)$$

where q_h is the velocity pressure at height h , GC_p is product of the gust factor G and external pressure coefficient C_p , and GC_{pi} is the internal pressure coefficient. In order to obtain the velocity pressure, q_h , several parameters had to be estimated. The equation for the velocity pressure is shown below and modified to account for the tornado loading as summarized by Amini and van de Lindt (2014)

$$q_h = 0.613K_zK_{zt}K_dK_cV^2 \quad (3.4)$$

$$q_h = 0.00256K_zK_{zt}K_dK_cV^2 \quad (3.5)$$

where K_z is the velocity pressure exposure coefficient, K_{zt} is the topographic factor, K_d is the wind directionality factor, K_c is the tornado amplification factor calculated by Haan *et al.* (2010), and V is the wind speed (3s gust at 10 m above ground level). In Eqn. 3.4, q_h is in SI with units of N/m^2 and V is in units of m/s . Similarly, in Eqn. 3.5, q_h has units of psf and V is expressed in mph .

The wind loading on the roof sheathing components was estimated using C&C while the roof-to-wall and wall-to-foundation connections used wind loading values for the MWFRS. The roof-to-wall connection was modeled as the MWFRS consistent with Amini (2012). This was under the assumption that diaphragm action of the roof was sufficient enough to model as the MWFRS rather than C&C. The directionality factor, K_d , accounts for the reduced probability of maximum wind speeds coming from a given direction and the reduced probability of the maximum pressure coefficient occurring for any given wind direction (ASCE 7-10). However, the maximum wind speed in tornadoes can occur from any direction, which may exert maximum pressure on buildings from any direction. Thus, K_d was conservatively neglected in the tornado wind load calculation and was set to 1. Similarly, local topographic effects are neglected so that the tornado wind load is not dependent on location. Therefore, K_{zt} was also set to one. The remaining parameters were treated as random variables and information on their statistical characteristics was summarized by Ellingwood and Tekie (1999), Lee and Rosowsky (2005), and Amini and van de Lindt (2014). Table 3.2 summarizes the wind loading parameters. The additional wind load parameters, GC_p and K_z , were not included in Table 3.2 since these values vary based on the five archetype structures and components used in this analysis.

Table 3.2: Values for select wind load parameters

Parameter	Classification	Nominal	Mean	COV	Distribution
K_d		1	-	-	N/A (Deterministic)
K_{zt}		1	-	-	N/A (Deterministic)
K_c^*	MWFRS	1.8-3.2	-	-	Uniform
	C&C	1.4-2.4	-	-	Uniform
GC_{pi}	Enclosed	± 0.18	0.15	0.33	Normal
	Partially Enclosed	± 0.55	0.46	0.33	Normal

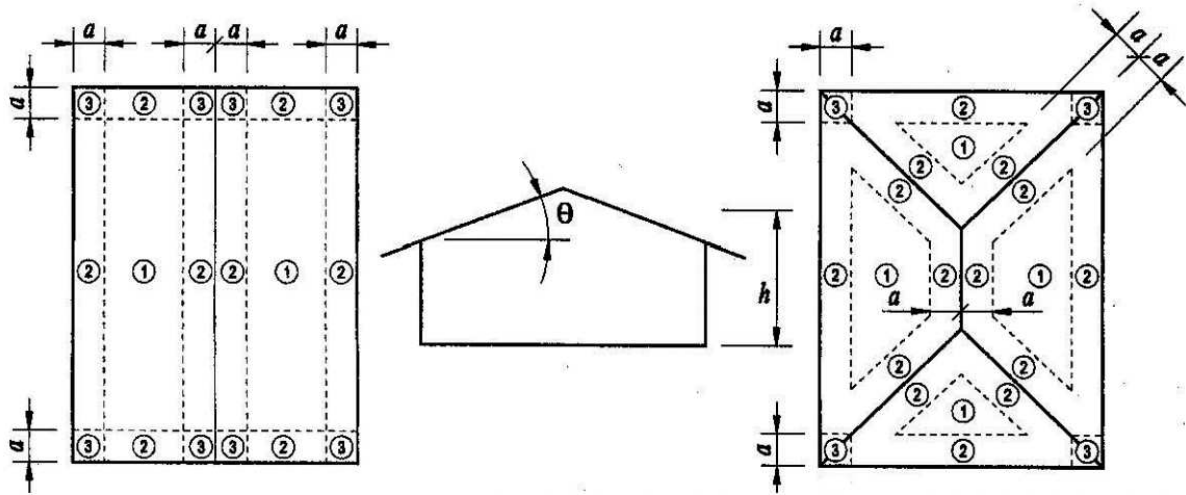
* Note: K_c was set to 1 for both the MWFRS and C&C when estimating the lower bound wind load using ASCE 7-16.

The external pressure coefficient, GC_p , for the roof sheathing was determined using both ASCE 7-10 and 7-16. Sheathing panels along the eaves, ridges, and corners experienced higher values of wind loading as compared to the interior portion of the roof. The external pressure coefficient for roof sheathing varied depending on location on the roof. Likewise, due to continued efforts in estimating wind loads, the external pressure coefficient differed between ASCE 7-10 and 7-16. For ASCE 7-10, the roof was divided into three zones. Interior regions were defined as Zone 1, eaves and ridges were located in Zone 2, and the corner regions were set as Zone 3 (ASCE 2010) as shown in Figure 3.7a. However, the roof zones in ASCE 7-16 varied slightly. There was a distinction between corner regions near the ridge versus the eave (Zone 3r and 3e respectively). Similarly, the edge regions were separated into locations at the ridge and along the eaves both parallel and perpendicular to the wind (Zones 2r, 2n, and 2e respectively). As with ASCE 7-10, Zone 1 is the interior portion of the roof. Figure 3.7b indicates the different roof zones used in ASCE 7-16 wind provisions for either hip or gable roofs.

Using either ASCE provision, the estimation of GC_p had to account for the fact that a single roof panel may be located in multiple zones. Thus, the values of GC_p were found for

individual roof sheathing panels using a weighted average method as described in Lee and Rosowsky (2005). Values for GC_p for each roof panel on each of the five structures using ASCE 7-10 wind provisions can be found in Amini (2012). Similarly, the values for GC_p using ASCE 7-16 are included in Appendix A.

a.) ASCE 7-10



b.) ASCE 7-16

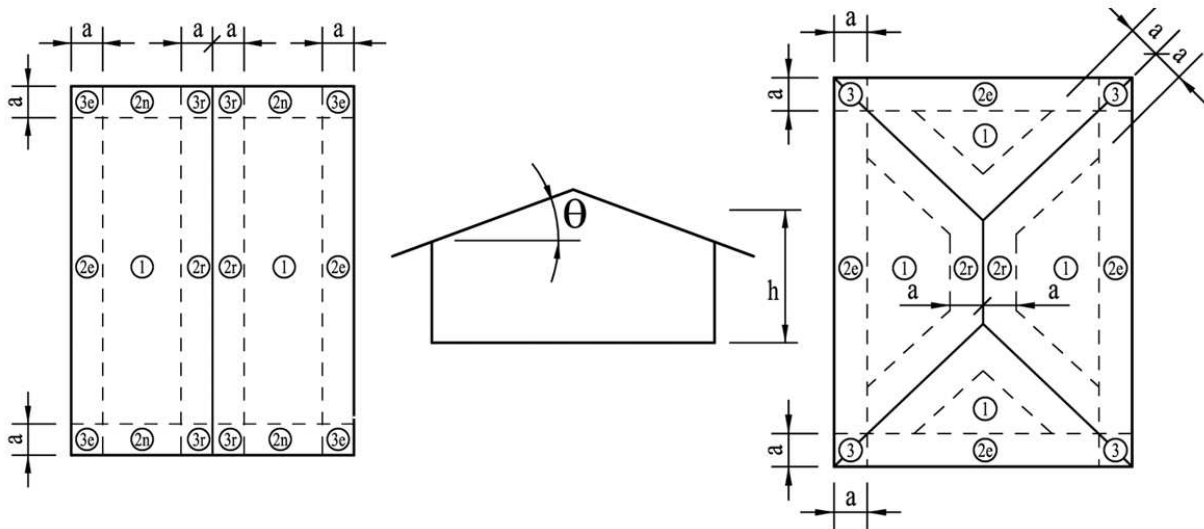


Figure 3.7: Location of roof wind zones for a.) ASCE 7-10 and b.) ASCE 7-16. The left hand side is for gable roofs while the right hand side shows hip roofs (ASCE 2010, Vickery 2015).

The value of K_z was determined for each of the designed structural archetypes and was calculated for the mean roof height. Wind direction refers to the orientation of the wind relative

to the structure therefore an EW wind implies a wind from either the east or west. Figures 3.1-5 assume a northern orientation. For instance, an EW wind would be from either the left or right. Similarly, a NS wind would be from the top or bottom of the page. It is known that wind speed and direction at the center of the tornado can vary significantly during the passage of a tornado. However, structures further away from the center of the tornado experience wind direction comparable to straight-line winds (Roueche and Prevatt 2013) and therefore, determining wind orientation was necessary. The locations on the fringe of the tornado damage path are locations that may most benefit from strengthened construction practices. To determine this, the orientation of the structure was varied with respect to the wind direction so that failure probabilities could be determined from either wind direction.

Table 3.3: Summary of K_z statistics for differing structure types

Structure Type	Wind Direction	Nominal	Mean	COV	Distribution
Type 1	EW	0.91	0.85	0.14	Normal
	NS	0.87	0.81		
Type 2	EW	0.95	0.89		
	NS	0.95	0.89		
Type 3	EW Main	0.90	0.84		
	EW Small	0.85	0.79		
	NS	0.90	0.84		
Type 4	EW	0.88	0.82		
Type 5	EW	0.95	0.89		
	NS	0.91	0.85		

The value of the external pressure coefficient for the roof-to-wall and wall-to foundation connections was found using the MWFRS. The roof-to-wall connection is assumed to experience only uplift forces. Thus, the value GC_p shown on the left hand side of Table 3.4 was used for the roof-to-wall connection. The wall-to-foundation connection is subjected to both uplift and shear loads. The uplift forces are transferred first from the roof sheathing to the roof-to-wall connection and finally to the walls and into the foundation. However, if the roof is removed, the walls are assumed to only experience shear forces. In the event of roof removal, wind loads are applied to the windward walls and are translated as shear forces on walls parallel with the wind. This behavior alters the value of GC_p , which is shown in Table 3.4 for wall racking.

Table 3.4: Summary of GC_p Values for Uplift and Wall Racking

Archetype	Roof or Wall Uplift		Wall Racking		COV	Distribution
	Nominal	Mean	Nominal	Mean		
1	-1.14	-0.92	0.98	0.78		
2	-0.94	-0.75	1.14	0.91		
3	-0.93	-0.75	1.11	0.89	0.17	Normal
4	-0.92	-0.74	1.14	0.91		
5	-0.97	-0.78	1.19	0.95		

Finally, for this dissertation, windborne projectiles (debris) were not included allowing for the assumption the structures remain nominally sealed and enclosed. Future work should include the impact of breaching the building envelope due to debris penetration which is recognized to be very important in tornado damage modeling.

3.5 Dead Load and Resistance Statistics

An extensive literature review was performed to obtain the statistics for the three main connections along the vertical load path. These statistics vary based on the type and size of the sheathing, nail type, nail spacing, fastener used, etc. Since different residential building codes were considered, these statistics were also dependent upon the building code at each of the locations. Thus the statistics for the roof sheathing, roof-to-wall, and wall-to-foundation connections varied as a function of location and are described in the following sections.

3.5.1 Roof Sheathing Connection

Tables 3.5-3.6 summarize information on the resistance and dead load statistics for the roof sheathing components from the limit state equation. The statistics shown in Table 3.5 are for 1.22 m x 2.44 m (4 ft x 8 ft) plywood sheathing with thickness based on code specifications.

The location in Dixie Alley had not adopted a residential code adoption, so 12 mm (15/32 in) sheathing was specified based on observations from tornado damage surveys (van de Lindt *et al.* 2013). The FRC 2010 specifies that sheathing be attached with 8d ring shank nails (63.5 mm (0.5 in) length, 2.87 mm (0.113 in) shank diameter). The remaining building codes used 8d common nails (63.5 mm (2.5 in) length, 3.33 mm (0.131 in) shank diameter) to attach roof sheathing. There were two different nailing schedules used: 150 mm/150 mm (6 in/6 in) and 150 mm/300 mm (6 in/12 in). The first number indicates the spacing along the edge of the sheathing panel while the second number indicates the field nailing or the nail spacing at interior locations. The FRC 2010 specifies a nail spacing of 150 mm/150 mm while the remaining building codes specify the roof sheathing nail schedule of 150 mm/300 mm.

Table 3.5: Roof sheathing statistics for panel uplift resistance based on local residential building code

Building Code	Nail	Spacing (mm/mm (in/in))	Mean (kPa (psf))	COV	Distribution	Source
AL Construction	8d common	150/300 (6/12)	2.76 (57.7)	0.2	Normal	Lee and Rosowsky 2005
IRC 2009	8d common	150/300 (6/12)	2.76 (57.7)	0.2	Normal	Lee and Rosowsky 2005
FRC 2010	8d ring shank	150/150 (6/6)	12.08 (252.4)	0.07	Lognormal	Datin 2011
ORC 2011	8d common	150/300 (6/12)	2.76 (57.7)	0.2	Normal	Lee and Rosowsky 2005
IRC 2012	8d common	150/300 (6/12)	2.76 (57.7)	0.2	Normal	Lee and Rosowsky 2005

Table 3.6: Roof sheathing statistics for panel dead load based on local residential building code

Building Code	Thickness (mm (in))	Mean (kPa (psf))	COV	Distribution	Source
AL Construction	12 (15/32)	0.168 (3.5)	0.1	Normal	Lee and Rosowsky 2005
IRC 2009	16 (0.625)	0.192 (4.0)	0.1	Normal	Lee and Rosowsky 2005
FRC 2010	16 (0.625)	0.192 (4.0)	0.1	Normal	Lee and Rosowsky 2005
ORC 2011	16 (0.625)	0.192 (4.0)	0.1	Normal	Lee and Rosowsky 2005
IRC 2012	16 (0.625)	0.192 (4.0)	0.1	Normal	Lee and Rosowsky 2005

Statistics on roof sheathing uplift capacity for 8d ring shank nails with a 150 mm/150 mm nail spacing and sheathing thickness of 16 mm (0.625 in) were not available. Therefore the statistics for 8d ring shank, 150 mm/150 mm, 13 mm (0.5 in) sheathing were used (12.08 kPa). Since FRC (2010) requires 16 mm (0.625 in) sheathing, using the statistics for 13 mm (0.5 in) sheathing will result in slightly conservative results when comparing the FRC 2010 to other regions of the U.S. The dead load statistics for 16 mm (0.625 in) sheathing was computed based on the values provided for 12 mm (0.469 in) sheathing by Lee and Rosowsky (2005). Their estimate included the weight of the sheathing, shingles, and other roof components. Therefore, the dead load weight of only wood structural sheathing was obtained from the Engineered Wood Association (APA 2011) in order to find the dead load statistics for the 16 mm (0.625 in) sheathing. The estimate of the dead load for the 12 mm (0.469 in) and 16 mm (0.625 in) sheathing was 0.067 kPa (1.4 psf) and 0.091 kPa (1.9 psf), respectively. Thus, the 16 mm (0.625 in) sheathing was 0.024 kPa (0.5 psf) heavier than the 12 mm (0.469 in) sheathing, so 0.024 kPa (0.5 psf) was added to the dead load statistics obtained from Lee and Rosowsky (2005). The coefficient of variation (COV) and distribution were assumed to remain the same.

3.5.2 Roof-to-Wall Connection

The statistics for the roof-to-wall connections were obtained based on the residential building code adopted at each location. Since the location in Dixie Alley did not have an adopted residential building code, the connection was determined based on observations from several tornado damage surveys after the devastating April 27, 2011 tornado outbreak (Dao 2014). Table 3.7 provides information on the roof-to-wall connection for each of the residential building codes used in this work.

Table 3.7: Roof-to-wall uplift resistance statistics based on local residential building code

Building Code	Connection	Mean (kN (lb))	COV	Distribution	Source
AL Construction	3-10d common toe nail	0.94 (211)	0.16	Normal	van de Lindt <i>et al.</i> 2012
IRC 2009	3-16d box toe nail	2.34 (525)	0.16	Normal	Shanmugam <i>et al.</i> 2008
FRC 2010	1-H2.5 clip	5.84 (1312)	0.12	Normal	Reed <i>et al.</i> 1997
ORC 2011	2-16d box toe nail	1.56 (350)	0.16	Normal	Shanmugam <i>et al.</i> 2008
IRC 2012	3-16d box toe nail	2.34 (525)	0.16	Normal	Shanmugam <i>et al.</i> 2008

Toe nailing is a common method to connect the roof rafters and top plate of walls and is shown in Figure 1.3. Nails are driven at an approximate 30° angle into the roof rafter 1/3 from the bottom. The nails are then able to penetrate both the rafter and the top plate connecting the roof to the walls. The type and number of nails used in this type of connection varied based on geographic region in the U.S. The H2.5 hurricane clip is a connection type specified in some

hurricane prone regions including Florida and is shown in Figure 3.8. This clip ties the roof framing members to the wall to better resist high wind loads. Statistics for this connection assume that the H2.5 clip is installed per the manufacturer recommendations.

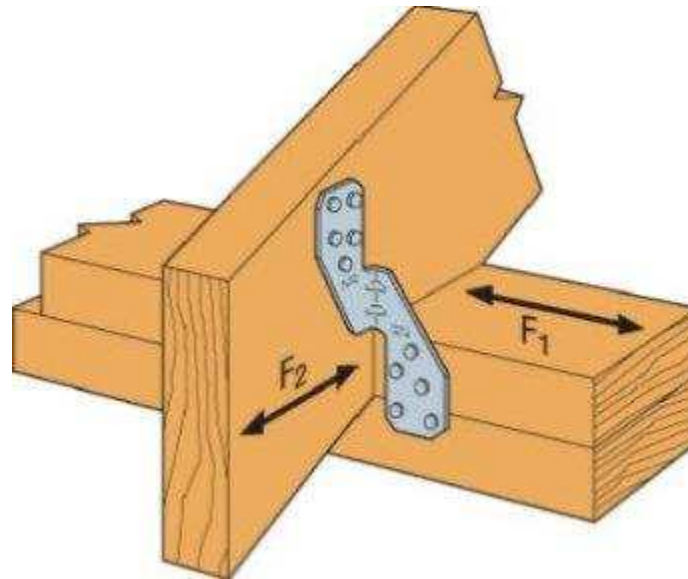


Figure 3.8: Simpson Strong-Tie H2.5 reinforcing clip connecting the roof rafter to a double top plate (Simpson Strong-Tie 2014a).

As discussed earlier, some of the values for the uplift resistance statistics were not immediately available from the literature and thus ratios between similar connections were used. The values for the 3-16d box toe nail connection were found by multiplying the uplift resistance of the 2-16d box toe nail capacity in Shanmugam *et al.* (2008) by 1.5. Similarly, the value for the 3-10d common toe nail was multiplied by 0.6 based on statistics from van de Lindt *et al.* (2012) for a 5-10d common toe nail connection. The authors chose to use the ratios of the number of nails due to the significant variability in capacity resulting from the type of nails, grade, moisture content, and wood. However, there has been research (Morrison and Kopp 2011) in the capacity of differing toe-nailed connections which may be considered in future work. As before, the COV and statistical distribution type were assumed to remain the same for

each of the connections found using this ratio approach. In addition, the dead load for the roof-to-wall connection was 0.717 kPa (15 psf) (Ellingwood *et al.* 2004).

3.5.3 Wall-to-Foundation Connection

Fragility analysis was also performed on the wall-to-foundation connection, since this is another critical component in transferring wind induced loads from the structure to the foundation. It is important to assess the performance of wood shear walls subjected to combined shear and uplift forces since this was similar to conditions experienced during a tornado, however this information was not readily available.

In order to perform fragility analysis for the wall-to-foundation connection, interaction curves were developed to assess the relationship between racking and uplift forces on wood shear walls. It is known that structures subjected to wind loads experience both uplift and shear simultaneously and recent studies have assessed this behavior (Yeh *et al.* 2009, Winkel and Smith 2010). Yeh *et al.* (2009) performed several experiments on combined shear and uplift using anchor bolts spaced 40.5 cm (16 in) on center. Likewise, Winkel and Smith (2010) did multiple tests to study behavior of walls subjected to in-plane and out-of-plane forces. In-plane forces (shear and uplift) were applied at a 1:1 ratio using wall anchorage spaced 61 cm (24 in) on center. While these studies are useful when determining shear wall behavior, neither study performed laboratory simulations using wall anchorage prescribed (and typically found) in current residential building codes, specifically with regard to anchor bolt spacing. Thus, laboratory testing of wood shear walls was performed at Colorado State University using wall specifications similar to current residential building codes. Results from these experiments were used directly in the subsequent fragility analysis.

Uplift forces are transferred to the wall from the roof-to-wall connection. It is assumed there is a continuous vertical load path existed when studying the wall-to-foundation connection for both one and two story structures (Amini 2012). Therefore, the roof sheathing and roof-to-wall connections continue to transfer the wind load without failure. The next portion of this work will address the performance of the entire system as a whole and takes into account all components along the vertical load path.

As described in Eqn. 3.2, the limit state for uplift includes the resistance, dead load, and wind load on the system. The dead load acts in a direction opposite of the wind load and is beneficial to the system. Thus, as long as the wind load is less than the dead load, the wall-to-foundation connection will not experience uplift forces and its performance is based on wall racking, not uplift. Therefore, the limit state when the wall-to-foundation connection experiences shear only is defined as

$$g(x)=R-W \quad (3.6)$$

where R is the racking resistance of the wall and W is the shear load applied to the wall. As before, once $g(x)$ becomes less than zero, failure is assumed to have occurred. Similarly, once the uplift forces exceed the roof dead load, the limit state for the wall performance is defined using Eqn. 3.2 and the wall resistance is found using an interaction curve.

3.5.3.1 Wall Test Specimen Descriptions

Shear wall testing was performed for four different wall types, termed Wall Types A-D, so that shear/uplift behavior could be assessed and interaction curves developed. The designs of Wall Types A-D were selected to model common construction practices at the six locations shown in Figure 3.6. There were a total of five walls tested for each wall type, each with varying

amounts of shear and uplift. This resulted in a total of 20 walls tested in the structural engineering laboratory at Colorado State University.

Wall dimensions were identical at 2.44 m by 2.44 m (8 ft by 8 ft) and were all framed in a similar manner. The materials used for framing the walls were the same for all 20 specimens. Studs were spaced 41 cm (16 inches) on center and were bottom nailed to a single bottom plate and double top plate using 16d common nails (89 mm (3.5 in) length, 4.11 mm (0.162 in) shank diameter). The wall construction is shown in Figure 3.9. The framing material was 2x4 dimension lumber (38.1 mm by 88.9 mm (1.5 in by 3.5 in)) No. 2 white fir purchased from a local lumber yard. The dimension members were kiln dried with estimated moisture content below 14%, which would be typical in-situ for an existing residential building. The walls were sheathed with 11 mm (0.438 in) oriented strand board (OSB) rated W24. Sheathing was attached with 8d common nails (63.5 mm (2.5 in) length, 3.33 mm (0.131 in) shank diameter).

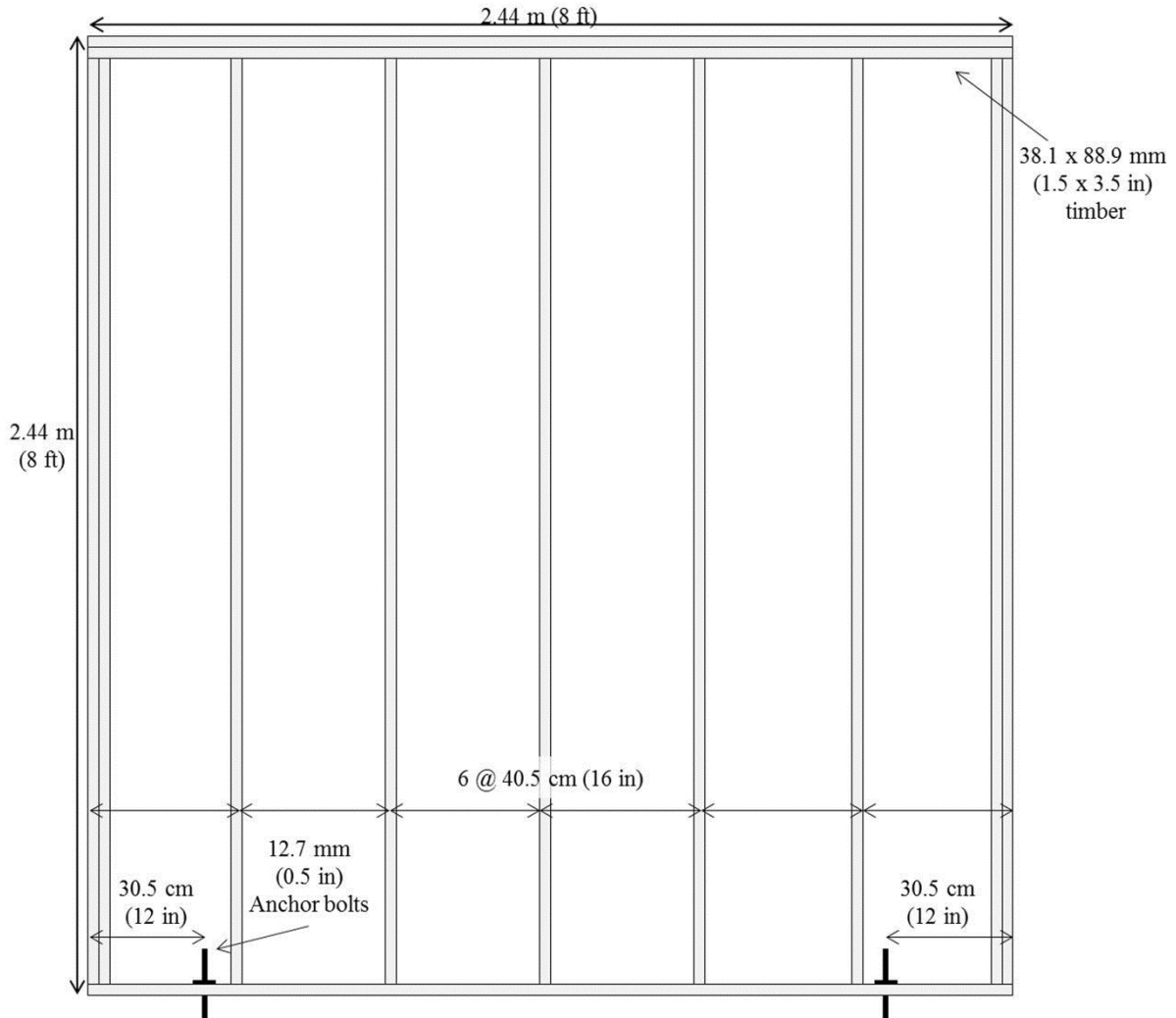


Figure 3.9: Design of the wood shear walls used in this study (wall sheathing not shown).

The differences between Wall Types A-D were based on the sheathing nail pattern and the inclusion of reinforcing ties. Wall Type A was designed with a sheathing nail spacing of 150 mm/300 mm (6 in/12 in). The first number indicates the edge nailing, signifying that the fasteners were spaced every 150 mm (6 inches). The second number is the field nailing of the sheathing to the interior studs, which was every 300 mm (12 inches). Wall Type B was similar to Wall Type A except that the sheathing nailing schedule was 102 mm/300 mm (4 in/12 in).

Thus there was a closer nail edge nail spacing for Wall Type B than Wall Type A. Both Wall Type A and B did not include reinforcing stud plate ties.

Wall Type C and Wall Type D had the same sheathing nail patterns as Wall Type A and Wall Type B, respectively. However, Wall Type C and Wall Type D were constructed using reinforcing stud plate ties. The RSP4 tie manufactured by Simpson Strong-Tie was used for reinforcing the walls. The stud plate ties are illustrated in Figure 3.10 and can be attached from the wall studs to either the bottom plate or double top plate. They were installed per manufacturer recommendations with Simpson Strong-Tie 8dx1 ½ nails (38.1 mm (1.5 in) length, 3.33 mm (0.131 in) shank diameter). Table 3.8 summarizes the wall types, construction, and loading protocol.

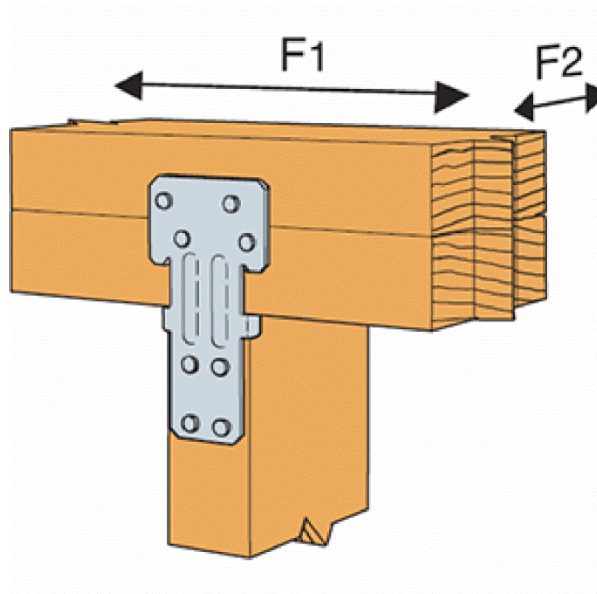


Figure 3.10: Simpson Strong-Tie RSP4 stud plate tie used as reinforcement for Wall Types C and D (Simpson Strong-Tie 2014b).

Table 3.8: Summary of Wall Types and Loading Protocol

Wall Type	Specimen Number	Sheathing Nail Pattern (mm/mm)	Reinforcing Ties	Uplift Percentage
A	SP01	150/300	None	100%
	SP02	150/300	None	75%
	SP03	150/300	None	50%
	SP04	150/300	None	25%
	SP05	150/300	None	0%
B	SP06	102/300	None	100%
	SP07	102/300	None	75%
	SP08	102/300	None	50%
	SP09	102/300	None	25%
	SP10	102/300	None	0%
C	SP11	150/300	RSP4	100%
	SP12	150/300	RSP4	75%
	SP13	150/300	RSP4	50%
	SP14	150/300	RSP4	25%
	SP15	150/300	RSP4	0%
D	SP16	102/300	RSP4	100%
	SP17	102/300	RSP4	75%
	SP18	102/300	RSP4	50%
	SP19	102/300	RSP4	25%
	SP20	102/300	RSP4	0%

3.5.3.2 Test Set Up

A test frame was built with lateral restraints so that the wall would remain in-plane when loaded. The walls were tested with three main components: (1) the base, bolted to the floor of the structural laboratory, (2) a horizontal actuator to apply shear loads, and (3) two horizontal actuators connected to a loader bar which applied a uniform uplift. Each specimen was bolted to the base with 12.7 mm (0.5 in) anchor bolts, consistent with current residential design guidelines. The shear load was applied with a horizontal actuator and the uplift was applied with two vertical actuators as shown in Figure 3.11. Furthermore, a loader bar was connected to all three actuators as well as to the double top plate of each wall specimen with threaded bolts and 51 mm (2 in) flat square washers. A hydraulic pump was used to first load the uplift actuators to their specified

intensity. Once the desired uplift force was reached, the horizontal actuator was activated and shear load was applied to each wall until failure.

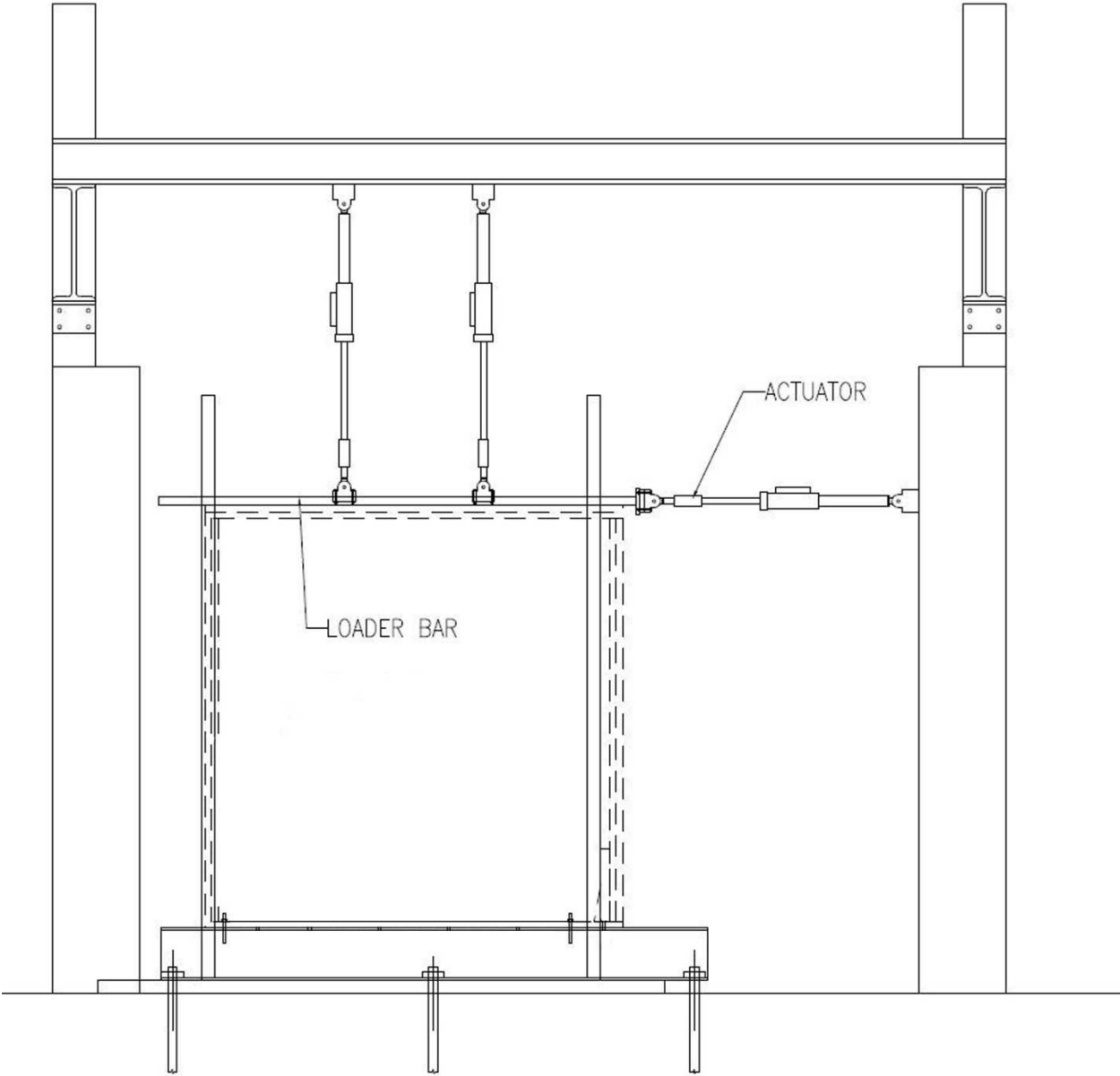


Figure 3.11: Experimental set-up for the combined shear and uplift test (modified from Bahmani 2014).

3.5.3.3 Test Procedure

The first specimens of each wall type (SP01, SP06, SP11, and SP16) were first loaded with pure uplift without any contribution from shear forces. The maximum value of uplift force was documented from the load data and was then assigned to be the uplift capacity of each particular wall type. After this value was determined, the remaining walls were loaded with 75%, 50%, and 25% of the estimated uplift capacity found from the pure uplift simulations. Once the specified uplift was reached, the horizontal actuator moved in displacement control until failure was achieved. The final walls of each wall type were tested in pure shear without any contribution from uplift forces. By varying the amount of uplift and the associated shear capacity, interaction curves were developed for each wall type.

3.5.3.4 Test Results

Each of the 20 walls was tested until failure and the performance of each wall and failure mode were documented with video and photographs. The walls without reinforcing stud plate ties (SP01-SP10) commonly failed due to nail withdrawal between the walls studs and bottom plate as shown in Figure 3.12. The walls with stud plate ties failed when the wood split around the anchor bolts as illustrated in Figure 3.13. There were not any observed failures of the reinforcing ties themselves.



Figure 3.12: Commonly observed failure with Wall Types A and B due to nail withdrawal.



Figure 3.13: Commonly observed failure with Wall Types C and D due to the wood splitting around the anchor bolt.

Interaction curves were developed using the applied uplift and the maximum value of shear at failure. As expected, as the uplift forces increased, the shear capacity decreased as

illustrated from the interaction curves shown in Figure 3.14. The axes of the interaction curve were normalized so that they could be applied to any length shear wall.

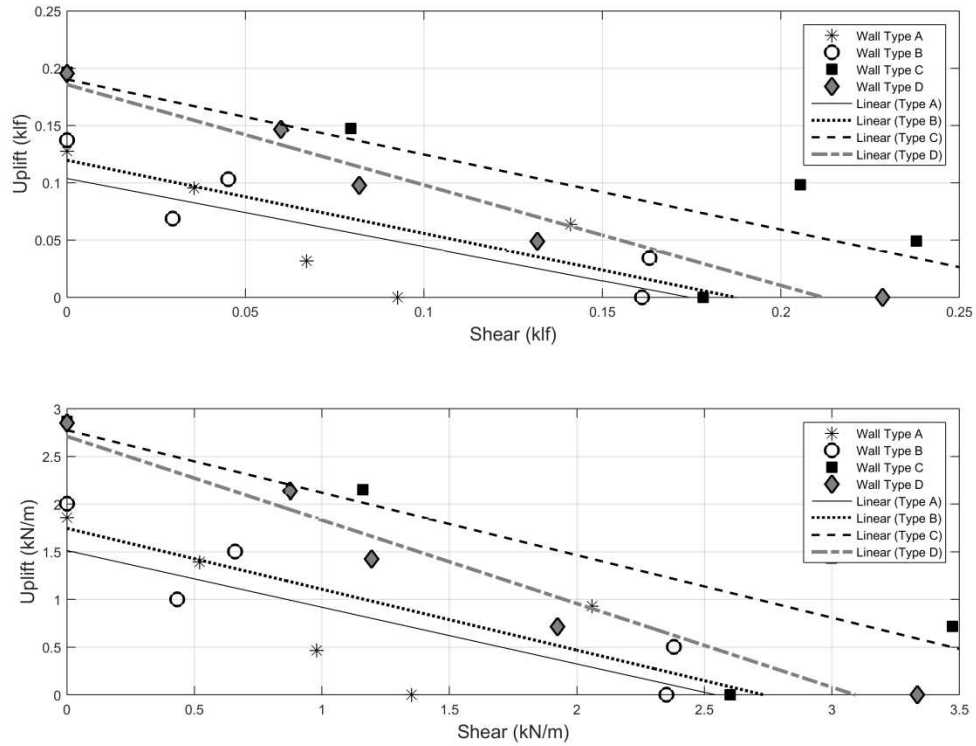


Figure 3.14: Interaction curves for Wall Types A-D. The top figure is in klf and the bottom figure is in kN/m.

In order to perform the fragility analysis, the results of the shear wall testing were used to determine the resistance of each wall type. This was performed iteratively using the interaction curves shown above in Figure 3.14. First, the uplift on the wall was calculated using Eqns. 3.3 and 3.4 (or 3.5) for wind speeds between 80-400 kph (50-250 mph) at 8 kph (5 mph) increments. The uplift was compared to the dead load carried by the wall. If the magnitude of the uplift was less than the dead load, wall performance was dictated by Eqn. 3.6 where R was the wall shear resistance obtained using the wall capacity of SP05, SP10, SP15, and SP20 for Wall Types A, B,

C, and D, respectively. The wind load, W , was found by converting the wind load on the windward wall to a shear force. Consistent with Amini (2012), only 70% of the wall length was assumed to be shear walls to account for any openings such as windows or doors.

Once the uplift exceeded the dead load, Eqn. 3.2 was used to determine wall performance. R was determined using the ratio of shear and uplift and the interaction curves. Table 3.9 summarizes the interaction curves and COV used to calculate the resistance statistics. R is the uplift resistance of the wall and S is the shear applied to the wall, calculated at every wind speed. The COV for Wall Type A is unusually large due to the performance of one shear wall during testing. This particular wall performed significantly better than remaining specimens built with the same specifications as indicated in Figure 3.14 with the right-most point of Wall Type A. Nevertheless, the remaining COVs are consistent with variability of typical wood-frame construction. The wind load, W , was calculated as the uplift of the wall based on Eqn. 3.3 and the roof tributary area for a given wall segment. The dead load was calculated individually for each archetype and accounted for the weight of the roof and wall, as well as the weight of any additional floors if the structure was more than one story. Table 3.10 includes a summary of the dead load statistics used in the wall-to-foundation analysis.

Table 3.9: Resistance Statistics for the Wall-to-Foundation Connection

Wall Type	Interaction Curve	COV
A	$R=-0.59*S+0.10$	0.704
B	$R=-0.64*S+0.12$	0.388
C	$R=-0.66*S+0.19$	0.511
D	$R=-0.88*S+0.19$	0.205

Table 3.10: Summary of Dead Load Statistics for the Wall-to-Foundation Connection Analysis

Component	Archetype	Mean (kPa (psf))	COV	Distribution Type	Source
Roof	All	0.717 (15)	0.1	Normal	Ellingwood <i>et al.</i> 2004
Wall	All	0.527 (11)			ASCE 7-10
Floor	2, 4, 5	0.479 (10)			U.S. Dept. of Housing and Urban Development 2000

3.6 Results of the Fragility Analysis

One research objective of this work was to quantitatively assess the impact of stricter building codes on structural performance when subjected to tornadic wind loads. Florida has included strict wind provisions in its residential building code after the extensive damage caused by Hurricane Andrew in 1992 (Keith and Rose 1994, Gurley and Masters 2011). However, there are currently no tornado design provisions included in residential building codes, even though extensive damage has been observed after violent tornadoes. Recall this is due to the fact that tornadoes are relatively rare, localized occurrences, impacting only a portion of a city. Hurricanes cover a much larger geographic region and thus stricter code provisions in coastal regions are more economical and logical.

However, often after damaging tornadoes, there is an increased interest in including tornado design provision in building codes (Prevatt *et al.* 2011a, 2011b, 2012, van de Lindt *et al.* 2013). Thus, this research aims to perform a quantitative analysis of the reduction in tornado damage by including stricter design guidelines in tornado prone areas. Each of the five structure types at each of the six locations were analyzed using current local, adopted residential building code and were also analyzed using the FRC 2010. The results of the fragility analysis shown below include the fragility curves for both the local design guidelines and the FRC 2010. For

both the roof sheathing system and roof-to-wall connection fragility analysis, the curves depicting Florida style construction, shown in dashed lines, are shifted to the right. For the wall-to-foundation connections, comparison of the four different wall types are shown where Wall Type A is indicative of standard construction and Wall Type C is representative of strengthened construction practices.

3.6.1 Roof Sheathing Results

Fragility analysis was performed to assess the performance of roof sheathing when subjected to tornado loads. The probability of failure was determined for the roof sheathing on a system level rather than individual roof sheathing panel performance (Lee and Rosowsky 2005). There were four different performance expectations analyzed in this work, consistent with Lee and Rosowsky (2005). These are referred to as damage states 1-4 (DS1-4) and are described as (DS1) no loss of roof sheathing; (DS2) less than or equal to 1 roof sheathing panel failure; (DS3) roof sheathing loss less than or equal to 10% of the number of roof panels; and (DS4) roof sheathing loss less than or equal to 25% of the number of roof panels.

Figures 3.15-19 illustrate the roof sheathing system fragility curves for each of the 5 structural archetypes and Appendix B includes the logarithmic parameters for the roof sheathing fragility curves. Each of the figures includes two sets of fragility curves. Figures 3.15-19a were created using ASCE 7-10 wind provisions and the tornado amplification factor, K_c , as described above when calculating the upper bound fragility curves. Similarly, Figures 3.15-19b are the fragility curves for the lower bound roof sheathing performance and were calculated using ASCE 7-16 without any amplification for tornadoes. Finally, the locations in Oregon, Oklahoma, Illinois, and South Dakota had identical code provisions for roof sheathing dimensions and attachment and the fragility curves for these locations are identified as IRC on the figures.

The fragility curves for the Alabama location are similar in magnitude to the IRC since the nail spacing was identical but the thickness of the sheathing was slightly less. Overall, it is evident that the Florida style construction performed significantly better than either the IRC or AL design for both the lower and upper bounds. For example for Structure Type 1 shown in Figure 3.15, the probability of the roof sheathing failure for the Florida style construction is approximately 0.01% until wind speeds reach approximately 240 kph (150 mph) for damage state 1 (DS1) for both the upper and lower bound. However, using IRC specifications, the probability of failure is near 100% for DS1 at wind speeds near 160 kph (100 mph) for the upper bound and 177 kph (110 mph) for the lower bound. Similar patterns are observed for DS2-DS4 for the remaining archetypes.

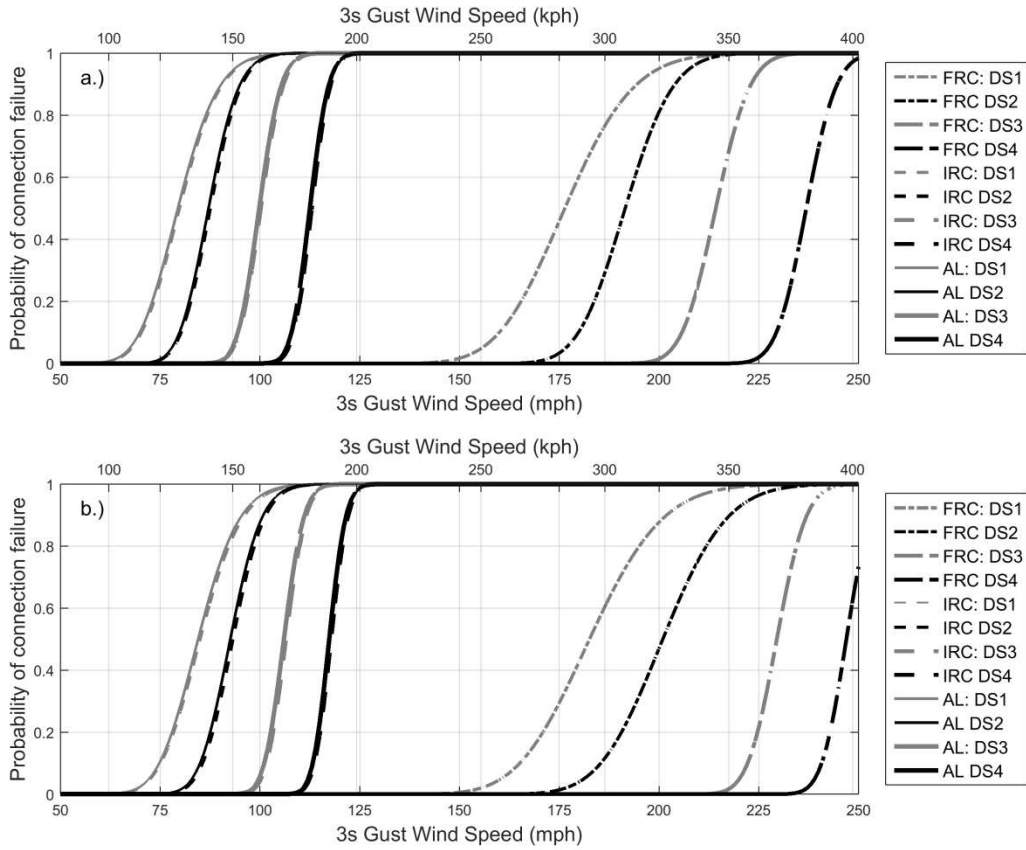


Figure 3.15: Roof system fragility curves for Structure Type 1 where a.) is the upper bound performance estimated using ASCE 7-10 and K_c and b.) is the lower bound performance found using ASCE 7-16 wind provisions without any tornado amplification. The improved performance of the Florida Residential Building Code is evident by the rightward shift of the curves.

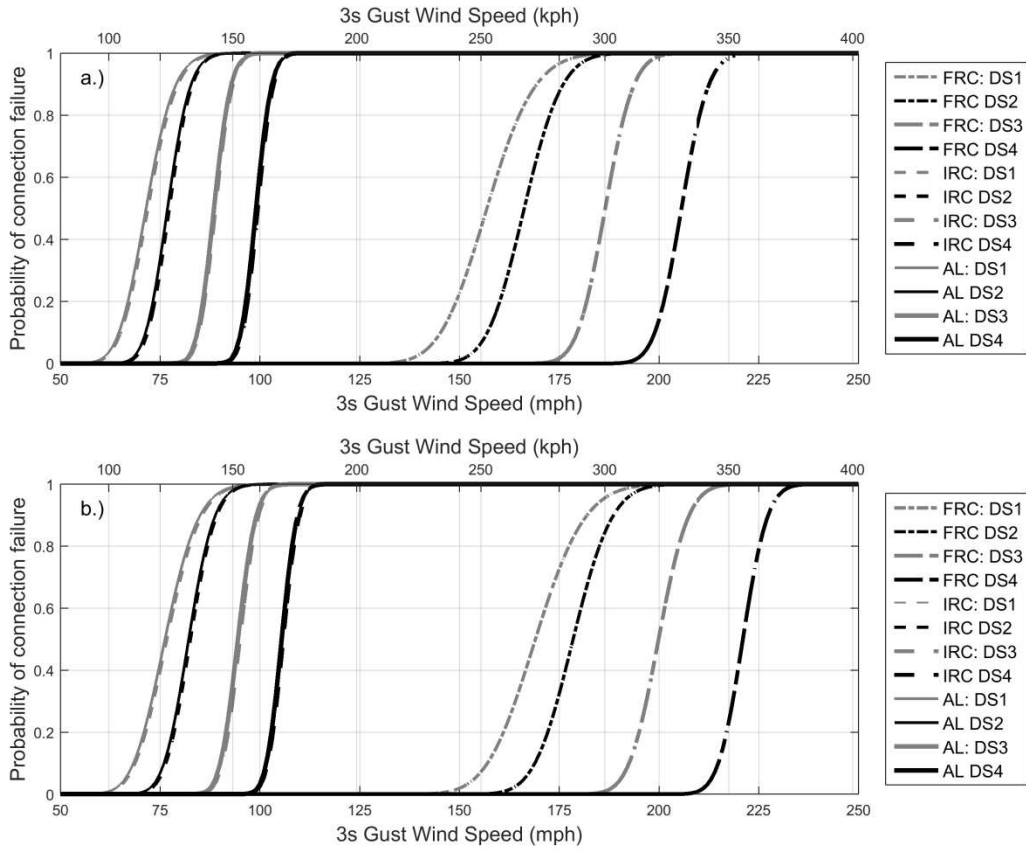


Figure 3.16: Roof system fragility curves for Structure Type 2 where a.) is the upper bound performance estimated using ASCE 7-10 and K_c and b.) is the lower bound performance found using ASCE 7-16 wind provisions without any tornado amplification. The improved performance of the Florida Residential Building Code is evident by the rightward shift of the curves.

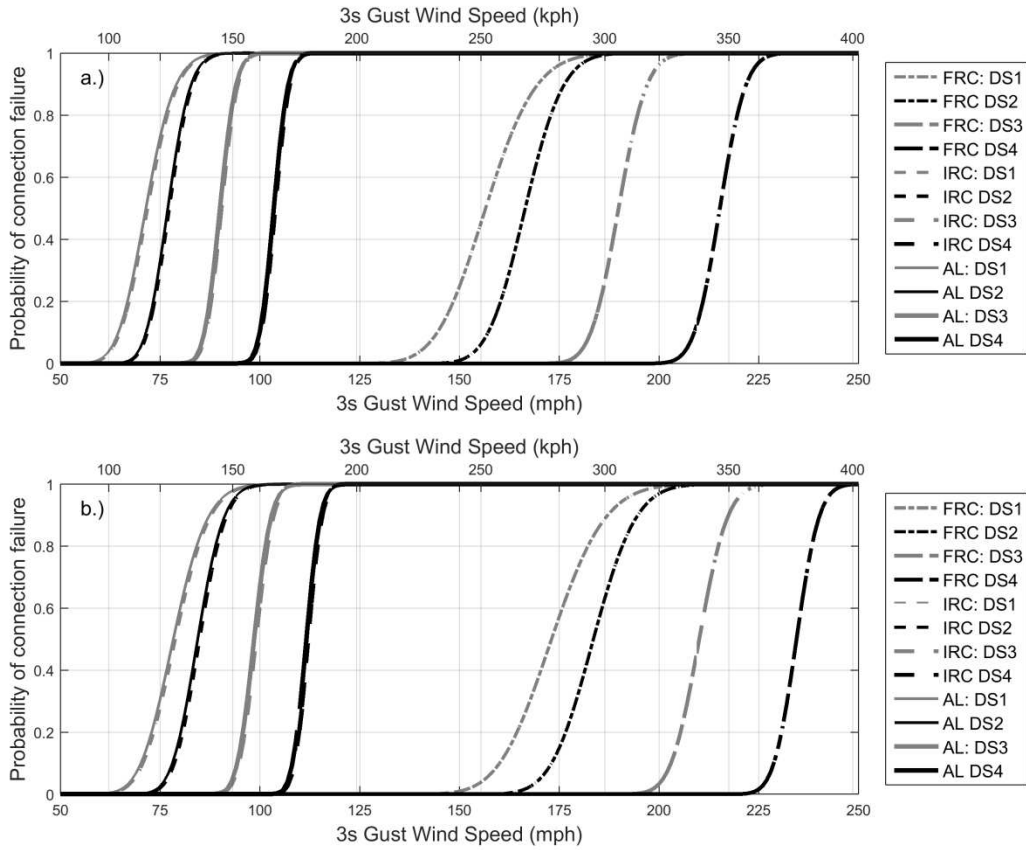


Figure 3.17: Roof system fragility curves for Structure Type 3 where a.) is the upper bound performance estimated using ASCE 7-10 and K_c and b.) is the lower bound performance found using ASCE 7-16 wind provisions without any tornado amplification. The improved performance of the Florida Residential Building Code is evident by the rightward shift of the curves.

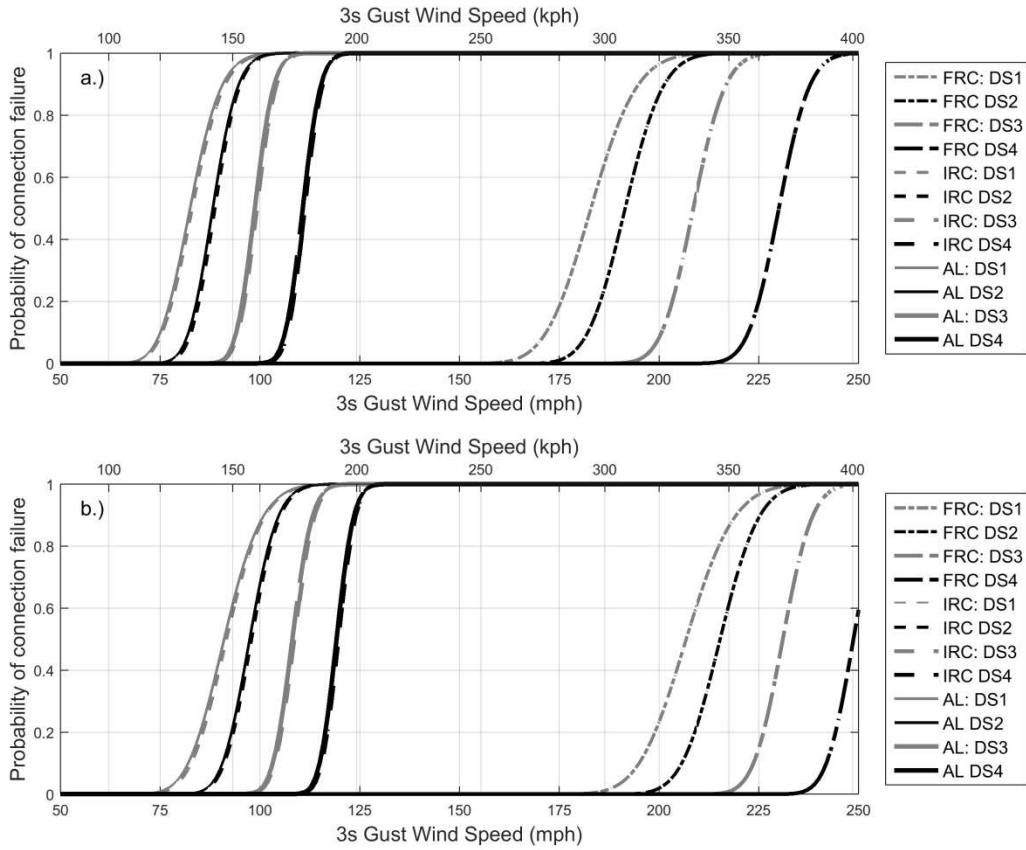


Figure 3.18: Roof system fragility curves for Structure Type 4 where a.) is the upper bound performance estimated using ASCE 7-10 and K_c and b.) is the lower bound performance found using ASCE 7-16 wind provisions without any tornado amplification. The improved performance of the Florida Residential Building Code is evident by the rightward shift of the curves.

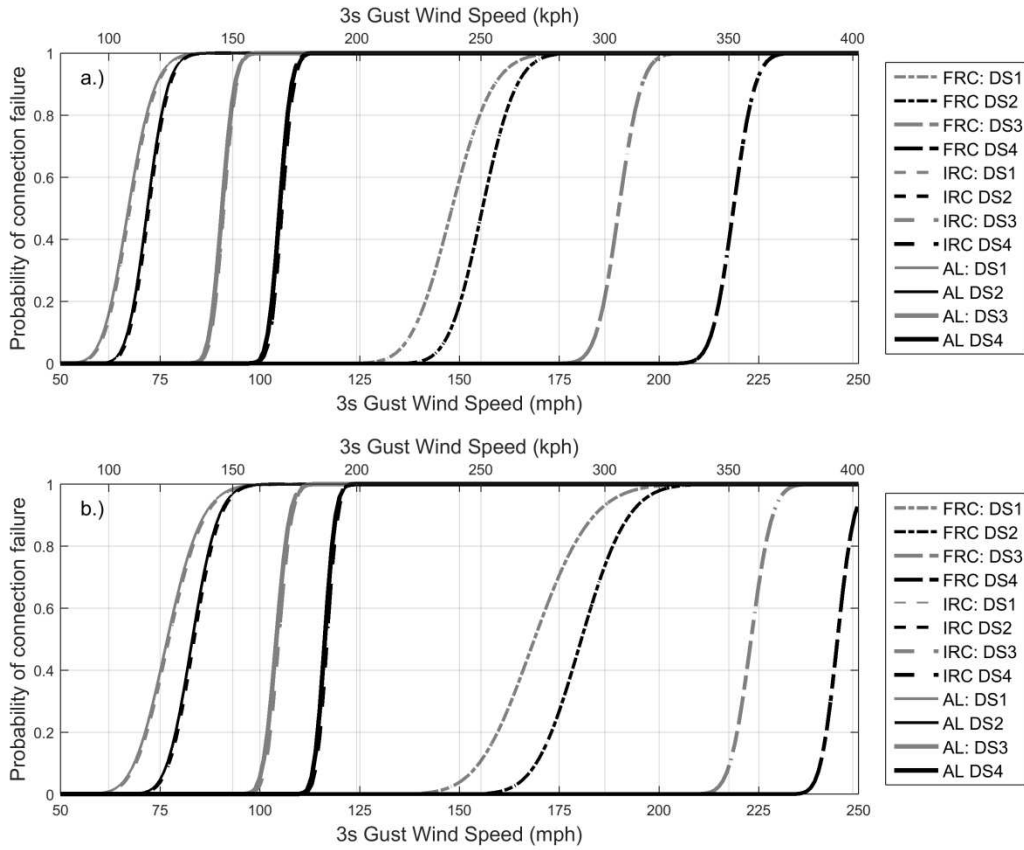


Figure 3.19: Roof system fragility curves for Structure Type 5 where a.) is the upper bound performance estimated using ASCE 7-10 and K_c and b.) is the lower bound performance found using ASCE 7-16 wind provisions without any tornado amplification. The improved performance of the Florida Residential Building Code is evident by the rightward shift of the curves.

For the roof sheathing fragility analysis, there was not a large difference between the upper and lower methods. This was especially true for the AL and IRC construction practices. There was some slight improvement of structural performance with the FRC using the ASCE 7-16, as observed with the right shift in the fragility curves. Overall, the similarities of the roof sheathing analysis using both methodologies were not surprising. The upper bound fragility method used ASCE 7-10 and a tornado amplification factor and the lower bound used updated values of GC_p found in ASCE 7-16. These updated values of GC_p were larger than those used in

ASCE 7-10. The net effect of increasing GC_p but neglecting the tornado amplification results in similar fragility curves using either methodology. Likewise, using the FRC construction standards drastically improved roof sheathing performance, as indicated on the fragility curves for all archetypes and for both upper and lower bounds.

3.6.2 Roof-to-Wall Connection Results

In addition to a roof sheathing system fragility analysis, the roof-to-wall connection performance was investigated. The fragility curves for each archetype are shown in Figures 3.20-24 and Appendix C includes the logarithmic parameters for the roof-to-wall fragility curves. As with the roof sheathing fragility curves, both the upper and lower bounds are included. The reader is referred to Tables 3.1 and 3.7 for information on the residential building code for each location and its respective roof-to-wall connection. As before, there is a rightward shift of the Florida style construction fragility curve with the use of the H2.5 hurricane clip for both ASCE 7-10 and 7-16. The fragility curve for the Alabama style construction performed the worst as this was the left-most curve for all archetypes. Another note is that the fragility curves are presented for the worst case wind loading. For instance, each structural archetype was subjected to both a north-south and east-west oriented wind. The controlling case has higher failure probabilities for lower wind speeds and thus is shown in Figures 3.20-24.

Another interesting feature of the fragility curves for the upper bound (3.20-24a) is that including the H2.5 clip does result in a rightward shift of the curves, but there is a limiting wind speed. At speeds above 241 kph (150 mph), the probability of failure is near 100% for Structure Types 1, 2, and 5. For the remaining archetypes, the probability of failure is approximately 90% or greater for a wind speed of 241 kph (150 mph). Thus, this implies that the inclusion of the H2.5 clip improves roof-to-wall connection performance at wind speeds below 241 kph (150

mph), but the loss of the roof or portions of the roof can be expected when wind speeds exceeding this value.

The performance of the roof-to-wall connection based on the lower bound methodology is seen in the lower set of fragility curves in Figures 3.20-24. With the IRC provisions (3-16d box toe nails), roof performance is significantly better than the upper bound. For Types 2 and 5, near absolute failure probabilities were not expected until wind speeds reached approximately 240 kph (150 mph). Failure of the remaining archetypes was not expected to occur until wind speeds exceeded at least 280 kph (175 mph). Similarly, the use of the H2.5 clip most drastically improved roof-to-wall performance. For Structure Type 5, near absolute failure probabilities were expected at wind speeds of approximately 300 kph (185 mph), yet for Types 1-4, the wind speed for near absolute failure exceeded 320 kph (200 mph).

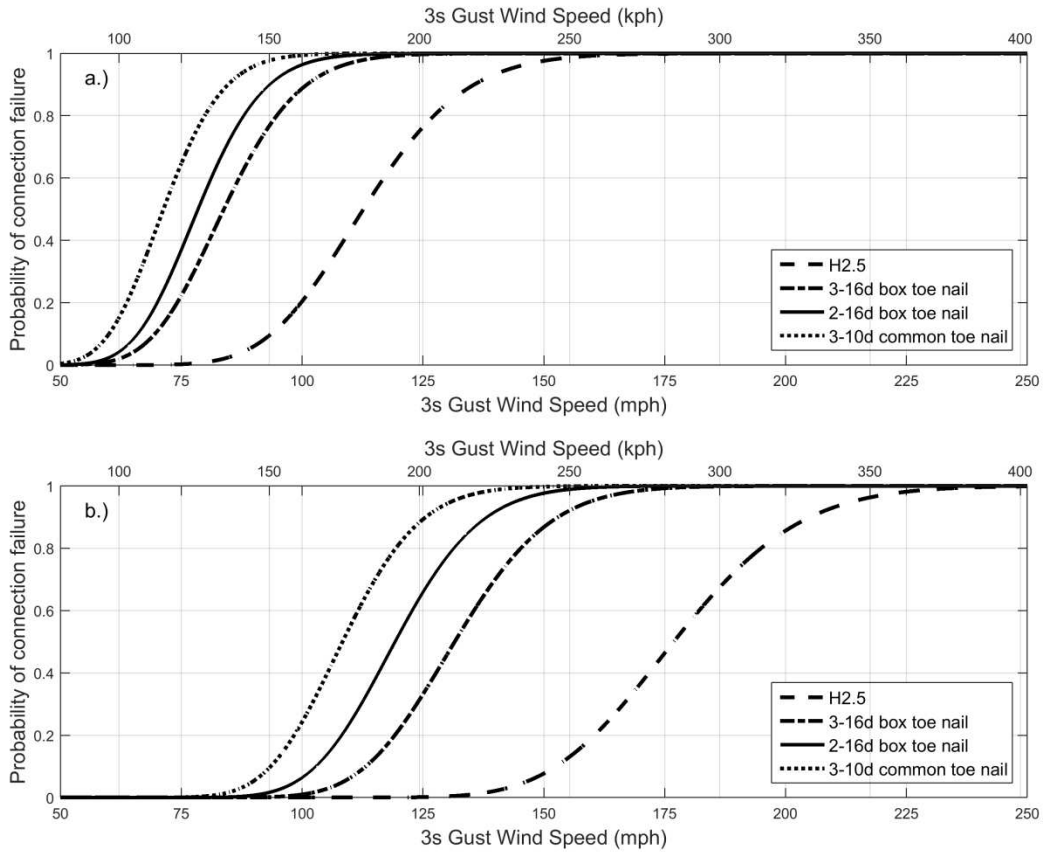


Figure 3.20: Fragility curves for Structure Type 1 for individual roof-to-wall connections prescribed by local residential building codes where a.) is the upper bound performance estimated using ASCE 7-10 and K_c and b.) is the lower bound performance found using ASCE 7-16 wind provisions without any tornado amplification.

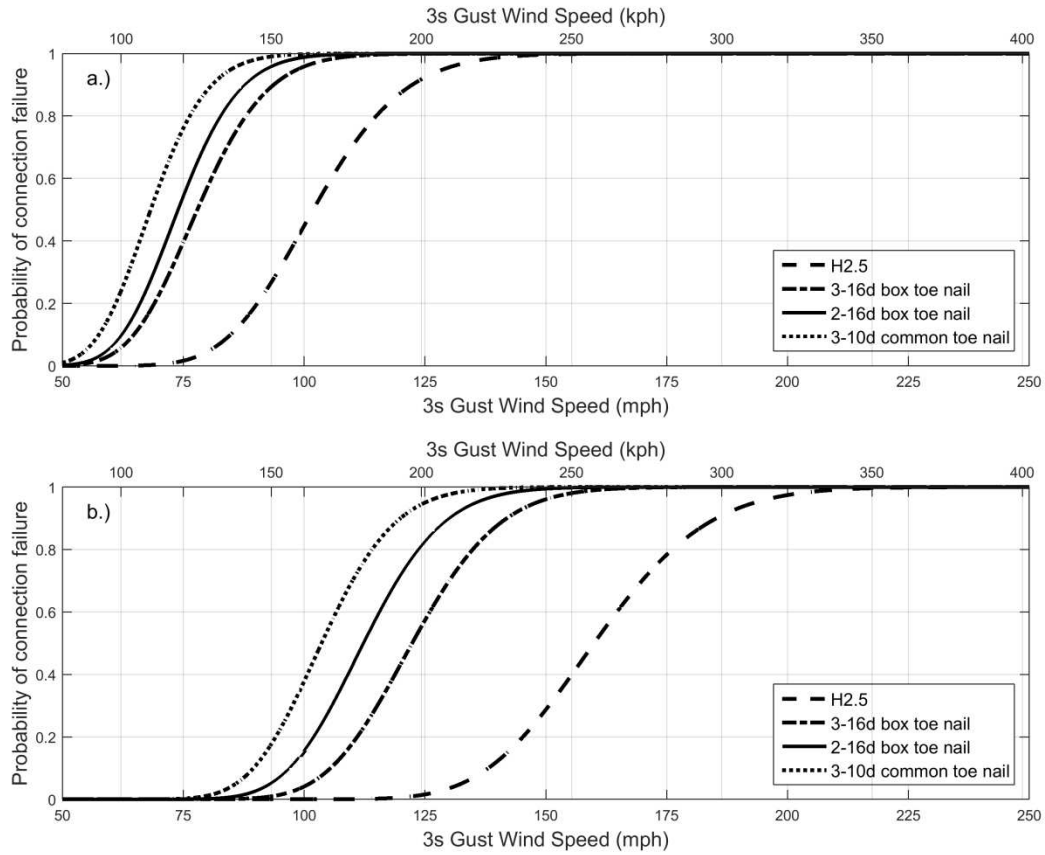


Figure 3.21: Fragility curves for Structure Type 2 for individual roof-to-wall connections prescribed by local residential building codes where a.) is the upper bound performance estimated using ASCE 7-10 and K_c and b.) is the lower bound performance found using ASCE 7-16 wind provisions without any tornado amplification.

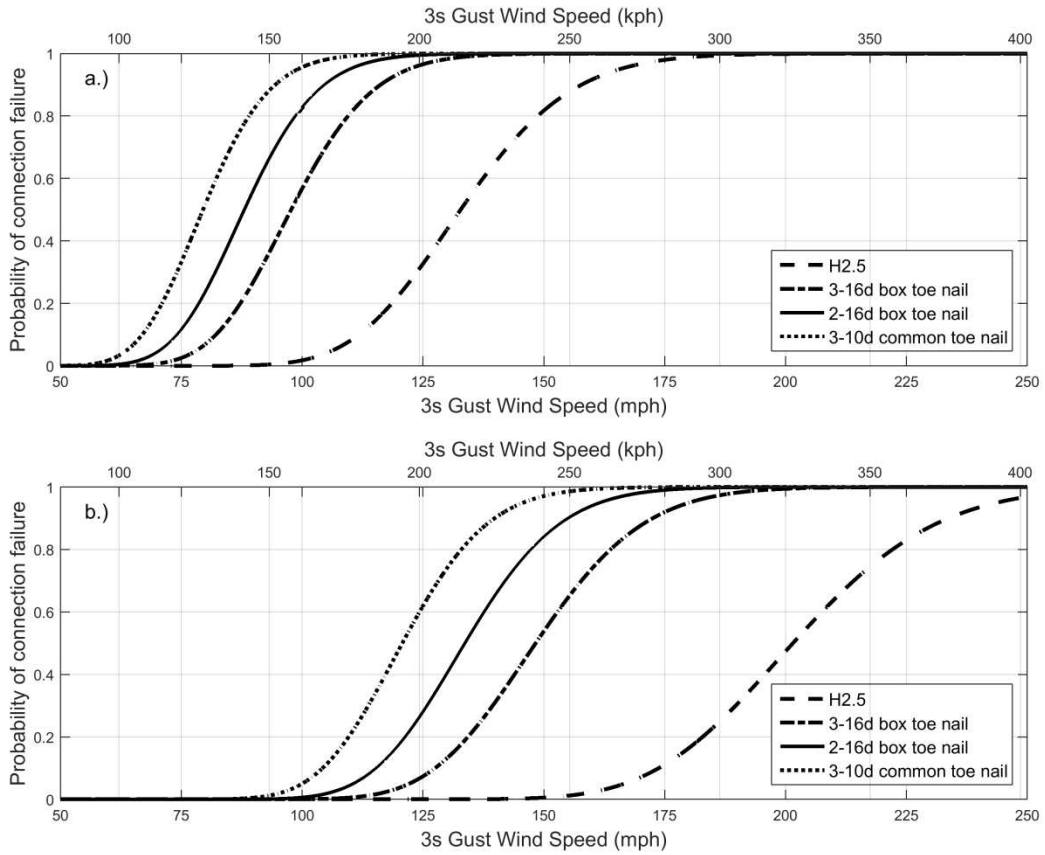


Figure 3.22: Fragility curves for Structure Type 3 for individual roof-to-wall connections prescribed by local residential building codes where a.) is the upper bound performance estimated using ASCE 7-10 and K_c and b.) is the lower bound performance found using ASCE 7-16 wind provisions without any tornado amplification.

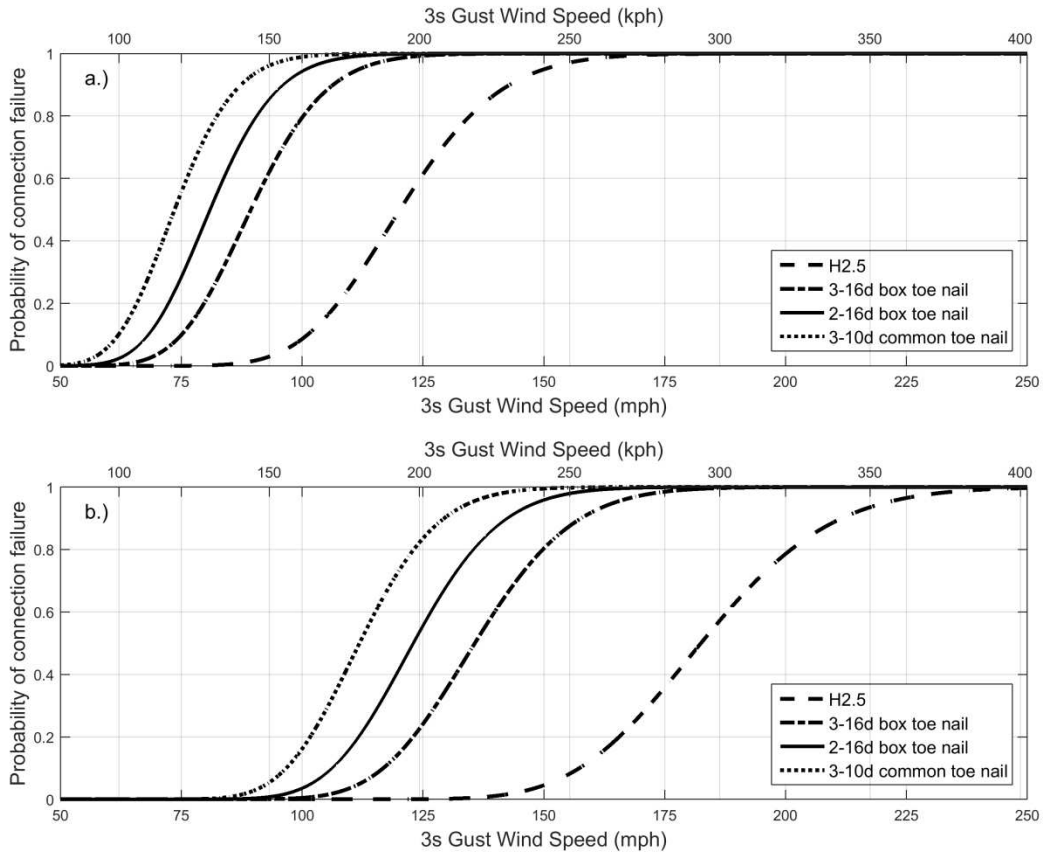


Figure 3.23: Fragility curves for Structure Type 4 for individual roof-to-wall connections prescribed by local residential building codes where a.) is the upper bound performance estimated using ASCE 7-10 and K_c and b.) is the lower bound performance found using ASCE 7-16 wind provisions without any tornado amplification.

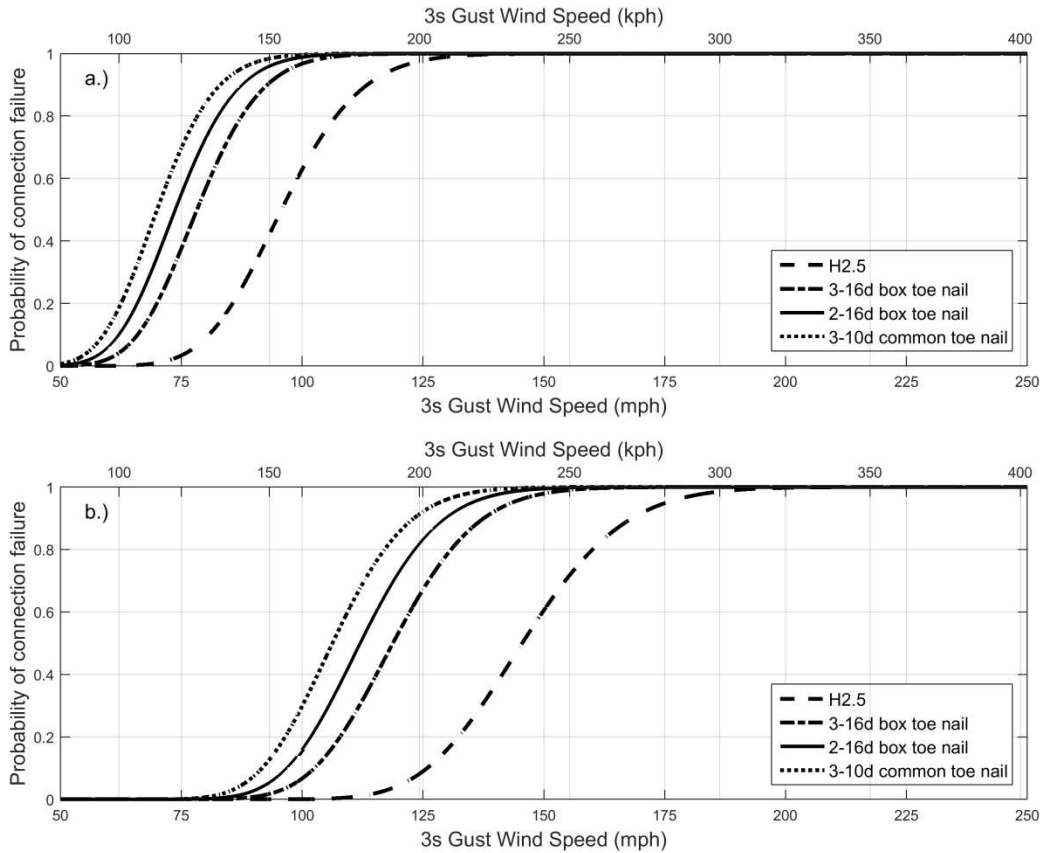


Figure 3.24: Fragility curves for Structure Type 5 for individual roof-to-wall connections prescribed by local residential building codes where a.) is the upper bound performance estimated using ASCE 7-10 and K_c and b.) is the lower bound performance found using ASCE 7-16 wind provisions without any tornado amplification.

The differences between the upper and lower bound fragility curves for the roof-to-wall connection were much larger than the roof sheathing. This was expected since the upper bound used a tornado amplification factor. The lower bound fragility curves were created using ASCE 7-16 provisions without any contribution from K_c . However, the main difference between ASCE 7-10 and 7-16 was the external pressure coefficient for C&C. The roof-to-wall connection is modeled as part of the MWFRS and thus there was no change in GC_p . Therefore, the only

difference between the upper and lower bounds is the inclusion of the tornado amplification resulting in an expected rightward shift of the lower bound fragility curves.

It should be noted that the fragility curves for the upper bound methodology are in better agreement with the damage for one- and two-family residences according to the Enhanced Fujita scale (see Table 2.3). The fragility curves for the IRC are most representative of standard construction practices across the U.S. For the upper bound fragility curves, near absolute failure probabilities for the IRC (3-16d box toenail) were expected for all archetypes in wind speeds between 160-210 kph (100-130 mph). According to the DOD for one- and two-family residences, uplift of the roof deck can be expected at wind speeds between 167-229 kph (104-142 mph). Therefore, the upper bound fragility curves are in agreement with the EF scale. By comparison, the lower bound fragility curves have near absolute failure probabilities of the roof-to-wall connection at wind speeds between 250-320 kph (155-200 mph).

3.6.3 Wall-to-Foundation Connection Results

Results of the fragility analysis indicate that strengthened connections at the wall-to-foundation interface did not drastically improve the performance of structures subjected to wind loads. This is attributed to the change in failure mechanisms for the different wall types. Figures 3.25-29 illustrate the common failure modes of the unreinforced (Wall Types A) and the reinforced (Wall Types C) walls, respectively. The dark fragility curves are for both wall types with an east-west oriented wind. Similar results were seen when comparing Wall Types B and D so their fragility curves were not included on the figures for clarity. However, the logarithmic parameters for the each of the four Wall Types and their respective fragility curves are included in Appendix D.

As is evident in Figures 3.25-29a, the fragility curves for Wall Type A and C have similar magnitudes for all wind speeds for both the EW and NS winds. The lower bound fragility curves (Figures 3.25-29b) had lower failure probabilities for a given wind speed when compared to the upper bound curves which was expected since the tornado amplification factor was not included. With the lower bound fragility curves, there was a larger spread between the unreinforced and reinforced fragility curves as compared to the upper bound. For example, with a N-S oriented wind shown on Figure 3.25a, there was a 50% failure probability at 150 kph and 165 kph (93 mph and 103 mph) for Wall Types A and C, respectively, which is a spread of 16 kph (10 mph). However, for the lower bound, there was a 50% failure probability at wind speeds of 236 kph and 262 kph (147 mph and 163 mph) for Wall Types A and C, respectively, as shown in Figure 3.25b. This is a spread of 26 kph (16 mph) which is 10 kph (6 mph) larger than the upper bound.

The results of the fragility analysis for the wall-to-foundation connection for Wall Types A and C were as expected. The unreinforced walls failed due to nail withdrawal while the reinforced walls failed when the wood split along the anchor bolt. In both cases, the failure mode was the wall separating from the foundation. The use of the RSP4 ties successfully kept the wall studs tied to the portion of the bottom plate that did not split around the anchor bolt. However, the limiting factor of the wall capacity against wind loads was the material used in the bottom plate. In all cases where the RSP4 tie was used, the wall studs and bottom plate remained connected, highlighting good performance of the tie itself. Thus the authors feel the use of the RSP4 tie is adequate, but would recommend decreased spacing of the anchor bolts or the use of a reinforcing plate between the anchor bolt and bottom plate similar to the results of Yeh *et al.* (2009).

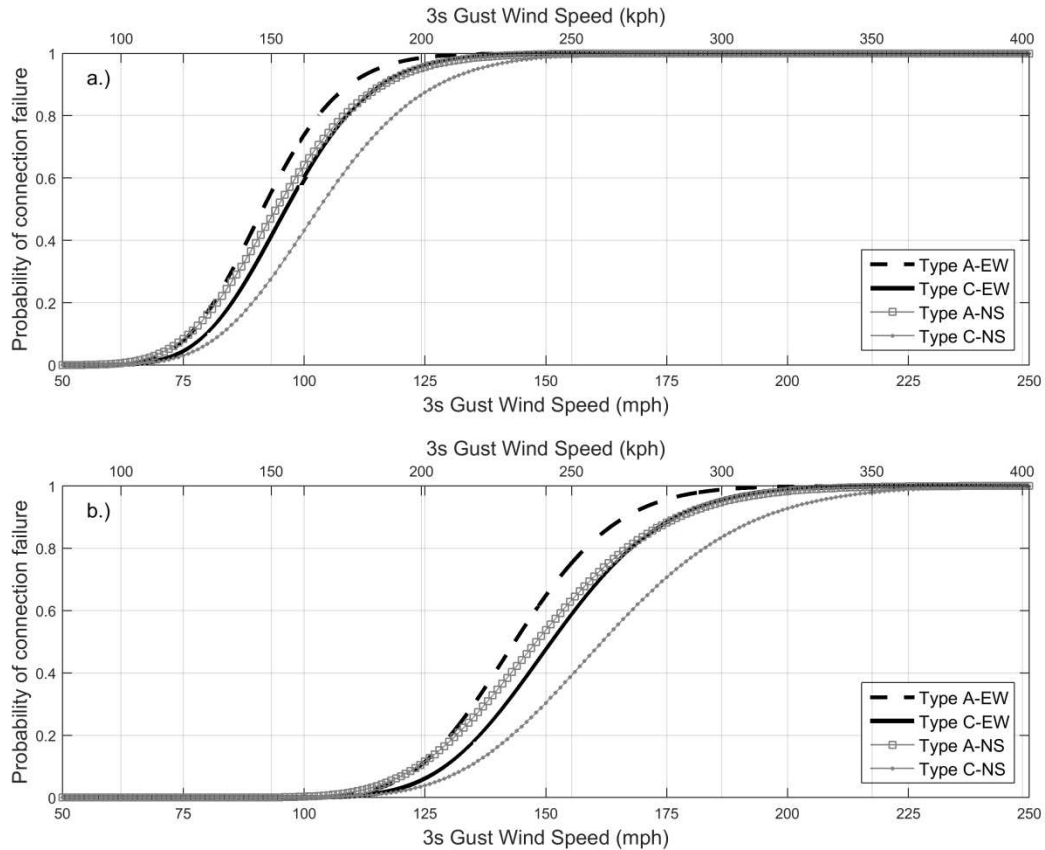


Figure 3.25: Fragility curves for Structure Type 1 for the wall-to-foundation where a.) is the upper bound performance estimated using ASCE 7-10 and K_c and b.) is the lower bound performance found using ASCE 7-16 wind provisions without any tornado amplification. It is evident that the inclusion of reinforcing ties did not drastically improve wall performance by comparing the curves for A and C for each wind direction.

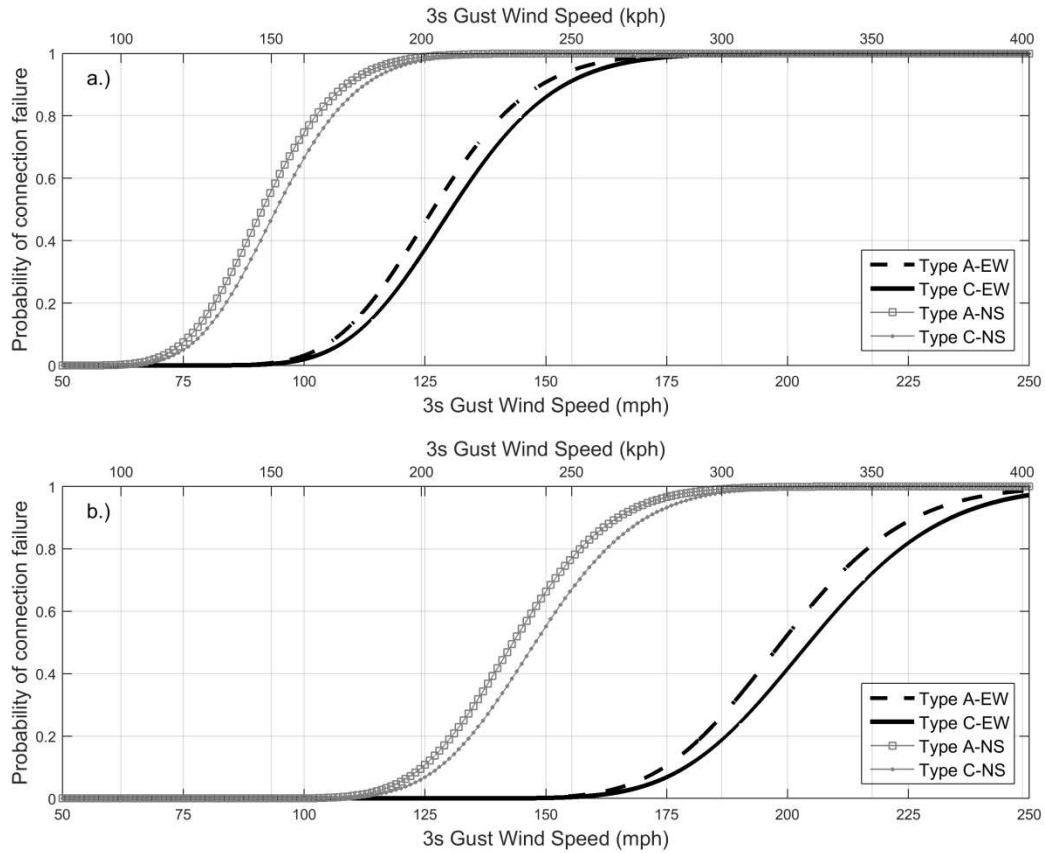


Figure 3.26: Fragility curves for Structure Type 2 for the wall-to-foundation where a.) is the upper bound performance estimated using ASCE 7-10 and K_c and b.) is the lower bound performance found using ASCE 7-16 wind provisions without any tornado amplification. It is evident that the inclusion of reinforcing ties did not drastically improve wall performance by comparing the curves for A and C for each wind direction.

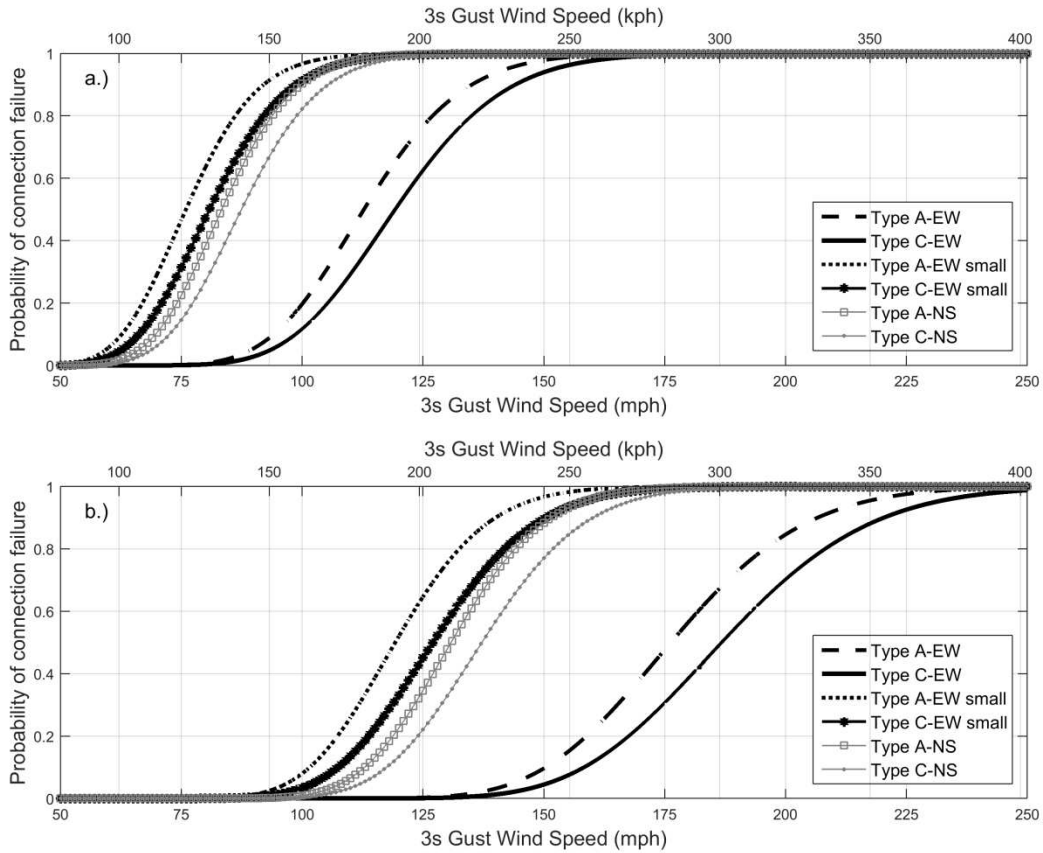


Figure 3.27: Fragility curves for Structure Type 3 for the wall-to-foundation where a.) is the upper bound performance estimated using ASCE 7-10 and K_c and b.) is the lower bound performance found using ASCE 7-16 wind provisions without any tornado amplification. It is evident that the inclusion of reinforcing ties did not drastically improve wall performance by comparing the curves for A and C for each wind direction.

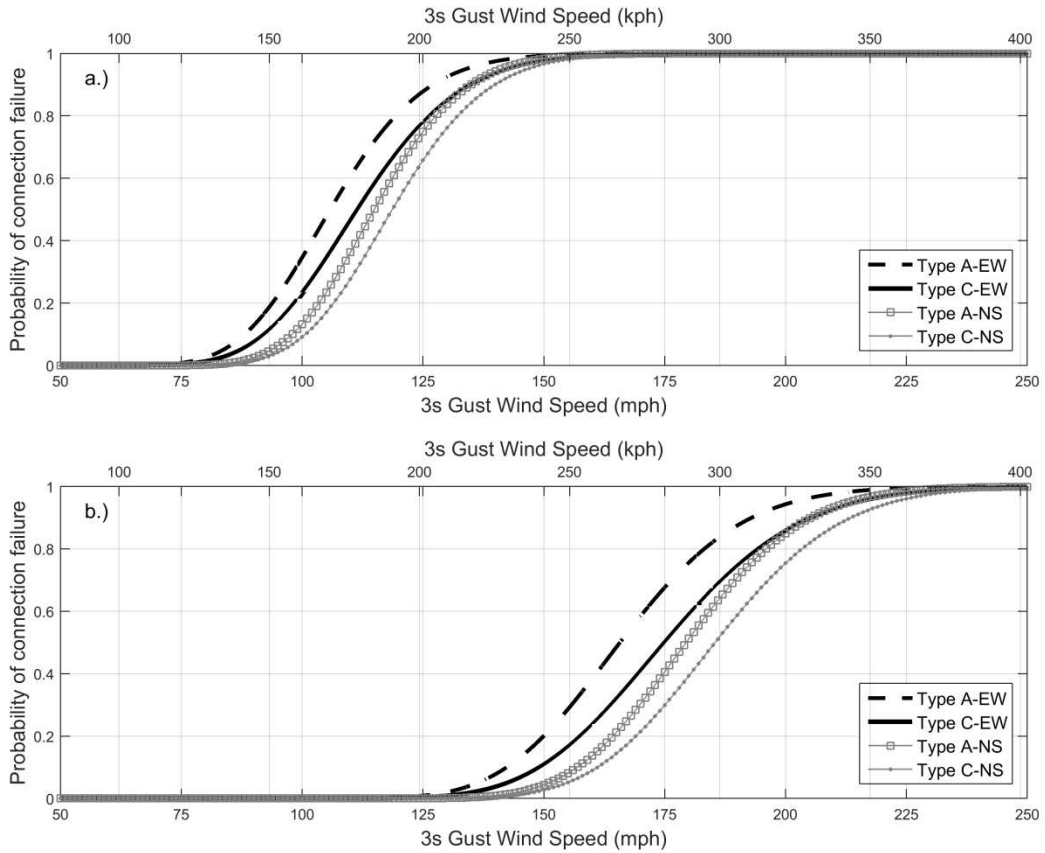


Figure 3.28: Fragility curves for Structure Type 4 for the wall-to-foundation where a.) is the upper bound performance estimated using ASCE 7-10 and K_c and b.) is the lower bound performance found using ASCE 7-16 wind provisions without any tornado amplification. It is evident that the inclusion of reinforcing ties did not drastically improve wall performance by comparing the curves for A and C for each wind direction.

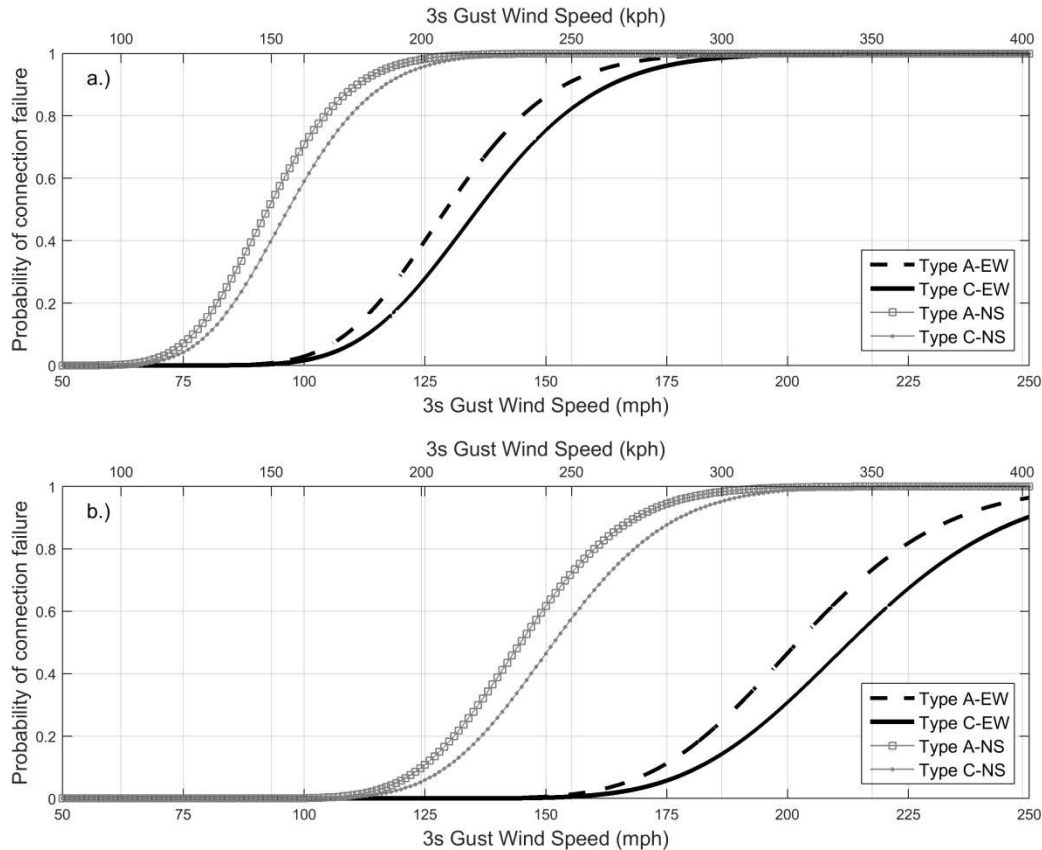


Figure 3.29: Fragility curves for Structure Type 5 for the wall-to-foundation where a.) is the upper bound performance estimated using ASCE 7-10 and K_c and b.) is the lower bound performance found using ASCE 7-16 wind provisions without any tornado amplification. It is evident that the inclusion of reinforcing ties did not drastically improve wall performance by comparing the curves for A and C for each wind direction.

As with the previous components, the difference between the upper and lower bound fragilities was studied. The upper bound wall-to-foundation curves were created using ASCE 7-10 wind provisions and the tornado amplification factor. Likewise, the lower bound fragility curves were created using ASCE 7-16 wind provisions without any amplification to account for tornado winds. However, since the wall-to-foundation connection is modeled as part of the

MWFRS, the ASCE 7-16 parameters are identical to ASCE 7-10, with the exception that K_c is set to unity.

As with the roof-to-wall connection, the fragility curves for the upper bound methodology are in better agreement with the EF scale DOD for one- and two-family residences as compared to the lower bound. Near absolute failure of the walls was expected for all archetypes in wind speeds between 177-240 kph (110-150 mph) using the upper bound. According to Table 2.3, failure of the exterior walls is expected in wind speeds between 182-246 kph (113-153 mph). By comparison, near absolute failure probabilities is not expected until 280-355 kph (175-220 mph) for the lower bound. This falls in the range of EF4-5 tornadoes, which result in catastrophic damage, often with the slab swept clean.

3.7 System Level Analysis

The next portion of this dissertation involved a reliability analysis for the roof to foundation load path which was modeled as a series system. Standohar-Alfano and van de Lindt (2015) performed an in-depth analysis on roof performance in tornadoes focusing on the roof sheathing and roof-to-wall connection. Their work assumed that the structure remained intact and that failure was initiated at the connection being investigated. For instance, when assessing the roof-to-wall connection performance, it is assumed the roof sheathing had not failed. While this is a useful assumption when investigating individual components, it is beneficial to investigate the performance of the entire structure as a system whose individual components have correlated dependence. Thus, for the next portion of this dissertation, the system level of each of the structural archetypes is analyzed. Three main components along the vertical load path were considered including the roof sheathing, roof-to-wall, and wall-to-foundation

connections. Detailed information about the roof sheathing, roof-to-wall, and wall-to-foundation connections can be found above in Sections 3.4 and 3.5.

3.7.1 Introduction to Positive Quadrant Dependence

In a series system, failure of any component results in failure of the system. In previous tornado efforts on system performance, it was commonly assumed that the components were independent (e.g. Amini 2012). However, components in the same system share the same loads and environment, and thus, the failure of one component affects the performance of the others (Lai and Xie 2003). For the load path analysis defined here as a system, the positive dependence between components had to be considered, commonly referred to as positive quadrant dependence.

In order to assess the system level performance, the dependencies between each of the components had to be established. This is not straight forward for structures subjected to tornado loads since the progression of failure of the components is not known. In order to determine the probability of failure of the system, Monte Carlo simulation was used to calculate the failure probabilities for each individual component along the vertical load path. An event tree was utilized to illustrate eight possible outcomes from the limit state analysis and is shown in Figure 3.30.

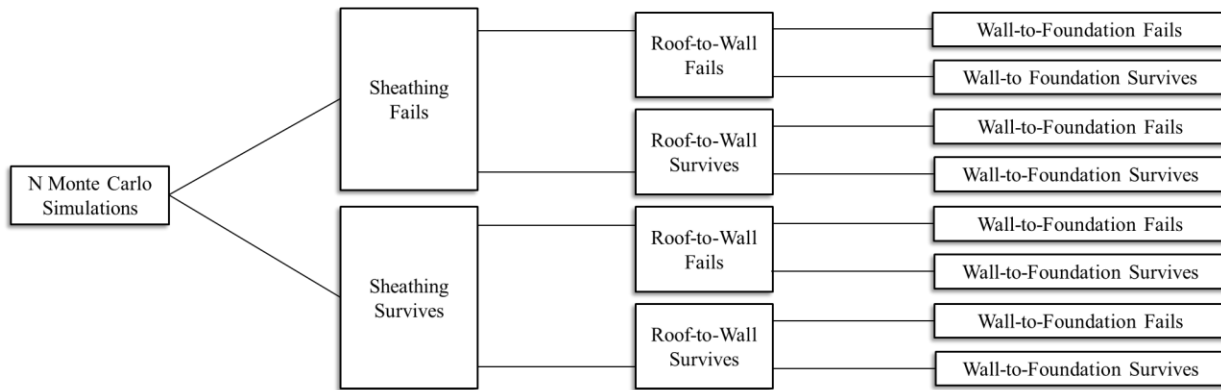


Figure 3.30: Event tree utilized for the system level performance.

The limit state analysis described differs from the individual component analysis in that it takes into account the impact of the performance of each component along the vertical load path. For example, the performance of the roof-to-wall connection depends on the performance of the roof sheathing connection. This is described in more detail below. As shown in Figure 3.30, there are eight possible outcomes from the limit state analysis. The probability of each of the eight outcomes was determined using 100,000 Monte Carlo simulations for every wind speed between 80 and 400 kph (50 and 250 mph) at 8 kph (5mph) increments. The individual outcomes are summarized in Table 3.11.

Table 3.11: Event Tree Component Details

Component Performance			
Event Number	Roof Sheathing	Roof-to-Wall Connection	Wall-to-Foundation Connection
1	Fails	Fails	Fails
2	Fails	Fails	Survives
3	Fails	Survives	Fails
4	Fails	Survives	Survives
5	Survives	Fails	Fails
6	Survives	Fails	Survives
7	Survives	Survives	Fails
8	Survives	Survives	Survives

The roof sheathing limit state was first calculated for the system level performance as shown in the event tree in Figure 3.30. Failure of the roof sheathing was defined as roof sheathing loss greater than or equal to 10% of the total number of roof panels (or DS3 from Section 3.6.1). Thus the roof sheathing was assumed to survive up until 10% of the roof sheathing was lost. While the failure progression in a tornado is not known, the authors assumed the roof sheathing would be the first connection to fail when subjected to extreme winds consistent with the Enhanced Fujita scale degree of damage for one- or two- family homes shown in Table 2.3 (Wind Science and Engineering Research Center 2006). At each wind speed investigated, the roof sheathing either failed (Events 1-4) or survived (Events 5-8), where failure is defined as loss of roof covering of 10% or more. The survival or failure of the roof sheathing was considered when assessing the roof-to-wall connection performance.

The next component investigated was the roof-to-wall connection as indicated on the second branch of the event tree in Figure 3.30. In order to determine the failure probabilities of the roof-to-wall connection, the performance of the roof sheathing was taken into account. In Table 3.11, Events 1-4 are associated with roof sheathing failure. In this case, at least 10% of the roof sheathing is removed, resulting in a large breach of the building envelope. Thus, it could no longer be assumed the structure was enclosed, and the change in the internal pressure coefficient, GC_{pi} had to be considered. This is indicated in Table 3.2 as the partially enclosed condition. Events 5-8 are the cases where the roof sheathing remains intact or loss is less than 10%. In these cases, the roof-to-wall connection is analyzed using an enclosed structure.

The wall-to-foundation was the final connection to be considered. With this connection, there were four different scenarios that had to be analyzed. The first was the cases where both the roof-to-wall and roof sheathing connections failed (Events 1-2). In this case, the wall-to-connection foundation used an open condition for the enclosure classification resulting in a null value for the internal pressure coefficient. Likewise, the loss of the roof system implied that there were no significant uplift forces being imposed on the remaining structure. Thus, the limit state of the wall-to-foundation connection used Eqn. 3.6 in which walls are only subjected to wind-induced shear forces.

The next scenario for the wall-to-foundation analysis was failure of the roof sheathing connection but survival of the roof-to-wall connection, allowing the roof structure to remain in place with some damage to the roof sheathing as indicated in Table 3.11 with Events 3-4. In this case, the limit state for the wall-to-foundation connection used Eqn. 3.2 accounting for uplift forces that are transferred from the roof-to-wall connection to the wall-to-foundation connection.

In the calculation of the wind load, the enclosure classification was set as partially enclosed and the tributary area of the roof structure was reduced to account for the loss of roof sheathing.

The third case for the wall-to-foundation case was survival of the roof sheathing but failure of the roof-to-wall connection as indicated with Events 5-6. In this case, the roof is removed but would remain relatively intact due to the survival of the roof sheathing. This is commonly observed in post-disaster investigations of extreme wind events. The limit state and enclosure classifications are the same as Events 1-2 for the wall-to-foundation connection as described earlier.

The final wall-to-foundation scenario was survival of both the roof sheathing and roof-to-wall connections. This is shown in Table 3.11 as Events 7-8. In this case, the structure remains enclosed and the analysis is identical to the previously discussed work in which the wall-to-foundation connection performance was investigated independently. The limit state is governed by Eqn. 3.2.

In any case, after the wall-to-foundation connection is analyzed, a total of 8 different event outcomes could have occurred as indicated by the third branch of the event tree shown in Figure 3.30. As stated before, failure of any component was deemed failure of the load path, i.e. the system. Thus, in order to determine the probability of system failure, Event 8 was utilized. Event 8 is the case where all connections along the vertical load path survive. This provided the system survival probability for every wind speed analyzed. Using this, system failure probabilities were calculated as

$$P_f = 1 - P_s \quad (3.7)$$

where P_f is the probability of failure and P_s is the probability of survival of the system. The system survival is calculated using the multiplication rule of probability. The probability that three events occur is written as $P(A \cap B \cap C)$, where A, B, and C can be thought of as survival of the roof sheathing, roof-to-wall, and wall-to-foundation connections, respectively. In order to determine the system survival probabilities, each branch of the event tree was analyzed. Thus, the survival probability can be written as

$$P(A \cap B \cap C) = P(C|A \cap B) * P(A \cap B) = P(C|A \cap B) * P(B|A) * P(A) \quad (3.8)$$

where A, B, and C, represent the roof sheathing, roof-to-wall, and wall-to-foundation connections respectively. When assessing the system survival probability, the first term on the right hand side of Eqn. 3.8, $P(C|A \cap B)$, represents the probability of survival of the wall-to-foundation connection, given that both the roof sheathing and roof-to-wall connection survive as described by Event 8 in Table 3.11. Similarly, the second term, $P(B|A)$, is the probability of survival of the roof-to-wall connection given that the roof sheathing survives. Finally, the last term, $P(A)$, is the probability that the roof sheathing survives.

The performance of each connection was documented for every iteration, allowing for an estimation of performance probabilities. The roof sheathing failure probability was simply the number of times the roof sheathing failed at a given wind speed divided by the number of Monte Carlo simulations, in this case 100,000. A similar approach was used for the survival probabilities. For example, assuming that the roof sheathing failed 10 times at 100 kph (62 mph), the probability of failure, P_f , would be equal to 10 divided by 100,000, or 0.0001.

3.7.2 Fragility Curves

The system level performance was analyzed at each of the six geographic locations using the locally adopted residential building codes. Details on the roof sheathing and roof-to-wall connections for each location are summarized in Sections 3.4 and 3.5. For the wall-to-foundation connection, the Florida Peninsula used Wall Type C, while the remaining five locations used Wall Type A. Simulations were performed for both wind orientations. Figures 3.31-35 present the fragility curves for the five structural archetypes with a north-south oriented wind direction. Appendix E includes the logarithmic parameters for the system level fragility curves. Additional fragility curves were created for the east-west orientation and are included in Appendix F.

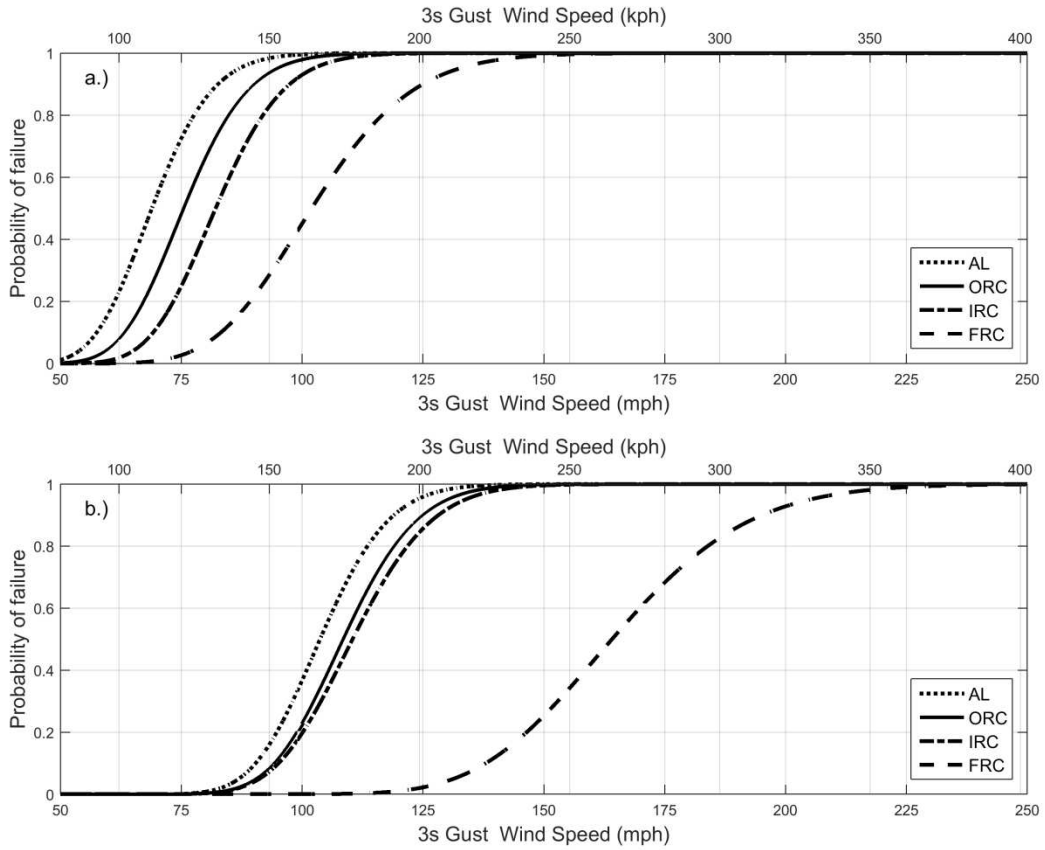


Figure 3.31: System level fragility curves for Structure Type 1 a.) is the upper bound performance estimated using ASCE 7-10 and K_c and b.) is the lower bound performance found using ASCE 7-16 wind provisions without any tornado amplification.

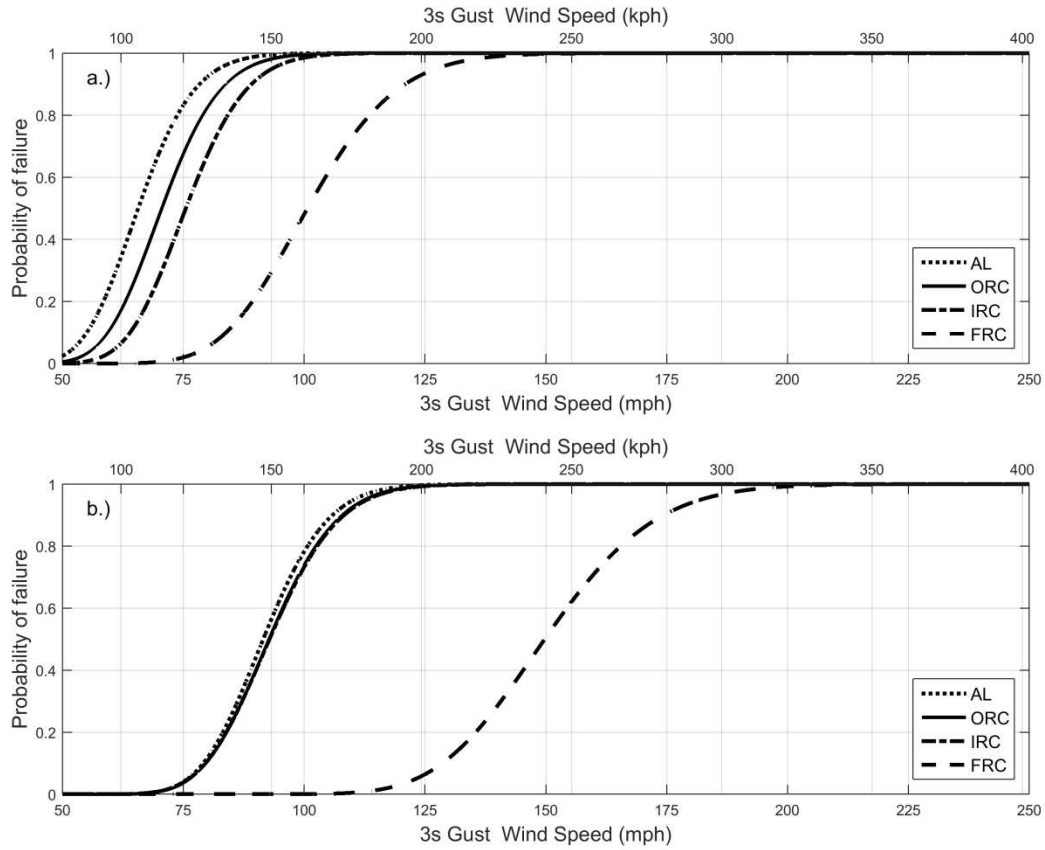


Figure 3.32: System level fragility curves for Structure Type 2 a.) is the upper bound performance estimated using ASCE 7-10 and K_c and b.) is the lower bound performance found using ASCE 7-16 wind provisions without any tornado amplification.

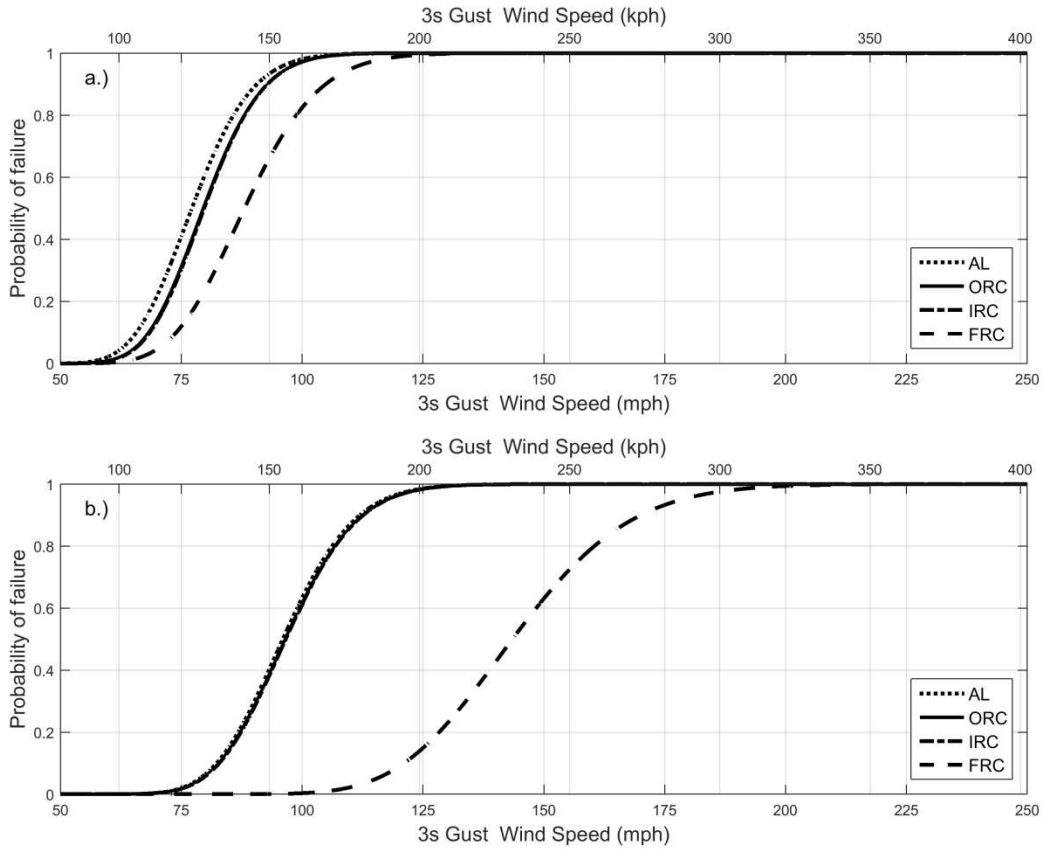


Figure 3.33: System level fragility curves for Structure Type 3 a.) is the upper bound performance estimated using ASCE 7-10 and K_c and b.) is the lower bound performance found using ASCE 7-16 wind provisions without any tornado amplification.

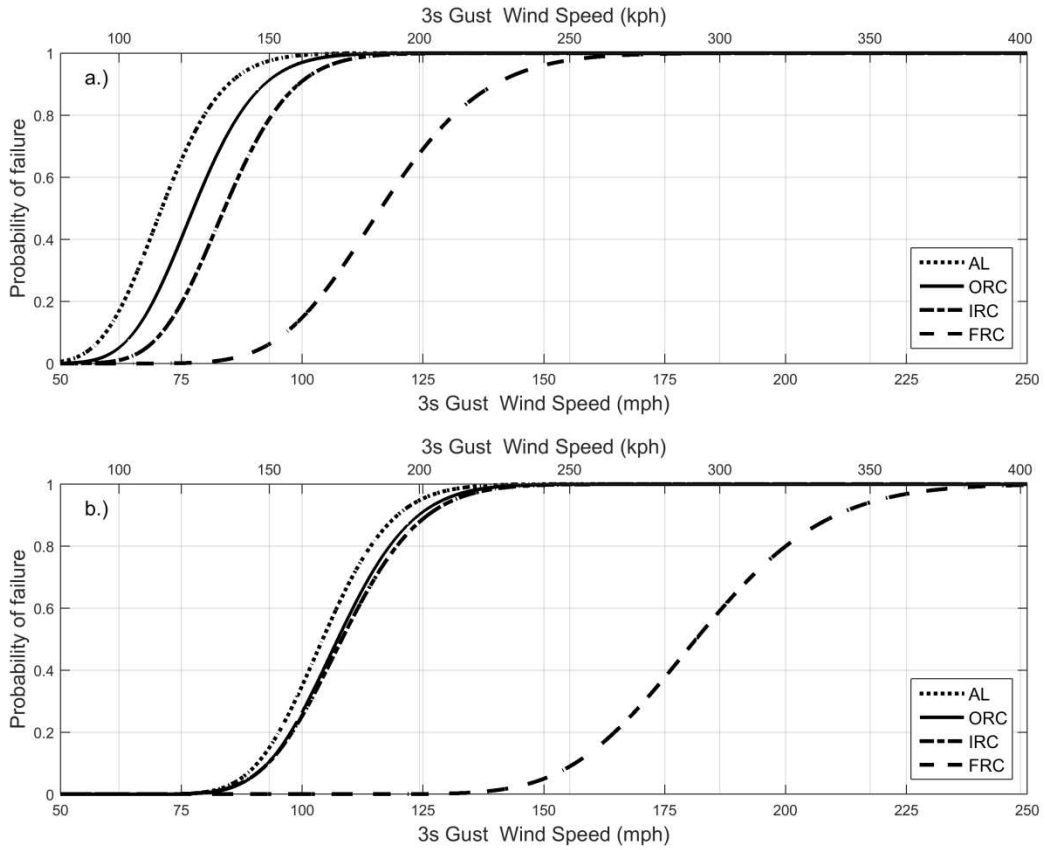


Figure 3.34: System level fragility curves for Structure Type 4 a.) is the upper bound performance estimated using ASCE 7-10 and K_c and b.) is the lower bound performance found using ASCE 7-16 wind provisions without any tornado amplification.

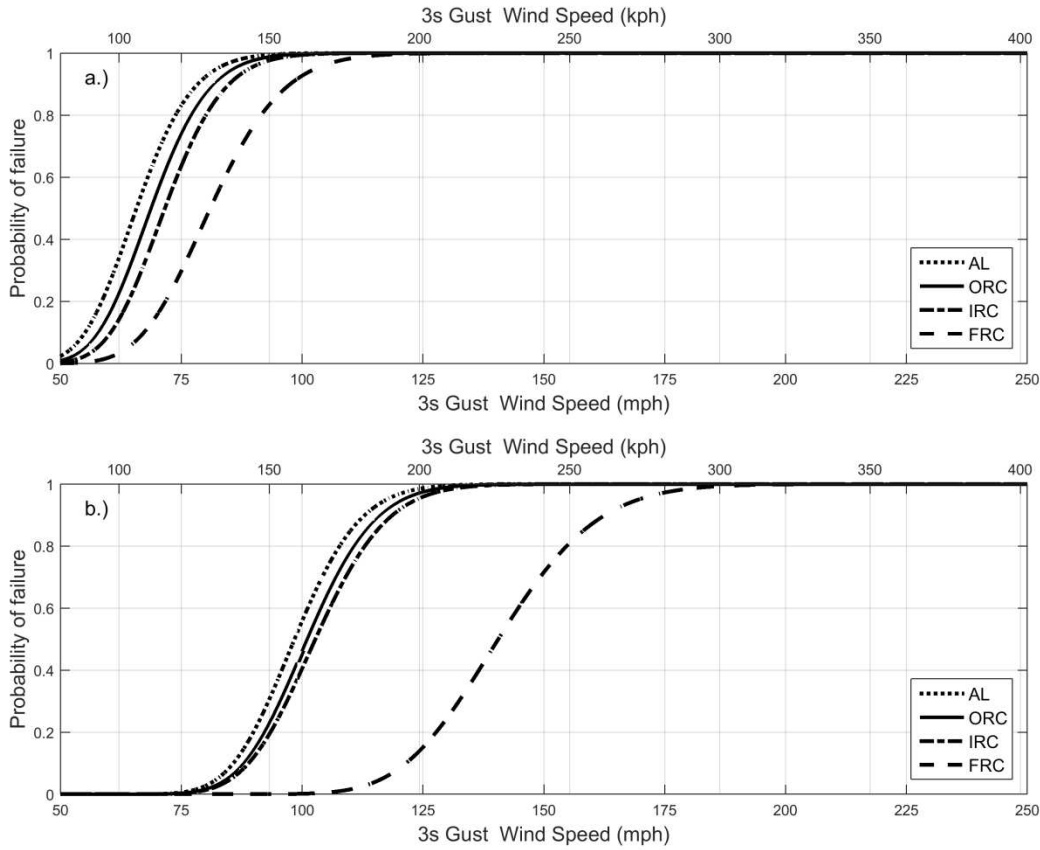


Figure 3.35: System level fragility curves for Structure Type 5 a.) is the upper bound performance estimated using ASCE 7-10 and K_c and b.) is the lower bound performance found using ASCE 7-16 wind provisions without any tornado amplification.

The system level fragility curves indicate the probability of failure of any component along the vertical load path. First, a comparison of the upper and lower bounds for the IRC was performed. The IRC was selected since it represents the most common construction practices across the majority of the U.S., with the exception of coastal or earthquake regions. The upper bound fragility curves indicated some type of failure along the vertical load path for wind speeds between 160-200 kph (100-125 mph). By comparison, the lower bound fragility curves indicated failure was expected for wind speeds between 200-240 kph (125-150 mph). As before,

the upper bound fragility curves are in better agreement with the DOD for one- and two-family residences per the EF scale. Likewise, by designing the archetypes using strengthened construction practices, structural performance was enhanced. For the upper bound approach, failure along the vertical load path wasn't expected until wind speeds ranged from 200-280 kph (125-175 mph) with the use of the FRC. Similarly, the lower bound FRC fragility curves indicate that failure wouldn't be expected until tornado wind speeds exceeded 300 kph (185 mph).

3.8 Summary

Fragility analysis was completed to assess structural performance of three individual components along the vertical load path, including the roof sheathing, roof-to-wall, and wall-to-foundation connections. Likewise, the system level behavior of the structure was also investigated. The use of fragility analysis took into account the uncertainty in resistance, dead load, and demand in order to obtain failure probabilities. In order to assess tornado risk across the U.S., several different building codes were used based on the six locations investigated.

Due to uncertainty with the magnitude and duration of tornado winds, two different approaches were used to bound structural performance. This first method utilized ASCE 7-10 coefficients as well as a tornado amplification factor estimated from laboratory experiments (Haan *et al.*2010). This represented the upper bound fragility curve since the tornado amplification factor resulted in higher failure probabilities for a given wind speed. Similarly, ASCE 7-16 provisions were used without a tornado amplification factor to represent the lower bound. This was primarily due to a lack of scientific consensus among engineers regarding the use of the tornado amplification factor.

The results from the fragility analysis using the lower bound methodology do not typically agree with the wind speeds associated with the EF scale or with damage observations from post-tornado investigations. This would support the idea of some type of amplification in wind loads due to tornado passage. Further research is required in order to understand the wind loads from tornadoes and the magnitude of amplification.

Strengthened construction, as indicated by the FRC, performed better than all the other building codes investigated and could improve structural performance when subjected to tornado wind loads. This is especially true for wind speeds lower than 220 kph (135 mph). Tornadoes rated EF2 or lower account for over 95% of all tornado reports. Likewise, while a tornado may be rated higher than EF2, only a small portion of the path will actually experience wind speeds in excess of 220 kph (135 mph) (see Figure 2.4). This implies that the majority of tornado winds across the U.S. fall within the EF2 range or lower, thus strengthened construction would be beneficial in tornado prone areas.

CHAPTER 4

CONVOLUTION OF FRAGILITY AND TORNADO HAZARD CURVES

4.1 Introduction to Convolution Analysis

The previous two chapters discussed the development of the tornado hazard and fragility curves. While fragility analysis is useful in determining failure probabilities, it is contingent on a particular hazard occurring. Thus, the analysis in Chapter 3 indicates the probability of failure of each component along the vertical load path if it was subjected to tornado wind speeds between 80-402 kph (50-250 mph). However, as discussed previously, the probability of any one particular structure being impacted by a tornado is quite small. Thus, the fragility curves were convolved with the tornado hazard curves to assess unconditional failure probabilities.

Chapter 3 of this dissertation included an in-depth fragility analysis on residential structures subjected to tornadic wind loads using typical wood-frame construction methodologies. However, fragility analysis assesses structural performance assuming tornado occurrence. Thus the work presented in Chapter 4 of this dissertation extends the fragility analysis found in Chapter 3 such that tornado hazard curves from Chapter 2 are convolved with the component and system level fragilities to determine the unconditional risk of tornado damage for typical wood-frame residential construction across the United States. Then, a comparison of structural performance with typical construction for several tornado-prone locations to the stricter wind provisions of the FRC 2010 was performed to quantitatively determine the reduction in tornado damage probabilities to residential structures when the FRC 2010 was applied in other regions of the U.S.

The probability of exceeding a limit state is described as

$$P(g(x) < 0) = \sum P(g(x) < 0 | De = x) P(De = x) \quad (4.1)$$

where $P(De=x)$ is the probability that the demand, De , will have a value of x , and $P(g(x) < 0 | De = x)$ is the conditional probability of the function, defined as the fragility. The demand, De , is any random variable describing intensity which, for the purposes of this dissertation, is the 3s gust wind speed. When the components of Equation 4.1 are continuous, then the summation becomes a convolution integral to assess failure probability (e.g. Rosowsky and Ellingwood 2002, Amini 2012). Numerical convolution of a tornado hazard curve and a fragility curve allows for the estimation of unconditional tornado risk. The convolution integral is expressed as

$$P_f = - \int_0^{\infty} P_f(v) \left(\frac{dH(v)}{dv} \right) dv \quad (4.2)$$

where $P_f(v)$ is the conditional probability of failure given a wind speed v , also referred to as the fragility, $H(v)$ is the tornado hazard probability or tornado hazard curve. The negative sign in front of the integration takes into account the fact that the derivative of the hazard curve is less than zero since the slope of the tornado hazard curve is negative. The convolution integral describes a fully coupled risk analysis in that the variability in structural performance (fragility analysis) and the demand are considered. As described earlier, tornado hazard curves shown in Figure 2.8 were developed using the methodology described in Chapter 2. Fragility analysis on different structure types across the country was performed for three different components individually as well as for the structures as a system in order to complete the convolution and hence a tornado risk analysis.

The demand in this case varied depending on the location within the United States. Since the tornado hazard is not identical between any two locations, individual hazard curves were needed. Figure 2.8 illustrates the hazard curves used in this work for the six selected locations and also highlights the natural variability in tornado hazard across the country. The convolution of the tornado hazard curve and fragility curves for each component and the entire system at each of the six locations was performed and is presented below. Failure probabilities are presented over a 50 year period. This value is in agreement with ASCE 7-05 return periods for non-hurricane wind speeds. In order to obtain the 50 year failure probability from the annual failure probability described in Equation 4.2, Equation 4.3 was used and is given as

$$P_{f50} \cong 1 - (1 - P_f)^{50} \quad (4.3)$$

where P_{f50} is the 50 year failure probability, and P_f is the annual failure probability obtained from Equation 4.2 (Luco *et al.* 2007). This approximate relationship is believed to be valid since variability in the fragility is small compared to the annual variability of the hazard.

4.2 Roof Sheathing

Overall, a comparison of the annual failure probabilities due to tornadoes with local building codes and with the FRC 2010 was performed and analyzed for both the upper and lower bounds. For the roof sheathing system, the 50 year failure probabilities were reduced as much as several orders of magnitude for most damage states at each of the sample locations when Florida style construction was used.

The results from convolving the structural fragilities and tornado hazard for the roof sheathing system connection are presented in tabular form below. Contour maps could be generated and shown in terms of risk, but because local jurisdictions have the ability to alter

broader model building codes locally, the number of designs that may be needed fall beyond the scope of this study. While the failure probabilities obtained from the fragility curves range from 0-1, the convolved values of unconditional risk remain quite small as evident in Tables 4.1-12. This is because the convolution integral takes into account the probability of a tornado occurring at a location which varies but has an occurrence probability in the range of 10^{-4} to less than 10^{-10} , even in highly active regions as shown earlier in Figure 2.8.

Tables 4.1-12 present the convolved 50 year failure probabilities from tornadoes for the roof sheathing system at each of the six locations for both the upper and lower bounds. Recall that the fragilities were created using two methodologies as described in Section 3.4. The upper bound was found using ASCE 7-10 with a tornado amplification factor, K_c described by Haan *et al.* (2010). The lower bound was found using ASCE 7-16 wind provisions, but the tornado amplification was neglected. As with the fragility analysis, convolution was performed for both the upper and lower bounds.

The impact of strengthened construction is immediately apparent. In Tornado Alley, the impact of strengthened construction is noticeable for all damage states shown in Tables 4.1 and 4.2. The left hand side of the tables presents the 50 year failure probabilities using the locally adopted residential building code, IRC 2009. Similarly, the 50 year failure probabilities are presented when the FRC 2010 design guidelines are used for residential construction in Tornado Alley. The failure probabilities obtained from numerical convolution utilize the same tornado hazard curve, but have different fragility curves based on different construction guidelines. For the upper bound DS1, the use of strengthened construction reduces the failure probability by an order of magnitude. However, for more severe damage states, DS3 and DS4, the reduction in the

50 year failure probabilities is quite large ranging from three to four orders of magnitude when estimating unconditional failure probabilities using the upper bound.

The lower bound failure probabilities indicate a similar pattern as shown in Table 4.2. Using the 2010 FRC reduces the failure probability by two orders of magnitude. As with the upper bound, for the more severe damage states (DS3-4), the reduction in 50 year failure probabilities is between three to four orders of magnitude. The failure probabilities using IRC 2009 had the same order of magnitude for both the lower and upper bounds. However, for DS1 and DS2 using FRC 2010, the difference between the upper and lower bounds is one order of magnitude. This is expected since the lower bound indicated better structural performance than the upper bound as shown by the rightward shift of the fragility curves shown in Chapter 3.

Table 4.1: Upper Bound Roof Sheathing System 50 year failure probabilities for Tornado Alley

Tornado Alley								
Building Code	IRC 2009				FRC 2010			
Damage State	0	<=1	<=10%	<=25%	0	<=1	<=10%	<=25%
Type 1	5.72E-03	5.12E-03	3.90E-03	2.66E-03	8.22E-05	7.39E-06	1.05E-06	7.80E-07
Type 2	6.37E-03	5.99E-03	5.10E-03	4.06E-03	2.67E-04	7.93E-05	6.65E-06	1.41E-06
Type 3	6.38E-03	5.99E-03	4.97E-03	3.60E-03	2.88E-04	7.78E-05	4.77E-06	9.72E-07
Type 4	5.62E-03	5.13E-03	4.10E-03	2.90E-03	1.99E-05	5.19E-06	1.28E-06	8.04E-07
Type 5	6.64E-03	6.33E-03	4.92E-03	3.42E-03	4.97E-04	2.12E-04	4.31E-06	8.93E-07
Average	6.14E-03	5.71E-03	4.60E-03	3.33E-03	2.31E-04	7.64E-05	3.61E-06	9.72E-07

Table 4.2: Lower Bound Roof Sheathing System 50 year failure probabilities for Tornado Alley

Tornado Alley								
Building Code	IRC 2009				FRC 2010			
Damage State	0	<=1	<=10%	<=25%	0	<=1	<=10%	<=25%
Type 1	5.34E-03	4.66E-03	3.37E-03	2.35E-03	2.31E-05	3.14E-06	8.08E-07	7.66E-07
Type 2	5.99E-03	5.58E-03	4.57E-03	3.50E-03	6.38E-05	1.73E-05	2.14E-06	8.97E-07
Type 3	5.82E-03	5.35E-03	4.05E-03	2.79E-03	4.82E-05	1.00E-05	1.10E-06	7.81E-07
Type 4	4.62E-03	3.97E-03	2.84E-03	1.75E-03	1.59E-06	9.43E-07	7.80E-07	7.61E-07
Type 5	5.93E-03	5.48E-03	3.58E-03	2.55E-03	7.93E-05	1.50E-05	8.46E-07	7.70E-07
Average	5.54E-03	5.01E-03	3.68E-03	2.58E-03	4.32E-05	9.29E-06	1.14E-06	7.95E-07

The 50 year failure probabilities for Dixie Alley are presented in Tables 4.3 and 4.4. The failure probabilities have similar magnitudes to those in Tornado Alley, except for the strengthened construction for DS3 and DS4. This is likely due to the fact that there is a slightly higher annual tornado probability at the Dixie Alley location compared to the Tornado Alley location as indicated in Figure 2.8. In addition, there was no locally adopted building code at the Dixie Alley location and design specifications were based on observations from damage surveys after the April 27th, 2011 tornado outbreak (van de Lindt *et al.* 2013). The roof sheathing used in this analysis for Dixie Alley was 9.5 mm (0.375 in) which was slightly lower than at the Tornado Alley location (12.7 mm (0.5 in)). These likely resulted in the slightly higher 50 year failure probabilities in Dixie Alley.

Table 4.3: Upper Bound Roof Sheathing System 50 year failure probabilities for Dixie Alley

Dixie Alley								
Building Code	AL Construction				FRC 2010			
Damage State	0	<=1	<=10%	<=25%	0	<=1	<=10%	<=25%
Type 1	8.20E-03	7.46E-03	5.76E-03	3.99E-03	7.32E-05	2.51E-05	5.48E-06	1.21E-06
Type 2	9.09E-03	8.52E-03	7.45E-03	6.01E-03	2.14E-04	9.23E-05	2.78E-05	9.24E-06
Type 3	9.10E-03	8.51E-03	7.31E-03	5.29E-03	2.29E-04	9.09E-05	2.33E-05	4.63E-06
Type 4	8.07E-03	7.49E-03	6.10E-03	4.32E-03	4.10E-05	2.30E-05	7.79E-06	1.53E-06
Type 5	9.54E-03	8.99E-03	7.26E-03	5.04E-03	3.85E-04	1.76E-04	2.25E-05	3.40E-06
Average	8.80E-03	8.20E-03	6.77E-03	4.93E-03	1.89E-04	8.15E-05	1.74E-05	4.00E-06

Table 4.4: Lower Bound Roof Sheathing System 50 year failure probabilities for Dixie Alley

Dixie Alley								
Building Code	AL Construction				FRC 2010			
Damage State	0	<=1	<=10%	<=25%	0	<=1	<=10%	<=25%
Type 1	7.74E-03	6.88E-03	4.98E-03	3.58E-03	1.23E-04	4.36E-05	9.68E-06	3.06E-06
Type 2	8.54E-03	7.99E-03	6.81E-03	5.14E-03	2.47E-04	1.23E-04	4.24E-05	1.61E-05
Type 3	8.32E-03	7.74E-03	6.00E-03	4.15E-03	1.97E-04	8.98E-05	2.37E-05	6.54E-06
Type 4	6.80E-03	5.87E-03	4.24E-03	2.71E-03	2.83E-05	1.68E-05	6.02E-06	1.35E-06
Type 5	8.49E-03	7.89E-03	5.29E-03	3.84E-03	2.67E-04	1.10E-04	1.33E-05	4.21E-06
Average	7.98E-03	7.28E-03	5.47E-03	3.89E-03	1.72E-04	7.67E-05	1.90E-05	6.26E-06

The Midwest roof sheathing system failure probabilities are shown in Tables 4.5-4.6. The use of strengthened construction resulted in a reduction of the failure probabilities ranging from two orders of magnitude for DS1 to three orders of magnitude for DS3 for the upper bound. Similarly, the lower bound failure probabilities are reduced by four orders of magnitude for DS3 and DS4. The 50 year failure probabilities have a slightly smaller magnitude compared to the probabilities at the Tornado Alley and Dixie Alley locations. This is likely due to the lower rate of strong tornadoes at the Midwest location, and thus indicates that the probability of

experiencing a tornadic wind speed that would cause DS 3-4 is lower in the Midwest than the Tornado Alley and Dixie Alley locations.

As before, there is a reduction in failure probabilities when the fragility curves were created using the lower versus the upper bounds. This was expected since the lower bound fragility curves indicated better structural performance under tornado wind loads. Due to this fact, the 50 year unconditional failure probabilities would be reduced. When comparing Tables 4.5 and 4.6, there is a reduction in the failure probabilities between one and two order of magnitudes with the IRC 2009 by using the two different methods to estimate structural performance. This is difference is increased when looking at the FRC 2010, where the difference between the upper and lower bounds ranges from two to three orders of magnitude.

Table 4.5: Upper Bound Roof Sheathing System 50 year failure probabilities for the Midwest

Midwest								
Building Code	IRC 2009				FRC 2010			
Damage State	0	<=1	<=10%	<=25%	0	<=1	<=10%	<=25%
Type 1	3.00E-03	2.07E-03	1.05E-03	4.83E-04	1.28E-05	2.34E-06	1.13E-06	1.11E-06
Type 2	4.37E-03	3.34E-03	1.99E-03	1.14E-03	3.77E-05	1.34E-05	2.28E-06	1.18E-06
Type 3	4.40E-03	3.35E-03	1.85E-03	8.69E-04	4.00E-05	1.32E-05	1.85E-06	1.12E-06
Type 4	2.79E-03	2.07E-03	1.18E-03	5.66E-04	4.39E-06	1.94E-06	1.16E-06	1.11E-06
Type 5	5.24E-03	4.13E-03	1.80E-03	7.78E-04	6.99E-05	2.99E-05	1.74E-06	1.12E-06
Average	3.96E-03	2.99E-03	1.57E-03	7.67E-04	3.30E-05	1.22E-05	1.63E-06	1.13E-06

Table 4.6: Lower Bound Roof Sheathing System 50 year failure probabilities for the Midwest

		Midwest							
Building Code		IRC 2009				FRC 2010			
Damage State		0	<=1	<=10%	<=25%	0	<=1	<=10%	<=25%
Type 1		5.43E-05	3.86E-05	1.97E-05	9.10E-06	1.39E-07	1.69E-08	1.62E-09	1.22E-09
Type 2		8.10E-05	6.34E-05	3.83E-05	2.17E-05	5.27E-07	1.94E-07	1.98E-08	2.39E-09
Type 3		8.14E-05	6.34E-05	3.57E-05	1.66E-05	5.60E-07	1.90E-07	1.29E-08	1.50E-09
Type 4		5.09E-05	3.89E-05	2.22E-05	1.07E-05	4.37E-08	1.30E-08	2.07E-09	1.24E-09
Type 5		9.78E-05	7.86E-05	3.49E-05	1.50E-05	1.02E-06	4.82E-07	1.16E-08	1.37E-09
Average		7.31E-05	5.66E-05	3.02E-05	1.46E-05	4.57E-07	1.79E-07	9.60E-09	1.54E-09

Results are shown in Tables 4.7 and 4.8 for the High Plains. Failure probabilities for the locally adopted residential code, IRC 2012, are smaller in magnitude than the previously discussed locations. This is likely due to the low occurrence of strong tornadoes. The impact of strengthened construction reduces the failure probabilities by two to three orders of magnitude for both the upper and lower bounds. The 50 year failure probabilities are shown for the Northwest in Tables 4.9-10. For all damage states, the failure probabilities in the Northwest are extremely small (on the order of 10^{-8}). Furthermore, the impact of strengthened construction is not noticeable except for DS1 and DS 2. This is due to the very low occurrence of tornadoes at this location. Results in Tables 4.9-10 indicate it would not be economical or cost effective to use strengthened construction at this location due to the negligible reduction in failure probabilities over a 50 year period.

Table 4.7: Upper Bound Roof Sheathing System 50 year failure probabilities for the High Plains

High Plains								
Building Code	IRC 2012				FRC 2010			
Damage State	0	<=1	<=10%	<=25%	0	<=1	<=10%	<=25%
Type 1	4.80E-04	2.79E-04	9.94E-05	2.70E-05	4.16E-07	2.83E-07	2.81E-07	2.81E-07
Type 2	7.94E-04	5.41E-04	2.61E-04	1.11E-04	9.10E-07	3.40E-07	2.82E-07	2.81E-07
Type 3	8.04E-04	5.42E-04	2.37E-04	7.09E-05	9.35E-07	3.39E-07	2.81E-07	2.81E-07
Type 4	4.29E-04	2.78E-04	1.19E-04	3.52E-05	2.93E-07	2.82E-07	2.81E-07	2.81E-07
Type 5	1.02E-03	7.24E-04	2.26E-04	5.87E-05	2.22E-06	5.21E-07	2.81E-07	2.81E-07
Average	7.05E-04	4.73E-04	1.88E-04	6.06E-05	9.54E-07	3.53E-07	2.81E-07	2.81E-07

Table 4.8: Lower Bound Roof Sheathing System 50 year failure probabilities for the High Plains

High Plains								
Building Code	IRC 2012				FRC 2010			
Damage State	0	<=1	<=10%	<=25%	0	<=1	<=10%	<=25%
Type 1	3.57E-04	1.99E-04	5.83E-05	1.86E-05	2.97E-07	2.81E-07	2.81E-07	2.81E-07
Type 2	5.70E-04	3.86E-04	1.76E-04	6.40E-05	3.44E-07	2.86E-07	2.81E-07	2.81E-07
Type 3	5.09E-04	3.27E-04	1.11E-04	3.02E-05	3.37E-07	2.83E-07	2.81E-07	2.81E-07
Type 4	2.08E-04	1.11E-04	3.35E-05	8.92E-06	2.81E-07	2.81E-07	2.81E-07	2.81E-07
Type 5	5.61E-04	3.59E-04	6.92E-05	2.27E-05	3.89E-07	2.86E-07	2.81E-07	2.81E-07
Average	4.41E-04	2.76E-04	8.95E-05	2.89E-05	3.30E-07	2.83E-07	2.81E-07	2.81E-07

Table 4.9: Upper Bound Roof Sheathing System 50 year failure probabilities for the Northwest

Northwest								
Building Code	ORC 2011				FRC 2010			
Damage State	0	<=1	<=10%	<=25%	0	<=1	<=10%	<=25%
Type 1	5.76E-06	1.07E-07	8.01E-08	8.00E-08	8.00E-08	8.00E-08	8.00E-08	8.00E-08
Type 2	1.14E-05	5.38E-07	8.52E-08	8.01E-08	8.00E-08	8.00E-08	8.00E-08	8.00E-08
Type 3	1.39E-05	5.61E-07	8.31E-08	8.00E-08	8.00E-08	8.00E-08	8.00E-08	8.00E-08
Type 4	4.46E-06	9.85E-08	8.02E-08	8.00E-08	8.00E-08	8.00E-08	8.00E-08	8.00E-08
Type 5	2.72E-05	1.93E-06	8.20E-08	8.00E-08	8.01E-08	8.00E-08	8.00E-08	8.00E-08
Average	1.26E-05	6.46E-07	8.21E-08	8.01E-08	8.00E-08	8.00E-08	8.00E-08	8.00E-08

Table 4.10: Lower Bound Roof Sheathing System 50 year failure probabilities for the Northwest

Northwest									
Building Code	ORC 2011				FRC 2010				
Damage State	0	<=1	<=10%	<=25%	0	<=1	<=10%	<=25%	
Type 1	1.41E-06	8.69E-08	8.00E-08	8.00E-08	8.00E-08	8.00E-08	8.00E-08	8.00E-08	
Type 2	2.49E-06	1.65E-07	8.08E-08	8.00E-08	8.00E-08	8.00E-08	8.00E-08	8.00E-08	
Type 3	1.06E-05	1.21E-07	8.01E-08	8.00E-08	8.00E-08	8.00E-08	8.00E-08	8.00E-08	
Type 4	3.02E-07	8.06E-08	8.00E-08	8.00E-08	8.00E-08	8.00E-08	8.00E-08	8.00E-08	
Type 5	1.17E-05	1.50E-07	8.00E-08	8.00E-08	8.00E-08	8.00E-08	8.00E-08	8.00E-08	
Average	5.29E-06	1.21E-07	8.02E-08	8.00E-08	8.00E-08	8.00E-08	8.00E-08	8.00E-08	

The 50 year failure probabilities for the Florida Peninsula are shown in Tables 4.11 and 4.12. Results indicate that the 50 year probability of failure is small (10^{-6}) for both the upper and lower bound. This is due to the tornado hazard curve for the Florida Peninsula and the impact of strengthened construction. While Florida does not experience a high number of strong tornadoes (wind speeds in excess of 241 kph (150 mph)), it does see a high occurrence of weak tornadoes. However, the stricter building codes implemented across the state results in relatively low failure probabilities, especially in wind speeds below 241 kph (150 mph).

Table 4.11: Upper Bound Roof Sheathing System 50 year failure probabilities for the Florida Peninsula

Florida Peninsula				
Building Code	FRC 2010			
Damage State	0	<=1	<=10%	<=25%
Type 1	1.10E-06	1.09E-06	1.09E-06	1.09E-06
Type 2	1.17E-06	1.09E-06	1.09E-06	1.09E-06
Type 3	1.15E-06	1.09E-06	1.09E-06	1.09E-06
Type 4	1.09E-06	1.09E-06	1.09E-06	1.09E-06
Type 5	1.66E-06	1.10E-06	1.09E-06	1.09E-06
Average	1.23E-06	1.09E-06	1.09E-06	1.09E-06

Table 4.12: Lower Bound Roof Sheathing System 50 year failure probabilities for the Florida Peninsula

Florida Peninsula				
Building Code	FRC 2010			
Damage State	0	<=1	<=10%	<=25%
Type 1	1.09E-06	1.09E-06	1.09E-06	1.09E-06
Type 2	1.09E-06	1.09E-06	1.09E-06	1.09E-06
Type 3	1.09E-06	1.09E-06	1.09E-06	1.09E-06
Type 4	1.09E-06	1.09E-06	1.09E-06	1.09E-06
Type 5	1.10E-06	1.09E-06	1.09E-06	1.09E-06
Average	1.09E-06	1.09E-06	1.09E-06	1.09E-06

4.3 Roof-to-Wall Connection

The reduction in the annual failure probabilities for roof-to-wall connections was also reduced but to a smaller degree. This is likely due to the limited uplift resistance a single H2.5 clip provides at wind speeds beyond 241 kph (150 mph) when estimating the wind load using the upper bound. There was greater variability in the roof-to-wall connection reductions due to the numerous types of roof-to-wall connections used as well as the variability in tornado hazard at each location.

The analysis for the roof-to-wall connection was performed in a similar manner to the roof sheathing system. The roof-to-wall connection results for each of the six locations are shown in Tables 4.13 and 4.14. As before, the 50 year failure probabilities for the locally adopted residential building codes are shown on the left and the 50 year failure probabilities with strengthened construction required by the FRC 2010 are presented on the right. The upper bound failure probabilities are shown in Table 4.13 whereas the lower bound failure probabilities are shown in Table 4.14. Recall that for the roof-to-wall connection, the only difference between the upper and lower bounds was the inclusion of the tornado amplification factor, K_c . Thus,

structural performance estimated using the lower bound was improved, which resulted in a rightward shift of the fragility curves as shown in Section 3.6.2.

Table 4.13: Upper Bound Roof-to-wall connection 50 year failure probabilities for the six sample locations

Building Code	Tornado Alley		Dixie Alley		Midwest	
	IRC 2009	FRC 2010	AL Const.	FRC 2010	IRC 2009	FRC 2010
Type 1	5.26E-03	2.70E-03	9.12E-03	4.01E-03	2.53E-03	6.52E-04
Type 2	5.73E-03	9.10E-04	9.42E-03	1.50E-03	3.23E-03	1.41E-04
Type 3	4.33E-03	1.54E-03	8.30E-03	2.38E-03	1.59E-03	2.78E-04
Type 4	5.04E-03	2.41E-03	8.89E-03	3.60E-03	2.26E-03	5.39E-04
Type 5	5.90E-03	4.50E-03	9.25E-03	6.53E-03	3.53E-03	1.71E-03
Average	5.25E-03	2.41E-03	9.00E-03	3.60E-03	2.63E-03	6.65E-04

Building Code	High Plains		Northwest		Florida Peninsula
	IRC 2012	FRC 2010	ORC 2011	FRC 2010	FRC 2010
Type 1	3.85E-04	5.84E-05	3.59E-06	8.08E-08	3.02E-05
Type 2	5.36E-04	6.21E-06	1.01E-05	8.00E-08	2.34E-06
Type 3	2.04E-04	1.68E-05	4.91E-07	8.01E-08	6.19E-06
Type 4	3.31E-04	4.42E-05	2.10E-06	8.04E-08	2.08E-05
Type 5	6.05E-04	2.26E-04	1.04E-05	1.43E-07	2.03E-04
Average	4.12E-04	7.03E-05	5.34E-06	9.29E-08	5.26E-05

The reduction in the 50 year upper bound failure probabilities for roof-to-wall connections is negligible for the Tornado Alley and Dixie Alley locations as shown in Table 4.13. Locations with moderate tornado activity (the Midwest and High Plains) experienced a reduction in 50 year failure probabilities of approximately one order of magnitude with the use of strengthened construction. As before, the 50 year failure probabilities in the Northwest are near zero due to the low occurrence of tornadoes. The small reduction in 50 year failure probabilities for the roof-to-wall connection is likely due to the fact that while a single H2.5 clip provides greater uplift resistance, it is not very effective in wind speeds above 240 kph (150 mph) as shown in the upper bound fragility curves for the roof-to-wall connections (Figures 3.20a-24a) (Amini and van de Lindt 2014). However, since the majority of tornadoes are rated

EF2 or lower (217 kph (135 mph) or lower), use of improved roof-to-wall connections may be beneficial at lower wind speeds. Likewise, as stated before, EF3-EF5 tornadoes only have a small percentage of area that experiences a high degree of damage (van de Lindt *et al.* 2013). Thus, even in the strongest tornadoes, it is likely an individual home will experience wind speeds below the highest EF rating, unless it receives a direct impact at the center of the tornado path.

Table 4.14: Lower Bound Roof-to-wall connection 50 year failure probabilities for the six sample locations

Building Code	Tornado Alley		Dixie Alley		Midwest	
	IRC 2009	FRC 2010	AL Const.	FRC 2010	IRC 2009	FRC 2010
Type 1	5.05E-05	1.47E-06	4.53E-03	2.20E-04	2.00E-04	1.04E-05
Type 2	1.90E-03	2.36E-04	5.16E-03	5.33E-04	3.41E-04	3.22E-05
Type 3	5.25E-04	8.27E-06	3.04E-03	6.28E-05	7.13E-05	2.39E-06
Type 4	1.05E-03	4.06E-05	4.08E-03	1.63E-04	1.55E-04	7.09E-06
Type 5	2.17E-03	6.01E-04	4.80E-03	1.08E-03	4.18E-04	8.13E-05
Average	1.14E-03	1.78E-04	4.32E-03	4.11E-04	2.37E-04	2.67E-05

Building Code	High Plains		Northwest		Florida Peninsula
	IRC 2012	FRC 2010	ORC 2011	FRC 2010	FRC 2010
Type 1	9.04E-06	3.57E-07	8.01E-08	8.00E-08	5.44E-05
Type 2	2.02E-05	7.60E-07	8.02E-08	8.00E-08	5.59E-05
Type 3	2.02E-06	2.85E-07	8.00E-08	8.00E-08	1.09E-06
Type 4	6.16E-06	3.20E-07	8.01E-08	8.00E-08	1.09E-06
Type 5	2.74E-05	2.32E-06	8.02E-08	8.00E-08	1.31E-06
Average	1.30E-05	8.09E-07	8.01E-08	8.00E-08	2.28E-05

The lower bound 50 year failure probabilities are shown in Table 4.14. There is a larger reduction in failure probabilities when comparing the adopted versus strengthened construction at the majority of locations. For Tornado Alley, Dixie Alley, and the Midwest, there is a one order of magnitude reduction in failure probabilities. In the High Plains, the reduction is slightly larger at two orders of magnitude when comparing IRC 2012 and FRC 2010. The Northwest

unconditional failure probabilities are again very small (10^{-8}) due to the low risk of tornado occurrence at that location. When comparing the upper and lower bound, the lower bound was smaller for both the standard and strengthened construction. This was expected since the wind loads for the lower bound were found using ASCE 7-16 provisions without any tornado amplification factor. Since the roof-to-wall connection is modeled as part of the MWFRS, there is no change between the parameters of ASCE 7-16 and ASCE 7-10, thus the lower bound structural performance was identical to estimating wind loads with straight line winds.

4.4 Wall-to-Foundation

Convolution of the tornado hazard curves and wall-to-foundation fragility curves are shown in Tables 4.15-20. As discussed in Sections 3.5 and 3.6, there was not a significant improvement of structural performance by including the RSP4 reinforcing clip. This was likely due to the similarity in failure mechanisms at the wall-to-foundation connection. As such, the reduction in 50 year failure probabilities is negligible between the different wall types. Thus, the unconditional failure probabilities for Wall Types A-D are approximately the same order of magnitude when found using either the upper bound or the lower bound.

While the unconditional failure probabilities have the same order of magnitude when comparing Wall Types A-D for a given methodology, there was a reduction in risk when the failure probabilities were calculated using the lower bound versus the upper bound in most locations as seen when comparing the left and right hand sides of Tables 4.15-20, with the exception of the location in Dixie Alley. The Tornado Alley location experienced a reduction in 50 year failure probabilities that was one order of magnitude when using the lower bound versus the upper bound. Similarly, locations in the Midwest and the Northwest had a reduction in risk between one to two orders of magnitude when convolving the lower bound fragility curve with

their respective tornado hazard curves. As before, the Northwest unconditional failure probabilities remained very small due to the limited tornado activity in this region. Finally, both the High Plains and Florida Peninsula experienced a reduction in 50 year failure probabilities when estimating risk using the lower bound as compared to the upper bound methodology. As with the roof-to-wall connection, this is due to the fact that the only difference between the upper and lower bounds is the tornado amplification factor described by Haan *et al.* (2010). Thus the lower bound fragility curves were found as if tornado winds were modeled as straight line winds.

Table 4.15: Wall-to-foundation 50 year failure probabilities for Tornado Alley

Tornado Alley								
Wall Type	Upper Bound 50 yr Failure Probabilities				Lower Bound 50 yr Failure Probabilities			
	A	B	C	D	A	B	C	D
Type 1	4.60E-03	4.50E-03	4.15E-03	4.31E-03	7.01E-04	5.60E-04	4.47E-04	4.50E-04
Type 2	3.60E-03	3.55E-03	3.35E-03	3.38E-03	6.84E-04	6.29E-04	5.21E-04	5.07E-04
Type 3	5.86E-03	5.80E-03	5.48E-03	5.53E-03	2.15E-03	2.00E-03	1.60E-03	1.60E-03
Type 4	1.97E-03	1.87E-03	1.63E-03	1.65E-03	1.69E-04	1.15E-04	8.97E-05	6.57E-05
Type 5	5.78E-03	5.71E-03	5.37E-03	5.42E-03	6.48E-04	5.75E-04	4.43E-04	4.18E-04
Average	4.36E-03	4.29E-03	4.00E-03	4.06E-03	8.71E-04	7.75E-04	6.21E-04	6.09E-04

Table 4.16: Wall-to-foundation 50 year failure probabilities for Dixie Alley

Dixie Alley								
Wall Type	Upper Bound 50 yr Failure Probabilities				Lower Bound 50 yr Failure Probabilities			
	A	B	C	D	A	B	C	D
Type 1	6.66E-03	6.53E-03	6.05E-03	6.27E-03	1.21E-03	1.02E-03	8.47E-04	8.64E-04
Type 2	5.27E-03	5.20E-03	4.93E-03	4.97E-03	1.20E-03	1.12E-03	9.63E-04	9.48E-04
Type 3	8.38E-03	8.28E-03	7.85E-03	7.92E-03	3.23E-03	3.01E-03	2.47E-03	2.46E-03
Type 4	2.98E-03	2.84E-03	2.50E-03	2.53E-03	4.15E-04	3.35E-04	2.65E-04	2.40E-04
Type 5	8.27E-03	8.16E-03	7.71E-03	7.77E-03	1.14E-03	1.04E-03	8.42E-04	8.13E-04
Average	6.31E-03	6.20E-03	5.81E-03	5.89E-03	1.44E-03	1.30E-03	1.08E-03	1.07E-03

Table 4.17: Wall-to-foundation 50 year failure probabilities for the Midwest

Midwest								
Wall Type	Upper Bound 50 yr Failure Probabilities				Lower Bound 50 yr Failure Probabilities			
	A	B	C	D	A	B	C	D
Type 1	1.82E-03	1.66E-03	1.46E-03	1.50E-03	1.10E-04	7.17E-05	6.32E-05	5.67E-05
Type 2	1.07E-03	1.04E-03	9.39E-04	9.39E-04	9.47E-05	8.46E-05	7.05E-05	6.62E-05
Type 3	3.51E-03	3.32E-03	2.89E-03	2.88E-03	4.30E-04	3.66E-04	2.85E-04	2.63E-04
Type 4	3.90E-04	3.52E-04	2.97E-04	2.86E-04	2.46E-05	1.71E-05	1.38E-05	1.08E-05
Type 5	3.37E-03	3.18E-03	2.74E-03	2.72E-03	9.04E-05	7.71E-05	6.04E-05	5.50E-05
Average	2.03E-03	1.91E-03	1.66E-03	1.66E-03	1.50E-04	1.23E-04	9.86E-05	9.04E-05

Table 4.18: Wall-to-foundation 50 year failure probabilities for the High Plains

High Plains								
Wall Type	Upper Bound 50 yr Failure Probabilities				Lower Bound 50 yr Failure Probabilities			
	A	B	C	D	A	B	C	D
Type 1	2.49E-04	2.12E-04	1.82E-04	1.84E-04	5.63E-06	1.68E-06	2.22E-06	1.15E-06
Type 2	1.17E-04	1.11E-04	9.69E-05	9.57E-05	3.01E-06	2.40E-06	1.98E-06	1.61E-06
Type 3	6.06E-04	5.56E-04	4.66E-04	4.56E-04	3.04E-05	2.20E-05	1.68E-05	1.30E-05
Type 4	2.74E-05	2.26E-05	1.82E-05	1.59E-05	7.03E-07	4.40E-07	4.49E-07	3.39E-07
Type 5	5.73E-04	5.25E-04	4.36E-04	4.24E-04	2.93E-06	2.14E-06	1.70E-06	1.32E-06
Average	3.14E-04	2.85E-04	2.40E-04	2.35E-04	8.53E-06	5.74E-06	4.64E-06	3.48E-06

Table 4.19: Wall-to-foundation 50 year failure probabilities for the Northwest

Northwest								
Wall Type	Upper Bound 50 yr Failure Probabilities				Lower Bound 50 yr Failure Probabilities			
	A	B	C	D	A	B	C	D
Type 1	1.82E-06	1.06E-07	5.23E-07	8.48E-08	1.69E-07	8.00E-08	8.09E-08	8.00E-08
Type 2	8.74E-08	8.52E-08	8.44E-08	8.27E-08	8.00E-08	8.00E-08	8.00E-08	8.00E-08
Type 3	6.77E-06	2.47E-06	2.67E-06	8.57E-07	8.05E-08	8.01E-08	8.01E-08	8.00E-08
Type 4	8.03E-08	8.01E-08	8.01E-08	8.01E-08	8.00E-08	8.00E-08	8.00E-08	8.00E-08
Type 5	5.74E-06	2.07E-06	2.40E-06	6.81E-07	8.00E-08	8.00E-08	8.00E-08	8.00E-08
Average	2.90E-06	9.62E-07	1.15E-06	3.57E-07	9.79E-08	8.00E-08	8.02E-08	8.00E-08

Table 4.20: Wall-to-foundation 50 year failure probabilities for the Florida Peninsula

Florida Peninsula								
Wall Type	Upper Bound 50 yr Failure Probabilities				Lower Bound 50 yr Failure Probabilities			
	A	B	C	D	A	B	C	D
Type 1	2.58E-04	1.69E-04	1.53E-04	1.33E-04	5.24E-06	1.21E-06	1.85E-06	1.14E-06
Type 2	7.81E-05	7.10E-05	5.93E-05	5.63E-05	1.48E-06	1.33E-06	1.29E-06	1.21E-06
Type 3	9.86E-04	8.25E-04	6.58E-04	5.95E-04	1.29E-05	7.22E-06	6.38E-06	3.74E-06
Type 4	1.16E-05	8.38E-06	6.94E-06	5.18E-06	1.14E-06	1.10E-06	1.11E-06	1.09E-06
Type 5	9.05E-04	7.55E-04	5.97E-04	5.31E-04	1.48E-06	1.29E-06	1.26E-06	1.17E-06
Average	4.48E-04	3.66E-04	2.95E-04	2.64E-04	4.45E-06	2.43E-06	2.38E-06	1.67E-06

4.5 System Level Analysis

Consistent with the individual connections along the vertical load path, the fragility curves were convolved with the tornado hazard curves for each of the six locations. This allowed for the calculation of the unconditional failure probabilities. As before, the failure probabilities are shown for a 50 year time frame as described with Eqn. 4.3. Tables 4.21-26 include the convolved failure probabilities for each location, structural archetype, and wind orientation.

Table 4.21: System Level 50-year Failure Probabilities for Tornado Alley

Tornado Alley					
Archetype	Orientation	Upper Bound 50 yr Failure Probability		Lower Bound 50 yr Failure Probability	
		IRC 2009	FRC 2010	IRC 2009	FRC 2010
Type 1	EW	5.17E-03	4.13E-03	3.11E-03	1.77E-04
	NS	5.44E-03	3.64E-03	2.92E-03	2.45E-04
Type 2	EW	5.23E-03	1.10E-03	4.54E-03	3.80E-06
	NS	5.94E-03	4.25E-03	4.55E-03	4.85E-04
Type 3	EW	5.13E-03	1.44E-03	4.20E-03	1.81E-05
	NS	5.66E-03	4.90E-03	4.20E-03	7.50E-04
	EW small	5.91E-03	5.42E-03	3.95E-03	1.41E-03
Type 4	EW	5.09E-03	2.58E-03	3.10E-03	7.05E-05
	NS	5.29E-03	2.47E-03	3.11E-03	4.49E-05
Type 5	EW	4.95E-03	4.35E-04	3.28E-03	1.40E-06
	NS	6.15E-03	4.80E-03	3.63E-03	8.01E-04
Average		5.45E-03	3.20E-03	3.69E-03	3.65E-04

Table 4.22: System Level 50-year Failure Probabilities for Dixie Alley

Dixie Alley					
Archetype	Orientation	Upper Bound 50 yr Failure Probability		Lower Bound 50 yr Failure Probability	
		AL Const.	FRC 2010	AL Const.	FRC 2010
Type 1	EW	8.65E-03	6.02E-03	4.92E-03	3.93E-04
	NS	9.13E-03	5.33E-03	5.17E-03	5.20E-04
Type 2	EW	8.41E-03	1.76E-03	6.64E-03	3.75E-05
	NS	9.47E-03	6.18E-03	6.79E-03	9.08E-04
Type 3	EW	7.91E-03	2.24E-03	6.17E-03	7.81E-05
	NS	8.58E-03	7.06E-03	6.20E-03	1.28E-03
	EW small	8.49E-03	7.78E-03	5.84E-03	2.20E-03
Type 4	EW	8.74E-03	3.84E-03	4.96E-03	2.17E-04
	NS	8.92E-03	3.69E-03	5.10E-03	1.73E-04
Type 5	EW	7.58E-03	8.01E-04	4.89E-03	1.27E-05
	NS	9.46E-03	6.93E-03	5.89E-03	1.36E-03
Average		8.67E-03	4.69E-03	5.69E-03	6.53E-04

Table 4.23: System Level 50-year Failure Probabilities for the Midwest

Midwest					
Archetype	Orientation	Upper Bound 50 yr Failure Probability		Lower Bound 50 yr Failure Probability	
		IRC 2009	FRC 2010	IRC 2009	FRC 2010
Type 1	EW	2.31E-03	1.42E-03	7.91E-04	2.56E-05
	NS	2.71E-03	1.16E-03	7.00E-04	3.50E-05
Type 2	EW	2.45E-03	1.80E-04	1.69E-03	1.63E-06
	NS	3.53E-03	1.53E-03	1.69E-03	6.60E-05
Type 3	EW	2.36E-03	2.84E-04	1.43E-03	3.64E-06
	NS	2.99E-03	2.08E-03	1.42E-03	1.11E-04
	EW small	3.49E-03	2.77E-03	1.25E-03	2.43E-04
Type 4	EW	2.25E-03	6.24E-04	7.87E-04	1.09E-05
	NS	2.49E-03	5.62E-04	7.91E-04	7.66E-06
Type 5	EW	2.16E-03	6.52E-05	8.73E-04	1.21E-06
	NS	3.99E-03	1.98E-03	1.04E-03	1.12E-04
Average		2.79E-03	1.15E-03	1.13E-03	5.61E-05

Table 4.24: System Level 50-year Failure Probabilities for the High Plains

High Plains					
Archetype	Orientation	Upper Bound 50 yr Failure Probability		Lower Bound 50 yr Failure Probability	
		IRC 2012	FRC 2010	IRC 2012	FRC 2010
Type 1	EW	3.36E-04	1.74E-04	7.47E-05	8.37E-07
	NS	4.19E-04	1.35E-04	6.22E-05	1.08E-06
Type 2	EW	3.68E-04	9.10E-06	2.19E-04	2.82E-07
	NS	6.02E-04	1.95E-04	2.19E-04	1.85E-06
Type 3	EW	3.51E-04	2.00E-05	1.73E-04	3.02E-07
	NS	4.79E-04	2.94E-04	1.72E-04	4.25E-06
	EW small	5.95E-04	4.38E-04	1.43E-04	1.35E-05
Type 4	EW	3.25E-04	5.64E-05	7.40E-05	3.89E-07
	NS	3.74E-04	4.69E-05	7.45E-05	3.26E-07
Type 5	EW	3.12E-04	2.58E-06	8.60E-05	2.81E-07
	NS	7.13E-04	2.75E-04	1.09E-04	3.72E-06
Average		4.43E-04	1.50E-04	1.28E-04	2.44E-06

Table 4.25: System Level 50-year Failure Probabilities for the Northwest

Northwest					
Archetype	Orientation	Upper Bound 50 yr Failure Probability		Lower Bound 50 yr Failure Probability	
		ORC 2011	FRC 2010	ORC 2011	FRC 2010
Type 1	EW	1.03E-06	1.02E-07	8.89E-08	8.00E-08
	NS	3.84E-06	1.11E-07	8.42E-08	8.00E-08
Type 2	EW	1.40E-06	8.00E-08	2.34E-07	8.00E-08
	NS	1.09E-05	1.28E-07	2.24E-07	8.00E-08
Type 3	EW	1.29E-06	8.02E-08	1.60E-07	8.00E-08
	NS	1.79E-06	3.27E-07	1.55E-07	8.00E-08
	EW small	4.34E-06	1.79E-06	1.21E-07	8.01E-08
Type 4	EW	1.23E-06	8.15E-08	8.67E-08	8.00E-08
	NS	2.39E-06	8.05E-08	8.67E-08	8.00E-08
Type 5	EW	8.22E-07	8.00E-08	8.89E-08	8.00E-08
	NS	1.58E-05	2.11E-07	9.47E-08	8.00E-08
Average		4.07E-06	2.79E-07	1.30E-07	8.00E-08

Table 4.26: System Level 50-year Failure Probabilities for the Florida Peninsula

Florida Peninsula			
Archetype	Orientation	Upper Bound	Lower Bound
		50 yr Failure Probability	50 yr Failure Probability
		FRC 2010	FRC 2010
Type 1	EW	1.33E-04	1.16E-06
	NS	1.04E-04	1.19E-06
Type 2	EW	3.36E-06	1.09E-06
	NS	1.67E-04	1.26E-06
Type 3	EW	9.38E-06	1.09E-06
	NS	3.02E-04	1.82E-06
	EW small	5.87E-04	4.85E-06
Type 4	EW	3.10E-05	1.10E-06
	NS	2.26E-05	1.09E-06
Type 5	EW	1.58E-06	1.09E-06
	NS	2.73E-04	1.56E-06
Average		1.49E-04	1.57E-06

The results of the upper bound load path system analysis indicate that the locations in Tornado Alley, Dixie Alley, and the Midwest have unconditional failure probabilities larger than

the remaining locations, as one would imagine. This increased risk is an order of magnitude larger than locations in the Florida Peninsula and the High Plains. Likewise, the failure probabilities are three orders of magnitude larger than the location in the Northwest, but this was expected since tornado occurrence is relatively rare west of the Rocky Mountains. In addition, results also indicate that failure of the vertical load path was near 100% once wind speeds reached 240 kph (150 mph) as shown in the upper bound fragility curves in Figures 3.31a-35a. Thus, failure of one or more connections along the vertical load path can be expected with tornadoes rated EF3 or greater with the upper bound estimation.

By comparison, the lower bound unconditional failure probabilities for the vertical load path analysis indicated a reduction in risk in most locations when compared to the results from the upper bound convolution. For Tornado Alley, Dixie Alley, the Midwest, and the High Plains, there was not a reduction in risk when using standard versus strengthened construction using the upper bound methodology. However, when using the lower bound, Tornado Alley and Dixie Alley experienced a reduction in risk of one order of magnitude and the Midwest and High Plains experienced a reduction in failure probabilities that was two orders of magnitude. This indicates that these would be the locations where it would be the most reasonable to consider strengthened construction practices. In the Northwest, the difference between the ORC 2011 and FRC 2010 was one order of magnitude for both the upper and lower bounds, however, the actual failure probabilities were reduced when comparing the upper and lower bound methods. When using the upper bound, the failure probabilities were 10^{-6} and 10^{-7} for the ORC 2011 and the FRC 2010 respectively, yet with the lower bound, these were reduced to 10^{-7} and 10^{-8} . As with the previous components, the difference between the upper and lower bound unconditional failure probabilities is attributed to the how the tornado wind load was calculated for the limit state

analysis. The approach using the ASCE 7-10 coefficients also utilized a tornado amplification factor, thus providing the upper bound, whereas ASCE 7-16 used updated external pressure coefficients for C&C, but did not account for any amplification due to the tornado vortex. Therefore, ASCE 7-16 provided the lower bound.

4.6 Summary

While the values of the annual failure probabilities may seem small, they can become meaningful over the lifetime of a building, especially in regions with high tornado activity as illustrated using the 50 year failure probabilities. Additionally, no structural or strength deterioration is included in the analysis which would only increase the failure probabilities. Use of strengthened construction methodologies in high risk areas would likely reduce the number of injuries and fatalities, and would also reduce the search and recovery, clean-up, and rebuilding efforts on a large scale thereby improving both recovery and contributing to resilience (and sustainability) objectives. Likewise, damage to a house can be minimized if the roof remains attached. By keeping the roof intact and in place, damage due to rain water intrusion (see e.g. Dao and van de Lindt 2012), wind damage, and structural collapse can be prevented.

While it may not be economical or reasonable to adopt tornado provisions in regions with low tornado activity, it is evident that improved construction could be beneficial in high activity areas such as Tornado Alley and Dixie Alley, and even in the Midwest. Florida style construction was especially beneficial in wind speeds above 145 kph (90 mph) and below 241 kph (150 mph), which includes the vast majority of reported tornadoes. Locations in Tornado Alley, Dixie Alley, and the Midwest had higher unconditional failure probabilities since they had the highest rate of tornado occurrence of six locations. Results also indicated that in wind speeds above 240 kph (150 mph) it becomes increasingly difficult to keep wood-frame construction

intact. However, strengthened construction may be beneficial in regions of high tornado activity since the majority of tornado wind speeds fall below 240 kph (150 mph). It should be noted that the majority of tornadoes are rated EF2 or lower. Even in the strongest tornadoes, the area of wind speeds in excess of 240 kph (150 mph) is quite small (van de Lindt *et al.* 2013). Thus, while strengthened construction practices may not be economical for a typical wood-frame building subjected to winds above this value, improved connections may be beneficial at lower wind speeds. This is especially true for roof sheathing performance. Failure of the roof sheathing changes the enclosure classification from enclosed to partially enclosed, increasing the internal pressure of the structure. This in turn increases the uplift load experienced by the roof-to-wall and wall-to-foundation connections.

It should be noted that in this dissertation the performance of five different structural archetypes were analyzed. While performance did vary by archetype, the results of the five archetypes are treated as an ensemble of typical construction. Thus the conclusions drawn from the fragility and convolution analyses can be applied to a broad range of residential construction in varying locations across the United States, but it is recognized that some differences in performance may occur compared to the archetype performance presented herein as a result of the moderate number of archetypes utilized herein.

Finally, there has been some discussion comparing the unconditional failure probabilities presented in this dissertation with the reliability indices presented in the ASCE 7-10 commentary. Specifically, the values of the unconditional failure probabilities from this dissertation for the high risk areas have a similar magnitude to those presented for Risk Category II structures. One important difference is that the failure probabilities in the ASCE 7 commentary are focused on risk to human life. However, for the work in this dissertation and for

performance-based wind engineering, the focus is on damage reduction. Thus, the current code limits damage based with the intent of protecting life safety, but not because it is controlling monetary loss.

CHAPTER 5

PROPERTY LOSS ESTIMATION FOR THE APRIL 25-28, 2011 TORNADO OUTBREAK

5.1 Summary of the April 25-28, 2011 Tornado Outbreak

The remarkable nature of the April 25-28, 2011 outbreak prompted significant research interest in understanding the impact of tornado hazards on the built environment (Prevatt *et al.* 2011a, Prevatt *et al.* 2012a, FEMA 2012, van de Lindt *et al.* 2013). This chapter aims to estimate property loss to wood-frame construction and manufactured homes from the tornadoes of the Super Outbreak of April 2011. Property loss was estimated using the fragility curves from Chapter 3 of this analysis, based on the locally adopted residential building codes as of 2011. Similar to Chapter 4, a comparison was performed using locally adopted residential codes versus the strengthened construction of the FRC 2010. This allowed for an estimation of the reduction of property loss from tornadoes when using strengthened construction methodologies.

The largest tornado outbreak in U.S. history occurred during a four-day period from April 25-28, 2011. Meteorologists began discussing a potential for a significant severe weather event across the southeast U.S. as early as April 18, 2011 (FEMA 2012). Confidence in the forecast in the days leading up to the event grew as model guidance converged and indicated atmospheric conditions favorable for long track, violent tornadoes. While the outbreak was well forecasted, it still resulted in significant damage, injuries, and loss of life.

A total of 350 tornadoes were reported across 21 states as shown in Figure 5.1 and summarized in Table 5.1. The forecast for long track, violent tornadoes was verified with a total of 15 tornadoes rated as EF4 or EF5. A summary of the tornado ratings for the April 25-28,

2011 outbreak is included in Table 5.2. Overall, the outbreak was responsible for more than \$5B in property loss, 324 fatalities, and at least 2906 injuries according to data obtained from the Storm Prediction Center (SPC 2011). While the outbreak did cover a large geographic region, Alabama, Tennessee, Georgia, and Mississippi received the brunt of the impact. Alabama was the hardest hit with over 70% (233) of the fatalities. Likewise, Mississippi and Georgia had 38 and 25 fatalities respectively and Tennessee had 19. The remaining fatalities occurred in Arkansas (5) and Virginia (4).

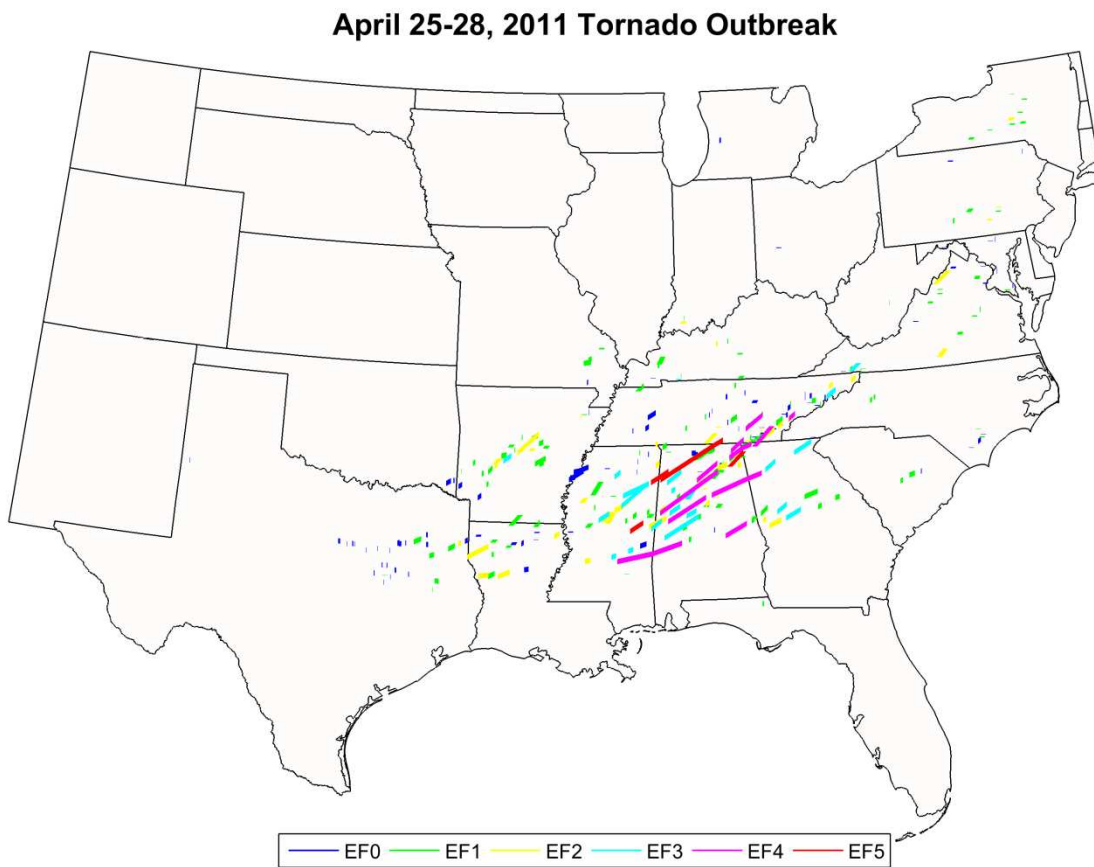


Figure 5.1: Map of all the reported tornadoes from the April 25-28, 2011 outbreak.

Table 5.1: Number of Tornadoes Reported per State

State Impacted	No. Tornadoes*
Tennessee	76
Alabama	62
Mississippi	42
Texas	34
Arkansas	31
Virginia	19
Louisiana	16
Georgia	16
North Carolina	14
Kentucky	13
Maryland	11
New York	9
Pennsylvania	7
Missouri	5
Oklahoma	3
Indiana	3
South Carolina	3
Florida	2
Michigan	1
Ohio	1
West Virginia	1

**Note: This is the total number of tornadoes reported in each state. Some tornadoes crossed state borders and thus impacted multiple states. In this case, it was included in the tornado count for both states in order to get the tornado count for each state.*

Table 5.2: Number of Tornadoes for each EF Intensity

EF5	EF4	EF3	EF2	EF1	EF0
4	11	22	49	138	126

April 27, 2011 was the most active day of the outbreak with 207 reported tornadoes. During the morning hours, an intense quasi-linear convective system moved across Alabama resulting in several strong tornadoes (EF2 and EF3). It is likely that many people suspected that the early morning round of storms were the severe weather that was forecasted and well-broadcasted for the area (FEMA 2012). Likewise, the early morning storms left many without

power and potentially unable to receive weather warnings in the afternoon. Several NOAA Weather Radio All Hazards transmitters were impacted by the power outages as well (NOAA 2011). Unfortunately, a second round of more intense severe weather occurred in the afternoon, which many may not have anticipated or have been prepared for. The afternoon storms consisted of numerous supercell thunderstorms which produced several long-lived strong tornadoes.

All the violent EF4 and EF5 tornadoes associated with this outbreak occurred on April 27. On average, the U.S. experiences a single EF5 tornado per year. However, with this outbreak, there were four reported EF5 tornadoes on one day. Tornadoes rated EF5 are the strongest on the EF scale with wind speeds in excess of 322 kph (200 mph). The Philadelphia-Kemper County EF5 tornado in Mississippi was so violent that it resulted in some of the deepest ground scouring ever observed (NWS JAN 2011) as shown in Figure 5.2. This highlights the violent nature of these tornadoes as well as the strong vertical velocities associated with tornado vortices as briefly described in Section 3.3. In addition to the strong wind associated with an EF4 or EF5 rating, favorable atmospheric conditions supported fast storm motions, resulting in catastrophic damage over a considerable length. One of the EF5 tornadoes and four of the EF4 tornadoes had damage paths in excess of 129 km (80 miles), with the Hackleburg-Phil Campbell EF5 tornado on the ground for 212 km (132 miles). Unfortunately, a number of these violent tornadoes coincided with densely populated areas such as the EF4 tornado that impacted the city of Tuscaloosa, AL.



Figure 5.2: Image of ground (top) and road (bottom) scouring from the Philadelphia-Kemper, MS EF5 tornado. Image courtesy of the Jackson, MS NWS Office (NWS JAN 2011).

The analysis in this section focuses primarily on the performance of wood-frame residential construction. Manufactured homes were included in the analysis since they comprise a large number of homes in the southeastern United States. Since manufactured home performance in tornadoes was not investigated in this dissertation, a methodology to relate hurricane winds and tornado winds was developed as described in Section 5.2.6.2. Property loss of commercial structures was not included since the majority of these structures are constructed with steel or reinforced concrete. Likewise, it should be noted that loss estimated in this dissertation is based on tangible property loss (damage to the structure) and does not include intangible loss such as fatalities, disruption to the economy, damage to interior contents, or damage to infrastructure.

5.1.1 Subset used for Analysis

Due to the magnitude of April 25-28, 2011 outbreak, a subset of the 350 reported tornadoes was used. The Storm Prediction Center provides detailed information regarding reported tornadoes including path length, width, EF rating, and property loss. Using this information, only tornadoes that resulted in over \$1M in property loss were used to in this chapter. There were a total of 60 tornadoes across 10 states that caused this level of property loss. While this is a significant reduction in the tornado reports, the subset was selected since it represents the tornadoes that had the largest economic impact and therefore likely damaged at least 50 homes.

The 60 tornadoes used in this subset account for only 17% of the reported tornadoes associated with this outbreak. Nevertheless, the tornadoes in this subset resulted in \$5.082B in property loss, which is over 99.5% of the estimated total property loss of \$5.107B (SPC 2011). Similarly, these 60 tornadoes included 311 fatalities (96% of total fatalities) and 2,868 injuries

(99% of total injuries). Thus, while the number of tornadoes in this analysis was greatly reduced, this subset adequately represented the tornadoes with the largest impact for the outbreak. Figure 5.3 illustrates the subset of tornado paths used for the estimation of property loss while Table 5.3 summarizes the reported tornadoes with over \$1M in property loss in each state.

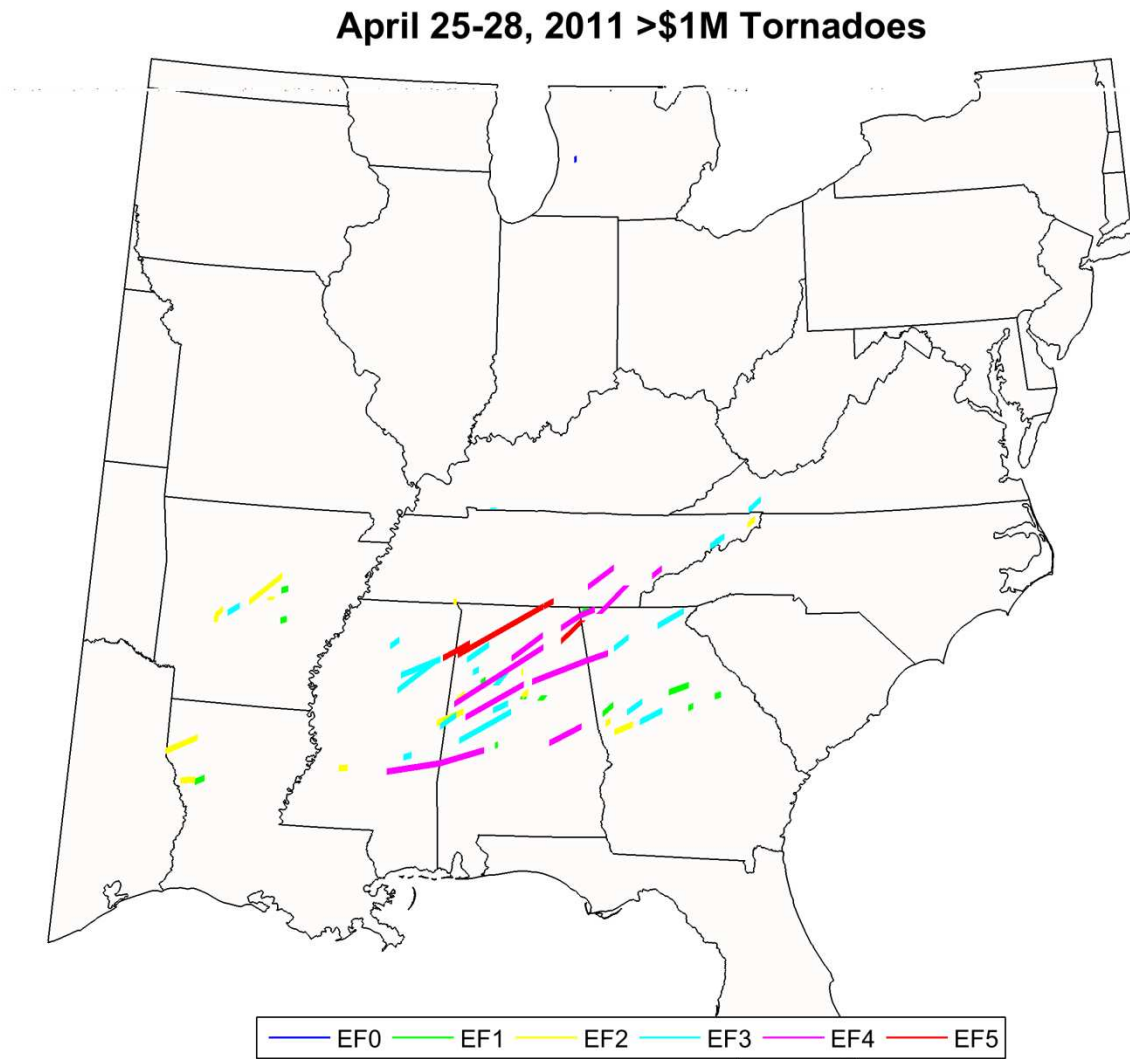


Figure 5.3: Map of all the reported tornadoes from the April 25-28, 2011 outbreak which caused over \$1M in property damage.

Table 5.3: Number of Tornadoes with over \$1M in Property Loss per State

State Impacted	No. Tornadoes*
Alabama	24
Georgia	15
Mississippi	9
Tennessee	8
Arkansas	7
Louisiana	3
Texas	1
Michigan	1
Kentucky	1
Virginia	1

**Note: This is the total number of tornadoes reported in each state. Some tornadoes crossed state borders and thus impacted multiple states. In this case, it was included in the tornado count for both states in order to get the tornado count for each state.*

5.2 Loss Estimation

The goal of this chapter is to estimate property loss to manufactured homes and wood-frame residential construction based on fragilities developed in Chapter 3. Similar to assessing unconditional risk, a comparison of property loss was performed using the locally adopted residential building code in place as of 2011 to the Florida Residential Code (FRC) 2010 in order to quantify the reduction in property loss when using strengthened construction methodologies. As stated before, the loss estimated in this chapter focuses solely on direct property loss related to structural damage. There was no attempt to estimate loss due to damage to infrastructure, interior contents of the home, or fatalities.

5.2.1 Building Code Assignment

In order to estimate the property loss based on the fragility curves created in Chapter 3, the locally adopted building code for each of the ten states in Table 5.3 had to be determined. Both Alabama and Mississippi did not have a residential building code at the time of the tornado

outbreak, so their fragility curves are based on the location in Dixie Alley. Michigan, Louisiana, Tennessee, and Virginia had adopted the IRC 2009 prior to the April 2011 outbreak and thus used the IRC fragility curves for Tornado Alley, the Midwest, and the High Plains. Finally, Arkansas, Kentucky, Texas, and Georgia had adopted the IRC 2006 for residential construction. The IRC 2006 most closely resembled the specifications of the IRC 2009 for the roof sheathing and wall-to-foundation connections. However, the roof-to-wall connection was the same as specified in the ORC 2011. For this reason, these four states used the fragility curves for the Northwest US. Table 5.4 summarizes the locally adopted building code for each state, as well as the fragility curves assigned to each state in order to estimate property loss.

Table 5.4: Locally Adopted Building Code and Assigned Fragility

State	Locally Adopted Residential Building Code (2011)	Assigned Building Code from Fragility Analysis
Alabama	N/A	AL Cons.
Arkansas	IRC 2006	ORC 2011
Georgia	IRC 2006	ORC 2011
Kentucky	IRC 2006	ORC 2011
Louisiana	IRC 2009	IRC 2009
Michigan	IRC 2009	IRC 2009
Mississippi	N/A	AL Cons.
Tennessee	IRC 2009	IRC 2009
Texas	IRC 2006	ORC 2011
Virginia	IRC 2009	IRC 2009

It should be noted that the estimation of property loss in this chapter is based on the performance of wood-frame residential structures built according to the building codes adopted in 2011. However, there is considerable variability in the age of homes across the U.S. implying that the types of connections (i.e. roof-to-wall connection) investigated in this dissertation vary both geographically and temporally. For the purposes of this work, only the geographic

variability is considered so all homes impacted are assumed to be built according to the current residential building code current in 2011. Future work should assess structural performance as a function of the age of the house.

5.2.2 Manufactured Homes

Manufactured homes are structures that are transportable in one or more sections and are built on a permanent chassis. They may or may not be attached to some type of permanent foundation (FEMA 2009). Manufactured homes are popular single family dwellings since they are relatively inexpensive as compared to permanent residential structures. The cost per square foot of manufactured homes is roughly half that of site built homes. It was estimated that a third of all new homes sold in the U.S. in 1985 were manufactured homes (McDonald and Mehnert 1989).

Despite their popularity, manufactured homes perform poorly when subjected to high winds and each year there are a large number of injuries, fatalities, and property loss resulting from their poor performance in tornadoes. One reason for the poor performance of manufactured homes in high winds is due to the fact that their failure mechanism includes stability failures, such as translation or overturning. While permanent structures can translate or overturn, the wind speed to cause this type of failure in manufactured homes is significantly lower. The units are lightweight and their geometry is often long and narrow, providing little resistance to overturning and sliding, especially if not properly anchored (McDonald and Mehnert 1989).

Wind loading requirements for manufactured homes were improved in 1994 following years of extensive damage, especially in the aftermath of Hurricane Andrew in 1992 (FEMA 2009). The 1994 requirements had wind loads similar to ASCE 7 and also defined wind zones

for manufactured homes as shown in Figure 5.4. For the work in this chapter, the manufactured homes are located in Zone I which corresponds to a maximum wind speed of 113 kph (70 mph). When estimating the reduction in property loss with strengthened construction methodologies, manufactured homes were designed for Zone III with a maximum wind speed of 177 kph (110 mph) which is required only along select coastal regions of the U.S. While manufactured home construction must follow the 1994 wind loading requirements, there is no regulation on the installation. As such, states and local jurisdictions dictate whether tie-downs are required (FEMA 2009).



Figure 5.4: Basic wind zone map for manufactured homes. Image courtesy of the Manufactured Housing Institute (MHI 2016).

Single unit manufactured homes are often supported on piers made of concrete masonry units (CMU). The home is held in place with metal frame tie-downs attached to the chassis or over-the-top tie-downs. These tie-downs are typically made of galvanized metal 0.9 mm (0.035

in) thick and 31.8 mm (1.25 in) wide with a specified minimum strength (McDonald and Mehnert 1989). The number and spacing of the tie-downs is specified by the manufacturer of the home. While it is recommended that all manufactured homes use tie-downs, it is ultimately up to the state or local jurisdiction on whether to require them. Likewise, even if tie-downs are required, there is often lax enforcement. Nevertheless, even with tie-downs installed, manufactured homes still perform poorly in high winds since these systems are often unreliable (FEMA 2009). Failure modes commonly include the home shifting off the CMU piers or pullout of the ground anchors. Tie-down performance is governed by soil type and condition, anchor type, installation practice, and maintenance which can drastically alter the pullout capacity of the tie-down. Failure of the tie-downs can lead to catastrophic damage to manufactured homes since the structure can tumble, roll, or become airborne (McDonald and Mehnert 1989). Figure 5.5 is a manufactured home that failed in an EF2 tornado in Perry County, Alabama on January 23, 2012. As indicated on the image, the manufactured home had tie-downs installed, but still failed catastrophically in wind speeds 217 kph (135 mph) or less. Thus, while a manufactured home may be designed for Zone III (wind speeds of 177 kph (110 mph)), failure can still occur if the home is not properly anchored. When comparing the reduction in property loss when using strengthened construction later in this chapter, it is assumed that the tie-downs are correctly installed and perform adequately.



Figure 5.5: Catastrophic damage to a manufactured home from an EF2 tornado in Perry County, Alabama. Tie-downs are indicated in the black circles.

The April 25-28, 2011 tornado outbreak primarily impacted the southeastern U.S. which has a high number of manufactured homes due a large number of the population living at or below the poverty level. Because of the high concentration of manufactured homes in states heavily impacted from the tornado outbreak, their performance had to be considered when estimating property loss. Manufactured homes are frequently destroyed by tornadoes rated EF1 or EF0 (177 kph (110 mph) or less) as shown in Figure 5.5. Damage to manufactured homes accounts for many of the deaths and injuries in tornadoes every year (McDonald and Mehnert 1989) and so their performance was quantified and is included in this chapter as discussed later.

5.2.3 Number of Homes Impacted

In order to estimate property loss for the subset of the April 25-28, 2011 outbreak used in this chapter, the number of residential structures in each of the tornado paths had to be determined. Many of the NWS offices impacted by the tornado outbreak had event web pages that included information from the damage surveys. In some cases, post-tornado damage surveys included a count of the number of homes impacted by tornadoes, however, this information is not commonly contained in NWS surveys. In the instances where a count of damaged residential structures was estimated, this information was used in the loss estimation.

In most cases, the NWS damage surveys did not estimate the number of homes impacted by a tornado due to the extensive nature of this outbreak and limitations on time and personnel. Thus, in this dissertation a methodology was developed to estimate the homes impacted by a given tornado. This was done overlaying tornado paths with census tract information using Geographic Information System (GIS) software. Each of the tornado paths contained information regarding the start and end coordinates, path width, and intensity (SPC 2011). Assuming that the tornado path was rectangular in shape and a straight line (Twisdale and Dunn 1983), the tornado path was plotted.

Census information was used to map the tracts in each of the ten states impacted by the tornadoes causing over \$1M in property loss. Census tracts are small, relatively permanent statistical subdivisions of a county and are updated before each census. While they range in population size between 1,200-8,000 people, the optimum size is typically 4,000 people (U.S. Census Bureau 2012). A census tract covers a broad geographic area which can vary considerably depending on population density. In urban settings, census tracts are considerably

smaller than those in rural regions. The number of housing units in each of the census tract was obtained from census information (U.S. Census Bureau 2011a).

With GIS, the tornado paths were plotted over the mapped census tracts. In order to obtain the number of homes impacted by each tornado path, a weighted average approach was used. First, the number of census tracts impacted by a given tornado path was determined using the intersect feature in GIS. The total area of the census tracts was found by summing the area of each of the individual census tracts that were in the tornado damage path.

$$A_{CT} = \sum_{i=1}^n A_i \quad (5.1)$$

where A_{CT} is total area of all the census tracts impacted by a given tornado, A_n is area of census tract i , and n is the total number of census tracts impacted by the tornado. The total number of homes in A_{CT} was found by summing the number of housing units in each individual census tract using the same approach as above,

$$N_{CT} = \sum_{i=1}^n N_i \quad (5.2)$$

where N_{CT} is total number of housing units in all the census tracts impacted by a given tornado and N_i is number of housing units in census tract i . As in Chapter 2, the tornado path area was found by multiplying the length by the width. Finally, the percentage of the total census tract area that was contained in the tornado path area was estimated. Using this percentage, the total number of homes impacted by the tornado was estimated as:

$$N = N_{CT} \times \left(\frac{lw}{A_{CT}} \right) \quad (5.3)$$

where N is the total number of homes impacted by a given tornado, l is the tornado path length, and w is the tornado path width. This was done for each of the tornadoes that did not have an estimate of the number of homes damaged included in an NWS storm survey.

It should be noted that the estimate of N did result in some values that were high. This was especially true in rural areas where the tornado did not impact a densely populated area. Engineering judgment was used to determine if the value of N was unreasonable based on the SPC reported property loss, path length, and path width. For instance, an estimate of N of 300 was deemed unreasonable if the tornado only caused \$1.5M in damage over a length of 13 km (8 miles) with a maximum width of 402 m (440 yds). In this case, the tornado path was overlaid on top of Google Maps, and the number of homes was counted. Fortunately, in most cases, the methodology summarized in Eqns 5.1-5.3 adequately estimated N .

Once the number of homes impacted from a tornado was established, the next step involved determining the intensity of winds each house experienced. As discussed in Chapter 2, winds vary in intensity along both the path length and width. As such, while a tornado may be rated EF5, in actuality, only a small portion of the damage path actually experiences EF5 wind speeds. Using the results from Chapter 2, the homes were randomly assigned an EF intensity based on the variation of intensity within the tornado path as shown in Table 2.5. For example, if a tornado was rated EF5, only 4.1% of the total number of homes impacted, N , experienced wind speeds above 322 kph (200 mph). Assigning an EF classification for each home was done in order to determine the structural performance and any associated property loss.

5.2.4 Archetype Assignment

Each of the homes impacted by a tornado was assigned an archetype based on the structures used in Chapter 3. Additionally, some of the structures in the tornado damage path were designated as a manufactured home. To determine the type and number of each of the homes in the path, county economic data from the U.S. Census was used. The U.S. Census provides information about income for individual households (U.S. Census Bureau 2011b). The particular dataset used in this analysis was Income in the Past 12 Months (in 2011 Inflation-Adjusted Dollars) obtained from the 2007-2011 American Community Survey 5-Year Estimates on a county level.

Economic income and archetype were related based on the size of the archetype. It was assumed that larger homes correlated with higher household incomes and vice versa. Therefore, the square footage of each archetype was estimated from the building foot print and the household income was broken into six brackets as summarized in Table 5.5. The percentages of households in a given income bracket were then related to percentages of archetypes. For instance, if 5% of the households in a county were in the \$35,000-74,999 income bracket, then 5% of the homes impacted by a tornado in that county would be assigned as Type 3.

Table 5.5: Income and Archetype Assignment

Archetype	Sq. Ft	Annual Household Income (2011 Dollars)
Manufactured Home	N/A	≤ \$14,999
Type 1	1253	\$15,000-\$34,999
Type 3	2337	\$35,000-\$74,999
Type 4	3180	\$75,000-\$149,999
Type 2	3657	\$150,000-\$199,999
Type 5	6300	≥\$200,000

5.2.5 Determining Real Market Value of Impacted Homes

In order to perform an estimate of property loss, the value of residential structures had to be determined. As with household income, this data was obtained from the U.S. Census. The particular dataset used in this portion of the analysis was the value of owner-occupied housing units obtained from the American Community Survey 5-year estimates (U.S. Census 2011c). The value of homes was broken into 24 brackets ranging from less than \$10,000 to homes worth over \$1M. The percentage of each home value bracket was determined for each county and used to assign an estimated real market value (RMV). For example, if 8% of the houses in the county were valued between \$90,000-99,999, then 8% of the homes impacted by the tornado, N , were randomly assigned an RMV falling in this range. In some cases, counties may not have had any homes in a certain RMV bracket, so no homes were assigned an RMV in that range. In addition, the RMV and archetype were sorted in order from lowest to highest. Thus, archetypes were initially assigned and ranked from lowest income bracket (manufactured home) to the highest income bracket (Type 5). RMV was also assigned to the archetypes from the lowest RMV bracket of under \$10,000 to the highest RMV bracket of over \$1M. This was done to ensure that manufactured homes or smaller archetypes were not assigned an RMV that was unreasonably large. The EF intensity was randomly assigned so that intensity was not related to the type or cost of home.

5.2.6 Determining Failure Probability

The probability of failure was a function of the building code, archetype, orientation (or anchorage), and EF intensity. The orientation for wood-frame residential construction was randomly assigned as either an EW or NS wind as described in Chapter 3. For manufactured home, orientation was not included. Rather, the performance of the manufactured home was

determined based on whether or not a tie-down was installed. In order to determine each of these characteristics and estimate property loss for a given house in the tornado path, a housing matrix was created. The matrix contained N rows and nine columns. The columns included a count of the homes (from 1 to N), archetype, RMV, EF intensity, orientation (or anchorage), and four columns of failure probabilities. An example housing matrix is shown in Table 5.6 for an EF4 tornado that impacted 20 structures.

Table 5.6: Sample Housing Matrix

Home Count	Archetype	RMV	EF Intensity	Orientation (Anchorage)	Pf – Local Code (Upper Bound)	Pf – FRC (Upper Bound)	Pf – Local Code (Lower Bound)	Pf – FRC (Lower Bound)
1	0	\$ 7,948.00	2	1	0.9960	0.6122	0.8994	0.1199
2	0	\$ 18,672.00	1	1	0.9689	0.0839	0.2439	0.0027
3	0	\$ 24,996.00	1	2	0.2691	0.3954	0.0452	0.0164
4	0	\$ 34,139.00	4	1	0.9999	0.9846	0.9971	0.6321
5	1	\$ 42,795.00	3	2	0.9999	0.9931	0.9906	0.9896
6	1	\$ 58,317.00	0	2	0.3339	0.1148	0.0035	0.0014
7	1	\$ 65,282.00	3	2	0.9999	0.9690	0.9854	0.9764
8	1	\$ 70,074.00	2	1	0.9928	0.9313	0.8606	0.7977
9	1	\$ 87,570.00	0	1	0.2212	0.0684	0.0014	0.0095
10	1	\$ 98,506.00	0	2	0.1641	0.0917	0.0091	0.0033
11	3	\$ 105,627.00	1	1	0.5070	0.1162	0.8511	0.5897
12	3	\$ 111,245.00	2	3	0.9988	0.9991	0.9742	0.9010
13	3	\$ 147,186.00	1	1	0.5750	0.0974	0.2804	0.3902
14	3	\$ 127,313.00	0	1	0.0911	0.0009	0.0373	0.0708
15	3	\$ 162,409.00	3	3	0.9999	0.9999	0.9972	0.9973
16	3	\$ 155,716.00	1	1	0.7623	0.1137	0.7954	0.4223
17	3	\$ 177,768.00	2	2	0.9981	0.9817	0.9358	0.9063
18	4	\$ 222,512.00	2	2	0.9978	0.6258	0.8657	0.7401
19	4	\$ 251,593.00	0	2	0.3948	0.0105	0.0062	0.0018
20	4	\$ 323,369.00	0	1	0.2820	0.0030	0.0197	0.0070

5.2.6.1 Wood-Frame Residential Construction

Once the building code, archetype, orientation (or anchorage), and EF intensity were established, the probability of failure was determined. Failure probabilities in this chapter were based on system level performance. Recall from Section 3.7, that the performance of each of the three main components along the vertical load path was considered in order to determine the system level behavior of a structure. Failure of any component along the vertical load path resulted in failure of the system. In this case, loss of over 10% of the roof sheathing, failure of the roof-to-wall connection, or failure of the wall-to-foundation connection resulted in failure of the system. While not considered in this dissertation, the performance of wood-frame residential construction can be established based on different damage states for an estimate of loss using performance based engineering.

Using the failure probabilities from the system level fragility curves, the probability of failure of the homes in the tornado path was determined. Once the building code, archetype, orientation, and EF intensity were established, the probability of failure was obtained. This was done by randomly assigning a wind speed based on the EF intensity that the structure experienced. The corresponding probability of failure at that particular wind speed was found based on the fragility curves for both the local and strengthened construction guidelines. For example, assume a home was assigned EF1 level damage for a Type 1 structure oriented in an east-west direction and built according to IRC 2009 specifications. The house was randomly assigned a wind speed between 138-177 kph (86-110 mph). For this example, assume the wind speed was 148 kph (92 mph). Based on the system level fragility curve for the IRC 2009, the probability of failure corresponding to a 148 kph (92 mph) tornado wind speed is 0.72 for the upper bound estimate. The same wind speed was used to find the failure probability for the

lower bound locally adopted residential code, and the upper and lower bound strengthened residential building codes.

The last four columns of the housing matrix (Table 5.6) contain the four different failure probabilities found using the methodology described above. The first failure probability column is for the upper bound P_f using the locally adopted residential building code, which varies depending on which state the tornado impacted. The next failure probability column is the upper bound P_f using strengthened construction. For wood-frame construction (Types 1-5), this was the FRC 2010 whereas for manufactured homes, this was designed for Zone III rather than Zone I. Similarly, the third and fourth failure probability columns were the lower bound P_f for the local and stricter residential building codes, respectively.

5.2.6.2 Manufactured Homes

Obtaining failure probabilities for manufactured homes was done using results from the HAZUS Hurricane Model created by FEMA. Fragility analysis was performed for manufactured homes subjected to extreme winds from hurricanes, however, tornado fragility curves are not in existence yet. Since the focus of this dissertation was on wood-frame residential construction, tornado fragility curves for manufactured homes subjected to tornadoes were approximated based on the results of the HAZUS model. Future work should focus on developing tornado specific fragility curves for manufactured homes to better estimate their performance.

As described in Section 3.1, fragility curves are modeled as a lognormal distribution (shown in Eqn. 3.1). Development of fragility curves is dependent on the demand, in this case 3s gust wind speed, the capacity R , the logarithmic median λ_R , and the logarithmic standard

deviation ξ_R . Therefore, the logarithmic parameters for tornado fragility curves for manufactured homes had to be calculated.

Hamid (2014) presented fragility curves for manufactured homes with several different designs. Based on these fragility curves, Masoomi and van de Lindt (2015) estimated the logarithmic parameters as summarized in Table 5.7. The hurricane fragility curves presented in FEMA (2009) were compared to those of Hamid (2014) and it was determined that the curves were most likely associated with failure probabilities for HAZUS Damage State 3 or 4. Damage State 3 implied that the manufactured home rolled onto its side, but the under-frame and structure were still attached, but it likely experienced significant damage to the roof and walls. Damage State 4 was when the manufactured home rolled or became airborne and the structure separated from the under-frame (FEMA 2009). In either case, the manufactured home experienced extensive damage and would be immediately uninhabitable.

Table 5.7: Logarithmic Parameters for Hurricane Fragility Curves

Type of Manufactured Home	λ_R	ξ_R
Pre-1994: No Tie-Down	4.73	0.2
Post-1994: Zone I	5.052	0.185
Post-1994: Zone II	5.13	0.185
Post-1994: Zone III	5.156	0.185

The fragility curves used in this chapter were for manufactured homes designed for post-1994 specifications in Zones I and III (shown in Figure 5.4), as well as for pre-1994 manufactured homes without tie-downs. However, Hamid (2014) focused solely on manufactured home performance in Florida, which includes Zone II and III, but not Zone I. The focus of this chapter is on the April 25-28, 2011 tornado outbreak which occurred over the

southeastern U.S., which is mostly in Zone I. The logarithmic median for Zone I was determined via linear interpolation using the logarithmic median and design wind speeds for Zones II and Zones III. The logarithmic standard deviation was assumed to remain the same.

In order to approximate the tornado fragility curves from the hurricane fragility curves, the methodology proposed by Masoomi and van de Lindt (2015) was used. In the case of hurricanes, the demand is the 3s gust wind, defined as V_H and the logarithmic parameters are summarized above in Table 5.7. Thus, in order to create the tornado fragility curves from the hurricane fragility curves, a relationship between the tornado demand (V_T) and hurricane demand (V_H) had to be determined so that the logarithmic parameters for tornadoes could be found. Eqns. 3.3 and 3.4 (or 3.5) are used to estimate the wind load applied on a structure, which is a function of wind speed. In theory, the same wind load, W , in a tornado and hurricane should result in the same probability of failure. However, the magnitude of wind which would result in this wind load would occur at a lower wind speed in tornadoes as compared to hurricanes as described in Section 3.3. Nevertheless, using the fact that the same wind loads in hurricanes and tornadoes (W_H and W_T respectively) would cause the same probability of failure, the relationship between the demands (V_H and V_T) could be estimated. This is shown below in Eqn. 5.3 below,

$$1 = \left(\frac{W_T}{W_H}\right) = \left(\frac{(K_z)_T}{(K_z)_H}\right) \left(\frac{(K_{zt})_T}{(K_{zt})_H}\right) \left(\frac{(K_d)_T}{(K_d)_H}\right) \left(\frac{(K_c)_T}{(K_c)_H}\right) \left(\frac{V_T}{V_H}\right)^2 \left(\frac{(GC_p - GC_{pi})_T}{(GC_p - GC_{pi})_H}\right). \quad (5.4)$$

The ratio of the terms on the right hand side was found for hurricanes (straight line winds) and tornadoes in order to relate V_H and V_T . The first term on the right hand side was dependent upon Exposure Category. The analysis in this dissertation assumed an Exposure Category C, thus this ratio was set to 1 (Masoomi and van de Lindt 2015). If the Exposure Category was B or D, the value of this ratio would be 1.43 or 0.87, respectively. The next ratio

was set to 1 since neither the hurricane or tornado wind loads were dependent upon local topographic features. The third term was the directionality factor. As described in Section 3.4 of this dissertation, this was set to 1. However, for straight line winds, this value is commonly set as 0.85 for the MWFRS. Therefore, this particular ratio had a value of $\frac{1}{0.85}$.

The fourth ratio involved the tornado amplification factor. The fragility analysis in this dissertation involved the estimate of upper and lower bound failure probabilities, thus, the value of this ratio varied depending on which methodology was being assessed. The upper bound methodology found the wind load using ASCE7-10 provisions as well as a tornado amplification factor (Haan *et al.* 2010). Hurricanes are treated as straight line winds, therefore, there is no amplification and K_c is set to 1. The lower bound methodology utilized the updated wind provisions included in ASCE 7-16 without any tornado amplification and, as with hurricanes, this value was thus set to 1. Therefore, the value of the fourth ratio was set as $\frac{2}{1}$ for the upper bound (Masoomi and van de Lindt 2015) and $\frac{1}{1}$ for the lower bound. The sixth ratio was set to 1 since there was no difference between the numerator and denominator when comparing tornadoes and hurricanes. Using the values of the aforementioned terms, a modification factor C_v was found where $C_v = \frac{V_T}{V_H}$. The modification factor was found to be 0.652 for the upper bound and 0.922 for the lower bound.

In order to obtain the tornado logarithmic parameters, the fragility curves for hurricanes and tornadoes were related as such

$$\Phi\left(\frac{\ln(V_H) - \lambda_R}{\xi_R}\right) = \Phi\left(\frac{\ln\left(\frac{V_T}{C_v}\right) - \lambda_R}{\xi_R}\right). \quad (5.5)$$

Based on Eqn 5.4, the logarithmic parameters can be determined for tornadoes. It can be seen that the logarithmic standard deviation is the same on both the left and right hand sides. However, the logarithmic median for tornadoes can be written as

$$\lambda'_R = \lambda_R + \ln(C_v) \quad (5.6)$$

where λ'_R is the logarithmic median for the tornado fragility curve. A summary of the logarithmic parameters for the upper and lower bound are shown in Table 5.8. Likewise, the fragility curves for manufactured home subjected to tornado wind loads are shown in Figure 5.6.

Table 5.8: Logarithmic Parameters for Tornado Fragility Curves

Type	Upper Bound		Lower Bound	
	λ'_R	ξ_R	λ'_R	ξ_R
Pre-1994: No Tie-Down	4.302	0.2	4.649	0.2
Post-1994: Zone I	4.624	0.185	4.971	0.185
Post-1994: Zone III	4.728	0.185	5.075	0.185

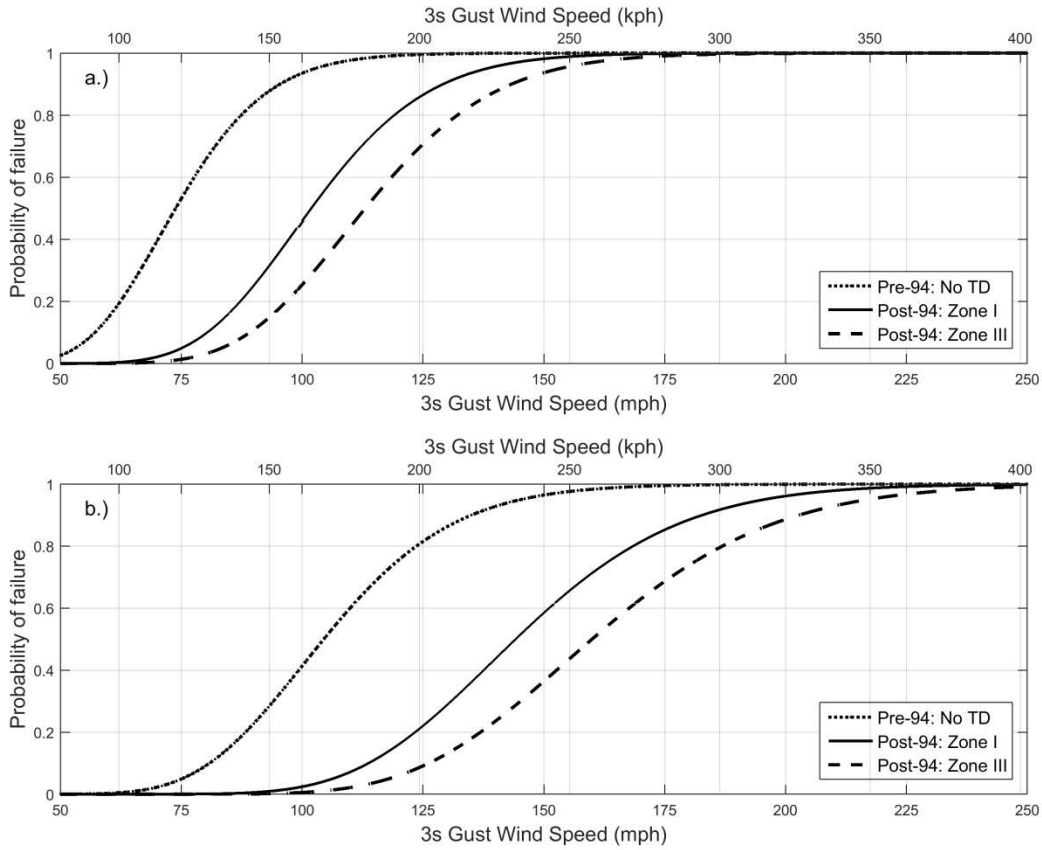


Figure 5.6: Fragility curves for manufactured homes where a.) is the upper bound performance estimated using ASCE 7-10 and K_c and b.) is the lower bound performance found using ASCE 7-16 wind provisions without any tornado amplification.

As with wood-frame construction, the manufactured homes were assigned an RMV, EF intensity, and anchorage (in lieu of orientation). The method for assigning an RMV and EF intensity was the same for manufactured homes and wood-frame construction and was described earlier. However, the anchorage for manufactured homes was considered. Anchorage classification was randomly assigned and manufactured homes without tie-downs used the fragility curves for the Pre-1994: No TD (tie-down) manufactured homes. Similarly, manufactured homes with tie downs were assigned the Post-1994: Zone I fragility curves. While

tie-downs are recommended for manufactured homes, it is up to the state or local jurisdiction as to whether to require tie-downs. It was decided to model some of the manufactured homes without tie-downs based on observations from tornado damage surveys across the state of Alabama. In multiple instances, damaged manufactured homes were observed without any tie-downs, resulting in significant damage. For the estimate of property loss using strengthened construction, the manufactured homes were assumed to be built to Post-1994: Zone III standards with tie-downs.

The failure probability assigned to each manufactured home was done by randomly selecting a wind speed within the bounds for each EF intensity. If the manufactured home was in an EF1 wind speed range and utilized tie-downs, a wind speed between 138-177 kph (86-110 mph) was randomly assigned. Assuming a properly anchored manufactured home was subjected to a tornado wind speed of 161 kph (100 mph), the upper bound failure probability was found to be 0.46. The same approach was used to find the failure probability for the lower bound locally adopted residential code, and the upper and lower bound strengthened residential building codes dependent upon anchorage and EF intensity.

5.2.7 Property Loss Estimation

Once the RMV and probability of failure were determined for each home, the property loss was estimated using a simplified model proposed by Weibe and Cox (2014). As stated before, this model estimated property loss based solely on structural damage and as such, damage to the interior contents or infrastructure was not taken into account. It is known that property loss is just a subset of the true economic loss from natural disasters, and future work should include an estimate of indirect tangible losses.

Fragility curves were used in Chapter 3 of this dissertation to estimate building performance when subjected to tornado wind loads. Using the fragility curves, damage was estimated for each individual home as described in Section 5.2.6. The property loss model used by Weibe and Cox (2014) provided an estimate for property loss from tsunamis at the community level by using the damage estimates from fragility curves and the RMV of structures located in Seaside, Oregon. While their work focused on tsunami hazards, their proposed methodology can be applied to tornado hazards.

Weibe and Cox (2014) proposed three different models to estimate the total probable loss from a natural disaster. Method 1 aggregated a percentage of the RMV for all buildings with a P_f greater than zero as shown below

$$P_{loss} = \sum_{i=1}^n RMV \times P_f \quad (5.7)$$

where P_{loss} is the estimated property loss, RMV is the real market value of the structure, P_f is the probability of failure, and n is the total number of structures with a value of P_f greater than zero. Method 2 aggregated the full RMV for all homes with a P_f greater than a threshold of 50% as shown below

$$P_{loss} = \sum_{i=1}^n RMV \text{ if } P_f > 0.5. \quad (5.8)$$

Method 3 from Weibe and Cox (2014) included a summation of loss based on the probability of failure for three different damage states. This was beyond the scope of this work since different damage states were not defined for the system level performance. However, once damage states are developed for tornado wind loads, Method 3 from Weibe and Cox (2014) can be used to estimate property loss.

Property loss for the April 25-28, 2011 tornado outbreak was found using both Method 1 and Method 2 of Weibe and Cox (2014). The property loss for each individual tornado was first calculated. Due to the random nature of assigning building characteristics (EF intensity, RMV, etc), the property loss estimate was performed ten times for each tornado and the average of the iterations was set as the property loss for the given tornado. The total property loss for the outbreak was found by summing the loss for individual tornadoes. Since fragility curves were created for standard and strengthened construction for both the upper and lower bound, property loss was estimated for each of these approaches. This resulted in a total of eight different estimates of property loss for a given tornado. An example of the property loss estimates for an EF2 tornado that impacted Arkansas is shown in Table 5.9.

Table 5.9: Sample Estimate of Property Loss from Tornadoes

EF Intensity	N	SPC Property Loss (\$M)	Method 1 Property Loss (\$M)				Method 2 Property Loss (\$M)			
			Upper		Lower		Upper		Lower	
			Local	FRC	Local	FRC	Local	FRC	Local	FRC
2	24	3	2.67	1.16	1.07	1.03	2.80	0.95	0.91	0.87

5.3 Comparison of Standard versus Strengthened Construction

Property loss for the subset of the April 25-28, 2011 tornadoes was performed and included in Table 5.10 below. This was done for both Methods 1 and 2 of Weibe and Cox (2014) as well as for the upper and lower bound estimates of failure probabilities for the local and strengthened construction methodologies. Table 5.10 includes a summation for all 60

tornadoes included in the property loss analysis. Appendix G contains the loss estimate for each of the individual tornadoes investigated in this dissertation.

Table 5.10: Loss Estimation for the April 25-28, 2011 Tornado Outbreak *

Total No. of Tornadoes	No. of Homes Impacted	SPC Record Property Loss	Property Loss			
			Method 1 – (\$M)			
			Upper Bound		Lower Bound	
			Local	FRC	Local	FRC
60	22,072	5,084.03	3,554.13	2,015.77	2,286.65	2,177.62
			Method 2 – (\$M)			
			Upper Bound		Lower Bound	
			Local	FRC	Local	FRC
			3,632.54	1,989.90	2,301.49	2,180.44

**Note this only includes tornadoes resulting at least \$1M in property loss*

The magnitude of the estimated property loss shown in Table 5.10 is lower than that provided by the Storm Prediction Center (SPC 2011). This is likely due to the fact that the SPC reports all property loss, including that of vehicles, interior contents, and/or commercial structures, whereas this dissertation focused on direct losses to residential structures. For example, one tornado in Arkansas struck an air force base and damaged several large aircraft resulting in an event estimate of \$125M in property loss (SPC 2011). However, the loss estimated using the simplified models was approximately \$25M. Since the work in this dissertation focused on direct losses to residential structures, the estimated property loss for the outbreak was well below the loss reported by SPC. While the property loss estimate using the simplified models was lower than SPC records for the entire outbreak, there were some individual tornadoes with estimated property loss greater than the SPC records, as shown in Appendix G. This is likely due to the over-estimate of N , especially in rural areas.

Both Method 1 and Method 2 resulted in similar magnitudes of property loss for the upper bound and lower bound methodologies for both standard and strengthened construction. The upper bound resulted in a larger estimate of property loss, which was expected. Recall, that failure probabilities for the upper bound were generated using ASCE 7-10 wind provisions as well as a tornado amplification factor. This resulted in a leftward shift of the fragility curves since the wind loads estimated for tornadoes were higher than those for straight line winds for the same reference velocity. In addition, the lower bound failure probabilities were estimated using ASCE 7-16 wind provisions without any amplification of the tornado wind.

For the upper bound estimate of property loss, there was a large difference between local and strengthened construction. The local code varied depending on the state where the tornado was reported, whereas for strengthened construction, all wood-frame residential construction was designed using the FRC 2010. Strengthened construction of manufactured homes followed design guidelines for wind Zone III. In any case, the loss estimated using strengthened construction resulted in a substantial reduction. For Method 1, this was a reduction of 43.28% and for Method 2, this was a reduction of 45.22%.

The lower bound estimate of property loss did not result in as large of a reduction in loss with standard versus strengthened construction. This was anticipated since the lower bound did not incorporate any amplification of the wind load from the tornado vortex, essentially treating tornado winds the same as straight-line winds. Using strengthened construction resulted in a reduction in loss of 4.77% and 5.26% for Method 1 and Method 2, respectively. It should be noted that with both Method 1 and Method 2, the local lower bound estimate of property loss was still over \$2B. Therefore a reduction of 5% still reduces property loss by over \$100M.

5.4 Conclusions

A simplified model was employed to estimate the reduction in property loss when using standard versus strengthened construction. This was applied to the tornadoes of April 25-28, 2011 since this was a well-documented tornado outbreak that resulted in widespread damage across the southeast U.S. During the outbreak, 350 tornadoes were reported and fifteen of those were deemed violent (EF4 or EF5). The April 2011 tornado outbreak resulted in over \$5B in loss, 324 fatalities, and 2906 injuries.

In order to estimate property loss to residential structures, the fragility curves from Chapter 3 were used in conjunction with U.S. census data. Since the southeast U.S. includes a large number of manufactured homes, their performance had to be considered. Using hurricane fragility curves for manufactured homes, an approximation of tornado fragility curves was performed and applied with the property loss model.

Results from the simplified model proposed by Weibe and Cox (2014) indicated that the reduction in property loss was small (~5%) when comparing standard and strengthened construction using the lower bound. However, as discussed earlier in Chapter 3, results from the fragility analysis indicate that there is likely some type of amplification of wind loads from tornado vortices as compared to straight line wind. Results from the upper bound fragility curves were in better agreement with the EF scale DOD for one- or two- family residences and observations from post-tornado investigations. Thus, the estimate of property loss included in this chapter is likely closer to the upper bound than the lower bound.

The reduction in property loss using the upper bound failure probabilities was substantial. For both Method 1 and 2, the reduction in loss exceeded 40%. This implies that adopting

strengthened design guidelines, similar to the FRC 2010, would result in significantly lower property losses from tornadoes. Areas with a high risk of tornado occurrence could benefit from stricter wind provisions, especially in Tornado Alley and Dixie Alley. Better performance of wood-frame residential construction and manufactured homes would result in a reduction in wind-borne debris, and likely decrease the chance of injury or fatalities to occupants sheltering in the home. Likewise, strengthened construction can improve a community's resiliency and reduce the economic impact from tornadoes.

The simplified model used in this chapter estimated direct property loss to the structure, but did not include loss to interior contents. Future research should consider indirect property losses, such as damage to contents from rain water intrusion. Likewise, the failure probabilities used in this chapter were based on the system level performance. It would be beneficial to develop tornado damage states that could be applied to a performance based engineering approach for tornadoes. This is currently being done with seismic and hurricane hazards and there is some discussion within the wind committees of ASCE. Finally, the development of the fragility curves for tornado damage states should include the structural response of debris impact, since tornadoes generate significant wind-borne projectiles which may strike a structure and result in a breach in the building envelope.

CHAPTER 6

ANTICIPATED CONTRIBUTIONS TO THE PROFESSION

The proposed and presented work is anticipated to offer several key contributions to the field of structural engineering, specifically to understanding the impacts of tornado wind loads on residential construction. The two major contributions include a multi-disciplinary approach to quantitatively assess tornado risk reduction and the development of a methodology to assess the dependencies of wood-frame residential structural components subjected to tornado wind loads.

6.1 Tornado Hazard Curves

The methodology to mitigate risk has been extensively explored for earthquake hazards. However, up to this point, tornado hazard curves had not been utilized for assessing unconditional failure probabilities. By updating the tornado hazard maps first introduced by Reinhold and Ellingwood (1982) and Schaefer *et al.* (1986), tornado hazard curves were able to be generated. These curves were shown in Figure 2.8 for the six select locations discussed in Chapter 3. While Reinhold and Ellingwood (1982) did develop tornado hazard curves in their work, their results were applied over a broad geographic region. By utilizing the tornado hazard maps of Standohar-Alfano and van de Lindt (2014), one could create a site-specific tornado hazard curve for any location within the contiguous United States.

6.2 Unconditional Failure Methodology for Tornadoes

In addition, a multi-disciplinary approach was utilized to quantitatively assess tornado risk reduction, specifically for residential wood-frame construction. After natural disasters,

especially tornadoes, there is often a good deal of discussion about improving residential design codes to reduce the damage observed in the aftermath. However, due to the relatively low probability of tornado occurrence at a given location, changes in the residential design codes are often not deemed economically viable. By utilizing the convolution analysis, unconditional failure probabilities are quantitatively generated for a given component or for the system level performance. Likewise, the unconditional failure probabilities were bounded by including an estimation of tornado wind loads using ASCE 7-10 (with a tornado amplification factor) and ASCE 7-16. This will provide a better, scientifically based assessment of the benefits of strengthened construction methods in regions of high tornado risk.

6.3 Positive Quadrant Dependence for Wood-frame Residential Structures

When determining the performance of the vertical load path of residential structures subjected to uplift forces, initial work assumed independence between the individual components (Amini 2012). This work utilized the theory of positive dependence to determine system level behavior of wood-frame residential structures subjected to tornado wind loads. Components in the same system share the same loads and environment, and therefore, the failure of one component affects the performance of the others. To account for this fact, the limit state analysis used in this work differed from the individual component analysis since it took into account the impact of the performance of each component along the vertical load path.

6.4 Property Loss Estimation

Using a methodology to estimate property loss from tsunami hazard curves, property loss from the April 25-28, 2011 tornado outbreak was estimated for both standard and strengthened construction. While the tornado convolution analysis estimated the reduction in risk by using

strengthened construction, risk can be difficult to understand and effectively communicate due to its small magnitude. By using property loss, the impact of strengthened construction in tornadoes can be better interpreted and communicated to decision-makers in a community or state. Using fragility analysis, property loss was estimated for a historical tornado outbreak to compute the reduction in loss when strengthened construction practices were utilized.

CHAPTER 7

MITIGATION STRATEGY AND CONCLUSIONS

7.1 Mitigation Strategy

While the work to develop unconditional failure probabilities is relevant, especially given the historic tornadoes of 2011, it would not be meaningful if a mitigation strategy was not developed. The final portion of the research will involve the development of a mitigation strategy, especially for regions that experience a high occurrence of tornadoes. In areas with limited tornado activity, it is not economical to implement strengthened construction methodologies to resist tornado wind loads. However, regions between the Rocky and Appalachian Mountains in the central U.S. see a high rate of tornado occurrence. States and local jurisdictions in this area can use the methodology and results presented in this dissertation to ascertain their tornado risk and any associated reduction in tornado damage by adopting stricter residential building codes. Ultimately though, in order to better prepare communities against tornado hazards, there must be continued collaboration between meteorologists and structural engineers in order to understand the wind field in tornadoes and the associated wind loads imparted onto the built environment.

7.1.1 Historical Approach to Residential Design against Tornadoes

The U.S. housing supply is extremely vulnerable, structurally, to damages from natural hazards, including tornadoes. Interest in tornado damage to residential structures increased in the 1970s with the implementation of the Fujita scale, as well as in the aftermath of the April 1974 Super Outbreak. However, damage surveys performed in the recent years have observed

similar failure modes as those described in the 1970s (Prevatt *et al.* 2012a) even with newer construction. These failure modes include discontinuities in the vertical load path, especially at the roof sheathing, roof-to-wall, and/or wall-to-foundation connections. This is due to the fact that current construction practices primarily design for gravity loads, but often perform poorly when subjected to uplift forces (van de Lindt *et al.* 2013). The failure modes seen from tornadoes are similar to damage observations from hurricanes. However, improved residential building codes in coastal regions have reduced damage to residential structures subjected to extreme wind loads (FEMA 2012, Prevatt *et al.* 2012a). Without any change to residential building practices across the majority of the country, considerable damage from tornadoes can be expected as the norm.

7.1.2 Distribution of Tornado Winds

Most homes are not built to withstand the extreme forces caused by high winds in strong to violent tornadoes (EF 3 or greater). However, the majority of tornadoes are rated EF2 or lower, implying maximum wind speeds below 217 kph (135 mph). Likewise, as described in Chapter 2, the highest wind speeds in strong tornadoes only occurs over a small area in the tornado damage path (Prevatt *et al.* 2012a, Standohar-Alfano and van de Lindt 2014). Research has shown that the highest intensities occur along the centerline of the tornado damage path (van de Lindt *et al.* 2013) and along the edges of the path, damage is consistent with lower EF ratings. This is consistent with observations from the April 25-28, 2011 tornado outbreak. This specific outbreak was extreme due to the large number of tornadoes, especially long track violent tornadoes. However, the FEMA Mitigation Assessment Team, which documented damage from the outbreak, determined that the majority of damage to wood-frame residential construction was a result of wind speeds of 217 kph (135 mph) or lower (FEMA 2012). While winds of this

magnitude can induce strong loads, damage can be mitigated through the use of enhanced wind-resistant construction, similar to provisions in the FRC 2010. Strengthening structural performance by maintaining the vertical load path and reinforcing connections has proven successful in mitigating damage from hurricanes and is an obvious model in which to base tornado-resistant construction methodologies (FEMA 2012). This was shown in Chapters 3-5 of this dissertation.

With improvements in the construction of residential structures, the damage can be limited, especially with the lower EF intensities. Regions in the central U.S., including Tornado Alley and Dixie Alley, have a higher risk of tornadoes. It is these locations that would benefit most from strengthened construction practices. Using the results presented in this dissertation, jurisdictions can determine their tornado hazard and assess the reduction in risk by adopting strengthened construction practices, similar to the FRC 2010.

7.1.3 Adoption and Enforcement of Residential Building Codes

Mitigation efforts are contingent upon changes in the residential building codes across the country. However, the FEMA Mitigation Assessment Team found that a large percentage of damage from the April 25-28, 2011 tornado outbreak occurred in municipalities that had not adopted any residential building code. Thus, adoption of a residential building code is imperative to improve construction quality and reduce the damage from tornadoes. While adoption of a residential building code may not improve performance of existing residential building stock, it does provide a benchmark for new construction. Similarly, it is recommended that codes be adopted at a state level. This not only improves residential construction performance across the state, but also in jurisdictions that have been unable to adopt a code through their own community processes (FEMA 2012). Finally, residential building codes that

are adopted at a state or local level must ensure that the minimum code requirements remain intact and that any amendments do not act to weaken the vertical and/or horizontal load paths. For example, the city of Tuscaloosa adopted a local residential building code after the April 2011 outbreak (the IRC 2006), however, a local amendment allows the use of concrete nails (known as cut nails) to attach the bottom plate to the foundation (FEMA 2012). This type of connection has commonly been observed in the aftermath of tornadoes and is known to be a weak point along the vertical and horizontal load paths.

In addition to adopting a residential building code, jurisdictions must enforce the design provisions (FEMA 2012, Prevatt *et al.* 2012a). Lax enforcement can lead to structures built below the standards specified in the building code resulting in failure under loads well below the minimum. Failure of residential homes can result in additional injuries, fatalities, as well as the generation of additional wind-borne debris which can damage homes and businesses downstream.

Finally, it is recommended that individual designer, builders, or homeowners voluntarily implement better design practices with new construction, especially in high risk areas. This could be done through enhanced performance packages offered by home builders. Since this is cost-based, it is the responsibility of the homeowner to select any strengthened construction methodologies. However, the additional cost of strengthened construction is estimated at 3-8% of the building costs associated with new construction (IBHS 2016). This includes wind resistant roofing, hurricane clips or straps at the roof-to-wall connection, impact and pressure resistant doors and windows, and a secure anchor of the home to the foundation. The estimate of the cost of strengthened construction is dependent upon location and jurisdictions with better design requirements typically do not see as large of an increase in additional costs.

7.1.4 Routine Maintenance

The average life expectancy of a house is approximately 80 years if it is well maintained (Prevatt *et al.* 2012a). The majority of residential construction in the U.S. is comprised of wood structural members. The structural systems that protect wood framing (i.e. siding, roof covering, etc) have a typical lifetime of 15-30 years. Failure of these systems can expose the main structural system to environmental conditions which are detrimental to its performance and can weaken the home. Wood framing has been known to deteriorate rapidly when exposed to water, wind damage, or pest infestations (Prevatt *et al.* 2012a). Any framing flaw can result in a reduction in structural capacity, especially when subjected to extreme loads, such as tornado wind loads. Therefore, routine maintenance is recommended along with routine inspections of the home focusing on the structural integrity of the MWFRS. Unfortunately, the catastrophic tornado outbreak of April 25-28, 2011 impacted many low-income communities across the southeast U.S. Many of these homes were not well-maintained and increased their vulnerability to tornado hazards.

7.1.5 Improved Connections

There is a limit in which damage and loss is unavoidable with tornadoes. It is safe to assume total destruction of wood-frame residential construction exposed to EF4-EF5 wind speeds (267 kph (166 mph) or greater) since it is not feasible or economical to design for wind speeds of this magnitude. However, as described in this dissertation, the majority of tornadoes are rated EF2 or lower. Furthermore, even in EF4 and EF5 tornadoes, there is only a small percentage of the damage area that experiences wind speeds above 267 kph (166 mph). Thus in areas with a heightened tornado risk, it is worthwhile to design for tornadoes rated EF2 or weaker.

This is done with improved connections and by ensuring continuous vertical and horizontal load paths (van de Lindt *et al.* 2013). By maintaining the load paths and structural systems, high wind loads are successfully able to be transferred to the foundation. While the home itself may still experience a degree of damage, the integrity of the MWFRS is maintained keeping the structure stable and the inhabitants better protected (FEMA 2012). Likewise, improved connections can keep the structure intact which can reduce damage from rainwater intrusion and limit the amount of wind-borne debris generated by the tornado. If a homeowner or community deems it economical to invest in strengthened construction methods, focus must be paid to ensuring a continuous vertical load path. This dissertation focused on three main components of the vertical load path and provided a comparison of the performance with standard and strengthened construction methods. These components included the roof sheathing, roof-to-wall, and wall-to-foundation connections, which are commonly observed to fail in high wind speeds.

7.1.5.1 Roof Sheathing Connection

Failure of the roof sheathing is commonly observed in the aftermath of tornadoes. Inadequate performance of the roof sheathing can be attributed to poor construction practices (i.e. fasteners not properly attached to roof structure) or internal pressurization of the home due to a breach in the building envelope. The majority of the U.S. residential design codes specify attachment of the roof sheathing with 8d common nails (see Section 3.5.1). However, ring shank nails are a cost effective fastener that can be used to dramatically improve roof sheathing performance as described in Sections 3.6.1 and 4.2 (Standohar-Alfano and van de Lindt 2015). The shanks around the body of the nail increase the uplift resistance of the fastener when compared to the smooth 8d common nails.

Recommendations from the FEMA Mitigation Assessment Team following the April 2011 outbreak include the use of ring shank nails as opposed to common nails. For panels in the interior of the roof, the recommended spacing of both the edge and field nails is 150 mm (6 in). Within 1.2 m (4 ft) of a gable end or along the edges of the roof, the recommended spacing is 102 mm/150 mm (4 in/6 in). FEMA did not recommend nail spacing smaller than 76 mm (3 in) due to the possibility of the roof truss splitting (FEMA 2012). Likewise, if using ring shank nails, they must be utilized on all roof panels since a system is only as strong as its weakest link. Finally, care must be taken to ensure that the nails hit the roof framing since missing the underlying truss can drastically reduce the panel uplift capacity. This can be done by the contractor or by a professional code inspector.

7.1.5.2 Roof-to-Wall Connection

The roof-to-wall is a common weak point along the vertical load path. Failure at this connection accelerates the damage to the entire structure and has also been hypothesized to be a critical phase in the progressive collapse of homes (FEMA 2012). With the exception of hurricane and earthquake regions, the roof is commonly attached with a toe-nail connection. This connection performs adequately under gravity loads, but has long been observed to perform poorly under uplift.

In this dissertation, the roof-to-wall connection was improved with the use of an H2.5 hurricane clip manufactured by Simpson Strong Tie. However, there are several different types of clips that can strengthen the roof-to-wall connection. The H2.5 clip used in this work ties the roof truss to the top plate and studs of the wall. Results from Section 3.6.2 and 4.3 indicate that the H2.5 clip performs significantly better than a toe-nailed connection, especially in wind speeds below 241 kph (150 mph). As with the roof sheathing, the reinforced connection must be

placed uniformly across the structure as failure will be initiated at the weakest point of the structure. Likewise, the clip should be installed per manufacturer specifications at any location where the roof truss intersects the wall. By maintaining the roof, damage due to rain water intrusion can be significantly reduced. Furthermore, the roof provides stability and bracing for the walls of a home. When the roof-to-wall connection fails and the roof is removed, the exterior walls of the home are more susceptible to collapse.

7.1.5.3 Wall-to-Foundation Connection

The final connection investigated in this dissertation was the wall-to-foundation connection. Failure of this connection can often be attributed to poor construction practices. For example, cut nails (or concrete nails) have been observed for years in place of anchor bolts (Marshall 2002, FEMA 2012). This type of anchorage does not provide significant resistance to shear or uplift loads. Thus, properly installed anchor bolts are critical to ensuring a structure does not overturn or translate. In the event that a house maintains a continuous vertical load path, the foundation must be of adequate strength. Likewise, a sufficient wall-to-foundation connection should ensure that the wall studs are properly tied to the bottom plate and that the wood does not split around the anchor bolts.

7.1.6 Additional Measures

Several other features have been identified as methods to improve residential wood-frame construction under extreme wind loads. While these were not investigated in this dissertation, they are mentioned for completeness. Such improvements include reinforced garage doors, impact resistant windows, and safe rooms.

Unprotected glazing is extremely susceptible to damage due to high winds or debris penetration. It is unlikely not to have damage to windows in wind speeds in excess of 177 kph (110 mph) unless the windows are impact resistant (FEMA 2012). Therefore, it is recommended that improved windows should be installed in a home aiming to reduce its vulnerability to tornadoes. Acceptable windows must protect against wind-borne debris and the high pressures of tornado wind loads. Garage doors have commonly been observed to fail in tornadoes. Failure of the garage door on attached garages leads to sudden internal pressurization of the home which can result in catastrophic damage to the roof and walls of the house. Thus, in order to protect a structure against tornadoes, pressure resistant garage doors are recommended. In addition to installing a strengthened garage door, proper fastening at each end of the door opening and appropriate track depth must be ensured (FEMA 2012).

The previous mitigation strategies described above focused on design improvements of wood-frame residential construction against tornado wind loads. However, in high risk areas, homeowners should also consider life safety. Even when built correctly, it is still improbable that a wood-frame structure can withstand an EF4-EF5 wind speed. Thus, installation of a safe room or tornado shelter is recommended (van de Lindt *et al* 2013). Any storm shelter should be built according to FEMA 361 specifications and must resist wind loads and debris impact. This is especially true in homes without a basement and manufactured homes.

7.1.7 Adoption of High Wind Provisions in Tornado Alley

Cities in regions of high tornado activity have begun to consider design guidelines for higher wind resistance, including the city of Moore, Oklahoma which was hit by its third violent tornado in fifteen years. As of March 17, 2014, Moore, Oklahoma requires that homes be to withstand 217 kph (135 mph) winds (City of Moore 2014). The new ordinance requires that the

roof sheathing is attached with 8d ring shank nails spaced at 102 mm/150 mm (4 in/ 6 in). Furthermore, the roof-to-wall connection requires the use of a hurricane clip at all truss to top plate connections. Additionally, any gable end must be tied to the structure and garage doors must be rated to 217 kph (135 mph). It is promising that cities located in regions of high tornado occurrence have begun to adopt strengthened construction methodologies to mitigate tornado hazards.

7.2 Summary

Tornadoes are one of the most devastating natural disasters that impact the U.S. on a local scale. While an average of 1,200 tornadoes are reported across the country each year, the annual likelihood of directly experiencing a tornado at a given location is quite small, even in the most active regions of the U.S. However, given the destructive nature of strong and violent tornadoes, it is necessary to determine a geographic tornado hazard as described in Chapter 2. This was done by using 38 years of tornado reports. This data was used in conjunction with results of damage surveys from the 1974 and 2011 Super Outbreaks in order to develop an empirical method that would estimate the tornado hazard at a particular location based on climatology as well as the gradient of wind speed along the tornado path length and width.

The results of the tornado hazard analysis were used to create maps that highlighted the regions of the U.S. with the highest risk of annual tornado occurrence, including an estimate of occurrence for each EF intensity. As expected, the locations with the highest tornado risk include locations between the Rocky and Appalachian Mountains, especially Tornado Alley and Dixie Alley. Finally, using the results for the tornado hazard analysis, tornado hazards curves were created. While these curves can be created at any location in the U.S., this dissertation focused on the tornado hazard curves for six locations with varying tornado activity. The hazard

curves were used with fragility curves to determine unconditional failure probabilities for component and system level performance.

In order to assess wood-frame residential performance under tornado wind loads, fragility analysis was used as described in detail in Chapter 3. Fragility analysis was used since it estimates performance under a given demand and accounts for uncertainty in both the demand and capacity of a structure. In this dissertation, the focus of the fragility analysis was on three main components along the vertical load path that have historically performed poorly under high wind loads. These include the roof sheathing, roof-to-wall, and wall-to-foundation connections. In addition to assessing the performance of each component individually, a vertical load path analysis was performed which took into account the performance of each of the components as a system. The fragility analysis was performed on five different residential structure archetypes in order to capture building to building variability.

Fragility analysis was performed at six different locations in the U.S. Since the building performance was dependent on construction methodology, the building code at each of these six locations was determined. The structural archetypes were modeled using the local code specifications at each of the six locations, as well as with the strengthened guidelines from the Florida Residential Code. This was done so that fragility curves could be created for standard and strengthened construction in order to illustrate the improvement in performance by using stricter design criteria.

In addition to estimating structural performance with standard and strengthened construction, fragility analysis was performed based on wind load estimates from two different ASCE 7 provisions. Scientific consensus has not been reached in regards to the best way to estimate tornado wind loads. While straight line winds have been well documented, there is a

fundamental gap in knowledge for tornado wind loads, primarily due to the difficulty in obtaining direct tornado measurements. Thus, the fragility curves in this dissertation were bounded by two methodologies in order to determine structural failure probabilities. The first method used the ASCE 7-10 wind provisions in conjunction with a tornado amplification factor obtained from laboratory experiments. The second method used ASCE 7-16 wind provisions without any amplification factor. The primary difference between ASCE 7-10 and 7-16 is an increase in the external pressure coefficients for C&C using ASCE 7-16, however, there is no change in the estimate of wind load for the MWFRS. Since the method using ASCE 7-16 resulted in lower failure probabilities for a given wind speed, it was the lower bound fragility curve. Similarly, the tornado amplification factor used with the ASCE 7-10 provisions resulted in higher failure probabilities for a given wind speed and was thus defined as the upper bound fragility curve. With both methods, the strengthened construction practices performed better than any of the locally adopted residential building codes indicating that the Florida Residential Code guidelines could result in better structural performance when subjected to tornado wind loads.

It should be noted that the results of the lower bound fragility analysis do not typically agree with the wind speeds associated with the EF scale DOD for one- or two- family residences or with observations from tornado damage surveys. This would support the idea that there is some type of amplification from tornado wind loads as compared to straight line winds, e.g. pressure deficit. The magnitude of this amplification requires continued research in methodologies to directly measure tornado winds and the associated tornado wind loads imparted on the built environment.

Structural performance based on the fragility analysis is contingent upon the actual hazard occurring. Thus, the fragility analysis in this dissertation only determined performance if a structure was subjected to a tornado. However, as previously discussed, the annual likelihood of a particular structure being impacted by a tornado is quite low. In order to estimate the unconditional risk of tornado damage, the tornado hazard curves and fragility curves were convolved to quantitatively determine the reduction in tornado damage probabilities to residential structures when strengthened construction was used instead of the locally adopted residential building codes. Results indicate that stricter building codes may be beneficial in areas with a high annual tornado risk, such as Tornado Alley and Dixie Alley.

The final portion of this dissertation applied the tornado fragility curves to a historical tornado outbreak. On April 25-28, 2011, the U.S. experienced over 350 tornadoes over 21 states. This particular outbreak was significant in that a total of 11 EF4 and 4 EF5 tornadoes occurred on a single day. Overall, it was estimated that the April 2011 tornado outbreak resulted in over \$5B in property loss, 324 fatalities, and 2906 injuries. Using data from the Storm Prediction Center, a subset of the 350 tornadoes was selected based on tornadoes with at least \$1M in reported property loss.

Using a simplified model, the property loss was estimated for both local and strengthened construction methods. This allowed for a real world application that quantitatively estimated the reduction in property loss by using the Florida Residential Code. Property loss was estimated by utilizing the failure probabilities calculated with both the upper and lower bound approaches. The lower bound estimate of the reduction in property loss was only ~5%. This was due to the fact that lower bound wind loads did not include any amplification to the wind load from the

tornado vortex. Thus, the difference between standard and strengthened construction was smaller as compared to the upper bound.

The reduction in property loss using the upper bound fragility curves indicated substantial improvement by using strengthened construction. Property loss was over 40% lower when structures were built according to the FRC 2010 (or manufactured homes in Zone III) as compared to the locally adopted residential codes. Results from the property loss estimate indicate it would be beneficial to adopt stricter building guidelines in areas with a high risk of tornado activity. Better home performance implies a decrease in the generation of wind-borne debris, as well as a reduction in injuries or fatalities to occupants seeking shelter in their home.

Tornado provisions are not currently considered in the residential design code due to their low probability of site-specific occurrence. However, tornadoes have the potential for catastrophic damage when they strike large urban communities as seen in Tuscaloosa, AL, Joplin, MO, and Moore, OK in the recent years. Since tornadoes will continue to be a part of the severe weather climatology of the U.S., it is likely that there will be increased damage, injuries, and fatalities from tornadoes as the population of the U.S. continues to rise. In order to mitigate this damage, residential building codes must be improved to account for the extreme winds from tornadoes.

7.3 Conclusions

The following conclusions are reached as a direct work presented in this dissertation.

1. Tornado hazard curves were created at select locations across the U.S. These curves indicated that the tornado risk varied significantly across country. Regions in

- Tornado Alley and Dixie Alley had a tornado risk that was several orders of magnitude larger than other locations.
2. Due to a lack of understanding of the tornado wind field, the associated tornado wind loads were estimated using two different methodologies. The first methodology, defined as the upper bound, utilized the wind load parameters from ASCE 7-10 along with a tornado amplification described in Haan *et al.* (2010). The second methodology was the lower bound and used ASCE 7-16 wind load parameters without any amplification of the wind load due to the tornado vortex. Results from fragility analysis indicate that the upper bound fragility curves were in better agreement with the estimated wind speeds associated with the EF scale and post-tornado observations. However, additional research is needed to determine the magnitude of any amplification of the wind load due to tornadoes.
 3. Fragility curves were generated for different residential building codes including the strengthened guidelines of the Florida Residential Building Code. Results indicated that strengthened construction performed better than standard construction.
 4. Convolution analysis quantified the reduction in the risk of tornado damage at varying locations across the U.S. High risk areas saw a reduction in risk that varied between one to two orders of magnitude depending on the component. These regions would benefit most from strengthened construction practices. In areas with low tornado activity, the risk of tornado induced damaged was significantly smaller.
 5. Property loss was estimated for a historical tornado outbreak using standard and strengthened construction. By using the guidelines of the Florida Residential Code (2010), property loss was reduced by over 40%. The direct application to a historical

tornado outbreak indicates that strengthened construction can result in a significant reduction in property loss.

7.4 Recommendations for Future Work

The work presented in this dissertation was performed in this dissertation provided a framework for assessing wood-frame residential construction performance under tornado wind loads. However, this is an area that will require continual research efforts in order to understand appropriate methods to mitigate damage from tornado hazards. The following are recommendations for future work based on the methodology and conclusions presented in this dissertation.

1. There must be continual refinement of the probabilistic tornado hazard methodology with additional post-tornado damage assessments in order to improve the understanding of the variation of intensity along the tornado damage path for all EF ratings.
2. Debris impact is a major source of tornado damage and the implications of projectiles and any associated breach of the building envelope should be considered in future fragility analysis.
3. Due to the uncertainty associated with the tornado wind field, there must be continued research on the applicability and magnitude of tornado amplification of wind loads.
4. Due to the limited improvement of shear wall performance with the RSP4 clip, additional experiments should be performed with reduced anchor bolt spacing or a reinforced sill plate for walls subject to combined shear and uplift. Results should be used to update the interaction curves in order to estimate the resistance of wood shear walls subjected to combined shear and uplift.

5. Due to changes in residential design standards with time, future fragility analysis should include the age of the home when assessing structural performance. This work should also consider the effects of strength deterioration.
6. The performance of manufactured homes subjected to tornado winds was assessed by approximating tornado fragility curves from the HAZUS hurricane fragility curves for manufactured homes. Future work should investigate manufactured home performance in tornadoes in order to create more accurate fragility curves.
7. Similar to hurricane and earthquake hazards, system level limit states for tornadoes should be developed for use in performance based design.
8. In order to assess the reduction in property loss from tornadoes with strengthened construction, future work should include the loss from damage to interior contents, commercial structures, and other infrastructure.

REFERENCES

- Anderson, Christopher J., Wikle, Christopher K., Zhou, Qin, and Royle, J. Andrew, 2007. Population Influences on Tornado Reports in the United States. *Weather and Forecasting*, **22**, 571-579.
- Amini, Mohammad Omar, 2012. Determination of Rational Tornado Design Wind Speed for Residential Woodframe Structures. University of Alabama, Tuscaloosa, Alabama, 1-92.
- Amini, M. Omar, and van de Lindt, John W., 2014. Quantitative Insight into Rational Tornado Design Wind Speeds for Residential Wood-Frame Structures Using Fragility Approach. *Journal of Structural Engineering*, 10.1061/(ASCE)ST.1943-541X.0000914, 1-15.
- APA—The Engineered Wood Association, 2011. Approximate Engineering Dead Load Weights of Wood Structural Panels. Technical Topics, TT-019B, Tacoma, Washington.
- ASCE, 2010. Minimum Design Loads for Buildings and Other Structures. Reston, Va.
- Ashley, Walker S., 2007: Spatial and Temporal Analysis of Tornado Fatalities in the United States: 1880-2005. *Weather and Forecasting*, **22**, 1214-1228.
- Bahmani, Pouria, 2014. AutoCAD drawing.
- Brooks, Harold E., Doswell III, Charles A., and Kay, Michael P., 2003: Climatological Estimates of Local Daily Tornado Probability for the United States. *Weather and Forecasting*, **18**, 626-640.

- Brooks, Harold E., 2004: On the Relationship of Tornado Path Length and Width to Intensity. *Weather and Forecasting*, **19**, 310-319.
- Changnon, Stanley A., 2009. Tornado Losses in the United States. *Natural Hazards Review*, **10(4)**, 145-150.
- Chowdhury, Arindam Gan, Canino, Iván, Mirmiran, Amir, Suksawang, Nakin, and Baheru, Thomas, 2012. Wind-Loading Effects on Roof-to-Wall Connections of Timber Residential Buildings, *Journal of Engineering Mechanics*, 10.1061/(ASCE)EM.1943-7889.0000512, 1-44.
- City of Moore, 2014. Ordinance No. 768 (14). Section 5-204 Adoption of Dwelling Code. Available at <http://www.cityofmoore.com/sites/default/files/main-site/high-winds-codes-passed.pdf>.
- Conner, Harold W., Gromala, David S., Burgess, Donald W., 1987. Roof Connections in Houses: Key to Wind Resistance. *Journal of Structural Engineering*, **113**, No. 12, 2459-2474.
- Dao, Thang Nguyen and van de Lindt, John W., 2012. Loss Analysis for Wood Frame Buildings during Hurricanes. I: Structure and Hazard Modeling. *Journal of Performance of Constructed Facilities*, **26(6)**, 729-738.
- Dao, Thang N., (2014, February 21). Personal Communication.

- Datin, Peter L., Prevatt, David O., Pang, Weichiang, 2011. Wind-Uplift Capacity of Residential Wood Roof-Sheathing Panels Retrofitted with Insulating Foam Adhesive. *Journal of Architectural Engineering*, **17**, 144-154.
- Davies-Jones, Robert, Trapp, R. Jeffrey, Bluestein, Howard B., 2001. Tornadoes and Tornadic Storms. *Severe Convective Storms*, Charles A. Doswell III, Ed., American Meteorological Society, 167-221.
- Dixon, P. Grady, Mercer, Andrew E., Choi, Jinmu, and Allen, Jared S., 2011: Tornado Risk Analysis: Is Dixie Alley an Extension of Tornado Alley? *Bulletin of the American Meteorological Society*, **April 2011**, 433-441.
- Efron, Bradley and Tibshirani, Robert J., 1994. An Introduction to the Bootstrap. Chapman & Hall/CRC Press.
- Ellingwood, B.R., Tekie, P.B., 1999. Wind Load Statistics for Probability-Based Structural Design. *Journal of Structural Engineering*, 1921-1930.
- Ellingwood, B.R., Rosowsky, D.V., Li, Y., Kim, J.H., 2004. Fragility Assessment of Light-Frame Wood Construction Subjected to Wind and Earthquake Hazards. *Journal of Structural Engineering*, 10.1061/(ASCE)0733-9445(2004)130:12(1921), 1921-1930.
- Federal Emergency Management Agency (FEMA), 2009. Multi-hazard Loss Estimation Methodology *Hurricane Model HAZUS-MH MR4* Technical Manual. August 2009.

Federal Emergency Management Agency (FEMA), 2012. Mitigation Assessment Team Report
Spring 2011 Tornadoes: April 25-28 and May 22 Building Performance Observations,
Recommendations, and Technical Guidance. P-908, May 2012.

FRC, 2010. Florida Residential Building Code, International Code Council, Country Club
Hills, IL.

Goliger, A.M., and Milford, R.V., 1998: A Review of Worldwide Occurrence of
Tornadoes. *Journal of Wind Engineering and Industrial Aerodynamics*, **74-76**,
111-121.

Graettinger, Andrew J., Grau, David, van de Lindt, John, and Prevatt, David O., 2012: GIS for
the Geo-Referenced Analysis and Rapid Dissemination of Forensic Evidence Collected in
the Aftermath of the Tuscaloosa Tornado. *Construction Research Congress*, 2170-2179.

Gurley, K.R. and Masters, F.J., 2011. Post-2004 Hurricane Field Survey of Residential Building
Performance. *Natural Hazards Review*, **12**, 177-183.

Haan Jr., F.L., Balaramudu, V.K., Sarkar, P.P., 2010. Tornado-Induced Wind Loads on a Low-
Rise Building. *Journal of Structural Engineering*, **136**, 106-116.

Hamid, S. S., 2014. The Florida Public Hurricane Loss Model. Retrieved March 1, 2016 from:
http://fphlm.cs.fiu.edu/docs/FPHLM_05_02_2014.pdf .

Hossain, Quazi, Mensing, Richard, Savy, Jean, and Kimball, Jeffery, 1999: A Probabilistic
Tornado Wind Hazard Model for the Continental United States. *United States-Japan
Joint Panel Meeting on Seismic and Wind Engineering*, Tsukuba, Japan, 9p.

Insurance Institute for Business and Homes Safety (IBHS), 2016. The IBHS Fortified Home Program. Retrieved March 1, 2016, from: <https://disastersafety.org/fortified/fortified-home/>.

IRC, 2009. International Residential Code for One- and Two-family Dwellings. International Code Council, Country Club Hills, IL.

IRC, 2012. International Residential Code for One- and Two-family Dwellings. International Code Council, Country Club Hills, IL.

Jordan, J. (2007) Tornado Damage Assessment for Structural Engineers. Forensic Engineering (2007): pp. 1-17. doi: 10.1061/40943(250)2

Karstens, Christopher D., Samaras, Timothy M., Lee, Bruce D., Gallus Jr., William A., and Finley, Catherine A., 2010. Near-Ground Pressure and Wind Measurements in Tornadoes. *Monthly Weather Review*, **138**, 2570-2588.

Keith, Edward L., and Rose, John D., 1994. Hurricane Andrew – Structural Performance of Buildings in South Florida. *Journal of Performance of Constructed Facilities*, **8**, 178-191.

Kopp, Gregory A., and Morrison, Murray J., 2011. Discussion of “Tornado-Induced Wind Loads on a Low Rise Building” by F.L. Hann Jr., Vasanth Kumar Balaramudu, and P.P. Sarkar. *Journal of Structural Engineering*, **137**, 1620-1622.

- Kopp, G. A., and Morrison, M.J., 2014. Component and cladding pressures and zones for the roof of low-rise buildings. To be submitted to *ASCE Journal of Structural Engineering*.
- Lai, C.D. and Xie, M., 2003. Concepts of Stochastic Dependence in Reliability Analysis. *Handbook of Reliability Engineering*, Hoang Pham, Ed., Springer, 141-156.
- Lee, Kyung Ho, and Rosowsky, David V., 2005. Fragility Assessment for Roof Sheathing Failure in High Wind Regions. *Engineering Structures*, **27**, 857-868.
- Luco, Nicolas, Ellingwood, Bruce R., Hamburger, Ronald O., Hooper, John D., Kimball, Jeffrey K., and Kircher, Charles A., 2007. Risk-Targeted versus Current Seismic Design Maps for the Conterminous United States. Structural Engineers Association of California 2007 Convention Proceedings, Squaw Creek, California.
- Manufactured Housing Institute (MHI), 2016: Basic Wind Zone Map. Retrieved March 2, 2016, from:
http://www.manufacturedhousing.org/lib/showtemp_detail.asp?id=203&cat=technical
- Marshall, Timothy P., 2002. Tornado Damage Survey at Moore, Oklahoma. *Weather and Forecasting*, **17**, 582-598.
- Masoomi, Hassan and van de Lindt, John W., 2015. Rough Estimation of Tornado Fragility Curves from Existing Hurricane Fragility Curves for Manufactured Homes. (2016, February 28). Personal Communication.
- McDonald, James R., and Mehnert, John F., 1989. Review of Standard Practice for Wind-Resistant Manufactured Housing. *Journal of Aerospace Engineering*, **2**, 88-96.

Mehta, Kishor C., Minor, Joseph E., and McDonald, James R., 1976. Windspeed Analyses of April 3-4, 1974 Tornadoes. *Journal of the Structural Division*, **102** (ST9), 1709-1724.

Minor, Joseph E., McDonald, James R., and Mehta, Kishor C., 1977. The Tornado: An Engineering-Oriented Perspective. National Oceanographic and Atmospheric Association Technical Memorandum ERL NSSL-82, National Severe Storms Lab, Norman OK, 1-196.

Mishra, A. R., James, D.L., and Letchford, C.W., 2008. Physical simulation of a single-celled tornado-like vortex, Part B: Wind loading on a cubical model. *Journal of Wind Engineering and Industrial Aerodynamics*, **96**, 1258-1273.

Morrison, Murray J., and Kopp, Gregory, A., 2011. Performance of toe-nail connections under realistic wind loading. *Engineering Structures*, **33**, 69-76.

National Oceanographic and Atmospheric Administration (NOAA), 2011. Service Assessment: The Historic Tornadoes of April 2011, *U.S. Dept. of Commerce*, December 2011.

National Weather Service, Jackson, Mississippi (NWS JAN), 2011: Neshoba/Kemper/

Winston/Noxubee Counties Tornado. Retrieved February 18, 2016,

from:

http://www.srh.noaa.gov/jan/?n=2011_04_25_27_neshoba_kemper_winston_noxubee.

ORC, 2011. Oregon Residential Specialty Code, International Code Council, Country Club Hills, IL.

Pan, Kai, Montpellier, Peter, and Zadeh, Masoud, 2002. Engineering Observations of 3 May 1999 Oklahoma Tornado Damage. *Weather and Forecasting*, **17**, 599-610.

Prevatt, David O., van de Lindt, John W., Graettinger, Andrew, Coulbourne, William, Gupta, Rakesh, Pei, Shiling, Hensen, Samuel, and Grau, David, 2011a. Damage Study and Future Direction for Structural Design Following the Tuscaloosa Tornado of 2011. National Science Foundation, 1-56.

Prevatt, David O., Coulbourne, William, Graettinger, Andrew J., Pei, Shiling, Gupta, Rakesh, and Grau, David, 2011b. The Joplin Tornado of 2011—Damage Survey and Case for Tornado Resilient Codes. American Society of Civil Engineers, 1-55.

Prevatt, David O., van de Lindt, John W., Back, Edward W., Graettinger, Andrew J., Pei, Shiling, Coulbourne, William, Gupta, Rakesh, and James, Darryl, 2012a: Making the Case for Improved Structural Design: Tornado Outbreaks of 2011. *Leadership and Management in Engineering*, **12**, 254-270.

Prevatt, David O., Roueche, David B., van de Lindt, John W., Pei, Shiling, Dao, Thang, Coulbourne, William, Graettinger, Andrew J., Gupta, Rakesh, and Grau, David, 2012b: Building Damage Observations and EF Classifications from the Tuscaloosa, AL and Joplin, MO Tornadoes. *Structures Congress*, 999-1010.

Ramsdell Jr., J.V., 2005: Tornado Climatology of the Contiguous United States. NUREG/CR-4461 – Pacific Northwest National Laboratory, U.S. Nuclear Regulatory Commission, Office of Nuclear Reactor Regulation, Washington, D.C. 266p.

Rapid Deployment Damage Assessment Team, 2011a: Joplin Tornado. Available at:

<http://esridev.caps.ua.edu/JoplinTornado/>.

Rapid Deployment Damage Assessment Team, 2011b: Tuscaloosa Tornado. Available at:

http://esridev.caps.ua.edu/tuscaloosa_tornado/.

Reed, T. D., Rosowsky, D.V., and Schiff, S.D., 1997. Uplift Capacity of Light-Frame Rafter to Top Plate Connections. *Journal of Architectural Engineering*, **3**, 156-163.

Reinhold, T.A., and Ellingwood, B., 1982: Tornado Damage Risk Assessment. NUREG-CR-2944/BNL-NUREG-51586 AN,RD – Center for Building Technology, National Bureau of Standards, Washington, D.C., 55p.

Rosowsky, David V., and Ellingwood, B.R., 2002. Performance-Based Engineering of Wood Frame Housing: Fragility Analysis Methodology. *Journal of Structural Engineering*, **128**, 32-38.

Roueche, David B., and Prevatt, David O., 2013. Residential Damage Patterns Following the 2011 Tuscaloosa, AL and Joplin, MO Tornadoes. *Journal of Disaster Research*, **8**, 1061-1067.

Schaefer, Joseph T., Kelly, Donald L., and Abbey, Robert F., 1986: A Minimum Assumption Tornado-Hazard Probability Model. *Journal of Climate and Applied Meteorology*, **25**, 1934-1945.

SellersPhoto, 2014: Flintville, TN Tornado. Available at:

<http://www.sellersphoto.com/20140428storm#hea1885a>.

Sengupta, A., Haan, F.L., Sarkar, P.P., and Balaramudu, V., 2008. Transient loads on buildings in microbursts and tornado winds. *Journal of Wind Engineering and Industrial Aerodynamics*, **96**, 2173-2187.

Shanmugam, Bagyalakshmi, Nielson, Bryant G., Prevatt, David O., 2008. Probabilistic Descriptions of in-situ Roof to Top Plate Connections in Light Frame Wood Structures, *American Society of Civil Engineers – Structures Congress*.

Simpson Strong-Tie, 2014a: H2.5 clip. Available at:

<http://www2.strongtie.com/drawings/index.asp>

Simpson Strong-Tie, 2014b: RSP4 clip. Available at:

<http://www2.strongtie.com/drawings/index.asp>

Standohar-Alfano, Christine D. and van de Lindt, John W., (2014). An Empirically-Based Probabilistic Tornado Hazard Analysis of the U.S. Using 1973-2011 Data. *Natural Hazards Review*, **10**.

Standohar-Alfano, Christine D. and van de Lindt, John W., (2015). Tornado Risk Analysis for Residential Wood-Frame Roof Damage across the United States. *Journal of Structural Engineering*, 10.1061/(ASCE)ST.1943-541X.0001353, 04015099.

Storm Prediction Center, 2011: Severe Weather Database Files.

Twisdale, Lawrence A., and Dunn, William L., 1983. Probabilistic Analysis of Tornado Wind Risks. *Journal of Structural Engineering*, **109**(2), 468-488.

United States Census Bureau, 2011a. TIGER/Line Shapefiles: Census. Available at:
<http://www.census.gov/cgi-bin/geo/shapefiles/index.php>.

United States Census Bureau, 2011b. INCOME IN THE PAST 12 MONTHS (IN 2011 INFLATION-ADJUSTED DOLLARS) 2007-2011 American Community Survey 5-Year Estimates. Available at: <http://www.factfinder.census.gov>.

United States Census Bureau, 2011c. VALUE: Owner-occupied housing units, 2009-2013 American Community Survey 5-Year Estimates. Available at:
<http://www.factfinder.census.gov>.

United States Census Bureau, 2012. Geographic Terms and Concepts. Retrieved March 1, 2016, from: https://www.census.gov/geo/reference/gtc/gtc_ct.html.

U.S. Department of Housing and Urban Development, 2000. Residential Structural Design Guide: 2000 Edition. Available online at:
<http://www.huduser.org/portal/Publications/pdf/residential.pdf>.

van de Lindt, John W. and Dao, Thang Nguyen, 2012. Loss Analysis for Wood Frame Buildings during Hurricanes. II: Loss Estimation. *Journal of Performance of Constructed Facilities*, **26**(6), 739-747.

- van de Lindt, John W., Amini, Mohammad Omar, Standohar-Alfano, Christine, Dao, Thang, 2012. Systematic Study of the Failure of a Light-Frame Wood Roof in a Tornado, *Buildings*, **2**, 519-533.
- van de Lindt, John W., Pei, Shiling, Dao, Thang, Graettinger, Andrew, Prevatt, David O., Gupta, Rakesh, Coulbourne, William, 2013. Dual-Objective-Based Tornado Design Philosophy, *Journal of Structural Engineering*, 251-263.
- Vickery, Peter J., 2015. (2015, November 30). Personal Communication.
- Weibe, Dane M. and Cox, Daniel T., 2014. Application of fragility curves to estimate building damage and economic loss at a community scale: a case study of Seaside, Oregon. *Natural Hazards*, **71**, 2043-2061.
- Wind Science and Engineering Research Center, 2006: A Recommendation for an Enhanced Fujita Scale, 111 pp. Available at: <http://www.depts.ttu.edu/weweb/efscale.pdf>
- Winkel, Michael, and Smith, Ian, 2010. Structural Behavior of Wood Light-Frame Wall Segments Subjected to In-Plane and Out-of-Plane Forces. *Journal of Structural Engineering*, **136**(7), 826-836.
- Wurman, Joshua, Kosiba, Karen, and Robinson, Paul, 2013. In Situ, Doppler Radar, and Video Observations of the Interior of a Tornado and the Wind-Damage Relationship. *Bulletin of the American Meteorological Society*, 835-846.

Yeh, Borjen, Williamson, Thomas, and Keith, Edward, 2009. Combined Shear and Wind Uplift Resistance of Wood Structural Panel Shearwalls. *American Society of Civil Engineers – Don't Mess with Structural Engineers.*

APPENDIX A

GC_p VALUES FOR EACH STRUCTURAL ARCHETYPE

Table A.1: External pressure coefficient, GC_p , for Structure Type 1 using ASCE 7-16 wind provisions.

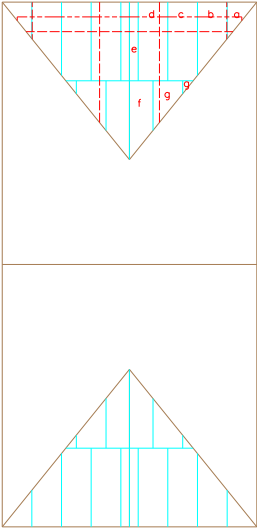
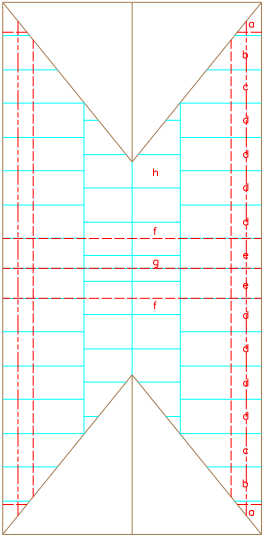
	Nominal	Mean	COV	
	a	-3.66	-3.473	0.12
	b	-2.12	-2.018	0.12
	c	-2.00	-1.895	0.12
	d	-2.01	-1.914	0.12
	e	-2.03	-1.927	0.12
	f	-1.74	-1.654	0.12
	g	-1.80	-1.710	0.12
	Nominal	Mean	COV	
	a	-3.53	-3.355	0.12
	b	-2.24	-2.132	0.12
	c	-2.05	-1.949	0.12
	d	-1.98	-1.879	0.12
	e	-1.98	-1.879	0.12
	f	-1.80	-1.710	0.12
	g	-1.80	-1.710	0.12
	h	-1.74	-1.651	1.12

Table A.2: External pressure coefficient, GC_p , for Structure Type 2 using ASCE 7-16 wind provisions.

	Nominal	Mean	COV	
	a	-3.75	-3.564	0.12
	b	-2.18	-2.075	0.12
	c	-2.34	-2.227	0.12
	d	-2.09	-1.986	0.12
	e	-2.34	-2.219	0.12
	f	-2.03	-1.932	0.12
	g	-1.77	-1.683	0.12
	h	-1.65	-1.570	0.12
	i	-1.80	-1.710	0.12
	j	-1.96	-1.860	0.12
k	-1.75	-1.663	0.12	
	Nominal	Mean	COV	
	a	-2.18	-2.066	0.12
	b	-2.20	-2.090	0.12
	c	-2.92	-2.774	0.12
	d	-2.00	-1.900	0.12
	e	-1.83	-1.739	0.12
	f	-3.19	-3.026	0.12
	g	-2.59	-2.456	0.12
	h	-2.03	-1.924	0.12
	i	-2.86	-2.716	0.12
	j	-2.72	-2.581	0.12
	k	-3.15	-2.988	0.12
	l	-3.00	-2.850	0.12
m	-3.50	-3.328	0.12	

Table A.3: External pressure coefficient, GC_p , for Structure Type 3 using ASCE 7-16 wind provisions.

	Nominal	Mean	COV
a	-1.95	-1.848	0.12
b	-1.95	-1.856	0.12
c	-2.85	-2.704	0.12
d	-1.76	-1.675	0.12
e	-1.72	-1.634	0.12
f	-2.50	-2.375	0.12
g	-1.80	-1.709	0.12
h	-1.67	-1.590	0.12
i	-1.99	-1.892	0.12
j	-1.80	-1.710	0.12
k	-2.20	-2.090	0.12

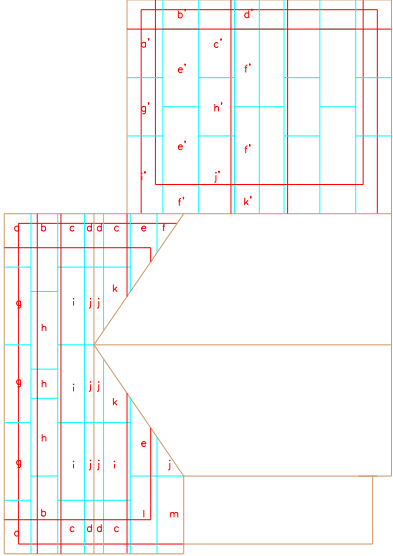
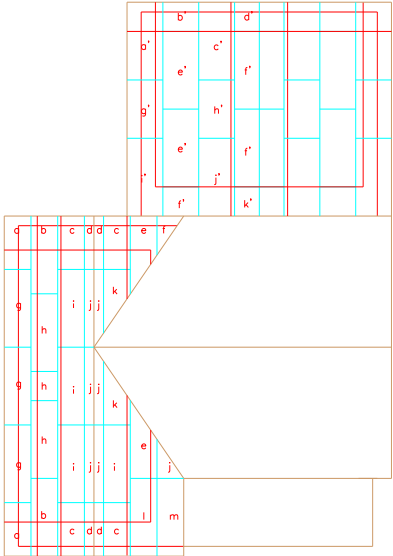
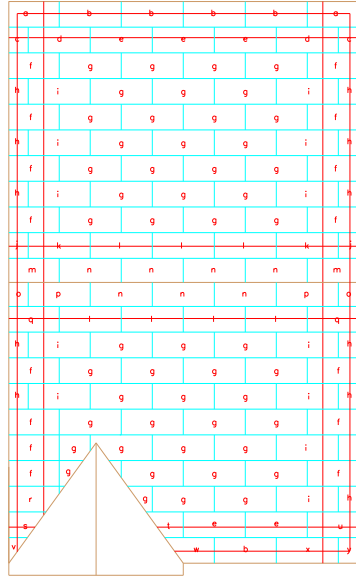
		Nominal	Mean	COV
	a	-3.09	-2.932	0.12
	b	-2.10	-1.997	0.12
	c	-2.07	-1.968	0.12
	d	-2.07	-1.968	0.12
	e	-2.05	-1.944	0.12
	f	-2.34	-2.227	0.12
	g	-2.01	-1.906	0.12
	h	-1.74	-1.652	0.12
	i	-1.70	-1.618	0.12
	j	-1.80	-1.710	0.12
	k	-1.78	-1.691	0.12
	l	-1.98	-1.883	0.12
	m	-1.97	-1.869	0.12
		Nominal	Mean	COV
	a'	-2.70	-2.563	0.12
	b'	-3.17	-3.007	0.12
	c'	-2.52	-2.398	0.12
	d'	-3.96	-3.765	0.12
	e'	-1.81	-1.716	0.12
	f'	-2.99	-2.836	0.12
	g'	-2.20	-2.085	0.12
	h'	-2.09	-1.987	0.12
	i'	-2.20	-2.085	0.12
	j'	-2.46	-2.340	0.12
	k'	-3.60	-3.420	0.12

Table A.4: External pressure coefficient, GC_p , for Structure Type 4 using ASCE 7-16 wind provisions.

	Nominal	Mean	COV
a	-2.21	-2.097	0.12
b	-2.23	-2.115	0.12
c	-2.40	-2.280	0.12
d	-2.01	-1.909	0.12
e	-1.50	-1.424	0.12
f	-2.41	-2.287	0.12
g	-2.05	-1.943	0.12
h	-1.99	-1.891	0.12
i	-2.40	-2.280	0.12
j	-1.70	-1.612	0.12
k	-1.42	-1.346	0.12
l	-2.19	-2.084	1.12

Table A.5: External pressure coefficient, GC_p , for Structure Type 5 using ASCE 7-16 wind provisions.

	Nominal	Mean	COV
a	-3.60	-3.420	0.12
b	-3.05	-2.898	0.12
c	-2.74	-2.599	0.12
d	-2.48	-2.356	0.12
e	-1.85	-1.758	0.12
f	-1.80	-1.710	0.12
g	-2.06	-1.961	0.12



	Nominal	Mean	COV
a	-2.55	-2.419	0.12
b	-1.96	-1.864	0.12
c	-2.80	-2.660	0.12
d	-1.96	-1.865	0.12
e	-1.76	-1.676	0.12
f	-2.05	-1.952	0.12
g	-1.63	-1.546	0.12
h	-2.34	-2.227	0.12
i	-1.77	-1.685	0.12
j	-2.32	-2.204	0.12
k	-1.85	-1.757	0.12
l	-1.77	-1.680	0.12
m	-2.07	-1.962	0.12
n	-1.64	-1.562	1.12
o	-2.34	-2.227	2.12
p	-1.78	-1.694	3.12
q	-2.08	-1.972	4.12
r	-2.09	-1.988	5.12
s	-2.64	-2.512	6.12
t	-1.80	-1.710	7.12
u	-2.39	-2.274	8.12
v	-3.75	-3.564	9.12
w	-1.96	-1.866	10.12
x	-2.39	-2.266	11.12
y	-3.74	-3.557	12.12

APPENDIX B

LOGARITHMIC PARAMETERS FOR THE ROOF SHEATHING FRAGILITY CURVES

Table B.1: Upper Bound Logarithmic Parameters for Structure Type 1

Damage State	FRC		IRC		AL	
	λ	ξ	λ	ξ	λ	ξ
DS1	5.173	0.076	4.380	0.099	4.375	0.100
DS2	5.255	0.049	4.472	0.068	4.467	0.068
DS3	5.367	0.032	4.608	0.043	4.603	0.043
DS4	5.468	0.025	4.728	0.032	4.723	0.033

Table B.2: Upper Bound Logarithmic Parameters for Structure Type 2

Damage State	FRC		IRC		AL	
	λ	ξ	λ	ξ	λ	ξ
DS1	5.055	0.060	4.276	0.078	4.270	0.078
DS2	5.113	0.045	4.348	0.057	4.342	0.058
DS3	5.229	0.030	4.487	0.037	4.483	0.037
DS4	5.326	0.026	4.600	0.031	4.596	0.031

Table B.3: Upper Bound Logarithmic Parameters for Structure Type 3

Damage State	FRC		IRC		AL	
	λ	ξ	λ	ξ	λ	ξ
DS1	5.053	0.063	4.275	0.079	4.269	0.079
DS2	5.115	0.045	4.348	0.057	4.343	0.057
DS3	5.246	0.029	4.504	0.034	4.500	0.035
DS4	5.372	0.024	4.643	0.027	4.639	0.027

Table B.4: Upper Bound Logarithmic Parameters for Structure Type 4

Damage State	FRC		IRC		AL	
	λ	ξ	λ	ξ	λ	ξ
DS1	5.209	0.049	4.419	0.074	4.413	0.074
DS2	5.255	0.039	4.486	0.054	4.480	0.056
DS3	5.340	0.030	4.598	0.038	4.592	0.038
DS4	5.438	0.026	4.712	0.031	4.707	0.032

Table B.5: Upper Bound Logarithmic Parameters for Structure Type 5

Damage State	FRC		IRC		AL	
	λ	ξ	λ	ξ	λ	ξ
DS1	4.998	0.054	4.211	0.076	4.206	0.077
DS2	5.048	0.043	4.279	0.055	4.274	0.056
DS3	5.247	0.024	4.510	0.027	4.506	0.027
DS4	5.388	0.020	4.659	0.022	4.654	0.022

Table B.6: Lower Bound Logarithmic Parameters for Structure Type 1

Damage State	FRC		IRC		AL	
	λ	ξ	λ	ξ	λ	ξ
DS1	5.207	0.078	4.442	0.096	4.437	0.095
DS2	5.303	0.063	4.535	0.066	4.528	0.067
DS3	5.436	0.025	4.669	0.036	4.664	0.037
DS4	5.509	0.020	4.770	0.028	4.765	0.028

Table B.7: Lower Bound Logarithmic Parameters for Structure Type 2

Damage State	FRC		IRC		AL	
	λ	ξ	λ	ξ	λ	ξ
DS1	5.130	0.058	4.339	0.085	4.334	0.085
DS2	5.184	0.043	4.414	0.060	4.409	0.061
DS3	5.298	0.029	4.554	0.037	4.548	0.037
DS4	5.398	0.022	4.662	0.029	4.658	0.029

Table B.8: Lower Bound Logarithmic Parameters for Structure Type 3

Damage State	FRC		IRC		AL	
	λ	ξ	λ	ξ	λ	ξ
DS1	5.154	0.061	4.367	0.085	4.361	0.085
DS2	5.213	0.046	4.442	0.060	4.436	0.061
DS3	5.347	0.027	4.596	0.034	4.590	0.034
DS4	5.457	0.019	4.720	0.024	4.715	0.025

Table B.9: Lower Bound Logarithmic Parameters for Structure Type 4

Damage State	FRC		IRC		AL	
	λ	ξ	λ	ξ	λ	ξ
DS1	5.332	0.046	4.518	0.079	4.511	0.081
DS2	5.372	0.036	4.584	0.056	4.579	0.057
DS3	5.443	0.025	4.688	0.036	4.683	0.036
DS4	5.516	0.022	4.785	0.028	4.781	0.028

Table B.10: Lower Bound Logarithmic Parameters for Structure Type 5

Damage State	FRC		IRC		AL	
	λ	ξ	λ	ξ	λ	ξ
DS1	5.129	0.067	4.346	0.088	4.341	0.089
DS2	5.196	0.051	4.425	0.061	4.420	0.061
DS3	5.408	0.019	4.651	0.024	4.646	0.025
DS4	5.500	0.014	4.760	0.018	4.756	0.018

APPENDIX C

LOGARITHMIC PARAMETERS FOR THE ROOF-TO-WALL FRAGILITY CURVES

Table C.1: Upper Bound Logarithmic Parameters for Structure Type 1

Building Code	NS		EW	
	λ	ξ	λ	ξ
FRC	4.725	0.144	4.826	0.145
IRC	4.429	0.145	4.514	0.146
ORC	4.363	0.135	4.409	0.144
AL	4.267	0.134	4.306	0.143

Table C.2: Upper Bound Logarithmic Parameters for Structure Type 2

Building Code	NS		EW	
	λ	ξ	λ	ξ
FRC	4.624	0.143	4.945	0.145
IRC	4.356	0.144	4.609	0.147
ORC	4.303	0.134	4.491	0.145
AL	4.223	0.133	4.370	0.142

Table C.3: Upper Bound Logarithmic Parameters for Structure Type 3

Building Code	NS		EW		EW Small	
	λ	ξ	λ	ξ	λ	ξ
FRC	4.889	0.135	5.068	0.145	5.079	0.146
IRC	4.582	0.135	4.728	0.147	4.714	0.149
ORC	4.478	0.134	4.607	0.145	4.579	0.146
AL	4.376	0.134	4.484	0.143	4.437	0.144

Table C.4: Upper Bound Logarithmic Parameters for Structure Type 4

Building Code	NS		EW	
	λ	ξ	λ	ξ
FRC	4.790	0.135	4.812	0.144
IRC	4.493	0.136	4.502	0.146
ORC	4.394	0.134	4.396	0.144
AL	4.299	0.134	4.292	0.142

Table C.5: Upper Bound Logarithmic Parameters for Structure Type 5

Building Code	NS		EW	
	λ	ξ	λ	ξ
FRC	4.562	0.133	5.071	0.145
IRC	4.360	0.133	4.747	0.146
ORC	4.301	0.134	4.634	0.144
AL	4.249	0.134	4.522	0.143

Table C.6: Lower Bound Logarithmic Parameters for Structure Type 1

Building Code	NS		EW	
	λ	ξ	λ	ξ
FRC	5.175	0.116	5.277	0.116
IRC	4.879	0.117	4.967	0.119
ORC	4.781	0.115	4.860	0.116
AL	4.685	0.115	4.756	0.115

Table C.7: Lower Bound Logarithmic Parameters for Structure Type 2

Building Code	NS		EW	
	λ	ξ	λ	ξ
FRC	5.075	0.115	5.395	0.115
IRC	4.807	0.116	5.060	0.119
ORC	4.721	0.114	4.941	0.117
AL	4.641	0.114	4.821	0.115

Table C.8: Lower Bound Logarithmic Parameters for Structure Type 3

Building Code	NS		EW		EW Small	
	λ	ξ	λ	ξ	λ	ξ
FRC	5.306	0.116	5.517	0.112	5.527	0.113
IRC	4.999	0.118	5.179	0.120	5.165	0.122
ORC	4.895	0.115	5.058	0.117	5.030	0.119
AL	4.794	0.115	4.935	0.115	4.888	0.116

Table C.9: Lower Bound Logarithmic Parameters for Structure Type 4

Building Code	NS		EW	
	λ	ξ	λ	ξ
FRC	5.207	0.116	5.264	0.116
IRC	4.911	0.117	4.953	0.118
ORC	4.812	0.114	4.848	0.116
AL	4.717	0.114	4.744	0.114

Table C.10: Lower Bound Logarithmic Parameters for Structure Type 5

Building Code	NS		EW	
	λ	ξ	λ	ξ
FRC	4.980	0.113	5.520	0.110
IRC	4.777	0.115	5.198	0.119
ORC	4.719	0.114	5.085	0.117
AL	4.666	0.115	4.972	0.114

APPENDIX D

LOGARITHMIC PARAMETERS FOR THE WALL-TO-FOUNDATION FRAGILITY CURVES

Table D.1: Upper Bound Logarithmic Parameters for Structure Type 1

Wall Type	EW		NS	
	λ	ξ	λ	ξ
Wall A	4.516	0.140	4.545	0.165
Wall B	4.526	0.129	4.566	0.149
Wall C	4.567	0.146	4.634	0.169
Wall D	4.549	0.130	4.626	0.145

Table D.2: Upper Bound Logarithmic Parameters for Structure Type 2

Wall Type	EW		NS	
	λ	ξ	λ	ξ
Wall A	4.841	0.127	4.514	0.136
Wall B	4.848	0.120	4.521	0.132
Wall C	4.871	0.129	4.546	0.139
Wall D	4.861	0.118	4.542	0.130

Table D.3: Upper Bound Logarithmic Parameters for Structure Type 3

Wall Type	EW		NS		EW Small	
	λ	ξ	λ	ξ	λ	ξ
Wall A	4.725	0.141	4.423	0.140	4.330	0.150
Wall B	4.737	0.130	4.434	0.132	4.344	0.141
Wall C	4.781	0.148	4.471	0.146	4.393	0.156
Wall D	4.765	0.130	4.463	0.131	4.387	0.141

Table D.4: Upper Bound Logarithmic Parameters for Structure Type 4

Wall Type	EW		NS	
	λ	ξ	λ	ξ
Wall A	4.662	0.143	4.744	0.125
Wall B	4.673	0.135	4.752	0.116
Wall C	4.713	0.149	4.776	0.128
Wall D	4.705	0.134	4.766	0.114

Table D.5: Upper Bound Logarithmic Parameters for Structure Type 5

Wall Type	EW		NS	
	λ	ξ	λ	ξ
Wall A	4.863	0.136	4.527	0.143
Wall B	4.873	0.124	4.537	0.138
Wall C	4.912	0.144	4.572	0.147
Wall D	4.891	0.125	4.569	0.137

Table D.6: Lower Bound Logarithmic Parameters for Structure Type 1

Wall Type	EW		NS	
	λ	ξ	λ	ξ
Wall A	4.967	0.115	4.997	0.141
Wall B	4.977	0.103	5.017	0.122
Wall C	5.018	0.123	5.085	0.146
Wall D	4.999	0.105	5.076	0.117

Table D.7: Lower Bound Logarithmic Parameters for Structure Type 2

Wall Type	EW		NS	
	λ	ξ	λ	ξ
Wall A	5.292	0.102	4.964	0.110
Wall B	5.298	0.094	4.971	0.107
Wall C	5.321	0.105	4.996	0.113
Wall D	5.310	0.092	4.991	0.104

Table D.8: Lower Bound Logarithmic Parameters for Structure Type 3

Wall Type	EW		NS		EW Small	
	λ	ξ	λ	ξ	λ	ξ
Wall A	5.172	0.124	4.874	0.115	4.781	0.125
Wall B	5.184	0.112	4.884	0.106	4.795	0.116
Wall C	5.230	0.129	4.921	0.121	4.844	0.131
Wall D	5.212	0.112	4.912	0.107	4.838	0.115

Table D.9: Lower Bound Logarithmic Parameters for Structure Type 4

Wall Type	EW		NS	
	λ	ξ	λ	ξ
Wall A	5.110	0.119	5.190	0.105
Wall B	5.122	0.110	5.197	0.097
Wall C	5.164	0.125	5.223	0.110
Wall D	5.154	0.110	5.210	0.097

Table D.10: Lower Bound Logarithmic Parameters for Structure Type 5

Wall Type	EW		NS	
	λ	ξ	λ	ξ
Wall A	5.308	0.118	4.975	0.119
Wall B	5.318	0.107	4.984	0.114
Wall C	5.360	0.124	5.022	0.124
Wall D	5.338	0.108	5.017	0.113

APPENDIX E

LOGARITHMIC PARAMETERS FOR THE SYSTEM LEVEL (VERTICAL LOAD PATH) FRAGILITY CURVES

Table E.1: Upper Bound Logarithmic Parameters for Structure Type 1

Building Code	EW		NS	
	λ	ξ	λ	ξ
FRC	4.568	0.144	4.625	0.159
IRC	4.450	0.122	4.408	0.134
ORC	4.389	0.132	4.324	0.138
AL	4.300	0.138	4.233	0.141

Table E.2: Upper Bound Logarithmic Parameters for Structure Type 2

Building Code	EW		NS	
	λ	ξ	λ	ξ
FRC	4.943	0.145	4.612	0.143
IRC	4.440	0.134	4.325	0.129
ORC	4.403	0.127	4.257	0.134
AL	4.335	0.128	4.185	0.138

Table E.3: Upper Bound Logarithmic Parameters for Structure Type 3

Building Code	EW		NS		EW Small	
	λ	ξ	λ	ξ	λ	ξ
FRC	4.880	0.170	4.478	0.136	4.405	0.144
IRC	4.453	0.141	4.379	0.119	4.331	0.130
ORC	4.440	0.134	4.376	0.120	4.329	0.130
AL	4.398	0.126	4.346	0.125	4.311	0.131

Table E.4: Upper Bound Logarithmic Parameters for Structure Type 4

Building Code	EW		NS	
	λ	ξ	λ	ξ
FRC	4.800	0.143	4.756	0.144
IRC	4.460	0.129	4.430	0.131
ORC	4.381	0.133	4.351	0.135
AL	4.287	0.139	4.262	0.139

Table E.5: Upper Bound Logarithmic Parameters for Structure Type 5

Building Code	EW		NS	
	λ	ξ	λ	ξ
FRC	5.028	0.168	4.395	0.145
IRC	4.475	0.143	4.271	0.133
ORC	4.467	0.135	4.231	0.135
AL	4.436	0.128	4.186	0.137

Table E.6: Lower Bound Logarithmic Parameters for Structure Type 1

Building Code	EW		NS	
	λ	ξ	λ	ξ
FRC	5.150	0.148	5.101	0.135
IRC	4.685	0.119	4.704	0.116
ORC	4.681	0.117	4.687	0.110
AL	4.660	0.110	4.642	0.107

Table E.7: Lower Bound Logarithmic Parameters for Structure Type 2

Building Code	EW		NS	
	λ	ξ	λ	ξ
FRC	5.369	0.120	5.009	0.119
IRC	4.531	0.120	4.531	0.120
ORC	4.533	0.121	4.530	0.118
AL	4.528	0.120	4.517	0.113

Table E.8: Lower Bound Logarithmic Parameters for Structure Type 3

Building Code	EW		NS		EW Small	
	λ	ξ	λ	ξ	λ	ξ
FRC	5.331	0.148	4.966	0.133	4.870	0.135
IRC	4.570	0.121	4.571	0.120	4.598	0.118
ORC	4.569	0.120	4.569	0.120	4.598	0.118
AL	4.566	0.121	4.564	0.120	4.593	0.119

Table E.9: Lower Bound Logarithmic Parameters for Structure Type 4

Building Code	EW		NS	
	λ	ξ	λ	ξ
FRC	5.191	0.126	5.201	0.116
IRC	4.686	0.119	4.684	0.118
ORC	4.681	0.116	4.676	0.113
AL	4.657	0.110	4.647	0.108

Table E.10: Lower Bound Logarithmic Parameters for Structure Type 5

Building Code	EW		NS	
	λ	ξ	λ	ξ
FRC	5.512	0.134	4.946	0.114
IRC	4.667	0.120	4.632	0.113
ORC	4.667	0.120	4.616	0.109
AL	4.663	0.120	4.589	0.107

APPENDIX F

SYSTEM LEVEL FRAGILITY CURVES FOR AN EAST-WEST ORIENTED WIND

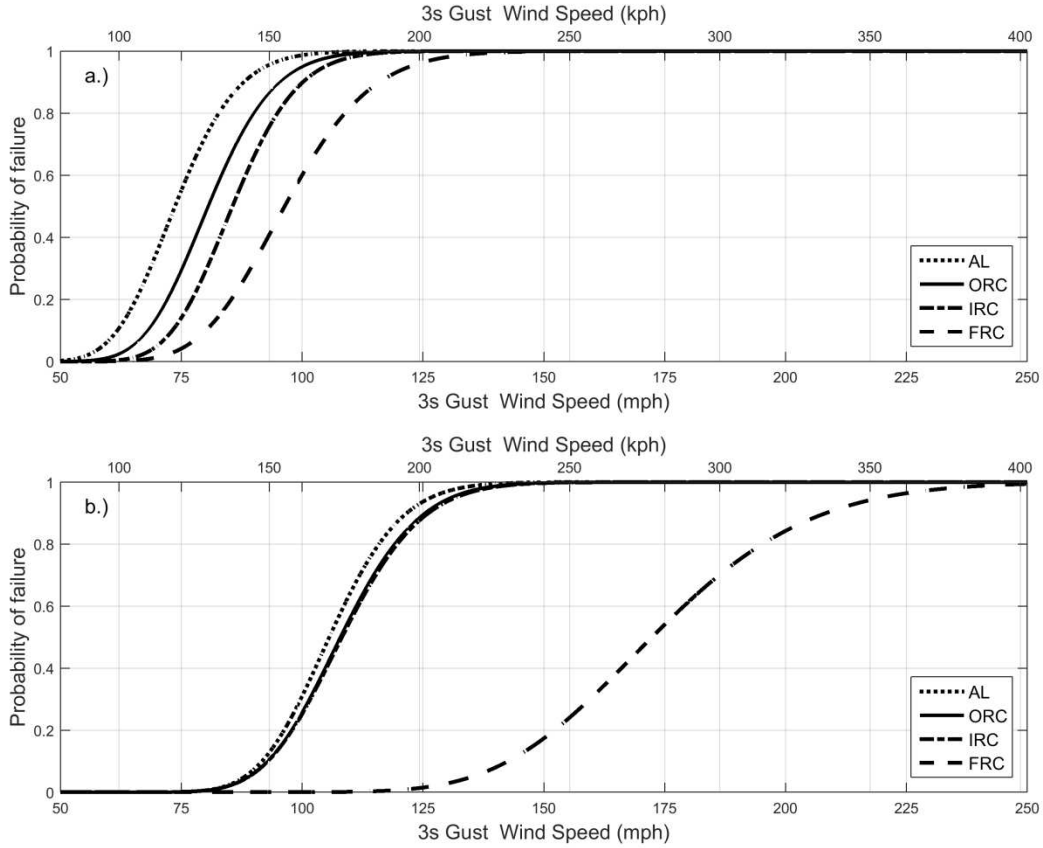


Figure F.1: System level fragility curves for Structure Type 1 a.) is the upper bound performance estimated using ASCE 7-10 and K_c and b.) is the lower bound performance found using ASCE 7-16 wind provisions without any tornado amplification.

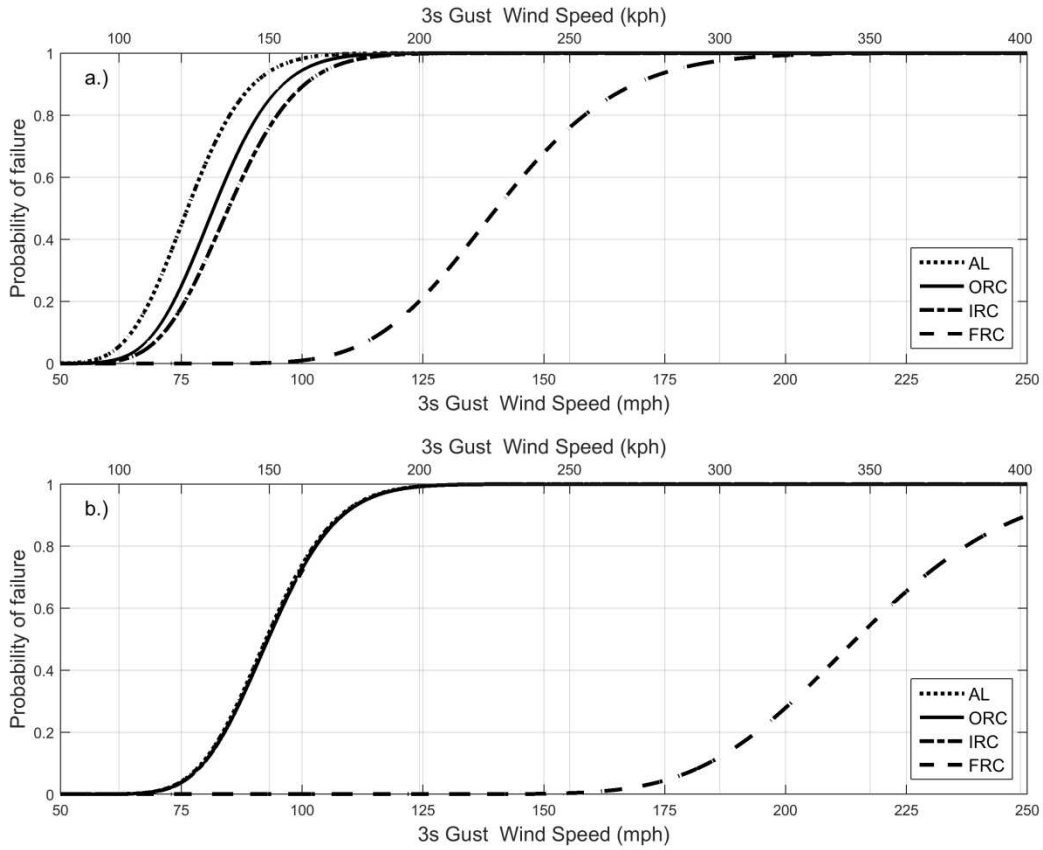


Figure F.2: System level fragility curves for Structure Type 2 a.) is the upper bound performance estimated using ASCE 7-10 and K_c and b.) is the lower bound performance found using ASCE 7-16 wind provisions without any tornado amplification.

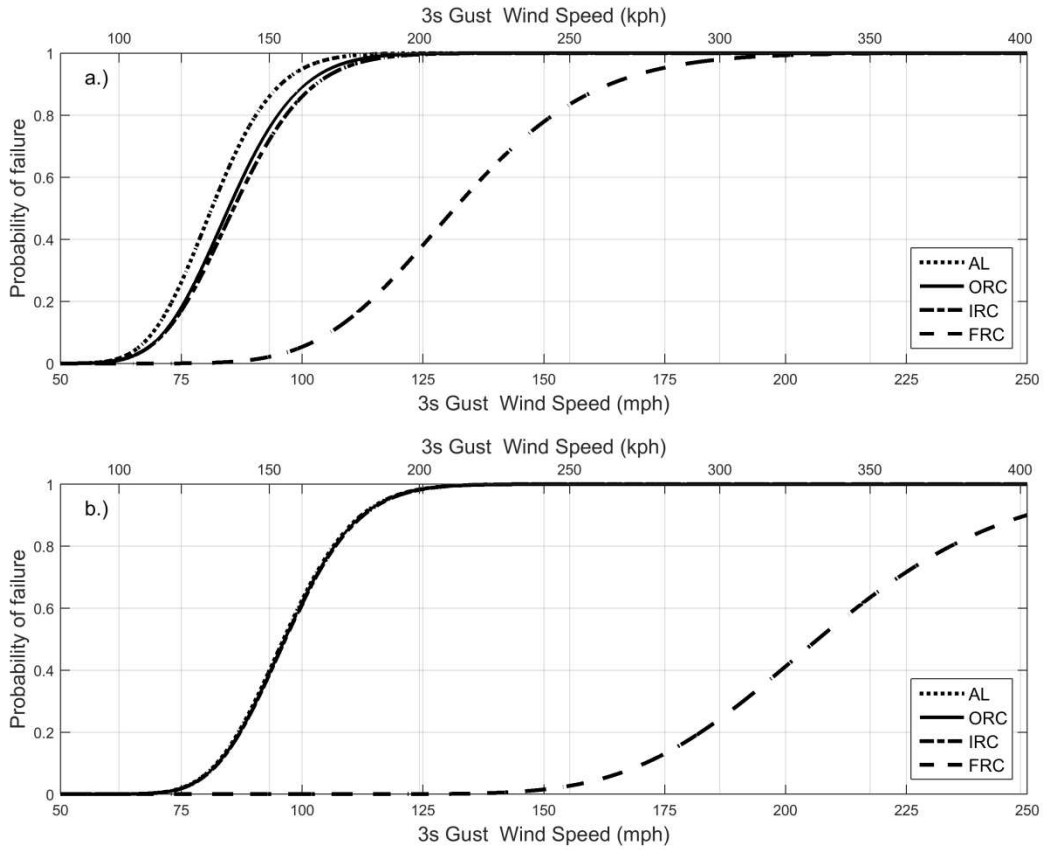


Figure F.3: System level fragility curves for the large EW portion of Structure Type 3 a.) is the upper bound performance estimated using ASCE 7-10 and K_c and b.) is the lower bound performance found using ASCE 7-16 wind provisions without any tornado amplification.

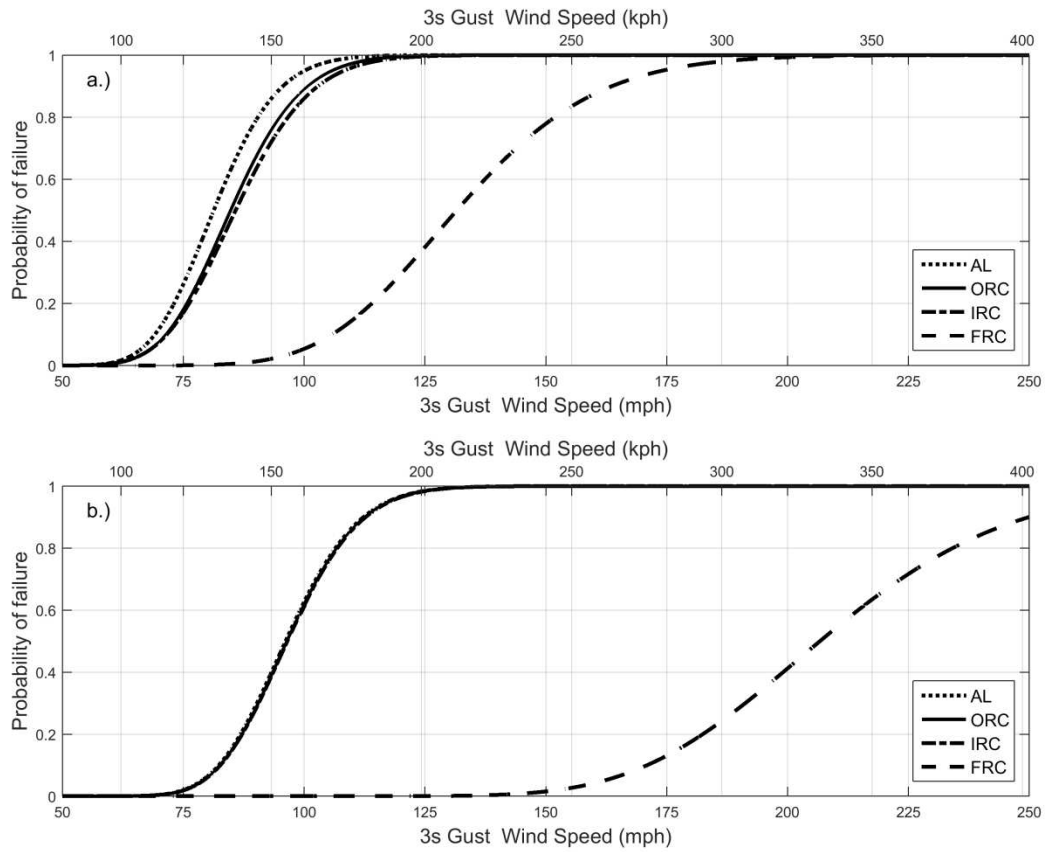


Figure F.4: System level fragility curves for the small EW portion of Structure Type 3 a.) is the upper bound performance estimated using ASCE 7-10 and K_c and b.) is the lower bound performance found using ASCE 7-16 wind provisions without any tornado amplification.

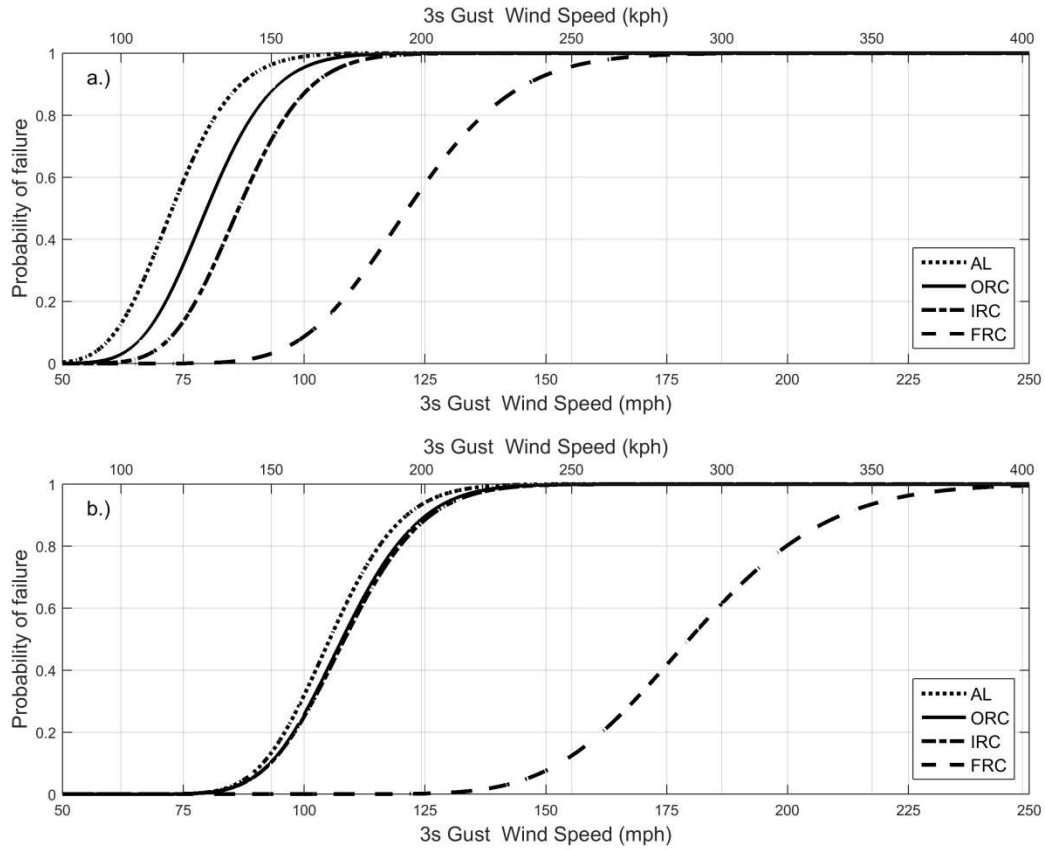


Figure F.5: System level fragility curves for Structure Type 4 a.) is the upper bound performance estimated using ASCE 7-10 and K_c and b.) is the lower bound performance found using ASCE 7-16 wind provisions without any tornado amplification.

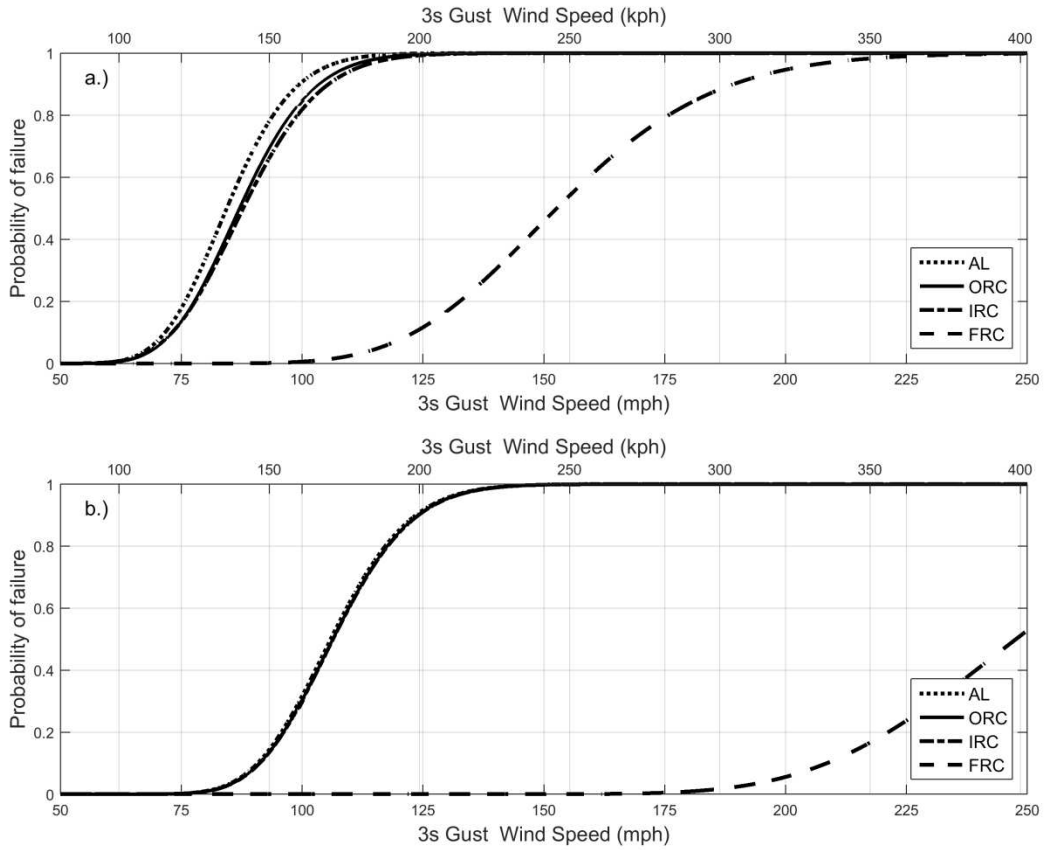


Figure F.6: System level fragility curves for Structure Type 5 a.) is the upper bound performance estimated using ASCE 7-10 and K_c and b.) is the lower bound performance found using ASCE 7-16 wind provisions without any tornado amplification.

APPENDIX G

PROPERTY LOSS ESTIMATES FOR INDIVIDUAL TORNADOES

Table G.1: Loss Estimate for Individual Tornadoes

Tor No.*	EF	length	width	N	Prop Loss (\$ mil)	Method 1 – Prop Loss (\$ mil)				Method 2 – Prop Loss (\$ mil)			
						Upper Bound		Lower Bound		Upper Bound		Lower Bound	
						Local	FRC	Local	FRC	Local	FRC	Local	FRC
301829	5	36.63	1320	1059	0.15	127.85	83.47	92.23	88.80	128.92	83.34	93.59	90.47
303562	5	37.1	1320	181	14.4	15.95	10.64	11.41	10.91	16.19	10.85	11.54	11.06
309488	5	132	2200	5997	1290	1025.40	649.48	739.89	712.91	1041.60	656.47	749.11	714.92
300459	4	40.16	880	119	17.25	12.85	8.43	8.90	8.76	12.90	8.36	9.07	8.92
301925	4	46.98	1260	172	25	23.46	12.66	15.28	14.80	24.10	12.22	15.27	14.64
301943	4	46.88	880	867	0	156.89	82.56	93.47	88.17	161.46	79.69	93.70	87.65
305268	4	48	800	514	68.25	86.66	53.64	58.14	57.33	85.39	54.34	58.24	57.42
307109	4	127.8	1408	2414	170.344	400.42	226.36	256.02	242.33	411.19	224.02	257.36	242.50
311079	4	122.04	1050	1594	27.813	120.61	64.58	72.19	66.86	123.94	63.98	72.15	66.66
314625	4	80.68	2600	5144	2450	993.98	537.74	626.23	590.01	1025.02	524.62	631.16	597.20
314829	4	97.33	1760	384	366.755	67.54	36.23	44.00	42.10	69.67	35.56	43.70	41.26
315331	4	44.18	880	555	167	107.03	58.39	67.05	63.08	108.29	57.42	69.95	63.02
353666	4	14.45	1320	3	1.05	0.90	0.24	0.34	0.34	1.01	0.21	0.28	0.28
289592	3	16.78	300	70	23	17.13	9.55	10.22	9.92	17.78	9.36	9.53	9.45
290471	3	2.57	300	4	1	0.95	0.51	0.66	0.65	0.97	0.49	0.70	0.61
297632	3	13.6	1000	96	8	13.62	7.98	6.95	6.78	13.27	7.56	6.68	6.50
298380	3	19.63	1320	56	5.25	11.64	6.61	6.64	6.58	12.63	5.74	6.23	6.17
303011	3	13.57	440	46	1.5	7.54	3.58	3.96	3.57	7.80	3.40	3.73	3.33
305917	3	23.05	880	101	23.35	16.04	7.76	9.41	9.22	16.33	7.49	9.37	9.15
306267	3	36.99	900	21	5.85	3.23	1.59	1.66	1.62	3.38	1.64	1.52	1.49
306606	3	21.68	880	141	25.4	22.55	12.05	13.86	13.51	22.91	12.56	13.74	13.39
306882	3	30.82	1056	162	15.04	20.74	10.41	11.66	11.36	21.31	10.33	11.58	11.20
309073	3	70.42	1800	83	5.4	6.53	3.26	3.82	3.54	6.73	3.15	3.83	3.53
310930	3	51.45	1320	20	3.27	1.48	0.77	0.86	0.79	1.49	0.75	0.83	0.77
311051	3	23.74	1056	10	3.1	1.85	0.74	0.85	0.78	1.90	0.60	0.84	0.79
311057	3	10.27	440	43	1	3.05	1.49	1.65	1.53	3.19	1.49	1.58	1.49
311603	3	20.26	200	76	9.28	11.56	5.69	6.66	6.13	11.90	5.50	6.73	6.23
314602	3	18.9	375	115	13.4	16.42	8.47	8.83	8.03	17.21	8.50	8.59	8.04
314709	3	31.84	1320	147	17	13.80	7.30	7.77	7.15	13.90	7.21	7.59	6.69
314725	3	72.13	1760	333	36	29.65	14.85	16.64	15.29	30.41	14.42	16.55	14.79
315350	3	7.96	880	37	3	2.83	1.43	1.63	1.50	2.90	1.46	1.61	1.47
347518	3	15.8	1500	114	8.01	18.72	9.26	11.57	11.36	19.28	8.85	11.32	11.06
289586	2	5.87	200	24	3	2.59	1.05	1.13	1.09	2.66	0.97	1.09	1.03
289587	2	14.44	300	24	5	3.03	1.39	1.42	1.36	3.04	1.27	1.40	1.30
289604	2	5.17	350	140	125	24.46	11.80	11.28	10.76	25.35	11.41	10.79	10.52
289605	2	68.1	2900	323	53.405	51.45	23.18	20.51	19.67	52.48	21.39	20.57	20.20
291143	2	42.37	850	38	10.025	3.31	1.48	1.52	1.50	3.24	1.35	1.44	1.42
291598	2	17.45	300	46	1	2.69	1.28	1.27	1.25	2.73	1.21	1.15	1.13
297650	2	12	250	65	1	4.96	2.56	2.46	2.41	4.93	2.37	2.29	2.26
303574	2	3.84	200	14	1.8	1.40	0.64	0.56	0.53	1.44	0.57	0.50	0.48
306600	2	6.73	440	65	10	11.63	3.46	4.87	4.75	11.71	2.64	4.83	4.72
306601	2	24.5	1320	62	8.5	6.38	2.26	2.83	2.76	6.41	2.01	2.63	2.58
310026	2	35.16	1410	27	3.16	2.00	0.50	0.47	0.39	2.24	0.34	0.37	0.28
311015	2	10.46	440	40	1	3.38	1.37	1.38	1.23	3.44	1.27	1.31	1.17
311310	2	14.36	1232	28	1.8	1.75	0.71	0.73	0.64	1.76	0.63	0.69	0.59
311613	2	7.76	200	153	18	34.31	14.74	16.45	15.05	35.53	12.44	16.90	14.18
312153	2	3.23	200	25	9.3	3.39	1.24	1.55	1.39	3.50	1.14	1.58	1.35
289738	1	8.31	800	17	1.75	1.28	0.36	0.34	0.33	1.27	0.28	0.29	0.26
290099	1	8.87	100	14	1	0.99	0.28	0.19	0.17	0.86	0.18	0.14	0.10
291638	1	12.66	880	56	2	2.70	0.94	0.68	0.66	2.22	0.76	0.50	0.48

Table G.1 Continued...						Method 1 – Prop Loss (\$ mil)				Method 2 – Prop Loss (\$ mil)			
						Upper Bound		Lower Bound		Upper Bound		Lower Bound	
Tor No.	EF	length	width	N	Prop Loss (\$ mil)	Local	FRC	Local	FRC	Local	FRC	Local	FRC
301964	1	9.9	100	24	1	1.68	0.64	0.47	0.44	1.65	0.52	0.44	0.37
306314	1	17.02	100	26	1.8	1.78	0.46	0.34	0.32	1.53	0.29	0.24	0.24
307092	1	25.21	880	50	8.15	10.99	2.96	1.93	1.90	11.14	1.56	1.26	1.20
307106	1	6.74	200	4	1.015	0.56	0.23	0.11	0.10	0.57	0.20	0.10	0.10
307167	1	7.76	440	8	1	0.57	0.11	0.07	0.07	0.61	0.09	0.04	0.04
311560	1	7.28	176	8	1.4	0.83	0.11	0.13	0.10	0.77	0.04	0.02	0.01
314573	1	3.39	100	84	3.715	14.32	3.58	2.96	2.55	13.82	2.79	2.87	1.98
315341	1	8.59	200	22	1.044	2.41	0.59	0.44	0.38	2.43	0.50	0.32	0.23
315353	1	4.24	100	2	1.3	0.17	0.08	0.10	0.09	0.17	0.07	0.10	0.09
289628	0	3.32	50	5	1	0.28	0.06	0.02	0.01	0.09	0.03	0.00	0.00

**The selection of tornadoes with over \$1M in property loss was based on SPC data. However, there were some well-documented tornadoes that resulted in over \$1M in property damage, but the property loss was not included or incomplete. These tornadoes were added to the analysis in dissertation and are shown in Table G.1 in italics.*

LIST OF ABBREVIATIONS AND SYMBOLS

λ_R – Logarithmic median of R

λ_R' – Logarithmic median for manufactured home tornado fragility curves

ξ_R – Logarithmic standard deviation of R

a_{EF_j} – Area of tornado path rated EF_j

A – Regional area of interest for tornado hazard estimation

A_{CT} – Total area of all census tracts impacted by a given tornado

A_i – Area of census tract i

ASCE – American Society of Civil Engineers

C&C – Components and cladding

CI – Confidence interval

CMU – Concrete masonry unit

COV – Coefficient of variation

C_p – External pressure coefficient

C_v – Modification factor

D – Dead load

De – Demand

DI – Damage indicator

DOD – Degree of damage

DS1 – Damage state 1: no loss of roof sheathing

DS2 – Damage state 2: loss of less than or equal to 1 roof sheathing panel

DS3 – Damage state 3: roof sheathing loss less than or equal to 10%

DS4 – Damage state 4: roof sheathing loss less than or equal to 25%

EF – Enhanced Fujita scale

EW – Orientation of wind from the east or west relative to a north-south oriented structure

F – Fujita scale

FEMA – Federal Emergency Management Agency

FRC – Florida Residential Building Code

G – Gust factor

GC_{pi} – Internal pressure coefficient

GIS – Geographic Information System

h – Height where wind load is being calculated

H_{EFj} – Annual probabilistic tornado hazard for tornado wind speeds classified as EF_j

i – Summing index for all tornadoes in A (Chapter 3)

i – Index for a given census tract (Chapter 5)

IRC – International Residential Code

j – Summing index for tornadoes rated EF0 to EF5

k – Summing index between 0 and 5

K_c – Tornado amplification factor

K_d – Wind directionality factor

K_z – Velocity pressure exposure coefficient

K_{zt} – Topographic factor

l – Tornado length

MWFRS – Main wind force resisting system

n – Number of tornadoes in A (Chapter 2)

n – Number of census tracts in the tornado damage path (Chapter 5.2.3)

n – Number of structures (Chapter 5.2.7)

N_{CT} – Total number of homes in all the census tracts impacted by a given tornado

N_i – Number of homes in census tract i

NS – Orientation of wind from the north or south relative to a north-south oriented structure

N – Total number of homes in the tornado damage path

NW - Northwest

NWS – National Weather Service

ORC – Oregon Residential Specialty Code

OSB – Oriented strand board

p_j – Probability that a tornado will be rated EF _{j}

P – Annual probability of tornado occurrence

P_f – Annual failure probability

P_{loss} – Estimated property loss

P_s – Annual survival probability

P_{f50} – 50 year failure probability

P_{EF_j} – Annual probability of experiencing a tornado rated EF _{j}

PDF – Probability density function

q_h – Velocity pressure at h

R – Resistance capacity for uplift or shear

RMV – Real market value

S – Swirl ratio (Chapter 1)

S – Shear load (Chapter 3)

SP – Specimen number for wall tests

SPC – Storm Prediction Center

TD – Tie-down

U.S. – United States of America

V – 3 s gust wind speed at 10 m

V_H – Hurricane demand (3 s gust wind speed at 10 m)

V_T – Tornado demand (3 s gust wind speed at 10 m)

w – Tornado width

W – Wind load in either uplift or shear

W_H – Hurricane wind load

W_T – Tornado wind load

Y – Number of years in the tornado data set